Implementation of Damage and Rupture models for composite materials

Auteur : Tomasetti, Romin
Promoteur(s) : Ponthot, Jean-Philippe; 7449
Faculté : Faculté des Sciences appliquées
Diplôme : Master en ingénieur civil physicien, à finalité approfondie
Année académique : 2018-2019
URI/URL : http://hdl.handle.net/2268.2/6732

Implementation and validation of a semi-analytical method for the prediction of material allowables for unidirectional composite materials

Master Thesis

TOMASETTI Romin

Liège University
Second Master in Engineering Physics

Academic Supervisor : J.-P. PONTHOT
Supervisor at e-Xstream : P. MARTINY

Academic Year: 2018-2019

Summary

Composite materials have very appealing properties. They are both lightweight and resistant, making their use of prior importance in reducing energy consumption in aeronautics and automotive sectors for instance. They are also widespread in the wind industry. However, the understanding of their behavior up to rupture is still an open question. Lot of work has been done in using advanced non-linear finite element models to predict ultimate failure of composites. Unfortunately, these methods result in very high computational costs, and generally require extensive material characterization, and as a result, material screening and preliminary optimization price goes up. In order to tackle both problems of computational costs and material characterization, this report implements and validates a semi-analytical framework for computing the strength of open-hole unidirectional Carbon Fiber Reinforce Polymer composite laminates. The framework requires only the longitudinal modulus and strength of the zero ply, as well as its $\mathscr{R}$-curve. Since the method does not involve finite elements, it is both time and mesh size independent and extremely fast. In this work, the method will be evaluated on several datasets. Afterwards, a method for calibrating the $\mathscr{R}$-curve from one open-hole strength is introduced to relieve the material characterization. Finally, the unnotched strength criterion used in the method will be enhanced. The overall framework performs very well at capturing the hole size effect on open-hole strength of unidirectional laminates, considering that very few material properties are used.

Acknowledgments

First of all, I would like to thank the team at e-Xstream Engineering for their support, in particular Philippe Martiny for his daily help and advice, and Laurent Adam for the master thesis proposal.

I am also grateful to Pr. Pedro Camanho and his two collaborators, Carolina Furtado and Albertino Arteiro, for their time.

Then, I express my thanks to my academic advisor, Pr. Jean-Philippe Ponthot.

Finally, thanks to all those who have been a part of my getting there, and those who will read this report.

Contents

List of Figures **117**

List of Tables **122**

List of Symbols

$\mathbb{C}$	elastic compliance tensor
l	crack extension at failure
T_{cure}	curing temperature
E_M^*	degradation factor
$\mathbb{E}$	elastic stiffness tensor
$\acute{E}$	equivalent modulus
v_F	fiber volume fraction
Y	finite-width correction factor
R	hole radius
ρ	in-plane orthotropy parameter
X_L	unnotched strength of the laminate
l_{fpz}	length of the fracture process zone
$\mathscr{G}_{Ic}$	mode I critical energy release rate
$\mathscr{G}_I$	mode I Energy Release Rate
$\mathscr{K}_{Ic}$	mode I fracture toughness
$\mathscr{K}_I$	mode I stress intensity factor
χ	orthotropy correction factor
X	longitudinal strength
S	shear strength
Y	transverse strength
ν_M	matrix Poisson ratio
ν_{12}	principal in-plane Poisson ratio
ν_{xy}	principal in-plane Poisson ratio in the global axes
ν_{21}	secondary in-plane Poisson ratio
ν_{yx}	secondary in-plane Poisson ratio in the global axes
$\Omega_0^{(i)}$	ratio between remote failure stress of the balanced sub-laminate (i) and the remote failure stress of the 0° sub-laminate
$\overline{\sigma}^0$	remote failure stress of the 0° sub-laminate
$\overline{\sigma}^{(i)}$	remote failure stress of the balanced sub-laminate (i)
σ_∞	remote stress
$\boldsymbol{\varepsilon}_R$	residual Cauchy strain tensor

$\boldsymbol{\sigma}_R$	residual Cauchy stress tensor
G_{12}	in-plane principal shear modulus
G_{F1}	fiber shear modulus
G_M	matrix shear modulus
G_{xy}	in-plane principal shear modulus in the global axes
F_{12}	in-plane shear strength
$F_{12}^{0.2\%}$	in-plane shear, strength at 0.2% offset
$F_{12}^{5\%}$	in-plane shear, strength at 5% strain
$\sigma_{xx}(0,y)$	stress distribution along the ligament section perpendicular to the loading direction
$\mathscr{R}_{ss}$	steady-state value of the $\mathscr{R}$-curve
$\boldsymbol{\varepsilon}$	Cauchy strain tensor
K_T	stress concentration factor at the edge of the hole of a finite plate
K_T^{∞}	stress concentration factor at the edge of the hole of an infinite plate
$\boldsymbol{\sigma}$	Cauchy stress tensor
T_{test}	temperature at which test is performed
α_L	longitudinal thermal expansion coefficient
α_T	transverse thermal expansion coefficient
$\boldsymbol{\alpha}$	thermal expansion tensor
W	width
E_1	longitudinal Young modulus
E_x	longitudinal Young modulus in the global axes
E_M	matrix Young modulus
E_2	transverse Young modulus
E_{F2}	transverse Young modulus of the fiber
E_y	transverse Young modulus in the global axes

Properties, stresses and strains can be expressed in the *local* and *global* axes, i.e. the ply orthotropic axe or the laminate orthotropic axes, respectively. In this report, the quantities expressed with subscripts 1,2 or 6 refer to the *local* axes whereas the subscripts x, y or z represent the quantities expressed in the *global* axes.

The superscript L denotes a laminate property. For instance, ν_{12}^L is the major/principal in-plane Poisson ratio of the laminate. The superscript 0 denotes a 0° ply property.

The reader is invited to consult the electronic version of the present report, in which any clickable symbol is colored in blue. Clicking on any of these symbols will enable automatic navigation to the present list of symbols.

List of Acronyms

BEST	Best Estimate of the unnotched STrength
CFRP	Carbon Fiber Reinforced Polymers
CPT	Cured Ply Thickness
CTD	Cold Temperature Dry
ETW	Elevated Temperature Wet, lower wet temperature
ETW2	Elevated Temperature Wet, higher wet temperature
FPF 0	First-Ply-Failure on the 0° ply only
LEFM	Linear Elastic Fracture Mechanics
LPF	Last Ply Failure
LPF MFH	Last-Ply-Failure with Mean-Field Homogenization for degradation of elastic properties
LPF mRoM	Last-Ply-Failure with modified Rules of Mixtures for degradation of elastic properties
LPT	Laminate Plate Theory
MFH	Mean-Field Homogenization
mRoM	modified Rules of Mixtures
MS	Max-Strain
OH	Open-Hole
OHC	Open-Hole in compression
OHT	Open-Hole in Tension
QI	Quasi-Isotropic
RTD	Room Temperature Dry
UC	Unit Circle
UCD	Unit Circle with Degraded ply properties
UN	Unnotched
UNC	Unnotched in Compression
UNT	Unnotched in Tension

The reader is invited to consult the electronic version of the present report, in which any clickable acronym is colored in blue. Clicking on any of these acronyms will enable automatic navigation to the present list of acronyms.

Introduction

Composite materials have been there for a long time. Their unrivaled properties, allowing for combination of low weight and high performances in harsh conditions, are very useful in a wide range of fields, varying from aircrafts to cars, bikes and even storage tanks. However, in order to meet the legal material requirements, extensive and expensive test campaigns have to be performed.

Indeed, substantiation of a composite structure is generally conducted by going through a building-block diagram, starting from coupons, elements, details, sub-components and ending with components of the structure [1] [2]. The coupon level requires a lot of experimental specimens to account for variability in material properties such as strength, fracture toughness and life due to the stochastic nature of matrix or fiber properties as well as fiber orientation for instance. These variabilities are generally accounted for by the use of A- or B-basis. On top of the material-linked variabilities, additional parameters such as hole size, environmental conditions or laminate lay-up must be investigated.

In order to reduce costs linked to complete experimental characterization of coupons, more and more researches are oriented towards virtual material models that can predict the strength of coupons to alleviate the number of tested specimens.

The present work focuses on unnotched and notched coupons, and more specifically on a semi-analytical framework to predict the strength of those coupons thanks to material elastic properties, strengths and $\mathscr{R}$-curve (or alternatively the mode I fracture toughness).

The advantages of such a semi-analytical framework are many. The most obvious benefits are the absence of mesh (and the related mesh and time step dependencies) and the reduced time required to obtain the open-hole coupon strength, allowing for fast computation of virtual B-basis [3].

The framework was initially proposed by Furtado et al. [4]. The core of the methodology uses three major building blocks. First of all, the laminate unnotched strength is predicted, based solely on material elastic properties, strengths, Laminate Plate Theory and a suitably chosen failure criterion. Then, an analytical model is used to relate the $\mathscr{R}$-curve (or the fracture toughness) of the material to that of the laminate. Finally, a coupled stress-energy criterion based on Finite Fracture Mechanics is used to predict the open-hole strength. Additionally, a calibration method is proposed to relieve the constraint of having an experimentally determined $\mathscr{R}$-curve.

1 A semi-analytical framework for predicting open-hole strength

This chapter is dedicated to the presentation of the semi-analytical framework as developed in [4]. The Laminate Plate Theory [5] [6] and Trace theory [7] are used for computing elastic properties of the laminate. A max-strain criterion is used to compute the unnotched strength. Then, an analytical model used for relating the $\mathscr{R}$-curve of the ply to that of the laminate, based on Camanho et al. [8], is presented. Eventually, a couple energy-stress criterion is solved in order to find the notched strength.

1.1 Laminate elastic properties

In this section, the Laminate Plate Theory (LPT) and Trace theory are presented. The LPT links the ply elastic properties to the laminate elastic properties, with some simplifying assumptions. The Trace theory is developed to find all elastic constants of the ply based solely on its longitudinal Young's modulus. This theory applies mainly on CFRP. It will be compared to the experimentally determined ply elastic constants.

1.1.1 Laminate Plate Theory

The Laminate Plate Theory is generally employed to determine the elastic properties of an orthotropic laminate based on its lay-up angles and 0° ply elastic properties. These ply elastic properties generally require three independent tests, namely longitudinal tension to determine the longitudinal Young modulus E_1 and in-plane Poisson ratio ν_{12}, transverse tension to determine the transverse Young modulus E_2 and ±45° cross-ply laminate in tension for determining the shear modulus G_{12}.

There are three main assumptions in LPT. The first one is constant through-the-thickness displacement, i.e. the plies are perfectly bonded. The second states that each ply is homogeneous and in plane stress state. The third assumption constraints normals to the mid-plane of the laminate to remain straight and normal after deformation, as well as the ply thickness to be unchanged. This is also

known as the Kirchhoff-Love assumption. The stiffness tensor of the laminate, $\mathbb{E}_L$, can be related to the stiffness tensor of each ply, $\mathbb{E}_k$, as follows:

$$\mathbb{E}_L = \frac{1}{t}\sum_{k=1}^{N} \mathbb{E}_k \cdot t_k, \tag{1.1}$$

where t_k is the thickness of the ply k, t is the thickness of the laminate and N is the number of plies in the lay-up. Then, the elastic properties of the laminate can be extracted from its compliance tensor $\mathbb{C} = \mathbb{E}^{-1}$, assuming relationships between compliance tensor and elastic properties for an orthotropic material hold.

1.1.2 Trace theory

As mentioned in Sect. 1.1.1, the full elastic characterization of the material system requires three independent tests. Moreover, those tests must be carried out multiple times to cope with material variability. A typical test methodology would be the one depicted in Fig. 1.1. For instance, for the sole characterization of E_1 in three different environmental conditions, at least 54 specimens are needed. The full elastic ply characterization in 3 different environmental conditions would require a minimum of 162 specimens.

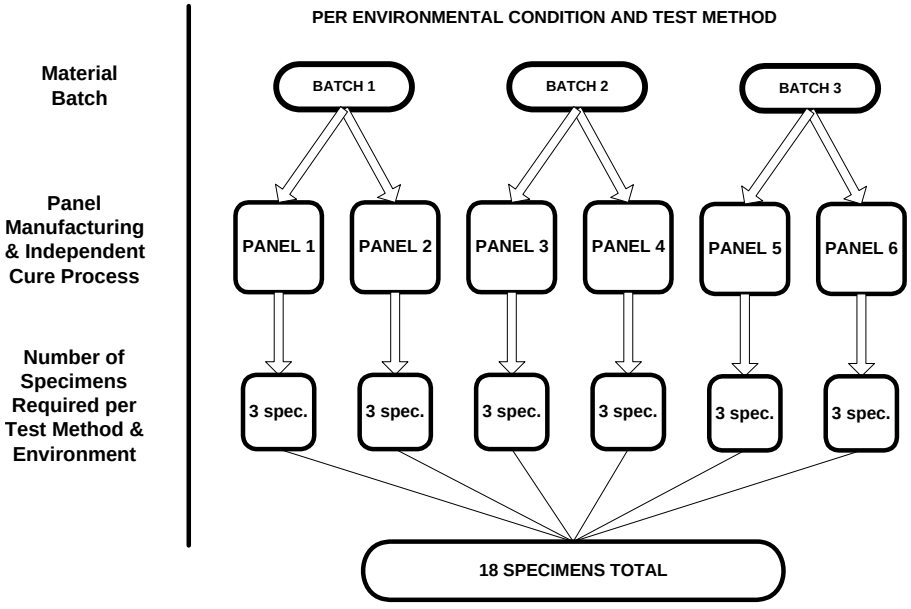

Figure 1.1: Specimen Selection Methodology, after [9].

In order to decrease the costs of a test campaign, the Trace theory may be used for Carbon Fiber Reinforced Polymers [7]. Indeed, thanks to this theory, the elastic constants of an orthotropic ply can be determined based solely on its longitudinal Young modulus E_1, with a remarkable accuracy.

The Trace theory is built upon the observation that the trace-normalized[1] elastic properties of a large number of carbon fiber/epoxy and thermoplastic composite materials are equal. As a reminder,

[1] By *Trace*, it is meant the trace of the in-plane stiffness matrix.

the in-plane stiffness matrix $\mathbb{E}$ is given by:

$$\mathbb{E} = \mathbb{C}^{-1} = \begin{bmatrix} \frac{1}{E_1} & \frac{-\nu_{21}}{E_2} & 0 \\ \frac{-\nu_{12}}{E_1} & \frac{1}{E_2} & 0 \\ 0 & 0 & \frac{1}{2G_{12}} \end{bmatrix}^{-1} \tag{1.2}$$

where the Voigt notations are used. From Eq. (1.2), it is straightforward to deduce the trace of the in-plane stiffness matrix:

$$\text{Trace} = 2G_{12} + \frac{E_1 + E_2}{1 - \nu_{21}\nu_{12}}.$$

Using the coefficients presented in Table 1.1, the 3 remaining elastic constants, E_2, ν_{12} and G_{12}, can be easily determined based only on the knowledge of E_1. The method was found to be quite accurate [4] [7]. In the following, an extensive accuracy study of the Trace theory will be conducted on the NIAR dataset [10].

E_1/Trace	E_2/Trace	G_{12}/Trace	ν_{12}
0.88	0.052	0.031	0.32

Table 1.1: Trace theory coefficients, according to [7].

The Trace theory has been evaluated on the NIAR dataset, see Table A.1, for 10 unidirectional material systems in 4 environmental conditions, namely CTD, RTD, ETW and ETW2. Only tensile properties are shown, but the same methodology can be followed for compressive properties, with more or less the same conclusions. The very first conclusion is that the coefficients from Table 1.1 are merely valid for RTD conditions. Indeed, if the elastic properties of quasi-isotropic laminates $[0/-45/45/90]$ are computed with trace theory coefficients of Table 1.1, there are non-negligible discrepancies between the values computed using the full ply elastic characterization and when trace theory is used, especially in ETW and ETW2 conditions, see Table A.2. If the coefficients are corrected with the help of Table A.1, see Table 1.2, the discrepancies vanish, see Table A.3.

Therefore, with coefficients adapted to the environmental conditions, the Trace theory captures well the relationship that exists between the trace-normalized properties of a wide range of CFRP. This empirical observation has been further validated in [11], wherein the authors used micro-mechanical models to relate the fiber volume fraction, the fiber/matrix stiffness ratios, and the trace-normalized engineering constants of unidirectional laminae and multidirectional laminates. They showed that under the conditions that the longitudinal fiber/matrix ratio is larger than 50 and the fiber volume fraction is between 50% and 70% —which is the case for most CFRPs —, the Trace theory gives very good results. The number of experimental tests required for characterizing the material system can thus significantly be reduced from three independent tests (E_1, E_2 and ν_{12}, G_{12}) to only one test which determines E_1.

Environment	E_1/Trace	E_2/Trace	G_{12}/Trace	ν_{12}
RTD	0.88	0.054	0.031	0.32
CTD	0.873	0.058	0.032	0.314
ETW	0.92	0.041	0.017	0.347
ETW2	0.93	0.037	0.014	0.368

Table 1.2: Corrected Trace theory coefficients.

1.2 Unnotched coupon strength

The unnotched strength predictions carried out in [4] were performed with a Maximum-Strain[2] (MS) criterion, which is therefore described hereunder.

The max-strain criterion is equivalent to the maximum-stress criterion. It states that when normal and shear strains in a ply exceed the maximum allowable values, the ply is considered as broken.

In this study, only longitudinal tension or compression tests are considered, so that the MS criterion reads as:

$$X_L = \frac{X}{E_1} \cdot E_x^L,$$

where X_L, X and E_x^L are the laminate unnotched strength, the ply longitudinal strength and the laminate longitudinal Young modulus, respectively. Note that the properties must be chosen either tensile or compressive. An in-depth analysis of unnotched strength prediction can be found in Chap. 4, wherein other criteria will be used.

1.3 Laminate $\mathscr{R}$-curve

In this section, the method to predict the $\mathscr{R}$-curve or the mode I critical enery release rate $\mathscr{G}_{Ic}$ of the laminate based on that of the 0° ply is presented. This method was proposed in [8].

1.3.1 Energy release rate of the laminate from that of the 0° ply

Camanho et al. [8] assume that a symmetric and balanced laminate, see Sect. G.1, subjected to a remote tensile stress σ_∞, contains a crack, see Fig. 1.2. The model deals only with a through-the-thickness macroscopic crack, considered identical in all plies[3]. Moreover, it neglects the three-dimensional stress field located in a boundary layer near the crack tip, excluding any failure mechanism due to those field. As a consequence, the model will not be valid in case of laminate failure driven by delamination. Camanho et al. [8] validated the model for lay-ups whose failure mode is fiber-dominated.

[2]Throughout the report, *max-strain* will be preferred over *maximum-strain*.

[3]The authors use the term *self-similar*. Unfortunately, it was unclear whether *self-similar* is used in the sense that the crack is identical through-the-thickness or if it means that under small crack growth, the stress fields at crack tip remain

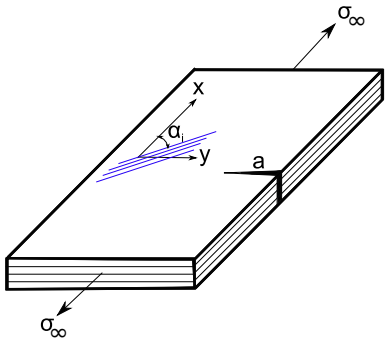

Figure 1.2: Multidirectional balanced laminate subjected to a remote tensile stress σ_∞, adapted from [8].

First of all, the method computes the ratio $\Omega_0^{(i)}$:

$$\Omega_0^{(i)} = \frac{\overline{\sigma}^{(i)}}{\overline{\sigma}^0},$$

where $\overline{\sigma}^{(i)}$ and $\overline{\sigma}^0$ are the remote failure stress of the balanced sub-laminate (i) and of the 0° sub-laminate[4]. This ratio can be determined based on the LPT only:

$$\begin{aligned}
\boldsymbol{\varepsilon}_L &= \mathbb{C}_L : \boldsymbol{\sigma}_L,\ \boldsymbol{\sigma}_L = \mathrm{diag}(\sigma_\infty, 0, 0),\\
\boldsymbol{\sigma}^{(i)} &= \mathbb{E}^{(i)} : \boldsymbol{\varepsilon}_L,\\
\overline{\sigma}^{(i)} &= \boldsymbol{\sigma}_{11}^{(i)}.
\end{aligned}$$

From LEFM, one can relate the remote failure stress to the fracture toughness of the material as follows:

$$\mathcal{K}_{Ic} = Y\chi\sigma_\infty\sqrt{\pi a}, \tag{1.3}$$

where χ is given by [12] [13]:

$$\chi = \left(1 + 0.1\left(\rho - 1\right) - 0.016\left(\rho - 1\right)^2 + 0.002\left(\rho - 1\right)^3\right)\left(\frac{1+\rho}{2}\right)^{-1/4}, \tag{1.4}$$

with:

$$\rho = \frac{\sqrt{E_x E_y}}{2G_{xy}} - \sqrt{\nu_{xy}\nu_{yx}}.$$

It is to be mentioned that the formula Eq. (1.4) is not the same as the one in Furtado et al. [4] and Camanho et al. [8]. Indeed, Eq. (1.4) has been adapted from the corrigenda of [12], see [13]. The influence of this correction will be discussed later on. Applying Eq. (1.3) to the sub-laminate (i) and the 0° sub-laminate, one has:

$$\mathcal{K}_{Ic}^{(i)} = \frac{\chi^{(i)}\Omega_0^{(i)}}{\chi^0}\mathcal{K}_{Ic}^0.$$

unchanged.

[4]The sub-laminate (i), of orientation θ, has the following stacking sequence: $[\theta, -\theta, -\theta, \theta]$.

The energy release rate of the sub-laminate (i) is given by:

$$\mathcal{G}_{Ic}^{(i)} = \frac{\left(\mathcal{K}_{Ic}^{(i)}\right)^2}{\acute{E}^{(i)}}, \tag{1.5}$$

where:

$$\acute{E}^{(i)} = \left(\frac{1+\rho^{(i)}}{2E_x^{(i)}E_y^{(i)}}\right)^{-1/2}\left(\frac{E_y^{(i)}}{E_x^{(i)}}\right)^{-1/4}.$$

Eventually, assuming self-similar crack propagation along all the plies of the laminate, its critical energy release rate can be computed as [8]:

$$\mathcal{G}_{Ic}^{L} = \frac{\sum_{(i)}^{N}\mathcal{G}_{Ic}^{(i)}t^{(i)}}{t}, \quad (i)\neq 90°, \tag{1.6}$$

wherein the contribution of the 90° plies is neglected, and t is the thickness of the laminate. Indeed, these plies fail by transerse cracking instead of fibre failure. The actual mode I fracture toughness of the matrix of these plies should be used, under the assumption that a single crack appears in the 90° ply, parallel to the crack in the 0° ply [8]. However, for carbon/epoxy systems such as those of interest in this study, this fracture toughness is generally several orders of magnitude lower than that of the 0° plies [14].

The method is very powerful in the sense that, through a very simple analytical framework, the fracture toughness of any balanced sub-laminate can be computed based solely on the fracture toughness of the 0° ply and the elastic properties of the material system at hand. Nevertheless, the method relies on formulas that are approximations, such as Eq. (1.4), and has thus a well-know range of applicability. For example, Eq. (1.4) is valid only in the range $0 \geq \rho \geq 6$ [13]. Moreover, it is based on LEFM and is therefore invalid in case of plastic deformation occurring in the vicinity of the crack tip or if delamination occurs. It also neglects any interaction between matrix cracking and fiber failure or between plies (known as the inter-laminar fracture toughness). Last but not least, the method is only valid for balanced sub-laminates.

Camanho et al. [8, Sec. 3.2] validated the method on several lay-ups with remarkable accuracy, with largest errors being imputed to occurrence of delamination between off-axis plies (such as ±45°). The model is thus appropriate for computing fracture toughness when laminates under scrutiny are dominated by fiber failure modes.

It is to be noted that at the moment, no standard test method exists to determine the fracture toughness (or $\mathcal{R}$-curve) of the 0° ply, and is generally found by carrying out Compact Tension and Compact Compression tests on cross-ply laminates[5]. Another method has also been investigated in [15]. Using double edge notched specimens of different sizes, the method predicts well the $\mathcal{R}$-curve of the 0° ply while circumventing the need for measuring the crack length during the test.

[5] By cross-ply laminates, it is meant [0/90] laminates.

1.3.2 $\mathscr{R}$-curve of the laminate from that of the 0° ply

In the previous section, the fracture toughness of the laminate and that of the 0° ply were related thanks to a closed-form analytical model. However, composite materials usually exhibit a fracture resistance behaviour (the $\mathscr{R}$-curve) that characterizes the growing resistance to cracking of the material as the crack length increases. According to [8], if the 0° ply exhibits a $\mathscr{R}$-curve, it makes sense to expect that the laminate will also exhibit a $\mathscr{R}$-curve. Leveraging the knowledge of the $\mathscr{R}$-curve of the 0° ply, and assuming that the length of the fracture process zone of the laminate is equal to that of the 0° ply, the $\mathscr{R}$-curve of the laminate is a simple rescaling of that of the 0° ply such that only the steady-state value of the laminate's $\mathscr{R}$-curve $\mathscr{R}_{ss}$ is unknown. Therefore, using the method presented in Sect. 1.3.1, it is easy to compute $\mathscr{R}_{ss}$ based on that of the 0° ply $\mathscr{R}^0_{ss}$ by replacing $\mathscr{G}_{Ic}$, $\mathscr{G}^{(i)}_{Ic}$ and $\mathscr{G}^0_{Ic}$ by $\mathscr{R}_{ss}$, $\mathscr{R}^{(i)}_{ss}$ and $\mathscr{R}^0_{ss}$, respectively. It was demonstrated in [16] that the use of the $\mathscr{R}$-curve has beneficial impacts on the prediction of the size effect. In-depth analysis of the $\mathscr{R}$-curve can be found in Sect. 2.1.2.

1.4 Notched coupon strength

In this section, the method to compute the open-hole tensile strength of composite laminates is presented. The considered geometry as well as loading are depicted in Fig. 1.3. The laminate has a central circular hole of radius R and its width is W. It is loaded in the longitudinal direction.

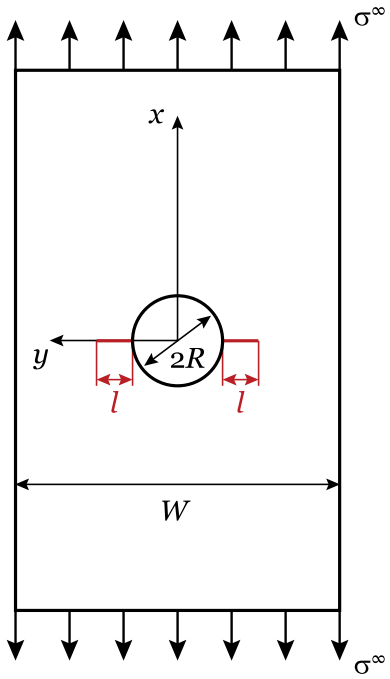

Figure 1.3: Notched plate with central circular hole, adapted from [4].

Assuming that only fiber failure occurs (either brittle fiber failure or pull-out), the crack will propagate in the y direction. Under these circumstances, it is possible to derive a coupled stress-energy criterion to predict failure of the open-hole laminate. The coupled stress-energy criterion is necessary in the sense that taken alone, neither the stress nor the energy criterion provide sound results.

Indeed, for crack-free bodies, the stress criterion stating that failure occurs if the stress reaches the ultimate stress works well. However, in the presence of large cracks, the stress criterion is useless since the stress field is singular near crack tip, leading to a zero failure load. In such cases, an energy criterion involving the fracture toughness can be used and provides sound results. Nevertheless, for crack-free bodies, the energy criterion also fails since the stress-intensity factor is zero. These criteria thus work for edge cases (crack-free bodies or large cracks). Cornetti et al. [17] proposed to introduce a characteristic material length l linking both criteria for handling intermediate cases, and considered a centered crack in an infinite plate under mode I loading. Their model can easily be transposed to an open-hole plate under same loading conditions [18].

1.4.1 Average Stress Criterion

The stress-based criterion states that failure occurs if the average stress along a segment of length l_S ahead of crack tip reaches the maximum allowable stress σ_u [19, 20]:

$$\int_R^{R+l_s} \sigma_{xx}(0,y)\mathrm{d}y = \sigma_u l_S. \tag{1.7}$$

The characterisitc length l_S is generally computed from experimental data, and must be calibrated for each lay-up [16]. It is noted that the expression of $\sigma_{xx}(0,y)$ can be adapted for either centered crack or open-hole plate.

1.4.2 Energy Criterion

Regarding the energy criterion, failure occurs only if the energy available for a l_E crack growth reaches $\mathcal{G}_{Ic}\ l_E$ [17]:

$$\int_R^{R+l_E} \mathcal{G}_I(a)\ \mathrm{d}a = \mathcal{G}_{Ic} l_E. \tag{1.8}$$

The reason why Eq. (1.8) should be used is well illustrated in [21]. The authors considered an infinite plate in tension, with a centered crack of length $2r$ perpendicular to the remote far stress field σ. From LEFM, one has $\mathcal{K}_I(r) = \sigma\sqrt{\pi r}$ and the crack propagates if $\mathcal{K}_I(r) = \mathcal{K}_{Ic}$, i.e. for $\sigma = \mathcal{K}_{Ic}/\sqrt{\pi r}$. With Eq. (1.8), the crack propagates for $\sigma = \mathcal{K}_{Ic}/\sqrt{\pi(r+l/2)}$. Indeed, using Eq. (1.5) and injecting $\mathcal{K}_I(r) = \sigma\sqrt{\pi r}$ in Eq. (1.8), one has:

$$\begin{aligned}
&\frac{1}{l_E}\int_r^{r+l_E} \mathcal{K}_I^2(a)\ \mathrm{d}a = \mathcal{K}_{Ic}^2 \\
\Leftrightarrow &\pi\sigma^2\,(l_E/2+r) = \mathcal{K}_{Ic}^2 \\
\Rightarrow &\sigma = \frac{\mathcal{K}_{Ic}}{\sqrt{\pi\,(l_E/2+r)}}.
\end{aligned}$$

The main advantage of Eq. (1.8) over the classical LEFM criterion $\mathcal{K}_I = \mathcal{K}_{Ic}$ is that for large cracks ($l_E/r \to 0$), both criteria converge to the same strength but in the small crack length limit ($l_E/r \to \infty$), Eq. (1.8) will predict a finite strength whereas the classical energy criterion $\mathcal{K}_I = \mathcal{K}_{Ic}$ diverges.

1.4.3 Coupled Stress-Energy criterion

Previous criteria have a physical meaning: crack growth happens by steps, in a *discontinuous* manner, hence the name Finite Fracture Mechanics [17]. However, as they are presented hereinabove, the fulfillment of one criteria does not imply the fulfillment of the other one. For instance, there is no reason for the energy released during crack growth to be equal to $\mathscr{G}_{Ic} l_S$ when the average stress criterion predicts crack growth. Cornetti et al. [17] proposed to weaken the hypothesis that l_S and l_E are material constants. The crack extension at failure l is now the result of the fulfillment of both criteria *at the same time*:

$$\begin{cases} \dfrac{1}{l}\displaystyle\int_R^{R+l} \sigma_{xx}(0,y)\,\mathrm{d}y = X_L, & \text{(1.9a)} \\ \dfrac{1}{l}\displaystyle\int_R^{R+l} \mathscr{G}_I(a)\,\mathrm{d}a = \mathscr{G}_{Ic}. & \text{(1.9b)} \end{cases}$$

Eq. (1.9) is thus a system of equation wherein σ_∞ and l are unknown. Cornetti et al. [17] presented Eq. (1.9) as a *necessary and sufficient* condition for crack propagation, whereas Eq. (1.7) and Eq. (1.8) are only *necessary* conditions for the crack to propagate.

If the material is better described with the help of a $\mathscr{R}$, Eq. (1.9) takes the following form:

$$\begin{cases} \dfrac{1}{l}\displaystyle\int_R^{R+l} \sigma_{xx}(0,y)\,\mathrm{d}y = X_L, & \text{(1.10a)} \\ \displaystyle\int_R^{R+l} \mathscr{G}_I(a)\,\mathrm{d}a = \int_0^{l} \mathscr{R}(\Delta a)\,\mathrm{d}\Delta a, & \text{(1.10b)} \end{cases}$$

where the $\mathscr{R}$-curve can be described as in Catalanotti et al. [15]:

$$\mathscr{R}(\Delta a) = \begin{cases} \mathscr{R}_{ss}\left[1-(1-\zeta\Delta a)^{\eta}\right] & ,\Delta a \le l_{\text{fpz}} \\ \mathscr{R}_{ss} & ,\Delta a > l_{\text{fpz}} \end{cases} \tag{1.11}$$

with l_{fpz} the length of the fracture process zone, and ζ and η some fitting parameters.

1.4.4 Finite Fracture Mechanics Model for open-hole laminated finite plates

Eq. (1.9) is a very general system of equations. It can basically be applied to any type of geometry, as far as the stress field and SIF can be expressed with analytical formulas or by numerical means. In the following, Eq. (1.9) is adapted to the particular case of open-hole laminated finite plates, such as the one depicted in Fig. 1.3.

1.4.4.1 Stress field

The stress field along the ligament, $\sigma_{xx}(0,y)$, appearing in Eq. (1.9a), is expressed as [22, 23]:

$$\begin{aligned}\sigma_{xx}(0,y) &= \frac{K_T^\infty}{K_T}\frac{\sigma_\infty}{2}\beta(y),\ y>R,\\ \beta(y) &= \left\{2+\left(\frac{R}{y}\right)^2+3\left(\frac{R}{y}\right)^3-\left(K_T^\infty-3\right)\left[5\left(\frac{R}{y}\right)^6-7\left(\frac{R}{y}\right)^8\right]\right\},\end{aligned} \tag{1.12}$$

where K_T^∞ is the stress concentration factor[6] at the edge of the hole of an infinite plate [22]:

$$K_T^\infty = 1+\sqrt{2\left(\sqrt{\frac{E_x}{E_y}}-\nu_{xy}\right)+\frac{E_x}{G_{xy}}} \tag{1.13}$$

and the ratio K_T/K_T^∞ takes into account the finite width of the open-hole laminate and is expressed as [22]:

$$\frac{K_T^\infty}{K_T} = \frac{3\left(1-2R/W\right)}{2+\left(1-2R/W\right)^3}+\frac{1}{2}\left(\frac{2R}{W}M\right)^6\left(K_T^\infty-3\right)\left[1-\left(\frac{2R}{W}M\right)^2\right]. \tag{1.14}$$

In Eq. (1.14), the parameter M has the following expression:

$$M^2 = \frac{\sqrt{1-8\left[\dfrac{3\left(1-2R/W\right)}{2+\left(1-2R/W\right)^3}-1\right]}-1}{2\left(2R/W\right)^2} \tag{1.15}$$

It is to be noted that the above framework is valid only for $2R/W<0.6$ [22]. If the latter is not fulfilled, the stress field in the criterion Eq. (1.9) must be evaluated with finite elements.

1.4.4.2 Stress Intensity Factor

It remains to define the Stress Intensity Factor appearing in Eq. (1.9b). The SIF of a finite open-hole isotropic plate, with identical cracks on both sides emanating from the hole edge, $\mathcal{K}_I$ is expressed as follows [24]:

$$\mathcal{K}_I(a) = \sigma_\infty \chi F_h F_w \sqrt{\pi a}, \tag{1.16}$$

with:

$$\begin{aligned}\lambda &= \frac{R}{a},\\ F_h(\lambda) &= \sqrt{1-\lambda}f_n,\\ F_w(a) &= \sqrt{\sec\left(\frac{\pi R}{W}\right)\sec\left(\frac{\pi a}{W}\right)},\\ f_n(\lambda) &= 1+0.358\lambda+1.425\lambda^2-1.578\lambda^3+2.156\lambda^4.\end{aligned}$$

[6] Not to be confused with a stress intensity factor.

1.4.5 Implementation

In this section, the system Eq. (1.9) incorporating the stress field Eq. (1.12) and the Stress Intensity Factor Eq. (1.16) is solved for both l and σ_∞.

Eq. (1.9b) can be rewritten thanks to Eq. (1.5):

$$\frac{1}{l}\int_R^{R+l} \frac{\mathcal{K}_I{}^2(a)}{\acute{E}}\mathrm{d}a = \mathcal{G}_{Ic} = \frac{\mathcal{K}_{Ic}{}^2}{\acute{E}}, \tag{1.17}$$

where $\acute{E}$ is given by:

$$\acute{E} = \left(\frac{1+\rho}{2E_xE_y}\right)^{-1/2}\left(\frac{E_y}{E_x}\right)^{-1/4}.$$

Introducing Eq. (1.16) in Eq. (1.17) leads to:

$$\frac{1}{l}\sigma_\infty{}^2\pi\chi^2\int_R^{R+l}(F_hF_w)^2\,a\,\mathrm{d}a = \mathcal{K}_{Ic}{}^2. \tag{1.18}$$

Using Eq. (1.12), Eq. (1.9a) can be rewritten:

$$\frac{1}{l}\frac{K_T^\infty}{K_T}\frac{\sigma_\infty}{2}\int_R^{R+l}\beta(y)\,\mathrm{d}y = X_L. \tag{1.19}$$

From Eq. (1.19), one has:

$$\sigma_\infty = 2lX_L\frac{K_T^\infty}{K_T}\left(\int_R^{R+l}\beta(y)\,\mathrm{d}y\right)^{-1} \tag{1.20}$$

Inserting Eq. (1.20) raised to the square in Eq. (1.18), one obtains easily

$$\mathcal{K}_{Ic}{}^2 = 4l\pi\chi^2X_L{}^2\frac{K_T^{\infty 2}}{K_T{}^2}\left(\int_R^{R+l}\beta(y)\,\mathrm{d}y\right)^{-2}\int_R^{R+l}(F_hF_w)^2\,a\,\mathrm{d}a. \tag{1.21}$$

Eq. (1.21) can be solved for l. Eventually, using Eq. (1.20), σ_∞ can be obtained.

The whole method has been implemented in C++. In the long term, if the method is proven sufficiently accurate, it might be included in Digimat[7]. For this reason, parts of the code such as tensor manipulation and input file reading have not been implemented from scratch but rather reused from existing libraries in Digimat. However, integration and root finding, necessary for solving Eq. (1.21), were implemented from scratch. For root finding, Brent's method was used [25]. For integration, a Lobatto quadrature was chosen [26].

The different building blocks presented hereinabove are summurized in a flowchart, see Fig. 1.4.

[7] https://www.mscsoftware.com/fr/product/digimat

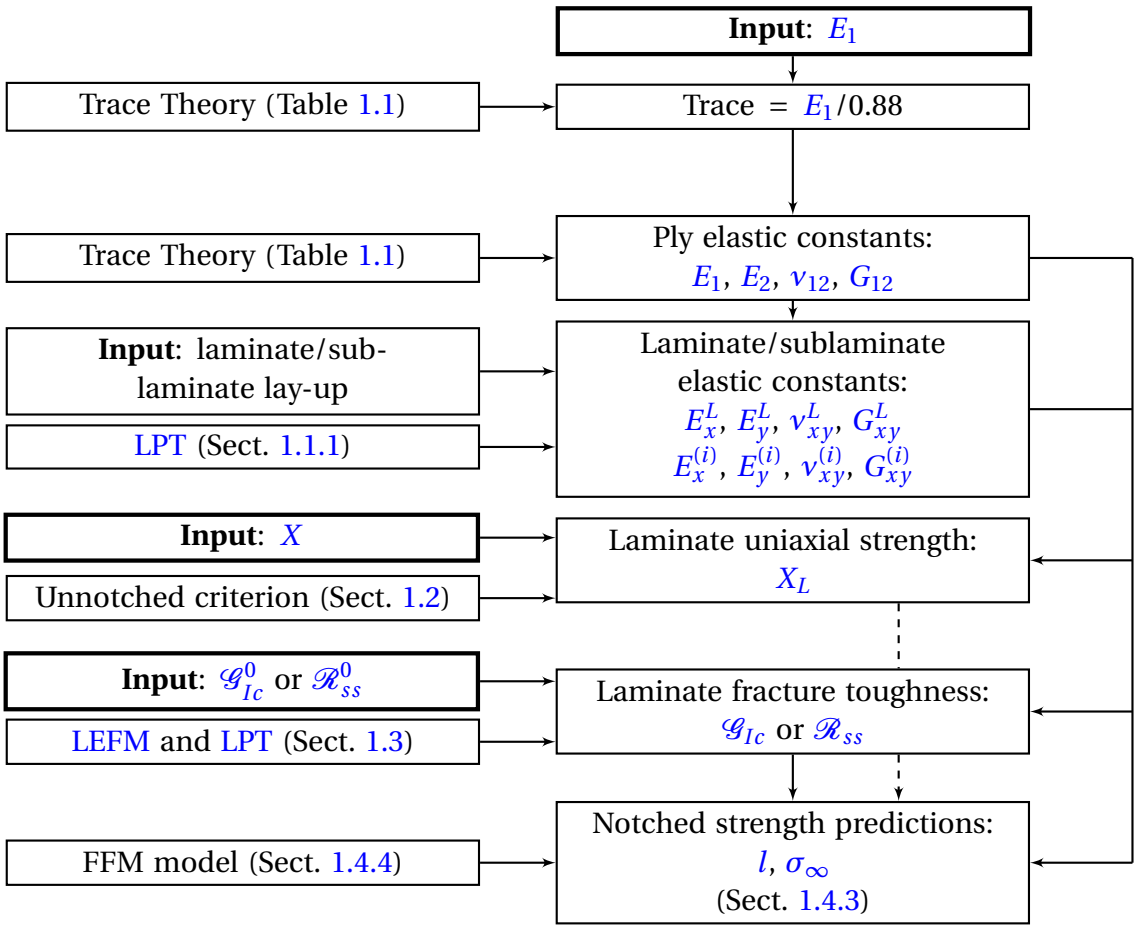

Figure 1.4: Workflow representing the steps followed by the semi-analytical framework, adapted from [4].

1.5 Validation of the framework

In this section, the results of Furtado et al. [4] are compared to the results of the present implementation, with and without the correction of Eq. (1.4), for validation purposes. For the sake of completeness, material properties reported in [4] are also reported in Chap. B.

Fig. 1.5 and Fig. 1.6 show a comparison of the predictions of Furtado et al. [4][8], labeled χ_{old}, with the results obtained after the correction of Eq. (1.4), labeled χ_{corr} and the experimental values of the notched strength of IM7/8552. Other results are available in Fig. 1.7f.

As seen in Fig. 1.5, the framework is capable of predicting not only one open-hole tensile strength but also the size-effect induced by the hole diameter. However, the framework seems less predictive for compressive open-hole strengths. For instance, the method underpredicts by more than 20% the open-hole compressive strength of the IM7/8552 (see Fig. 1.6a), which, according to [4], is due to a too low compressive longitudinal strength (see Table B.2). Indeed, other works reported a much higher ply compressive strength (e.g. [29], [31]). Using the compressive longitudinal strength reported in [29],

[8] It is to be noted that these results were also reproduced by the present C++ code, thereby validating the implementation of the framework as presented in [4].

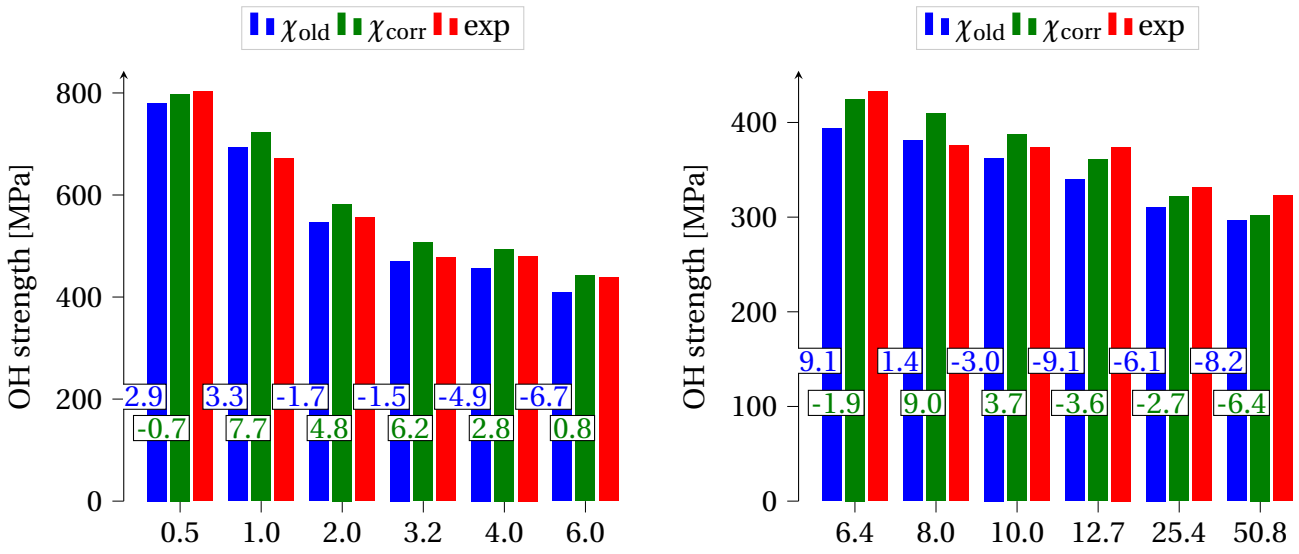

Figure 1.5: Comparison between predicted tensile open-hole strength and experimental results [27, 28] for quasi-isotropic IM7/8552 laminate. The x-axis is the hole diameter [mm]. Hole diameter-to-width ratios $2R/W$ are 0.031 for $2R = 0.5$, 0.062 for $2R = 1$, 1/6 for $2R \in \{2,4,6,8,10\}$ and 0.2 otherwise. The lay-up is $[90/0/-45/45]_{3S}$ for ratios of 1/6, and $[90/0/-45/45]_{4S}$ otherwise. χ_{corr}: results obtained after correction of Eq. (1.4). Material data from Tables B.1 and B.2.

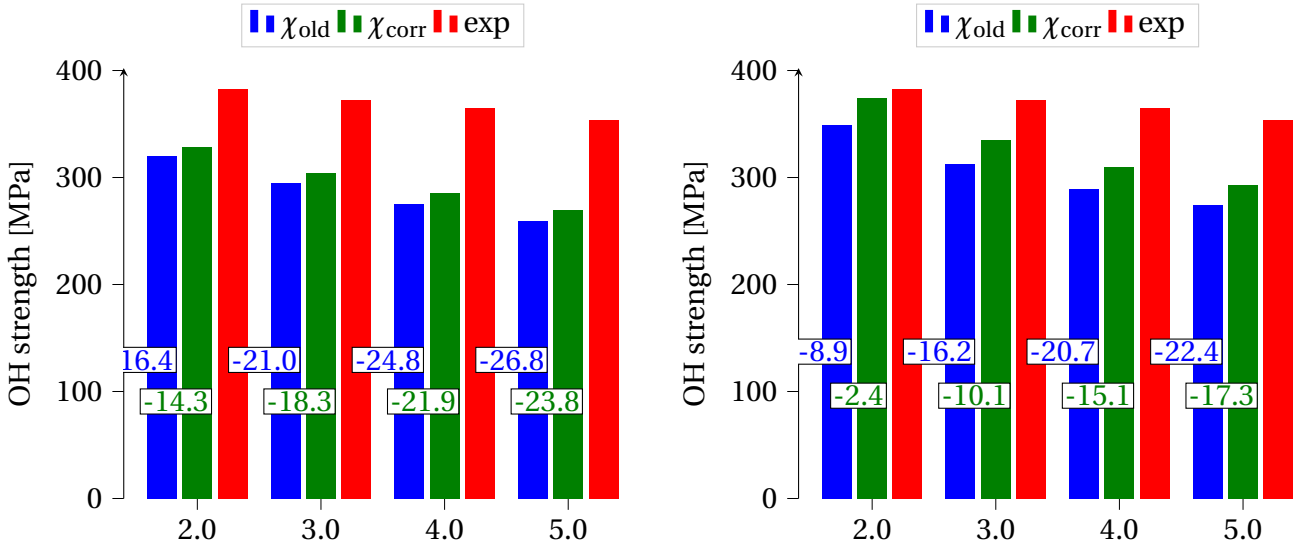

(a) IM7/8552, ply strength from [4].

(b) IM7/8552, ply strength from [29].

Figure 1.6: Comparison between predicted compressive open-hole strength and experimental results [30] for quasi-isotropic $[90/0/-45/45]_{3S}$ IM7/8552 laminate. The x-axis is the hole diameter [mm]. The hole diameter-to-width is $2R/W = 1/6$. χ_{old}: results from Furtado et al. [4]. χ_{corr}: results obtained after correction of Eq. (1.4). Material data from Tables B.1 and B.2.

the predicted unnotched strength of the laminate is enhanced[9], resulting in better predictions of the notched strength, at least for small hole diameters, see Fig. 1.6b.

[9]Indeed, the unnotched strength predicted with the max-strain criterion is changed from 458.3 to 645.6 MPa, which is much closer to 600.2 MPa, reported in [31].

The method performs very well on M40JB/ThinPreg 80EP/CF, with all predicted strengths within a 3% error range, see Fig. 1.7d. The important point is to notice that all the strengths are obtained using only the longitudinal Young's modulus, the strength (either tensile or compressive) and the $\mathscr{R}$-curve of the 0° ply. Furtado et al. [4] also showed that using the complete elastic characterization of the ply can help improving the results by a few percent.

It remains to analyse the influence of the correction of Eq. (1.6). From Fig. 1.5 to 1.7, it is clear that the corrected framework predicts open-hole strengths that are a few percent higher. Indeed, the computed critical energy release rate (or $\mathscr{R}_{ss}$) of the laminate Eq. (1.6) is now larger, because the ratio $\chi^{(i)}/\chi^0$ has increased.

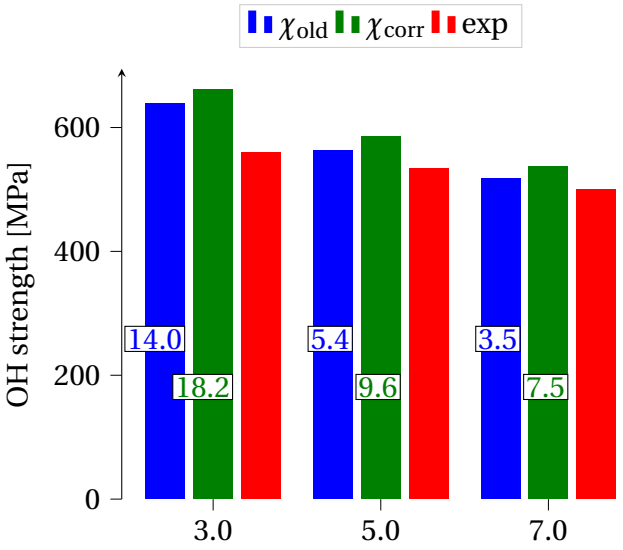

(a) Quasi-isotropic $[90/45/0/-45]_{3S}$ tensile strength of T800/M21, experimental strength from [32], $2R/W = 1/4$.

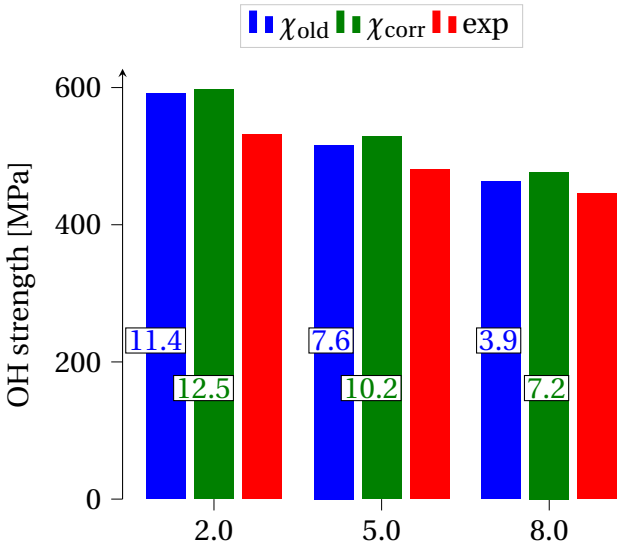

(b) Quasi-isotropic $[90/45/0/-45]_{3S}$ tensile strength of T700/M21, experimental strength from [33], $2R/W = 1/6$.

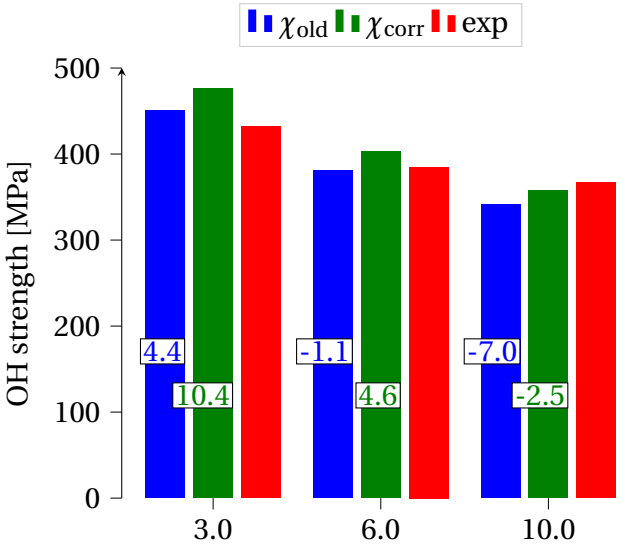

(c) Quasi-isotropic $[0/-45/90/45]_{6T}$ tensile strength of T700/AR2527, experimental strength from [34], $2R/W = 1/4$.

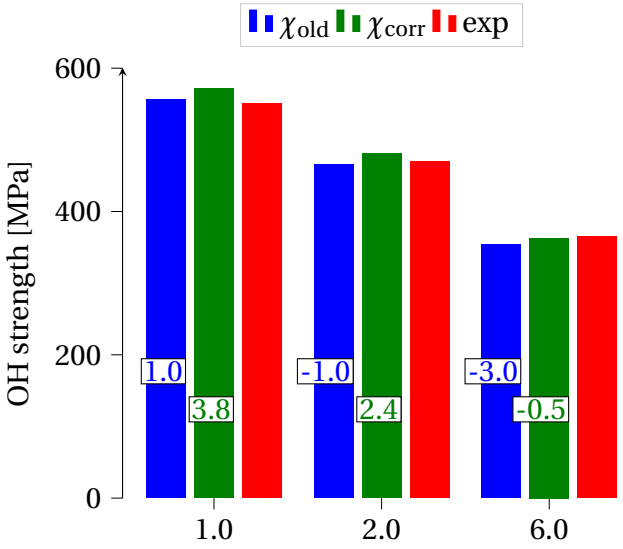

(d) Quasi-isotropic $[45/90/-45/0]_{10S}$ tensile strength of M40JB/ThinPreg 80EP/CF, experimental strength from [33], $2R/W = 1/6$.

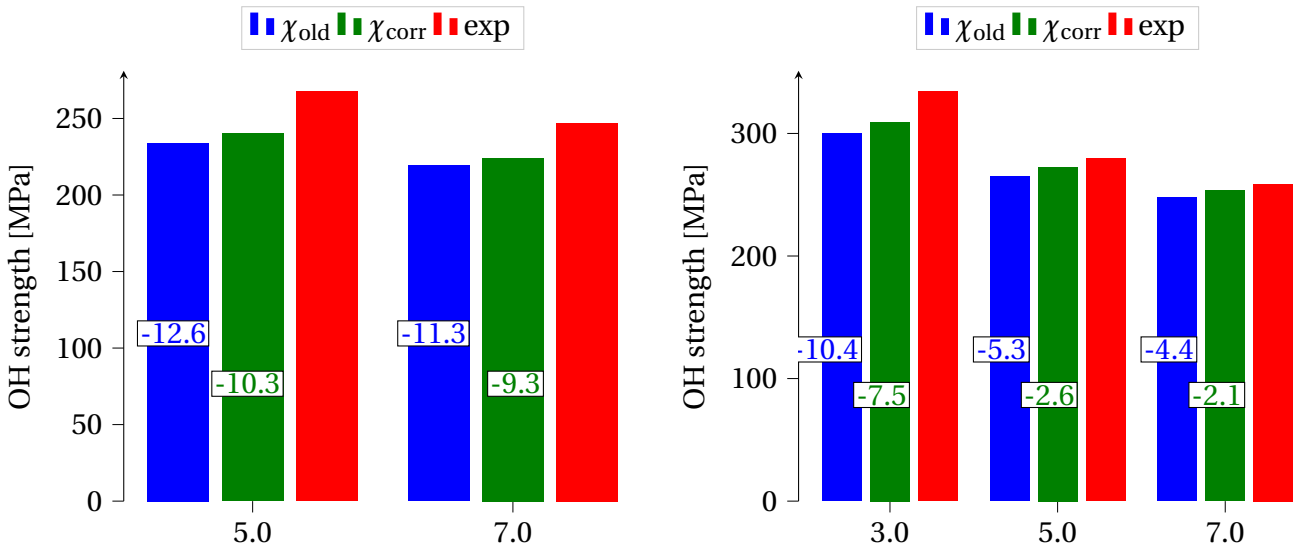

(e) Quasi-isotropic $[0/-45/90/45]_{6T}$ compressive strength of T700/AR2527, experimental strength from [34], $2R/W = 1/4$.

(f) Quasi-isotropic $[90/45/0/-45]_{3S}$ compressive strength of T800/M21, experimental strength from [32], $2R/W = 1/4$.

Figure 1.7: Comparison between non-corrected and corrected framework. χ_{old}: results from Furtado et al. [4]. χ_{corr}: results obtained after correction of Eq. (1.4). Material data from Tables B.1 and B.2.

1.6 On the size effects

It must be noted that as the width-to-hole ratio is kept constant, the stress field of larger specimens is an image of the one in smaller specimens, thus making the sole stress analysis for predicting open-hole strength impractical, except if one introduces empirical characteristic lengths in the model. This is what is done in the point stress and average stress criterions [19]. It is thus required to introduce the notions of energy and damage.

That being said, there are two trends in open-hole size effects. The first one is concerned with thin ply laminates, mainly governed by fiber failure (either pull-out or fiber breaking) and exhibiting a decreasing strength as the hole size is increased. This is the trend the present framework is concerned with. The second trend is linked to thick ply-block laminates[10], whose strength increases with increasing hole diameter [35]. This *inverse* hole size effect is also noticed for thick ply laminates.

It seems that for thin laminates, the open-hole size effect is caused by the development and propagation of non-critical ply-level damage mechanisms, i.e. not causing failure of the coupon, that differ from one hole size to another [36]. This ply-level damage might be regarded as a fracture process zone. For a twice larger specimen, the energy available for crack growth is also two times larger, explaining why the larger coupons fail earlier.

For thicker ply laminates, it seems that failure is mainly governed by delamination or matrix-dominated

[10]Thick ply-block laminate refers here to a laminate with the same orientations as a thin laminate and same overall thickness, but with ply bunching, i.e. several plies of identical orientation are put together.

failure mode [35] [37]. If the hole size gets higher, the ligament width[11] increases as well. Therefore, it requires more energy to propagate delamination through the coupon width, thereby increasing the open-hole strength. The strength prediction of laminate exhibiting matrix-dominated failure modes or delamination can not be considered in an analytical way and should be tackled with non-linear finite element analysis [37].

1.7 Perspectives of improvement

From the discussion made hereinabove, meaningful comments can be provided, especially regarding the already identified weaknesses as well as the possible improvements.

First of all, as already mentioned, the framework is not applicable for cases in which delamination or any other non-fibre-dominated damage mechanisms are involved. Moreover, the method only considers self-similar cracks that are growing perpendicularly to the remote applied stress. Any configuration leading to angled failure must be handled carefully, as will be discussed later on.

Regarding the different parts of the methods, each of them is built upon simplifying assumptions and approximations, thus making room for improvements. Possible ways to enrich the current framework can be investigated, requiring either more material data or more computationally intensive computations.

Lay-up A very important point is that the framework is not sensitive to the number of repetitions of the lay-up, ply ordering, ply bunching or ply thickness. For instance, LPT predicts the same laminate properties whether the lay-up is a $[0/90/-45/45]_{3S}$ or a $[90/0/45/-45]_{10S}$. The method can predict different strengths if the ply thicknesses are not uniform across the laminate, see Eq. (1.6) for instance[12]. However, as can be easily deduced from Eq. (1.6), if the ply thickness is uniform across the laminate, a change in ply thickness does not change the strength prediction. In short, if all plies have the same thickness, the method is only sensitive to the relative proportion of ply orientations. Last but not least, the method does not make use of the *in situ* strength of the plies. Indeed, the strength of a given ply might depend on its thickness, as well as of its position within the laminate [38], e.g. inner or outer plies.

Stress distribution The stress field along the ligament Eq. (1.12) is an approximate solution. Firstly, it is based on [23], in which an approximate solution is built for an infinite orthotropic plate with a central circular hole. On top of this approximate, a correction must be brought to account for finiteness of the plate. Carrying out an in-depth verification of the validity and accuracy of Eq. (1.12) would be therefore very interesting, especially when $2R/W$ tends to the validity limit stated as being 0.6. However, such an investigation requires extensive use of finite element simulations and is out of the scope of this report.

[11] The ligament refers to the uncracked material between crack tip and free edges of the coupon.

[12] Even if it is possible to predict some $\mathcal{G}_{Ic}$ that is sensitive to non-uniform ply thickness, there is still no evidence that it would provide sound results.

Another concern related to the stress field Eq. (1.12) is that it does not account for any plastic deformation near crack tip, that would limit the stress field. However, since no experimental evidence is available to ascertain that non-negligible plastic deformations occur, this concern can be dropped for the moment.

Stress Intensity Factor Similarly to the stress field, the stress intensity factor is also an approximate solution, built at the very beginning for isotropic materials. In order to stress the validity of having an orthotropic plate in plane stress with the laminate elastic properties describing the whole laminate fracture toughness, an extensive study should be conducted to determine its accuracy compared to a three-dimensional lay-up. As for the stress field, such a study is out of scope.

$\mathscr{R}$-curve of the laminate The method to compute the $\mathscr{R}$-curve of the laminate from that of the 0° ply is also questionable. Indeed, it neglects any interaction between the plies (i.e. inter-laminar fracture toughness), and requires the crack to growth in a similar fashion in each ply, without being deviated from its initial direction, i.e. normal to the loading direction. This is a very limiting hypothesis as even angled failure modes are rejected. Moreover, even if the use of a $\mathscr{R}$-curve seems more physical, measuring it is still a challenge, adds non-negligible costs to a test campaign, and no standardized measuring method has been released at the moment.

Unnotched strength Recalling Sect. 1.5, in which a wrongly evaluated longitudinal strength lead to worsened predictions, it seems that the predicted unnotched strength has a large impact on the method, and could have been foreseen since Eq. (1.9a). Whereas for the stress field and stress intensity factor, it seemed difficult to change the formulation of the framework without bringing additional computational costs and complexity, the unnotched strength of composite laminates can be easily evaluated with very simple criteria, requiring very few computational resources. Among them are the unit circle, the Tsai-Wu criterion, the Hashin criterion, and many others. However, these criteria require in general more than the sole longitudinal strength of the ply.

It should also be noted that the unnotched strength depends on the stacking sequence (ply ordering), ply thickness and plate dimensions. Those parameters are not dealt with in the present framework and will not be dealt with if simple unnotched criteria as mentioned above are used.

1.8 Conclusion

Using only three ply properties, namely the longitudinal Young modulus, the longitudinal strength and the $\mathscr{R}$-curve of the 0° ply of a given CFRP, it is possible to predict, within an acceptable range of accuracy for preliminary design, the strength of balanced open-hole coupons. The size effect is well predicted by the method, especially for tensile strength. However, the framework has a tendency to underestimate the compressive strength. This might be an indication that other phenomena, not described by the present method, take part in the failure process. The method also exhibits non-negligible sensitivity to the predicted unnotched strength, which shall be investigated further thereafter.

2 On the need for calibration

In this chapter, a method that can be used when no data is available for the $\mathscr{R}$-curve or $\mathscr{G}_{Ic}$ is presented. This method was developed to assess the capabilities of the present framework on the NIAR dataset, which lacks information about the $\mathscr{R}$-curve or $\mathscr{G}_{Ic}$. At the end of this chapter, preference shall be given to either the $\mathscr{R}$-curve or $\mathscr{G}_{Ic}$ for futur use. Moreover, a sensitivity analysis will be conducted to determine on which lay-up it is preferable to calibrate the energy part of the coupled stress-energy criterion.

2.1 Method

In the NIAR dataset, there are generally two tables per material system, listing the lamina elastic properties and strengths and the laminate strengths for 3 lay-ups: a quasi-isotropic lay-up, a hard lay-up and a soft lay-up[1]. The laminate strengths are given for both unnotched and open-hole laminates, in several environmental conditions, namely CTD, RTD, ETW and ETW2.

2.1.1 Critical Energy Release Rate

In the following, one of the three laminate open-hole strengths (quasi-isotropic, hard or soft) is used to calibrate a critical energy release rate $\mathscr{G}_{Ic}$. Therefore, once the calibration is done, the calibrated $\mathscr{G}_{Ic}$ can be used to assess the framework on the two remaining experimental points.

The first step of the method consists in evaluating the unnotched strength of the lay-up chosen for calibration, X_L, as previously.

The second step is to use Eq. (1.9a), in which both X_L and σ_∞ are known:

$$\frac{1}{l}\int_R^{R+l} \sigma_{xx}(0,y)\,\mathrm{d}y = X_L, \tag{2.1}$$

[1] A hard lay-up has a majority of 0° plies, whereas a soft lay-up has more 45° plies.

from which l can be extracted numerically.

The third step consists in using Eq. (1.9b). The left-hand side being completely characterized once l is known, it remains to integrate it to deduce $\mathscr{G}_{Ic}$:

$$\mathscr{G}_{Ic} = \frac{1}{l}\int_{R}^{R+l} \mathscr{G}_I(a)\,\mathrm{d}a. \tag{2.2}$$

Once $\mathscr{G}_{Ic}$ has been obtained, which is related to the whole laminate, the last step is concerned with the back-calculation of $\mathscr{G}^0_{Ic}$, see Sect. 1.3.

2.1.2 Mean $\mathscr{R}$-curve

In the previous section, calibration was performed on a critical energy release rate. Such a calibration is meaningful for brittle-like materials only. Indeed, considering Eq. (1.9), the crack grows instantaneously, *as a singular event* [16]. This can be a good approximation if the final crack length at failure is small, i.e. damage occurs just before ultimate failure. However, for laminates that fail with a large final crack length, the damage process can not be considered as a singular event and is rather a continuous process.

This growing crack length that lot of CFRP systems generally exhibit can be described with a $\mathscr{R}$-curve, also called *resistance curve*. The $\mathscr{R}$-curve is an appropriate mean to describe some load drops in a stress-strain curve of a coupon test, due to the crack growing by some finite steps. These steps are attributed to both the loading redistribution arising from micro-cracking, splitting and delamination at the local level and to fiber bridging, which is an extrinsic toughening mechanism as opposed to intrinsic ones such as development of a plastic zone ahead of crack tip which is typical of metals.

The $\mathscr{R}$-curve, which is associated with the intra-laminar energy release rate, can be experimentally characterized [15, 39]. However, this characterization can be costly and is generally not available since not included in usual test campaigns. Therefore, the following will address a methodology that can be used to calibrate a $\mathscr{R}$-curve based on one open-hole strength.

In order to keep the overall framework as much analytical as possible, the $\mathscr{R}$-curve can be characterized as in Eq. (1.11). It should be noted that the resistance curves generally found in the litterature do not start from zero. However, keeping up with the idea of a continuous fracture process starting at the very beginning of the loading, it makes sense to choose a representation of the $\mathscr{R}$-curve starting from zero. As a side note, the steady-state value of the $\mathscr{R}$-curve defined in Eq. (1.11) is interpreted as the energy release rate of the material for an infinite plate [16].

Keeping in mind that only one open-hole strength should be used to calibrate the $\mathscr{R}$-curve, some hypotheses must be made on the parameters l_{fpz}, ζ and η of Eq. (1.11). The choice that was made is to find an average $\mathscr{R}$-curve, based on the data presented in [4], and reported in Table B.3. The remaining parameter $\mathscr{R}^0_{ss}$ is calibrated based on the given open-hole strength.

The average $\mathscr{R}$-curve, alongside with the 4 $\mathscr{R}$-curves that are available in [4], are depicted in Fig. 2.1, normalized w.r.t. their steady-state value. The parameters of the average $\mathscr{R}$-curve are given in Table 2.1.

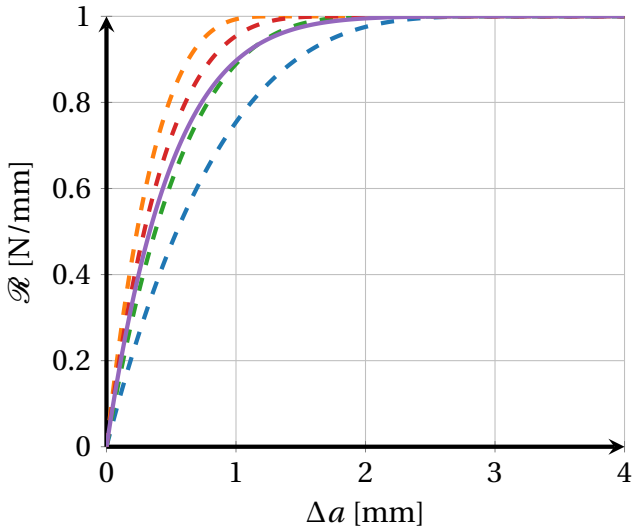

Figure 2.1: $\mathscr{R}$-curve for IM7/8552 in tension (– –), T800/M21 in tension (– –), T700/AR2527 in tension (– –), IM7/8552 in compression (– –) and average fitted $\mathscr{R}$-curve (——). The $\mathscr{R}$-curves' parameters are given in Table B.3.

l_{fpz} [mm]	ζ [mm^{-1}]	η [-]
$1/\zeta \approx 4.347$	0.23	8.69

Table 2.1: Parameters of the average $\mathscr{R}$-curve depicted in Fig. 2.1.

Regarding the calibration procedure, it is broadly similar to the one for $\mathscr{G}_{Ic}$. After having solved Eq. (2.1) for the final crack length l, it remains to solve Eq. (1.10b), which can be rearranged as:

$$\mathscr{R}_{ss} = \int_R^{R+l} \mathscr{G}_{Ic}(a)\,\mathrm{d}a \cdot \begin{cases} \left(l - \dfrac{1-[1-l\zeta]^{\eta+1}}{\zeta(1+\eta)} \right)^{-1} & , l \le l_{\text{fpz}} \\ \left(l_{\text{fpz}} - \dfrac{1-\left[1-l_{\text{fpz}}\zeta\right]^{\eta+1}}{\zeta(1+\eta)} + l - l_{\text{fpz}} \right)^{-1} & , l > l_{\text{fpz}} \end{cases} \tag{2.3}$$

Eventually, $\mathscr{R}^0_{ss}$ can be back-calculated as for $\mathscr{G}^0_{Ic}$, see Sect. 1.3.

2.2 Comparison of calibration and experimental characterization

In order to validate the proposed methodology that copes with the lack of information about the energetic part of the open-hole failure criterion, the latter should be applied on the results of [4] and compared in order to evaluate the loss of accuracy, as well as how close the calibrated values of $\mathscr{R}^0_{ss}$ or $\mathscr{G}^0_{Ic}$ are to the experimental ones. This comparison will be helpful to determine which one of the two calibration methods should be preferred. Moreover, the chosen calibration method will be evaluated on other datasets to evaluate how it generally behaves w.r.t. experimental open-hole strength.

To set the procedure up, a choice must be made regarding the diameter of the hole on which cali-

bration will be performed. Since in the NIAR dataset, the hole diameter is always 6.35 mm, the chosen hole diameter will always be the closest to 6.35 mm. For instance, in the results of Furtado et al. [4], the calibration for T800/M21 in compression will be made using the experimental notched strength for a hole of 7 mm. The calibrated values of $\mathscr{R}^0_{ss}$ and $\mathscr{G}^0_{Ic}$ are shown in Table 2.2.

Material system	Loading	Hole diameter [mm]	$\mathscr{R}^0_{ss}$ [N/mm]	$\mathscr{G}^0_{Ic}$ [N/mm]	$\mathscr{R}^{0,\text{calib.}}_{ss}$ [N/mm]	$\mathscr{G}^{0,\text{calib.}}_{Ic}$ [N/mm]
M40JB/ThinPreg80EP	OHT	6.0	-	47.7	87.2	48.9
T700/M21	OHT	5.0	-	391.0	287.9	250.7
IM7/8552	OHT	6.0	205.0	-	168.6	125.2
T700/AR2527	OHT	6.0	254.0	-	221.6	146.3
T800/M21	OHT	7.0	283.0	-	259.4	177.4
T700/AR2527	OHC	7.0	-	43.0	99.1	67.9
T800/M21	OHC	7.0	-	37.0	67.8	41.0
IM7/8552	OHC	5.0	61.0	-	240.7	228.2
IM7/8552-CCS	OHC	5.0	61.0	-	102.3	80.6

IM7/8552-CCS has the same properties as IM7/8552, except for the longitudinal compressive strength X^C which is taken from [29].

Table 2.2: Calibrated values of the steady-state $\mathscr{R}$-curve $\mathscr{R}^{0,\text{calib.}}_{ss}$ or critical energy release rate $\mathscr{G}^{0,\text{calib.}}_{Ic}$, for the results shown in [4]. The loading is either tensile (OHT) or compressive (OHC). The hole diameter chosen for calibration is also shown, as well as experimental values from [4].

As may be seen in Table 2.2, when $\mathscr{R}^0_{ss}$ is calibrated, it is generally close to the experimental value. However, the calibration does not render the exact experimental value for three obvious reasons. The first one is the inaccuracy of the framework. Indeed, it is not expected that the framework be perfect. The second one is the error made on the unnotched strength by the max-strain criterion, thereby influencing the calibration process. The last reason is due to the average $\mathscr{R}$-curve parameters, that are by definition averages. It can also be observed that, for the case of IM7/8552 in compression, the calibrated value is way above the experimental one; it is explained by the fact that because the predicted unnotched strength is by far under-estimated, the energetic criterion must compensate for that and the calibrated steady-state value of the $\mathscr{R}$-curve is thus far beyond the expected experimental value so that the given experimental open-hole strength can be reached. This conclusion is correlated by the result of IM7/8552-CCS in compression, for which the longitudinal compressive ply strength has been changed from 1200 MPa, reported in [4], to 1690 MPa, reported in [29]. The predicted unnotched strength is therefore higher and the calibrated steady-state value gets closer to the experimental one. Another explanation for the over-estimation would be that, referring to Fig. 1.6 or any result in compression, the method always under-predicts the strength. This might be due to a physical damage mechanism that occurs in compression and is not included in the framework. Therefore, when calibrating, the method artificially over-predicts the $\mathscr{R}$-curve steady-state value to match with the provided open-hole strength, see Fig. 2.4. However, there is a lack of evidence at the moment to validate such an explanation.

As can be seen in Fig. 2.3, the predictions from calibrated values (either $\mathscr{R}^0_{ss}$ or $\mathscr{G}^0_{Ic}$) are very close to the experimental open-hole strength. Furthermore, the framework performs equally, whether the input of the energetic criterion is from experimental data or calibration. It is very important to note at this point that the proposed calibration method is very interesting in the sense that it relaxes the costs of experimental campaigns: it requires only one open-strength instead of a $\mathscr{R}$-curve. All the results

from [4] were successfully reproduced using either calibration method, without noticeable loss of accuracy, except for IM7/8552 in compression that will be discussed in the next paragraphs. Therefore, since the calibration of the average $\mathscr{R}$-curve and $\mathscr{G}_{Ic}^0$ perform equally, the $\mathscr{R}$-curve will be chosen for later use. Indeed, the observed physical behaviour is characterized by a $\mathscr{R}$-curve. Moreover, $\mathscr{R}_{ss}^{0,\text{calib.}}$ is close to the experimental value, see Table 2.2. Last but not least, the use of a constant energy release rate should be avoided since it is more an artificial quantity than a physically sound variable. It must be noted that the calibrated steady-state value $\mathscr{R}_{ss}^0$ (or $\mathscr{G}_{Ic}^0$) can vary quite a lot depending on the hole size on which calibration is performed. An example is shown in Table C.1, where calibration of the tensile steady-state value was carried out for IM7/8552, for all the hole diameters reported in [4]. Quite remarkable is the tiny difference between the calibrated value on the 6 mm hole diameter (168.6 [N/mm], see Table 2.2) and the mean value of $\mathscr{R}_{ss}^{0,\text{calib.}}$ (174.32 [N/mm], see Table C.1). It does not seem to be a lucky break. Indeed, it is clear from Table C.1 that calibrating on hole sizes not too small neither too large give an acceptable narrow range of calibrated values, thus supporting the choice of calibrating on 6 mm holes (or the closest).

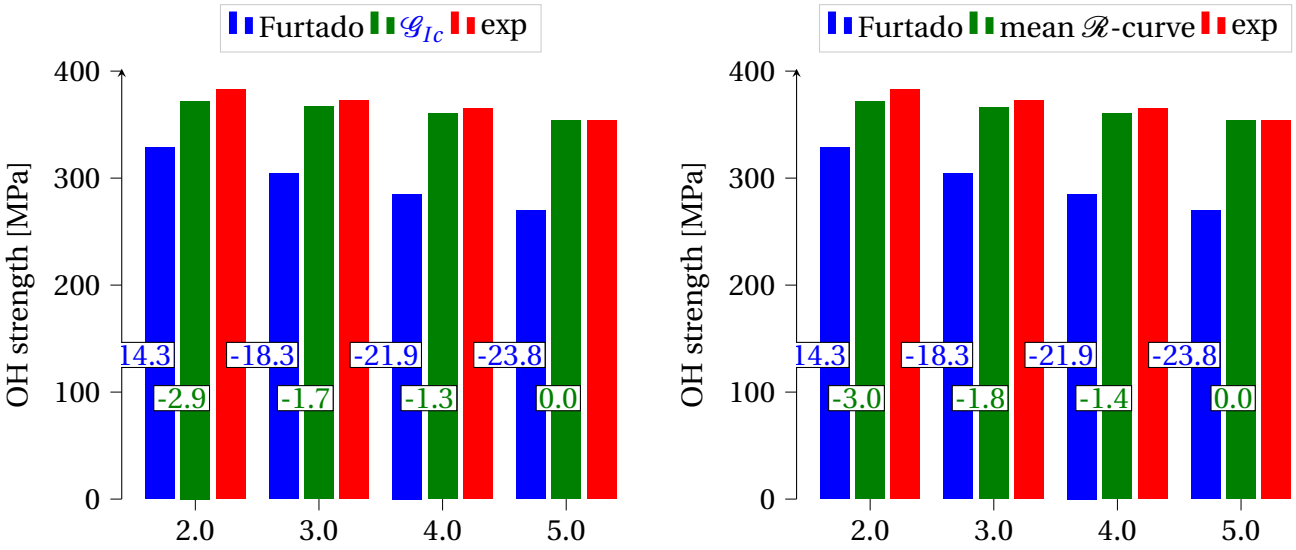

Figure 2.2: Comparison between predicted open-hole compressive strength and experimental values, when the energetic characterization of the IM7/8552 material system comes from calibration of either $\mathscr{G}_{Ic}^0$ or $\mathscr{R}_{ss}^0$ or from the experimental $\mathscr{R}$-curve reported in [4]. The x-axis is the hole diameter [mm]. Material data from Tables B.1 and B.2 and experimental strengths from [30]. The hole-to-width ratio is 1/6.

Contrary to what one may think, even if the calibration on IM7/8552-CCS seems to lead to better calibrated values of $\mathscr{R}_{ss}^{0,\text{calib.}}$ than calibration on IM7/8552, see Table 2.2, the predicted open-hole strength are very disappointing for IM7/8552-CCS in compression, see Fig. 2.4, and the next paragraphs are dedicated to an attempt of explanation of these poor results. A first remark on the predicted strengths shown in Fig. 2.4 is that results are equally poor, whatever the calibration method (i.e. energy release rate or $\mathscr{R}$-curve). Therefore, the explanation should be looked for elsewhere.

The first step in the understanding of Fig. 2.4, which shows predicted compressive strengths for the IM7/8552-CCS[2] is to look at Fig. 2.2, showing the compressive open-hole strengths for IM7/8552. Un-

[2]As a reminder, IM7/8552-CCS is the same material as the IM7/8552, except that the compressive longitudinal strength

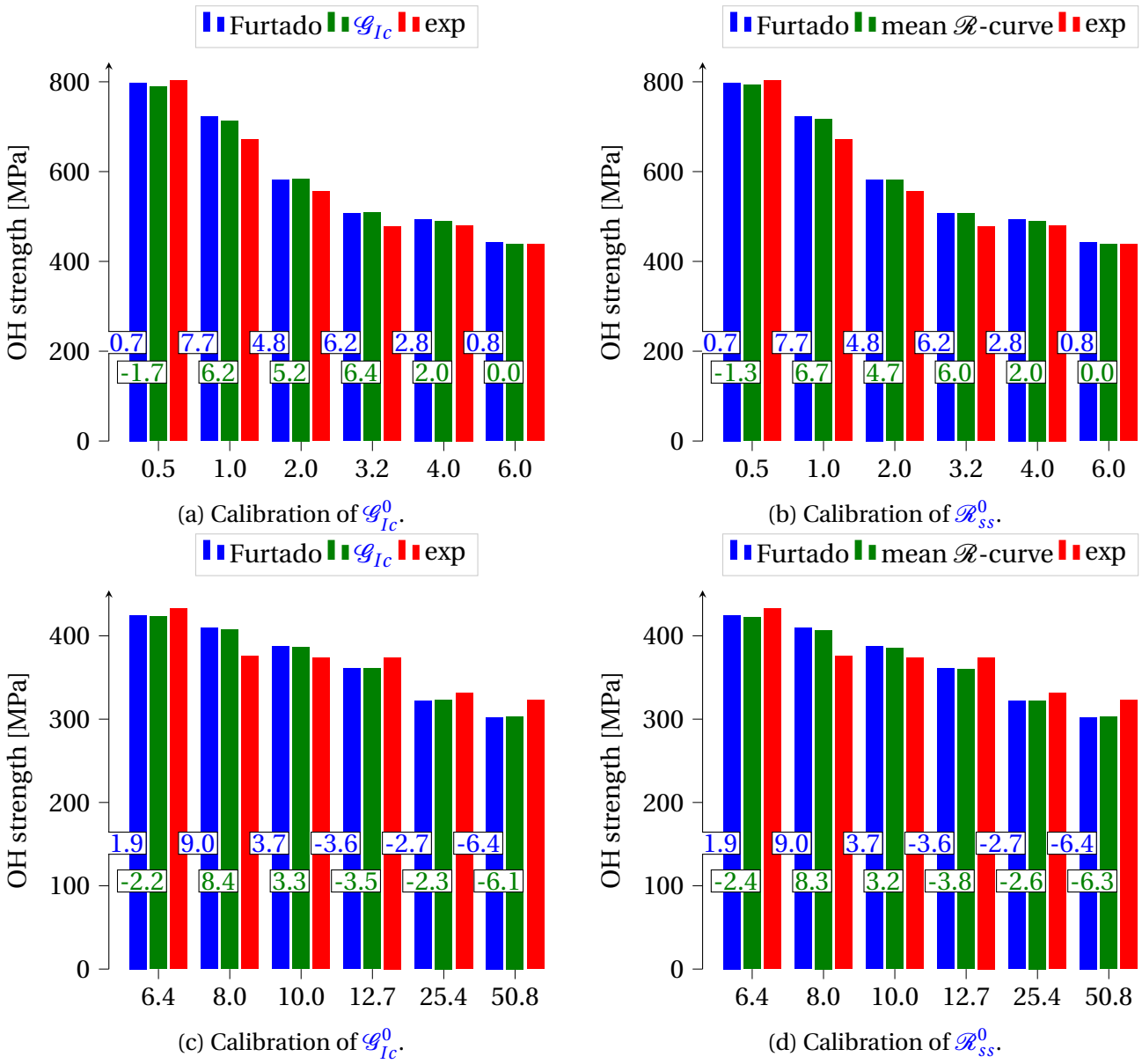

(a) Calibration of $\mathscr{G}^0_{Ic}$.

(b) Calibration of $\mathscr{R}^0_{ss}$.

(c) Calibration of $\mathscr{G}^0_{Ic}$.

(d) Calibration of $\mathscr{R}^0_{ss}$.

Figure 2.3: Comparison between predicted open-hole tensile strength and experimental values, when the energetic characterization of the IM7/8552 material system comes from calibration of either $\mathscr{G}^0_{Ic}$, $\mathscr{R}^0_{ss}$ or experimental $\mathscr{R}$-curve. They are labeled as $\mathscr{G}^0_{Ic}$, *mean $\mathscr{R}$-curve* and *Furtado*, respectively. The experimental strength is denoted *exp*. The x-axis is the hole diameter [mm]. Material data from Tables B.1 and B.2. Experimental strengths from [27, 28]. Calibration was performed on the coupon with a hole diameter of 6 mm.

expectedly, the predictions are very good with IM7/8552, even if its compressive longitudinal strength is now known as being too low. Referring to Table 2.2, the calibrated steady-state values of the $\mathscr{R}$-curve are 240.7 [N/mm] for IM7/8552 and 102.3 [N/mm] for IM7/8552-CCS, while the experimentally determined value is 61 [N/mm][3]. That major difference is due to the difference in longitudinal compressive

is from [29].

[3]The reader should keep in mind that the calibrated value is not expected to ever be equal to the experimental value, see above.

stress, as stated earlier, and is very relevant to grasp what is going on. Indeed, as shown in Fig. C.1, the larger the calibrated value, the smaller the sensitivity of the predictions to the hole diameter. This observation was also made in [18] and is the key for understanding why calibration on IM7/8552 works better than with IM7/8852-CCS.

In fact, looking at the experimental compressive open-hole strengths of IM7/8552, they are very insensitive to the hole diameter, going from 383 MPa to 353 MPa, for hole diameters of 2 mm and 5 mm, respectively. That is a -8.3% variation in notched strength for a 2.5 larger specimen. By comparison, compressive notched strength of T800/M21 decreases from 334.45 MPa to 258.82 MPa, for a hole diameter varying from 3 mm to 7 mm, a variation of -29.2% strength for 2.3 times larger specimen. The compressive strength of T700/AR2527 varies between 267.8 MPa and 247.1 MPa for holes of 5 mm and 7 mm, thus exhibiting a variation of -8.38% in strength for a 1.4 bigger specimen. The experimental notched strength of IM7/8552 will never be correctly predicted by the framework, if the experimental $\mathscr{R}$-curve is to be used, for the obvious reason that the experimental steady-state value of the $\mathscr{R}$-curve is so low that the framework will always predict a strong hole-size-dependency, which is not representative of the experimental strengths. However, taking IM7/8552 open-hole strengths from Hodge et al. [40], the framework still works very well, see Fig. C.2 (p. 84) for instance. These new strenghts are sufficiently hole size dependent for the method to provide good accuracy. It should be noted, though, that while the results from [4] are for constant hole-to-width ratio, the strengths from [40] are for constant plate width, and are thus by nature more size dependent.

The fact that the IM7/8552 compressive OH strengths can not be predicted with the experimental $\mathscr{R}$-curve raises the question whether the experimental strengths used in [4] for IM7/8552, coming from [30], are valid. Another explanation for the insensibility to hole diameter of the compressive open-hole strength of IM7/8552 reported in [30] could be based on the ply thickness of the tested laminates. Indeed, thicker plies exhibit a reversed trend: when the hole diameter is increased, the open-hole strength increases too [37] [35]. The hole size effect is therefore expected to be less and less significant as the ply thickness increases, which might explain the weak hole-size-dependency of the compressive strengths of IM7/8552 reported in [30]. However, the ply thickness of compressive open-hole coupons reported in [30] is 0.125 mm, which can be considered as a thin ply laminate. As a comparison, IM7/8552 tensile coupons were reported to have a nominal thickness of 0.131 mm [27]. The compressive strengths reported in [30] should therefore be further investigated in order to understand why they show such a small hole-size-dependency.

Only quasi-isotropic lay-ups have been considered so far. However, the method also quite remarkably apply for $[60/0/-60]_{3S}$ and $[30/60/90/-60/-30]_{2S}$ IM7/977-3 laminates from [41], at least in compression, see Fig. C.3 (p. 85). It is to be noted that in the case of [45/−45/0/90] and [60/0/−60] laminates, LPT predicts the same laminate elastic properties[4], and so the predicted unnotched strengths using the max-strain criterion are equal, even if it is not experimentally the case.

The hole size effect was also strikingly captured on 24 open-hole strengths of the AS4/3501-6 material system reported in [42], in tension and in compression, for both RTD and ETW conditions, see Fig. 2.5. It is important to note that, since the longitudinal Young modulus and strength of the 0° ply were not given in [42], they were back-calculated from the Young modulus and strength of a unnotched $[45/0/-45/90]_{2s}$ coupon, using the Trace theory and the max-strain criterion, for each environmental condition and loading.

[4]This observation can be experimentally validated, as in [41].

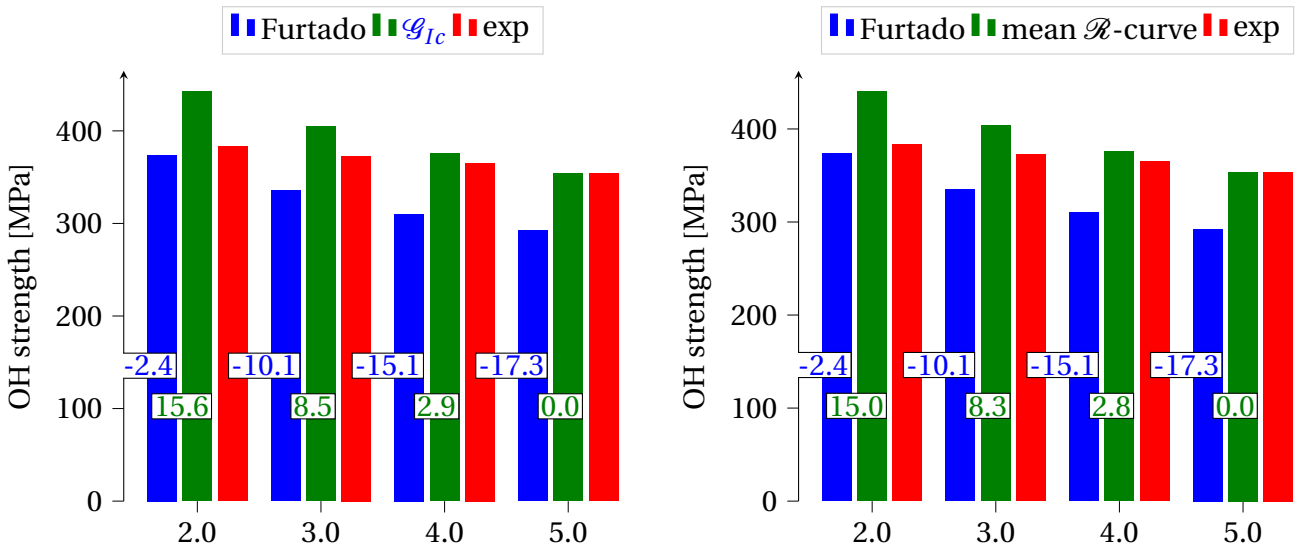

Figure 2.4: Comparison between predicted open-hole compressive strength and experimental values, when the energetic characterization of the IM7/8552-CCS material system comes from calibration of either $\mathscr{G}^0_{Ic}$ or $\mathscr{R}^0_{ss}$. Results from [4] (*Furtado*), from calibration (either $\mathscr{G}_{Ic}$ or $\mathscr{R}_{ss}$) and experimental values (*exp*) [30].

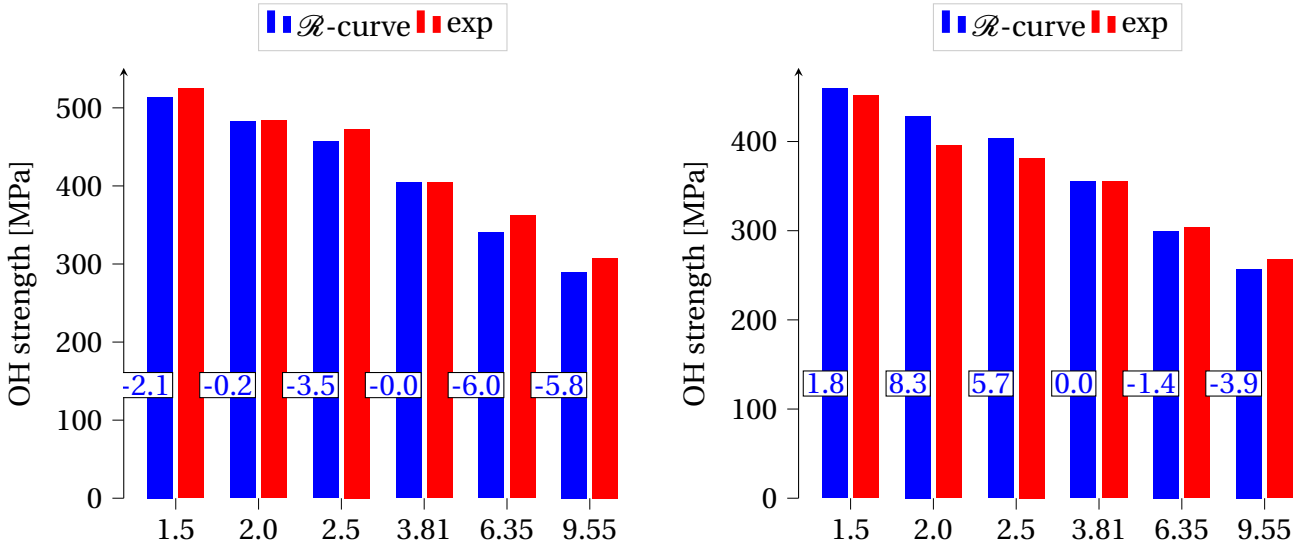

(a) Tensile strength prediction in RTD conditions.

(b) Compressive strength prediction in RTD conditions.

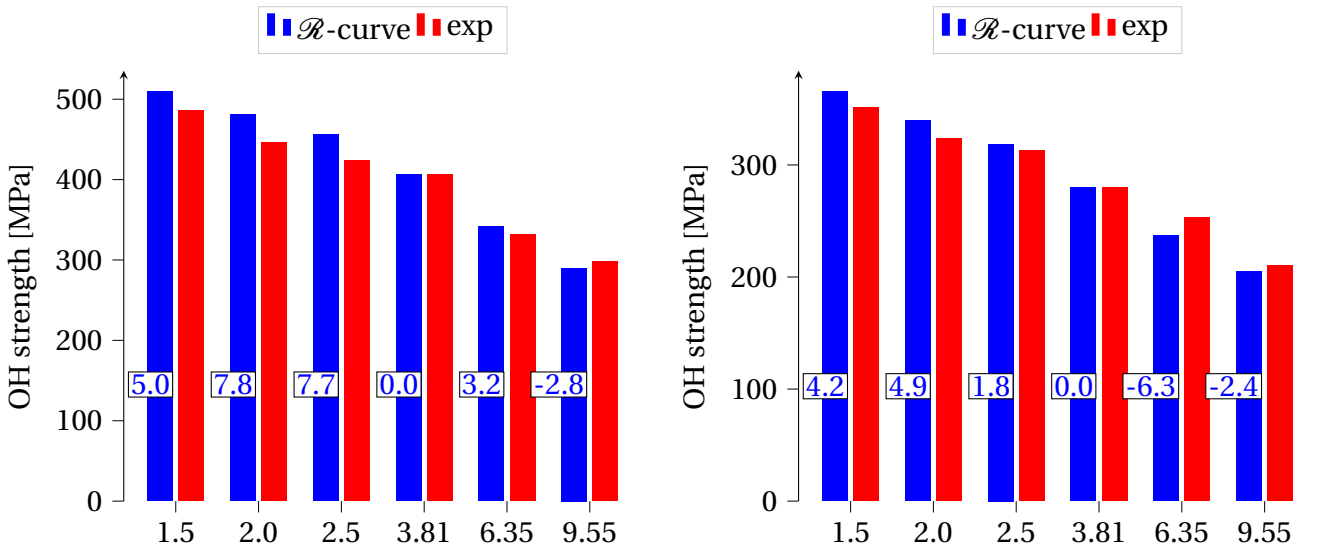

(c) Tensile strength prediction in ETW conditions.

(d) Compressive strength prediction in ETW conditions.

Figure 2.5: Prediction of open-hole strength of AS4/3501-6 [42], with calibration of $\mathscr{R}^0_{ss}$ on experimental strength with 6.35 mm hole. The x-axis represents the hole diameter [mm]. The lay-up is $[45/0/-45/90]_{2s}$. The width W is always equal to 38.1 mm.

2.3 Sensitivity

In the previous section, the calibration was proved effective, at least on the results presented in [4] and [42]. Furthermore, preference will be given to the calibration of $\mathscr{R}^0_{ss}$. Indeed, it is more representative of the physical behaviour that is generally observed. Moreover, the calibrated value is close to the experimentally measured steady-state value. However, before extending the method on the NIAR dataset, a choice must be made regarding the lay-up on which calibration will be performed. Indeed, three lay-ups are available in the NIAR dataset: quasi-isotropic, hard and soft.

In order to show sufficient grounds for that choice, a sensitivity analysis must be performed. It will consist in analyzing the sensitivity of the calibrated $\mathscr{R}^0_{ss}$ to both unnotched (UN) and notched (OH) strengths. In the end, the calibration should be performed on the lay-up that minimizes the sensitivity to the unnotched strength in order to cope with the errors induced by the unnotched strength criterion. On the contrary, it should maximize the sensitivity to the notched strength, for the obvious reason that a small sensitivity to the experimental open-strength would probably lead to ineffective calibration. Such a sensitivity analysis is shown in Fig. C.4, for RTD conditions on the NIAR dataset. It is based on the following finite difference formula:

$$\begin{aligned}
&\text{sensitivity w.r.t. OH strength:} && \frac{\mathscr{R}^{0,\text{calib.}}_{ss}\left(\text{OH}^{+10\%}\right)-\mathscr{R}^{0,\text{calib.}}_{ss}\left(\text{OH}^{-10\%}\right)}{\text{OH}^{+10\%}-\text{OH}^{-10\%}}\frac{\text{OH}_{\text{exp}}}{\mathscr{R}^{0,\text{calib.}}_{ss}\left(\text{OH}_{\text{exp}}\right)} && \text{at } \text{UN}_{\text{exp}},\\
&\text{sensitivity w.r.t. UN strength:} && \frac{\mathscr{R}^{0,\text{calib.}}_{ss}\left(\text{UN}^{+10\%}\right)-\mathscr{R}^{0,\text{calib.}}_{ss}\left(\text{UN}^{-10\%}\right)}{\text{UN}^{+10\%}-\text{UN}^{-10\%}}\frac{\text{UN}_{\text{exp}}}{\mathscr{R}^{0,\text{calib.}}_{ss}\left(\text{UN}_{\text{exp}}\right)} && \text{at } \text{OH}_{\text{exp}},
\end{aligned} \tag{2.4}$$

where the superscripts −10% and +10% mean that the value is taken as 90% or 110% of the experimental value, and the subscript *exp* means that the value is the experimental one. When analyzing the sensitivity to UN strength, the OH strength is kept constant and equal to the experimental value, and *vice versa*. The finite difference is always normalized. For instance, if the sensitivit to OH strength is considered, the finite difference is multiplied by the experimental OH strength and divided by the calibrated steady-state value of the $\mathscr{R}$-cure $\mathscr{R}_{ss}^{0,\text{calib.}}$, so that the computed sensitivity can be compared with the other material systems. It must be noted, though, that the dependency between the $\mathscr{R}$-curve and the open-hole and unnotched strengths is not linear, but is monotonous.

As a preliminary remark, it must be noted that the sensitivity w.r.t. UN strength is negative, whereas the sensitivity to OH strength is positive. Indeed, at fixed OH strength, $\mathscr{R}_{ss}^{0,\text{calib.}}$ must decrease if the UN strength is increased so that the given OH strength can be predicted by the coupled stress-energy criterion, see Eq. (1.10). On the contrary, for fixed UN strength, an increase in the open-hole strength must lead to a higher steady-state value of the $\mathscr{R}$-curve as the open-coupon appears stronger.

The first conclusion that can be drawn from Fig. C.4 is that soft lay-ups are too sensitive to the unnotched strength and should be discarded for calibration, in both tension and compression. It remains to make a choice between calibration on quasi-isotropic and on hard lay-ups.

Regarding tension, it is clear that while calibration on quasi-isotropic strength maximizes the sensitivity of $\mathscr{R}_{ss}^{0}$ w.r.t. the open-hole strength, it is the calibration on hard lay-ups that minimizes the sensitivity to the unnotched strength, see Fig. C.4. Therefore, a more in-depth analysis of the results shown in Fig. C.4 is necessary for the obtainment of a clear calibration rule in tension. On the one hand, it is noted that the calibration on hard lay-up is generally either twice less sensitive or equally sensitive to the unnotched tensile strength than calibration on quasi-isotropic lay-ups, see Fig. C.4c. On the other hand, calibration on quasi-isotropic lay-up is not drastically more sensitive to the open-hole tensile strength than calibration on hard lay-up is, see Fig. C.4a. Therefore, hard lay-ups should be preferred over quasi-isotropic ones when calibration of the average $\mathscr{R}$-curve is required. Regarding compression, the conclusions are essentially the same.

2.4 Conclusion

First, a calibration method was proposed to cope with the lack of information on the energetic part of the failure criterion, i.e. Eq. (1.9) for $\mathscr{G}_{Ic}^{0}$ and Eq. (1.10) for $\mathscr{R}_{ss}^{0}$. Because calibration of a critical energy release rate and average $\mathscr{R}$-curve lead to similar open-hole strength prediction, calibration of an average $\mathscr{R}$-curve was preferred. Indeed, the $\mathscr{R}$-curve is more representative of the physical behavior of failure of unidirectional coupons in uniaxial loading. Moreover, the calibrated value of $\mathscr{G}_{Ic}^{0,\text{calib.}}$ is artificially to low and not representative of the steady-state value of the $\mathscr{R}$-curve. Then, the calibration was shown effective in reproducing the hole size effect on several datasets, both in tension and compression and even in ETW environmental condition. Eventually, a sensitivity analysis over 10 material systems under both tension and compression and 3 different lay-ups lead to the conclusion that if available, a hard lay-up should be preferred over a quasi-isotropic or a soft one for calibration.

3 Validation of the framework on a real dataset

In the previous chapters, a framework was proposed to compute the open-hole strength of unidirectional coupons in a semi-analytical manner. Moreover, in order to compensate for the lack of an experimentally measured $\mathscr{R}$-curve, a calibration method based on an average $\mathscr{R}$-curve was proposed. In this chapter, the aforementioned framework, combined with the calibration method, will be applied on the NIAR dataset [10]. Supplementary information, such as the list of all unidirectional materials covered and the link to their data report can be found in Chap. D.

In Chap. 2, it was concluded that it would be preferable to apply the calibration of the $\mathscr{R}$-curve on hard lay-ups. However, the first lay-up that is generally tested for is a quasi-isotropic one. Therefore, in this chapter, calibration will always be performed on QI lay-ups. The sole purpose of this chapter is to present the results that can be obtained on a real dataset with the method presented earlier. The influence of using the experimental unnotched strength will also be discussed, while focusing mainly on RTD conditions. It is worth noting that since NIAR gives the complete elastic characterization of the lamina, the Trace theory will be discarded unless otherwise specified. Also, the NIAR open-hole geometry is always the same: a hole diameter of 6.35 mm and a width of 38.1 mm. Therefore, the method's ability to reproduce the hole size effect will not be addressed.

3.1 Extraction of the data from NIAR

The NIAR database contains a lot of datasheets, predominantly woven and unidirectional material systems [10]. Ten unidirectional material systems were identified. For each of them, a large material report of more than 200 pages is emitted. It contains at least one table with elastic properties and strengths of the lamina in different environmental conditions, mainly RTD, CTD and ETW, as well as a table containing the unnotched and open-hole strength of QI, hard and soft laminates in the aforementioned environmental conditions, whose stacking sequences are shown in Table 3.1. Because of the huge amount of data it represents, a Python code was produced for automating the extraction of material data. The material data report also contains an exhaustive listing of each test performed, with the observed predominant failure mode, representing a gigantic amount of data. Unfortunately, these tables were not formatted in a way that the extraction process can be automated, and it thus required a manual extraction method. It is to be noted that the material properties are most of the time

reported as measured and normalized w.r.t. nominal ply thickness. Indeed, to provide comparable material properties, they are always normalized w.r.t. cured ply thickness (CPT):

$$\text{Normalized Value} = \text{Measured Value} \cdot \frac{\text{Measured CPT}}{\text{Nominal CPT}}.$$

The default values were taken as the normalized ones. However, if the normalized value is not supplied, the measured value was used. It is important to keep in mind that the present framework is not sensitive to ply ordering, and that ply ordering may affect the ultimate strength of coupons. For instance, 10/80/10 and 9/73/18 coupons will experimentally differ in ultimate unnotched strength not only because the proportions are not strictly equal but also because ply ordering is very different, see Table 3.1.

Layup name	Angles	Proportions
Quasi-Isotropic (QI)	$[45,0,-45,90]_{2S}$	(25/50/25)
Hard	$[0,45,0,90,0,-45,0,45,0,-45]_S$	(50/40/10)
	$[0,45,0,-45,0,90,0,-45,0,45,0]_S$	(55/36/9)
Soft	$[45,-45,0,45,-45,90,45,-45,45,-45]_S$	(10/80/10)
	$[0,45,0,-45,0,90,0,-45,0,45,0]_S$	(9/73/18)

Table 3.1: Common stacking sequences found in the NIAR dataset, for Quasi-Isotropic (QI), hard and soft lay-ups. The repeating sequence might differ from one unidirectional material system to another.

3.2 Prediction of open-hole strength in RTD conditions

The results of the present framework on the NIAR dataset in RTD conditions[1] are shown in Fig. D.2 to D.4, both when a max-strain criterion is used to predict the unnotched strength and when the experimental unnotched strength is used. The calibrated value of the steady state $\mathscr{R}$-curve is also shown (see Fig. D.2), alongside with the observed predominant failure mode. It is to be noted that the only failure mode that fulfills the hypotheses of the framework is the lateral failure mode. For a complete overview of the failure identification codes, refer to Sect. D.3.

The first comment regarding the results depicted in Fig. D.2, is that when the unnotched strength is over-predicted w.r.t. the experimental value, the calibrated $\mathscr{R}^0_{ss}$ is smaller than the one that is obtained by calibration with the experimental UN strength. This observation was already mentioned earlier in Chap. 1. As a reminder, it is due to the fact that since the over-prediction of the UN strength artifically strengthen the material, the calibrated crack resistance curve must decrease in order to match with the experimental OH strength.

The open-hole strength prediction of the hard lay-ups in tension is in very good agreement with experimental data, generally in a ten percent error range, except for cases exhibiting multi-mode failure, see Fig. D.3. As a reminder, this failure mode does not fulfill the requirements of the present framework. The results in compression are less good.

[1] As a reminder, the full elastic characterization is used, with a max-strain criterion for the unnotched strength. An average $\mathscr{R}$-curve is calibrated on an OH QI strength.

Regarding the results for soft lay-ups, the results are clearly not in agreement with available experimental data. The framework always under-estimates the open-hole soft strength, see Fig. D.4. It is noted that very few soft lay-ups are failing in lateral mode, thus at odds with the basic assumption of the developed framework. It should also be noticed that soft lay-ups in compression might be more prone to non-negligible plasticity near crack tip, as well as local delamination[2], thus worsening the infringement of the framework's hypothesis.

It must be noted that the framework with the max-strain criterion seems to work as good as when the experimental unnotched strength is used. However, it must be noted that the max-strain criterion generally over-predicts the QI tensile strength, thereby under-predicting $\mathscr{R}_{ss}^{0,\text{calib}}$, which in turn compensates for the over-estimation of the unnotched soft or hard tensile strength when predicting soft or hard notched strength. Therefore, if one uses the max-strain criterion with an experimentally determined $\mathscr{R}$-curve, there are big chances that the notched predictions will be very disappointing since the aforementioned compensation mechanism will not come into play. It therefore seems desirable to improve the unnotched strength criterion. The following chapter shall look in that direction.

3.3 Comparison with experimental $\mathscr{R}$-curve

In order to further validate the use of a calibrated average $\mathscr{R}$-curve on a QI open-hole strength, a comparison is made between the predictions of notched strength of IM7/8552 (from the NIAR dataset) using the experimental $\mathscr{R}$-curve reported in [4] and using calibration of $\mathscr{R}_{ss}^{0,\text{calib}}$, for QI, hard and soft lay-ups in tension and compression. The results are shown in Table 3.2. The experimental unnotched strength was used. Firstly, it is noticed —once again —that the calibrated $\mathscr{R}_{ss}^{0}$ is not the same as the experimental one, and that the calibrated value on IM7/8552 with properties from NIAR is not the same as the one computed on IM7/8552 with properties from [4], see Table 2.2. In addition to the reasons given in Chap. 2, the difference in the calibrated steady-state value of the $\mathscr{R}$-curve is explained by slight differences in material properties.

The predicted OH QI tensile strength using the experimental $\mathscr{R}$-curve is extremely accurate, as was already the case for IM7/8552 tensile strengths from Furtado et al. [4]. However, the compressive strength is largely under-estimated and it originates from the very different steady-state $\mathscr{R}$-curve values, i.e. that from [4] and the calibrated one. The results for hard and soft lay-ups are even better with the calibrated average $\mathscr{R}$-curve than with the experimentally determined one. It is important to note that when using the $\mathscr{R}$-curve from [4] to predict the open-hole compressive strength of the soft lay-up, there was no solution to the coupled stress-energy criterion Eq. (1.10), hence the −100% error in Table 3.2. It is very important to observe that if the experimental $\mathscr{R}$-curve is used in conjunction with the max-strain criterion instead of the experimental unnotched strength, the predictions are really poor, see Table 3.3.

[2]These observations lack from robust evidence and reference but were exposed by Albertino Arteiro during a telephone conference on May 14th 2019.

Layup	Loading	Expected [MPa]	$\mathscr{R}$-curve from Furtado [4]			Calibration		
			OH strength [MPa]	Error [%]	$\mathscr{R}^0_{ss}$ [N/mm]	OH strength [MPa]	Error [%]	$\mathscr{R}^{0,\text{calib.}}_{ss}$ [N/mm]
QI	OHT	406.8	408.8	0.5	205.0	406.8	-0.0	184.2
QI	OHC	338.4	250.0	-26.1	61.0	338.4	0.0	142.1
Hard	OHT	597.0	598.0	0.2	-	610.2	2.2	-
Hard	OHC	436.0	355.5	-18.5	-	479.0	9.8	-
Soft	OHT	301.0	255.4	-15.1	-	255.3	-15.2	-
Soft	OHC	267.5	0.0	-100.0	-	226.1	-15.5	-

An error equal to -100% means that no solution was found to the coupled energy-stress criterion Eq. (1.10).

Table 3.2: Comparison of the prediction of open-hole strength for the material system IM7/8552 in RTD conditions, when the $\mathscr{R}$-curve from [4] is used and when calibration of an average $\mathscr{R}$-curve is performed on the QI lay-up. The material characterization (elastic properties and strength) comes from the NIAR dataset. The experimental unnotched strength is used.

Layup	Loading	Expected OH strength [MPa]	Predicted OH strength [MPa]	Error [%]
QI	OHT	406.8	398.03	-2.2
	OHC	338.4	249.1	-26.4
Hard	OHT	597.0	566.44	-5.1
	OHC	436.0	358.1	-17.9
Soft	OHT	301.0	0.0	-100.0
	OHC	267.5	0.0	-100.0

Table 3.3: Prediction of notched strength of IM7/8552 from NIAR, in RTD. The experimental $\mathscr{R}$-curve from [4] is used, with a max-strain failure criterion.

3.4 On the use of the Trace theory

Earlier in this report, it was mentioned that using the Trace theory can give very good approxition of the elastic properties of the lamina based solely on the longitudinal Young modulus E_1. Furtado et al. [4, Table 6] showed that using the Trace theory or the full elastic characterization of the ply does not induce noticeable drop in accuracy, for QI OH strength prediction. In this report, this observation is further validated on the RTD open-hole strengths found in the NIAR dataset. A comparison of the strength prediction with and without the Trace theory is shown in Fig. D.5 to D.7, for the 10 material systems found in NIAR, for both tensile and compressive strength with three different stacking sequences (QI, hard and soft). The calibration of the average $\mathscr{R}$-curve was performed on QI lay-ups, using the max-strain unnotched criterion. The calibrated steady-state value $\mathscr{R}^{0,\text{calib.}}_{ss}$ are shown in Table D.4.

The prediction of the unnotched strength of QI and hard lay-ups is nearly not affected by the use of the Trace theory, with a maximum difference of around 3%. The calibrated steady-state value of the average $\mathscr{R}$-curve is nearly the same, whether Trace theory is used or not, see Table D.4. The accuracy

of hard open-strength prediction is not degraded at all.

Regarding the prediction of the unnotched strength of soft coupons, larger differences are observed, such as 11.8% for the tensile UN strength of CytecT40-800/Cycom5215 (index 6). Therefore, bigger changes are seen in the predicted open-hole strength of soft coupons. It seems that using the Trace theory generally predict a higher UN strength so that notched strength is also generally higher.

Recalling that the Trace theory uses only the longitudinal Young modulus of the ply, it is quite remarkable that the open-hole predictions are nearly equal to those predicted with full elastic characterization. This is of course expected, as the Trace theory was shown to be very accurate in predicting the laminate properties of QI lay-ups, see Sect. 1.1.2.

3.5 Conclusion

In this chapter, it was demonstrated that the proposed framework, i.e. calibration of an average $\mathscr{R}$-curve on QI lay-ups and a max-strain criterion for estimating the unnotched strength, can give good accuracy regarding the prediction of hard lay-up strengths, with largest errors generally obtained for lay-ups whose failure mode is not lateral. However, the method always under-estimates the strength of soft coupons, especially in compression. Nevertheless, it must be noted that nearly no soft coupon fails by lateral mode, and therefore not agreeing with the hypotheses of the framework. A summary of the accuracy of notched strength prediction is shown in Table 3.4.

Layup		Hard		Soft	
Loading		OHT	OHC	OHT	OHC
Number of predictions in	±10%	7/10	3/10	2/10	0/10
	±15%	8/10	8/10	6/10	0/10

Table 3.4: Summary of the accuracy of the framework, with full elastic characterization, a max-strain criterion for the unnotched strength and calibration of an average $\mathscr{R}$-curve on the strength of a QI lay-up. Case by case prediction can be found in Fig. D.2 to D.4.

The use of a calibrated $\mathscr{R}$-curve was also compared with an experimental $\mathscr{R}$-curve with no degradation of the prediction, if the experimental unnotched strength is used. The hard and soft strengths were even better with the calibrated $\mathscr{R}$-curve. However, when the max-strain criterion is used in conjunction with the experimental $\mathscr{R}$-curve, the predictions are not satisfying. Therefore, the unnotched criterion should be improved so that it predicts strength closer to the experimental one, thus improving the overall framework.

In Chap. 1 to 3, the framework proposed in [4] was validated for computing the notched strength and capturing the hole size effect of QI lay-ups in tension and compression, using either an experimentally measured $\mathscr{R}$-curve or a calibrated average $\mathscr{R}$-curve. Using 10 material systems found in the NIAR dataset, it was further validated for computing the notched strength of hard lay-up, provided the $\mathscr{R}$-curve is calibrated on QI lay-ups. However, the framework predict very conservative tensile soft strength and is not capable of predicting the compressive notched strength of soft lay-up, even if the experimental unnotched strength is used.

4 Prediction of unnotched strength: a review

As mentioned earlier in this report, the open-hole predictions are generally better when the unnotched strength is taken as the experimental one. Therefore, this chapter presents other failure criteria for composite laminates in order to find the best compromise between accuracy and material characterization. Moreover, a comprehensive study will try to determine which unnotched criterion should be used under given circumstances, so that the open-hole predictions are best. Among those, the usual Tsai-Wu criterion will be addressed, as well as a failure criterion based on the longitudinal strengths only, namely the Unit Circle (UC), that was proposed recently in the litterature [43].

4.1 Tsai-Wu in Strain Space

In this section, the Tsai-Wu failure criterion is used, with some modifications. The First Ply Failure criterion relies on the Tsai-Wu failure envelope of each ply of the laminate, based on the intact lamina elastic properties. It is generally observed that this criterion predicts an under-estimated laminate unnotched strength. The Last Ply Failure criterion has emerged to alleviate the under-prediction. It also relies on the Tsai-Wu failure envelope of each ply of the laminate, but is based on degraded elastic properties of the lamina. Finally, the First Ply Failure on the 0° ply relies on the Tsai-Wu failure of the 0° ply only. It is to be noted that because all these three criteria make use of five material strengths, namely longitudinal and transverse strengths in tension and compression and the in-plane shear strength, using the Tsai-Wu criterion requires more extensive test campaigns compared to using only a max-strain criterion for instance.

4.1.1 First Ply Failure

Tsai et al. [7] proposed to use the Tsai-Wu failure criterion in the strain space, because the failure envelope of a given ply is then independent of the other plies. The laminate failure envelope is thus obtained by superimposing the individual failure envelopes of each ply orientation in the lay-up. The use of the Tsai-Wu criterion is significant. Indeed, in contrast to other failure criteria such as Hashin or max-strain (see Sect. 1.2), the Tsai-Wu criterion is based on tensors and can be easily translated

from the stress to the strain space and *vice versa*.

The Tsai-Wu criterion is a quadratic criterion in the stresses for plies in plane-stress state. In the 1-2 symmetry axes, it writes:

$$F_{ij}\sigma_i\sigma_j + F_i\sigma_i = 1, \quad (i,j) \in \{1,2,6\}, \tag{4.1}$$

where Voigt notation is used and the matrix $[F]$ and vector $\{F\}$ are parameters in the stress space based on the material strengths:

$$\begin{aligned} F_{11} &= \frac{1}{X^C X^T}, & F_{22} &= \frac{1}{Y^C Y^T}, \\ F_1 &= \frac{1}{X^T} - \frac{1}{X^C}, & F_2 &= \frac{1}{Y^T} - \frac{1}{Y^C}, \\ F_{66} &= \frac{1}{S^2}, & F_{12} &= -\frac{F_{12}^*}{\sqrt{X^T X^C Y^T Y^C}}, \end{aligned}$$

where $0 \leq F_{12}^* \leq 1$[1] for closed failure envelopes [6]. Indeed, unclosed envelopes would predict unphysical infinite strength under particular combined loads. It is to be noted that because only orthotropic materials are considered, F_{16}, F_{26} and F_6 vanish, and only five independent strengths exist: X and Y in tension and compression and the in-plane shear strength. Moreover, the interaction term F_{12}^* is generally taken equal to 0.5 [6].

In the following, the stress-based failure criterion Eq. (4.1) will be transformed to a strain-based criterion of the same form, i.e. quadratic:

$$G_{ij}\varepsilon_i\varepsilon_j + G_i\varepsilon_i = 1, \tag{4.2}$$

where $[G]$ and $\{G\}$ are strain-space parameters also based on the material strengths. Still, the relationship between material strengths and the strain-space parameters is not defined yet. Nevertheless, the translation to the strain space is straightforward. Using the stress-strain relations of elasticity [6, p. 237]:

$$F_{ij}\sigma_i\sigma_j = F_{ij}Q_{ik}\varepsilon_k Q_{jl}\varepsilon_l = G_{kl}\varepsilon_k\varepsilon_l, \tag{4.3}$$

where Q is the in-plane stiffness matrix for plies under plane-stress. It implies that $G_{ij} = F_{kl}Q_{ki}Q_{lj}$. One also has:

$$F_i\sigma_i = F_i Q_{ij}\varepsilon_j = G_j\varepsilon_j, \tag{4.4}$$

and therefore, $G_i = Q_{ji}F_j$.

There remains to transform the envelope described hereinabove from the 0° to the θ° orientation, i.e. going from the envelope of the ply in the *local* axes to that of the *global* axes. For a ply with

[1] The interaction term can be determined by carrying out a combined-stress test so that both σ_1 and σ_2 are non-zero, but it is generally very difficult to perform.

orientation $\theta°$, the failure envelope for loadings in the 0° direction is given by [6]:

$$\begin{Bmatrix} U_1 \\ U_2 \\ U_3 \\ U_4 \\ U_5 \end{Bmatrix} = \begin{pmatrix} \frac{3}{8} & \frac{3}{8} & \frac{1}{4} & \frac{1}{2} \\ \frac{1}{2} & -\frac{1}{2} & 0 & 0 \\ \frac{1}{8} & \frac{1}{8} & \frac{-1}{4} & \frac{-1}{2} \\ \frac{1}{8} & \frac{1}{8} & \frac{3}{4} & \frac{-1}{2} \\ \frac{1}{8} & \frac{1}{8} & \frac{-1}{4} & \frac{1}{2} \end{pmatrix} \begin{Bmatrix} G_{11} \\ G_{22} \\ G_{12} \\ G_{66} \end{Bmatrix} \qquad , \begin{Bmatrix} U_6 \\ U_7 \end{Bmatrix} = \begin{pmatrix} \frac{1}{2} & \frac{1}{2} \\ \frac{1}{2} & \frac{-1}{2} \end{pmatrix} \begin{Bmatrix} G_1 \\ G_2 \end{Bmatrix},$$

$$\begin{Bmatrix} G_{xx} \\ G_{yy} \\ G_{xy} \\ G_{ss} \\ G_{xs} \\ G_{ys} \end{Bmatrix} = \begin{pmatrix} U_1 & U_2 & U_3 & 0 & 0 \\ U_1 & -U_2 & U_3 & 0 & 0 \\ U_4 & 0 & -U_3 & 0 & 0 \\ U_5 & 0 & -U_3 & 0 & 0 \\ 0 & 0 & 0 & \frac{U_2}{2} & U_3 \\ 0 & 0 & 0 & \frac{U_2}{2} & -U_3 \end{pmatrix} \begin{Bmatrix} 1 \\ \cos(2\theta) \\ \cos(4\theta) \\ \sin(2\theta) \\ \sin(4\theta) \end{Bmatrix}, \begin{Bmatrix} G_x \\ G_y \\ G_s \end{Bmatrix} = \begin{pmatrix} U_6 & U_7 & 0 \\ U_6 & -U_7 & 0 \\ 0 & 0 & U_7 \end{pmatrix} \begin{Bmatrix} 1 \\ \cos(2\theta) \\ \sin(2\theta) \end{Bmatrix}.$$

The above relations seem over-complicated. There are just a convenient way to circumvent the use of high powers of trigonometric functions. Other transformations can be found in [6], that use higher powers of the trigonometric functions.

The failure envelope of the ply in the *global* axes is then given by [6]:

$$G_{xx}\varepsilon_x^2 + G_{yy}\varepsilon_y^2 + 2G_{xy}\varepsilon_x\varepsilon_y + 2G_{xs}\varepsilon_x\gamma_{xy} + 2G_{ys}\varepsilon_y\gamma_{xy} + G_{ss}\gamma_{xy}^2 + G_x\varepsilon_x + G_y\varepsilon_y + G_s\gamma_{xy} = 1. \tag{4.5}$$

Since the problem at hand is not concerned with shear strains in the global x-y axes, see Sect. F.2, only ε_x and ε_y remain in the above equation, and can thereby be interpreted as an ellipse. The laminate unnotched strength is given as:

$$\underset{\theta\in\Theta}{\operatorname{argmin}}\ E_x^L \cdot \varepsilon_{\mathbb{L}\cap\mathbb{E},x}, \tag{4.6}$$

where Θ is the ensemble of all ply orientations in the laminate and $\varepsilon_{\mathbb{L}\cap\mathbb{E},x}$ is the ε_x value of the intersection point in the $(\varepsilon_x, \varepsilon_y)$ space of the failure envelope of the $\theta°$ ply and the line of slope $-\nu_{xy}^L$, since the problem at hand is pure longitudinal tension or compression. It is important to note that the tensile strength is located in the fourth quadrant and the compressive strength in the second quadrant, since the laminate Poisson ratio is positive for composite laminates. Envelopes can be found in Fig. 4.5 for IM7/977-3 and have been validated against [43].

4.1.2 Last Ply Failure

As the loading is increased, cracks can form in the matrix, especially the matrix of off-axis plies, while the laminate is not yet completely broken and can still sustain loads. In general, micro-cracks form

in the matrix where micro-defects caused stress concentrations. With the load increase, these cracks coalesce and cause fiber debonding. Because of those cracks and debonding arising and growing in number, the laminate elastic properties change. For example, there can be stiffness drops. However, LPT deals with continuous media. Therefore, there is a need for homogenization of the degraded plies.

Tsai et al. [6] cope with the matrix cracks by introducing a new matrix with lower stiffness, see Fig. 4.1. Instead of using the intact matrix Young modulus E_M, a degraded one is used, which is given by $E_M^* \cdot E_M$, where E_M^* is the degradation factor. Therefore, the ply elastic constants must be computed again. In what follows, two methods will be exposed to back-compute the ply properties accounting for the change in matrix Young modulus.

Another reason for degrading the ply properties is because the First Ply Failure criterion yields overly conservative predictions. This will be discussed later on, see Sect. 4.3.

It is to be noted that other analytical degradation methods exist, see for instance Carraro et al. [44]. However, they were not investigated in this work.

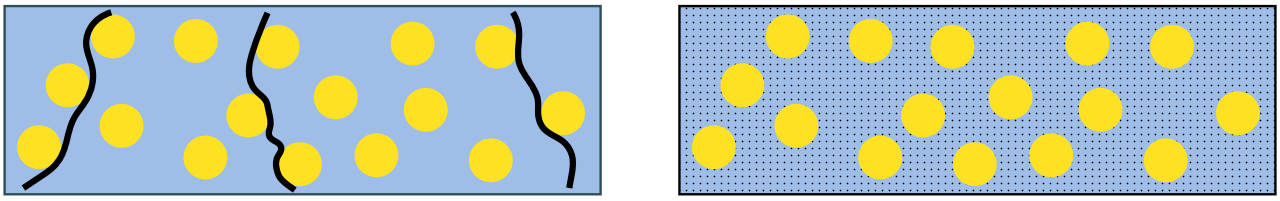

(a) Degradation of the ply caused by emerging transverse cracks, inducing debonding.

(b) Degraded ply is replaced by a quasi-homogeneous ply with a reduced Young modulus.

Figure 4.1: Proposed degradation procedure, in accordance with [6].

4.1.2.1 Modified Rules of Mixtures

The well known rules of mixtures give the lamina elastic properties based on those of its constituents, namely the fibers and the matrix [45, 46]. However, the basic rules of mixtures are based on the simplifying hypothesis that the fiber is a plate, embedded in another plate of equal thickness representing the matrix, with the supplementary hypothesis of perfect bonding between the two, see Fig. 4.2a. This model is not representative of the embedded fibers of CFRP, that are better described as concentric cylinders, see Fig. 4.2b. Then, to simplify the derivation of rules of mixtures based on a concentric cylinders model, Tsai et al. [45] note that the matrix being much softer than the fibers, one can write:

$$\begin{cases} \bar{\sigma}_{M,2} = \eta_2 \bar{\sigma}_{F,2} & , 0 < \eta_2 \leq 1, \\ \bar{\sigma}_{M,6} = \eta_6 \bar{\sigma}_{F,6} & , 0 < \eta_6 \leq 1, \end{cases}$$

where $\bar{\sigma}_{M,2}$, $\bar{\sigma}_{M,6}$, $\bar{\sigma}_{F,2}$, $\bar{\sigma}_{F,6}$ are the average matrix (M) and fiber (F) stresses in transverse (2) and shear (6) loading, η_2 and η_6 are *stress partitioning* parameters, that link the average stresses in the matrix with those of the fiber. The homogenized degraded ply properties are then given by [45]:

$$E_1^{\text{degr.}} = E_1,$$

$$
\begin{aligned}
\nu_{12}^{\text{degr.}} &= E_M^* \nu_{12}, \\
E_2^{\text{degr.}} &= \left(\frac{1}{1+\upsilon_2^*} \left[\frac{1}{E_{F2}} + \frac{1}{E_M^*} \frac{\upsilon_2^*}{E_M} \right] \right)^{-1}, \\
G_{12}^{\text{degr.}} &= \left(\frac{1}{1+\upsilon_6^*} \left[\frac{1}{G_{F1}} \frac{\upsilon_6^*}{G_M} \right] \right)^{-1}, \\
\upsilon_2^* &= \eta_2 \frac{\upsilon_F}{\upsilon_F}, \\
\upsilon_6^* &= \eta_6 \frac{1-\upsilon_F}{\upsilon_F}, \\
E_{F2} &= \left(\frac{1+\upsilon_2^*}{E_2} - \frac{\upsilon_2^*}{E_M} \right)^{-1}, \\
G_{F1} &= \left(\frac{1+\upsilon_6^*}{G_{12}} - \frac{\upsilon_6^*}{G_M} \right)^{-1},
\end{aligned}
$$

whose derivation can be found in Tsai et al. [45, p. 394] and is very similar to the derivation of the usual rules of mixtures. Tsai et al. [6] proposed to take $\eta_2 = 0.5161$ and $\eta_6 = 0.316$ for usual CFRP, with a degradation factor $E_M^* = 0.15$. Moreover, the default values for the matrix properties were chosen equal to 3400 MPa for the Young modulus and 1260 MPa for the shear modulus. The volume fraction is either taken as the nominal volume fraction if given, as is generally the case in the NIAR dataset, or back-computed with $\upsilon_F \approx E_1 / E_F$, E_F being the fiber Young modulus found in data sheets, see Table E.1. The degradation methodology is then as follows:

1. Assuming the matrix is linear elastic and isotropic, use ν_M and E_M to compute G_M.
2. Using η_2, η_6, υ_F, E_2, G_{12}, E_M and G_M, compute E_{F2} and G_{F1}.
3. With the degradation factor E_M^*, compute the degraded transverse Young modulus $E_2^{\text{degr.}}$, in-plane shear modulus $G_{12}^{\text{degr.}}$ and in-plane Poisson ratio $\nu_{12}^{\text{degr.}}$. The longitudinal modulus is considered not affected by the degradation procedure.

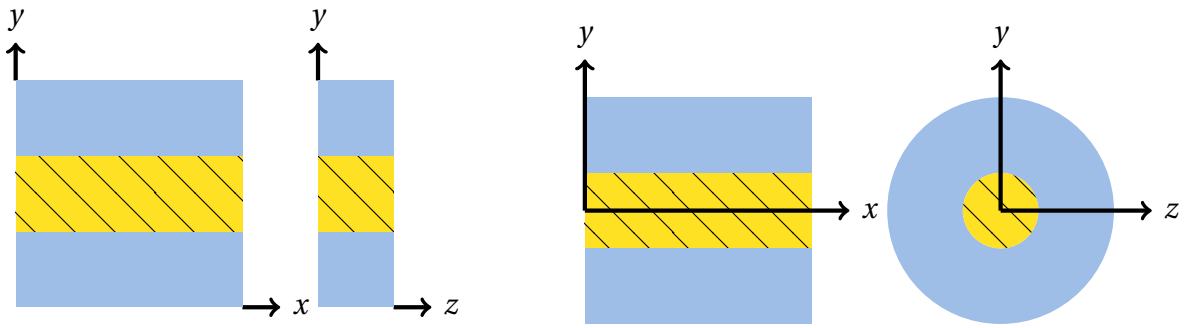

(a) Fiber plate embedded in matrix plate.

(b) Concentric cylinder model.

Figure 4.2: Representative volume element of a composite, with matrix ● and fiber ◍, in accordance with [45].

4.1.2.2 Degradation of elastic properties *via* Mean-Field Homogenization

A less empirical method for degradation of elastic properties can be built upon with a mean-field homogenization technique, whose analytical nature allows for fast evaluation, in line with the philosophy of the present framework. Because there was a possibility of including the present tool in Digimat, the adopted Mean-Field Homogenization (MFH) technique is the Mori-Tanaka model since it is implemented in Digimat[2] [47] [48]. In theory, the Mori-Tanaka model can be used only for low fiber volume fractions, and an inversed Mori-Tanaka or a Balanced Model should be used for high fiber volumes. However, the Mori-Tanaka model still gives good predictions beyond the low fiber volume limit and is therefore the method that will be used. The Mori-Tanaka model is based on the following concentration tensor[3] [47] [49]:

$$\boldsymbol{A} = \left[\boldsymbol{S} : \left(\mathbb{E}_M^{-1}\mathbb{E}_F - \mathbb{I}\right) + \mathbb{I}\right]^{-1},$$

with $\mathbb{E}_F$ and $\mathbb{E}_M$ the elastic stiffness tensors of the fiber and matrix phases, respectively, and $\boldsymbol{S}$ the Eshelby tensor, whose expression depends on $\mathbb{E}_M$ and the shape and orientation of the inclusions, i.e. the fibers. In the present case, the unidirectional composite laminate can be assimilated to a transversly isotropic inclusion phase (the fibres) in an isotropic host phase (the matrix). Expressions for the Eshelby tensor can be found in [50].

The theoretical part being presented, the method followed to degrade the elastic ply properties is as follows:

1. From the input data, i.e. E_1, E_2, ν_{12}, G_{12}, υ_F, E_M and ν_M, compute the fiber properties assuming it is transversely isotropic.
2. Use the MFH model described hereinabove, in which only the matrix Young modulus E_M is degraded: $E_M^{\text{degr.}} = E_M^* \cdot E_M$, to compute the degraded elastic properties of the homogenized ply.

4.1.2.3 Comparison between degradation methods

The examination of both degradation methods has lead to some reserves about the modified rules of mixtures presented in Sect. 4.1.2.1. Indeed, the fact that the Poisson ratio is decreased by the degradation factor is questionable. Taking $E_M^* = 0.15$, the ply's Poisson ratio is decreased by 85%. This is not in line with the results provided by the MFH degradation method of Sect. 4.1.2.2. Moreover, from a more physical point of view, it is unclear why, under longitudinal tensile loading, the Poisson ratio of a degraded ply should be decreased that much, since the cracks will tend to close and a usual behaviour might be found back. However, in order to decide which of the two methods provide the most sound results, a shear-lag analysis should be conducted [44].

A comparison of both methods is performed for IM7/8552 in RTD conditions. The degraded ply properties and corresponding QI laminate properties are reported in Table 4.1. The Tsai-Wu failure envelopes in the strain space are shown in Fig. 4.3, for both degradation methods. It is clear that the anchor points of the failure envelopes drawn with the MFH or mRoM degradation methods are very similar, for the simple reason that the degraded longitudinal Young modulus of the ply is nearly equal

[2] The method was received as a compiled C++ dynamic library.

[3] The concentration tensor links the mean-field strains of the matrix and fiber: $\langle\boldsymbol{\varepsilon}\rangle_F = \boldsymbol{A} : \langle\boldsymbol{\varepsilon}\rangle_M$.

for both methods, see Table 4.1b. The ultimate unnotched strengths computed with 0°, 45° and 90° envelopes are reported in Table 4.2.

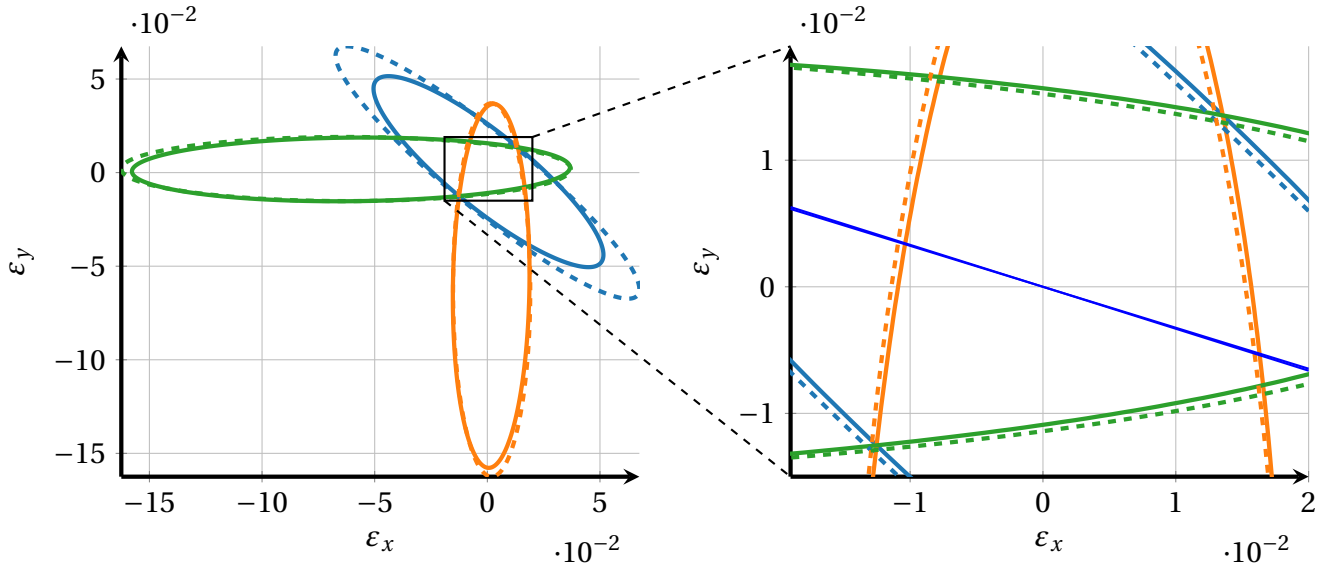

Figure 4.3: Tsai-Wu failure criterion: failure envelopes in the strain space ε_x-ε_y of IM7/8552 (NIAR, RTD), for a quasi-isotropic lay-up in tension (left) and a zoom on the inner envelope (right). Degradation with mRoM: 45° (——), 0° (——), 90° (——). Degradation with MFH: 45° (- - -), 0° (- - -), 90° (- - -). The blue line (——) is in fact composed of two blue lines whose slopes are $\nu_{12}^{L,\text{degr.}} = 0.331433$ for the MFH method and $\nu_{12}^{L,\text{degr.}} = 0.323539$ for the mRoM method, see Table 4.1b.

The major difference between mRoM and MFH lies in the lamina degraded Poisson ratio. While the mRoM predicts a very small —even negligible —Poisson ratio, the MFH does not predict such a drop, see Table 4.1. However, the degraded properties of a QI laminate are not very different in the end, and will not be helpful in determining which degradation method is best for predicting the unnotched strength.

Lamina properties				QI laminate properties			
E_1	E_2	ν_{12}	G_{12}	E_x^L	E_y^L	ν_{xy}^L	G_{xy}^L
158511	8963.2	0.316	4688.4	59653.4	59653.4	0.314808	22685.2

(a) Intact lamina and QI laminate tensile elastic properties.

	Degraded ply properties				Degraded QI properties			
	$E_1^{\text{degr.}}$	$E_2^{\text{degr.}}$	$\nu_{12}^{\text{degr.}}$	$G_{12}^{\text{degr.}}$	$E_x^{L,\text{degr.}}$	$E_y^{L,\text{degr.}}$	$\nu_{xy}^{L,\text{degr.}}$	$G_{xy}^{L,\text{degr.}}$
mRoM	158511	1811.84	0.0474	976.672	54285.4	54285.4	0.323539	20507.7
MFH	157322	1761.87	0.315263	727.761	53610.3	53610.3	0.331433	20132.6

(b) Comparison of degraded tensile properties of lamina and QI laminate, when ply properties are degraded with mRoM and MFH methods.

Table 4.1: Elastic properties of IM7/8552 (NIAR, RTD). The unit system is MPa.

From Table 4.2, it is clear that the two degradation methods give quite different ultimate strengths, and that the MFH method gives better results. Indeed, recalling Eq. (4.6), the ultimate strength is the

smallest intersection between the envelopes and a straight line of slope $-\nu^L_{xy}$, which is in this case always given by the 0° ply. This suggests that a failure criterion based on the envelope of the 0° ply only might also give appreciable results.

A complete comparison of both degradation methods is presented in Table E.2, where both criteria are put to the test on the whole NIAR dataset in RTD conditions. The mean error and standard deviation are presented in Table 4.3. It is easy to see that the MFH result is overall more predictive, i.e. providing better strengths, than the mRoM method as far as the unnotched strength is concerned. The only case in which the mRoM degradation method should be prefered is for hard lay-ups in compression, see Tables 4.3 and E.2. It should be noted, though, that both criteria lead to very similar results, both regarding unnotched and notched strength, see Tables 4.2 and E.2.

	X^T_L [MPa]		X^C_L [MPa]	
Ply orientation (°)	mRoM	MFH	mRoM	MFH
0	885.214	853.883	562.483	589.263
45	1922.3	1950.56	1777.37	1950.34
90	1125.24	1165.63	3145.17	3087.59
Experimental X_L	721.8		600.2	

Table 4.2: Comparison of the laminate unnotched strength (X_L) prediction with the Tsai-Wu failure criterion, with degraded properties computed either with mRoM or MFH method. Material is IM7/8552 (NIAR, RTD), lay-up is QI. The laminate properties are those in tension for tensile strength and in compression for compressive strength. The strength is computed as the intersection of the Tsai-Wu envelope of the θ° ply in the *global* axes with a line of slope equal $-\nu^L_{12}$, where $-\nu^L_{12}$ is the laminate major in-plane Poisson ratio.

Layup	Loading	LPF mRoM		LPF MFH	
		μ[%]	σ[%]	μ[%]	σ[%]
QUASI	UNT	6.1	10.8	4.1	11.2
	UNC	-14.1	9.0	-11.2	8.5
HARD	UNT	-2.9	13.8	-3.4	11.6
	UNC	1.8	8.9	5.5	9.7
SOFT	UNT	-21.6	13.7	-20.4	14.0
	UNC	-36.5	10.3	-35.1	10.1

Layup	Loading	LPF mRoM		LPF MFH	
		μ[%]	σ[%]	μ[%]	σ[%]
QUASI	OHT	-0.0	0.0	-0.0	0.0
	OHC	0.0	0.0	0.0	0.0
HARD	OHT	-9.3	9.7	-8.6	9.8
	OHC	16.2	6.9	15.6	6.8
SOFT	OHT	-23.5	8.2	-22.7	8.1
	OHC	-32.2	4.9	-32.1	5.0

Table 4.3: Mean error of the unnotched strength prediction and open-hole strength prediction, for Last Ply Failure criterion with mRoM (LPF mRoM) and MFH (LPF MFH) degradation methods. Error closest to zero is colored in blue. For detailed case by case unnotched prediction, refer to Table E.2. For detailed case by case open-hole strength prediction, refer to Table E.6. Mean (μ) and standard deviation (σ) are provided, in percent. Calibration is performed on QI lay-ups.

4.1.3 First Ply Failure on 0° ply only

Earlier in this report, it was mentioned that when using failure envelopes in the strain space like those produced with the Tsai-Wu criterion using degraded ply properties, the ultimate strength of the unnotched laminate was dictated by the 0° envelope only, see Sect. 4.1.2.3. Moreover, in order to reduce

the uncertainties related to properties degradation, it is proposed to use the intact lamina properties. This choice can be motivated by the fact that since the criterion relies only on the 0° ply, which is assumed to be fiber-failure dominated, the degradation of the matrix will not affect the results and might even be detrimental. The procedure to compute the unnotched strength is thus the following:

1. Compute the failure envelope of the 0° ply with intact ply properties.
2. Compute the intersections of this envelope with a straight line of slope $-\nu_{xy}^{L}$.
3. Choose the intersection lying in the fourth quadrant for tensile strength and in the second quadrant for compressive strength.

This failure criteria, named FPF 0 hereinafter, is expected to better describe hard lay-ups that are predominantly populated with 0° plies.

An extensive comparative study is shown in Table E.3, in which the FPF 0 criterion is compared to LPF mRoM and LPF MFH for the prediction of the unnotched strength. Mean error and standard deviation are provided in Table 4.4, alongside with the prediction of notched strength. Astonishingly, the First Ply Failure on 0° ply works in general even better than LPF MFH or LPF mRoM, at least for unnotched prediction. Nevertheless, all three criteria are generally way too conservative on soft compressive UN strength. The open-hole predictions will be discussed afterwards, see Sect. 4.3.2.

Layup	Loading	LPF mRoM		LPF MFH		FPF 0	
		μ[%]	σ[%]	μ[%]	σ[%]	μ[%]	σ[%]
QUASI	UNT	6.1	10.8	4.1	11.2	13.3	12.1
	UNC	-14.1	9.0	-11.2	8.5	-0.8	8.8
HARD	UNT	-2.9	13.8	-3.4	11.6	4.9	9.6
	UNC	1.8	8.9	5.5	9.7	2.3	8.0
SOFT	UNT	-21.6	13.7	-20.4	14.0	14.5	21.0
	UNC	-36.5	10.3	-35.1	10.1	-29.9	9.2

Layup	Loading	LPF mRoM		LPF MFH		FPF 0	
		μ[%]	σ[%]	μ[%]	σ[%]	μ[%]	σ[%]
QUASI	OHT	-0.0	0.0	-0.0	0.0	-0.0	0.0
	OHC	0.0	0.0	0.0	0.0	0.0	0.0
HARD	OHT	-9.3	9.7	-8.6	9.8	-9.0	8.6
	OHC	16.2	6.9	15.6	6.8	9.2	6.4
SOFT	OHT	-23.5	8.2	-22.7	8.1	-9.5	10.2
	OHC	-32.2	4.9	-32.1	5.0	-31.2	4.9

Table 4.4: Mean error of the unnotched strength prediction (left) and open-hole strength prediction (right), for Last Ply Failure criterion with mRoM (LPF mRoM) and MFH (LPF MFH) degradation methods and the First Ply Failure on the 0° ply only (FPF 0). Error closest to zero is colored in blue. For detailed case by case unnotched prediction, refer to Table E.3. For detailed case by case open-hole strength prediction, refer to Table E.6. Mean (μ) and standard deviation (σ) are provided, in percent. Calibration is performed on QI lay-ups.

4.2 Unit Circle

Last Ply Failure and First Ply Failure on 0° ply approaches require the 4 elastic constants[4] and 5 strengths of the ply, and in the case of LPF, the elastic properties must be degraded, with the batch of questions degradation raises. In order to alleviate the need for such a strong ply characterization, another approach can be followed. This new method is based on the observation that for many CFRPs, the Last Ply Failure envelope is governed by the 0° and 90° envelopes only, see Fig. 4.3 for instance. Therefore, a circle-like criterion inscribed in the Last Ply Failure envelope can be defined, see Fig. 4.4, and has been named Unit Circle (UC) by Tsai et al. [43]. It must be noted that even if it seems that both LPF and UC have the same anchor points, it is not the case. Indeed, in the case of the LPF envelope, the point X^T/E_1 is a little below the ε_x axis. It should be noted that since the 0° LPF envelope is very steep near the anchor points of the UC, the influence of the ply Poisson ratio is insignificant on the intersection between the ε_x axis and the 0° LPF envelope.

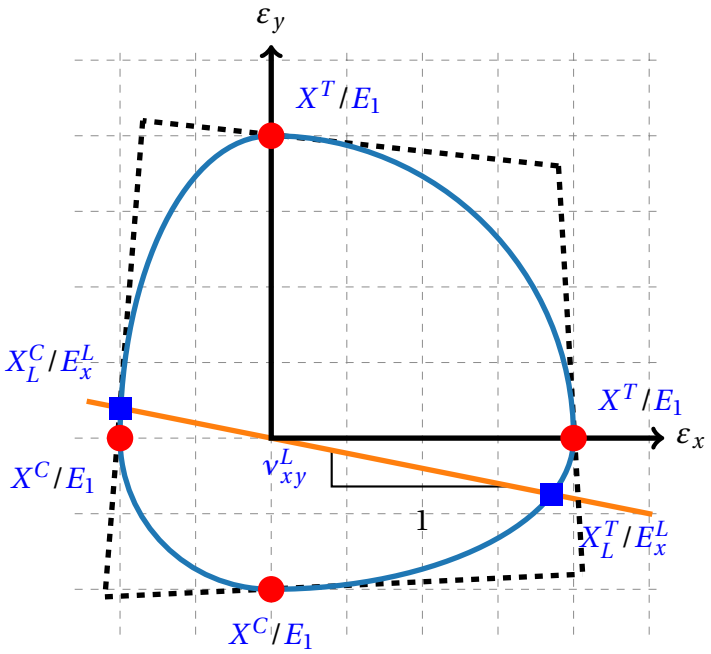

Figure 4.4: Unit Circle in strain space. Red dots represent the anchor points of the UC envelope. Blue squares are the intersection of the unit circle with a straight line of slope $-\nu_{xy}^L$. The Young moduli should be taken as the compressive or tensile Young moduli, according to the strength of interest. The dashed black lines represent a fictitious last ply failure envelope. The vertical dashed black lines come from the 0° envelope whereas the horizontal ones are from the 90° envelope, see Fig. 4.5.

A fictitious unit circle is constructed in Fig. 4.4[5]. It is composed of two quarter of circle of radius X^T/E_1 and X^C/E_1, see quadrants I and III respectively, and two ellipses whose axis are the longitudinal strains to failure X^T/E_1 and X^C/E_1, see quadrants II and IV. A unit circle embedded in a last ply failure envelope is depicted in Fig. 4.5 for the IM7/977-3 material system from [43]. The ultimate

[4] Alternatively, one can use the Trace theory if only E_1 is known.

[5] The last ply failure envelope depicted in Fig. 4.4 is purely fictitious and has been drawn for the reader's information. Tsai et al. [43, Fig. 4] have drawn several LPF envelopes and corresponding unit circles.

unnotched strengths of the composite X_L is then found by intersecting the unit circle envelope with a straight line of slope $-\nu_{xy}^L$, and multiplying the ε_x value of the intersection by the laminate longitudinal Young modulus E_x^L.

Tsai et al. [43] proposed that the degraded ply properties should be used to compute the laminate stiffness matrix in order to go to the stress space representation of the unit circle. This makes sense since the Unit Circle is proposed to be an approximation of a Last Ply Failure envelope. Therefore, one should use the degraded laminate Poisson ratio $\nu_{xy}^{L,\text{degr.}}$ and longitudinal Young modulus $E_1^{L,\text{degr.}}$. However, the construction of the unit circle requires the intact longitudinal Young modulus E_1, see Fig. 4.4. The MFH degradation method was chosen, since it gave better results that the mRoM method, see Sect. 4.1.2.3.

When the unit circle was first implemented in the C++ code, it was noticed that using the intact Poisson ratio and longitudinal Young modulus of the laminate instead of the degraded one provided in general better results. Indeed, a comparative study of both criteria (i.e. unit circle with intact and degraded elastic properties) on the NIAR dataset in RTD conditions shows that the unit circle with intact properties outperforms the unit circle with degraded ply properties, except for quasi-isotropic lay-ups in tension and hard ones in compression, see Tables 4.5 and E.4. It should be noted that even if the unit circle with intact properties is definitely better for soft lay-ups, the unnotched strength for such lay-ups is still under-predicted, sometimes dramatically. This phenomenon might be explained by the fact that since soft lay-ups have very large in-plane Poisson ratio, compared to quasi-isotropic ones, the intersection of the straight line of slope $-\nu_{12}^L$ and the unit circle envelope lies in a more conservative zone w.r.t. the LPF envelope, see Fig. 4.4. Both criteria are not very well suited for prediction of open-hole hard and soft strength, see Table 4.5.

Layup	Loading	UC		UCD	
		μ[%]	σ[%]	μ[%]	σ[%]
QUASI	UNT	3.6	12.7	-8.3	10.7
	UNC	-4.5	7.8	-16.2	6.7
HARD	UNT	-10.8	9.3	-19.2	8.0
	UNC	8.8	10.2	1.0	10.3
SOFT	UNT	-9.2	14.6	-35.5	12.2
	UNC	-19.3	7.6	-42.2	7.0

Layup	Loading	UC		UCD	
		μ[%]	σ[%]	μ[%]	σ[%]
QUASI	OHT	-0.0	0.0	-0.0	0.0
	OHC	0.0	0.0	0.0	0.0
HARD	OHT	-10.1	8.9	-9.2	9.2
	OHC	12.9	6.5	16.8	6.6
SOFT	OHT	-17.3	9.2	-29.0	9.0
	OHC	-25.7	4.3	-34.5	5.0

Table 4.5: Mean error of the unnotched strength prediction (left) and open-hole strength prediction (right), for Unit Circle with intact (UC) and degraded (UCD) elastic properties. Error closest to zero is colored in blue. For detailed case by case unnotched prediction, refer to Table E.4. For detailed case by case open-hole strength prediction, refer to Table E.6. Mean (μ) and standard deviation (σ) are provided, in percent. Calibration is performed on QI lay-ups.

4.3 Comparison and best practice

The prediction of the unnotched strength was identified to be a key parameter in the accuracy of open-hole strength prediction, see Chap. 3 for instance. Earlier in this chapter, 5 unnotched strength criteria have been described: UC, UCD, LPF mRoM, LPF MFH and FPF 0. Adding the max-strain crite-

rion, see Sect. 1.2, it remains to compare those 6 criteria both when used for predicting the unnotched strength alone and when they are incorporated in the method to compute the open-hole strength on a real dataset, i.e. a dataset without $\mathscr{R}$-curve measurements.

4.3.1 Unnotched strength

The failure envelopes of the Last Ply Failure criterion using mRoM degradation method, First Ply Failure and Unit Circle are depicted in Fig. 4.5 for the material system IM7/977-3 [43]. It can readily be seen that if one uses the First Ply Failure criterion for predicting the tensile strength of a quasi-isotropic laminate for instance, it will lead to premature failure because of the intact failure envelopes of the 45° and 90° plies, hence the introduction of the degradation of the matrix, see Sect. 4.1.2. Properties degradation leads to very different envelopes, see Fig. 4.5. As already exposed hereinabove, the unit circle envelope is inscribed in the failure envelope of LPF, whose inner envelope are defined by the 0° and 90° plies only[6].

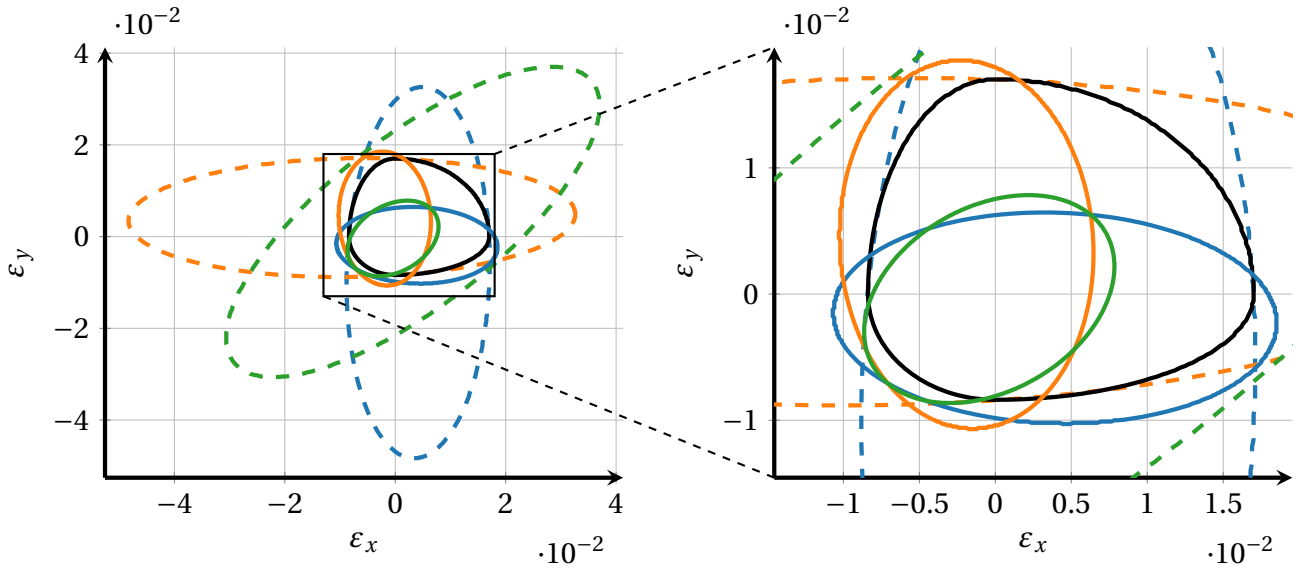

Figure 4.5: Comparison of Unit Circle, Last Ply Failure width mRoM degradation and First Ply Failure envelopes in the strain space for IM7/977-3 [43]. The First Ply Failure envelopes are represented by solid colored lines: 0° (——), 90° (——) and 45° (——). The Last Ply Failure envelopes are represented by dashed colored lines: 0° (- -), 90° (- -) and 45° (- -). The Unit Circle criterion is represented by the solid black line (——).

The unnotched criteria were compared on the NIAR dataset, for RTD conditions. Mean errors and standard deviations are provided in Table 4.6. Detailed case by case predictions can be found in Table E.5. Before diving in the conclusions, it is important to keep in mind that an error close to 0 is not a good indicator of the accuracy of a criterion. Indeed, a criterion providing wrong strengths scattered around zero might have a smaller mean error than a criterion providing conservative strength. Therefore, one has to look not only to means and standard deviations but also to case by case behaviour. That being said, the following conclusions can be drawn:

[6] In order to lighten Fig. 4.5, the envelopes corresponding to other ply orientations such as 15° or 60° were not plotted. However, it does not change the conclusion that the envelopes of the 0° and 90° plies are governing failure when considering LPF criterion [43].

- **Overall UN trend**:
  Without looking into details which criterion is best under particular loading and lay-up, the max-strain criterion seems to provide good predictions as it was the closest to the experimental UN strength on 18 case out of more than 57 experimental strengths, see Table E.5. It must be noted that the unit circle is ranked second.
- **QI UNT**:
  The unit circle with degraded elastic properties (UCD) is mostly useful for quasi-isotropic lay-ups in tension. Indeed, it showed the least error on 6 cases out of 10. It is more conservative than all the other criteria, whose tendency is generally to over-estimate the quasi-isotropic UNT. Unfortunately, the cases for which the UCD is not the best QI UNT criterion, it is quite far from the experimental value, e.g. IM7G/MTM45-1.
- **QI UNC**:
  Regarding quasi-isotropic compressive unnotched strength, it seems that no criterion stands out. However, the max-strain and FPF 0 criteria give generally comparable predictions, see Table E.5 and Table 4.6. Since FPF 0 requires more material strength data than the MS criterion, the latter should be preferred, especially during material screening campaigns.
- **Hard UNT and soft UNT**:
  The unit circle with intact properties (UC) is without doubt the most predictive criterion for hard and soft lay-ups in tension. Moreover, it is noted that when the UC is not the most predictive criteria, it generally provides a conservative prediction. Looking at Table 4.6 would lead to the conclusion that LPF mRoM and LPF MFH are better for hard lay-ups in tension: both criteria have a mean error closer to zero. However, the individual errors of those criteria are more scattered around zero than the UC criterion, with unsafe (e.g. IM7/8552 hard UNT) or too conservative (e.g. IM7G/MTM45-1 hard UNT) predictions. The advantage of UC is to provide most-of-the-time safe predictions.
- **Hard UNC**:
  It seems that the prediction of compressive hard strength should be performed with the Last Ply Failure criterion using the modified Rules of Mixtures degradation method (LPF mRoM). Indeed, even if it is not always the closest to experimental data, it is generally very close, see Table E.5. It must be noted however that the degraded unit circle (UCD) always provides a strength that is very close to that of LPF mRoM, while requiring only one strength, see Table E.5 and Table 4.6.
- **Soft UNC**:
  The max-strain criterion is by far the best of all 6 criteria concerning soft compressive strengths. It is always conservative[7]. Unfortunately, the predicted UN strength is always under-estimated, sometimes up to more than 30%. Nevertheless, the MS criterion is still the one for which the error is the smallest.

[7] The MS criterion is not conservative for soft MR60H-NB4708 in compression, but the error is nearly zero.

Layup	Loading	MS		UC		UCD		LPF mRoM		LPF MFH		FPF 0	
		μ[%]	σ[%]	μ[%]	σ[%]	μ[%]	σ[%]	μ[%]	σ[%]	μ[%]	σ[%]	μ[%]	σ[%]
QUASI	UNT	15.9	13.4	3.6	12.7	-8.3	10.7	6.1	10.8	4.1	11.2	13.3	12.1
	UNC	-2.4	8.1	-4.5	7.8	-16.2	6.7	-14.1	9.0	-11.2	8.5	-0.8	8.8
HARD	UNT	8.1	7.8	-10.8	9.3	-19.2	8.0	-2.9	13.8	-3.4	11.6	4.9	9.6
	UNC	13.1	10.3	8.8	10.2	1.0	10.3	1.8	8.9	5.5	9.7	2.3	8.0
SOFT	UNT	20.9	18.3	-9.2	14.6	-35.5	12.2	-21.6	13.7	-20.4	14.0	14.5	21.0
	UNC	-14.1	7.6	-19.3	7.6	-42.2	7.0	-36.5	10.3	-35.1	10.1	-29.9	9.2

Table 4.6: Mean error of the unnotched strength prediction, for Max-Strain (MS), Unit Circle with intact (UC) and degraded (UCD) elastic properties, Last Ply Failure criterion with mRoM (LPF mRoM) and MFH (LPF MFH) degradation methods and the First Ply Failure on the 0° ply only (FPF 0). Error closest to zero is colored in blue. For detailed case by case unnotched strength prediction, refer to Table E.5. Mean (μ) and standard deviation (σ) are provided, in percent.

It is to be noted that the above criteria will predict the same unnotched strength whatever the thickness of the plies, provided the ply thickness is uniform accross the laminate. Also, they will predict equal strengths for $[45/90/-45/0]_{10s}$ with 30g/m^2 plies or $[45/90/-45/0]_s$ with 300g/m^2 plies, i.e. they are insensitive to ply bunching. However, the experimental unnotched strengths are not the same for such laminates. For instance, M40JB/ThinPref 80EP/CF laminates with the aforementioned stacking sequences were tested in [37], and the unnotched strength varied from 814 MPa to 612 MPa. It is generally noticed that thinner plies lead to a more brittle-like behavior, the onset of damage mechanisms appearing nearly at ultimate failure stress and are thereby awaited to be better described with aforementioned unnotched strength criteria. It is very important to keep in mind that the criteria used hereinabove are not sensitive to ply ordering, while it makes sense to expect very different strengths whether 0° plies are inside or on the outside of the laminate, for instance.

4.3.2 Open-hole strength

It was shown earlier that having a very good prediction of the unnotched strength might be beneficial to the presented method for computing the open-hole strength. Because an unnotched criterion is more predictive than all the others on a specific case (i.e. given loading and lay-up) does not imply that this criterion should be used for predicting the open-hole strength. Indeed, the calibration of the average $\mathscr{R}$-curve now comes into play, as well as the remaining of the semi-analytical framework presented earlier.

An extensive comparison of the open-hole strength prediction depending on which unnotched criterion is used can be found in Table E.6. Mean errors and standard deviations are shown in Table 4.7. The calibration was performed on QI lay-ups since they are more common in usual test campaigns. The calibrated steady-state value of the $\mathscr{R}$-curve depends on the unnotched strength, as mentioned earlier, and will thereby vary from one UN criterion to another. Eventually, two factors are influencing open-hole strength: the unnotched strength and $\mathscr{R}_{ss}^{0,\text{calib.}}$. Therefore, the following is dedicated to discussing which unnotched criterion is best for predicting hard and soft open-hole strength based on the calibration of an average $\mathscr{R}$-curve on QI lay-ups, if only one UN criterion is to be used irrespective of the lay-up.

As a preliminary remark regarding results shown in Table E.6, it should be noted that the value of $\mathscr{R}_{ss}^{0,\text{calib.}}$ can significantly vary from one criterion to another. For instance, it can vary by as much as 30% in the case of IM7G/MTM45-1 in tension. It should also be noted that as far as the calibrated value in tension is concerned, it is always higher when calibrated with the degraded unit circle (UCD). As a reminder, it was concluded that the UCD provides the best quasi-isotropic tensile unnotched strength, the other criteria predicting larger strengths. This is consistent with the observation made several times ealier in this report: the higher the unnotched strength, the smaller the calibrated steady-state value of the $\mathscr{R}$-curve in order to match with the given open-hole strength on which calibration is performed. Since the calibration is performed on QI lay-ups, only hard and soft notched strengths will be discussed.

- **Hard OHT**:
  For hard lay-ups in tension, the LPF MFH method can be used quite safely, see Table E.6. Indeed, even if the method is not always the most accurate, it is in most cases very close to the experimental strength. A noticeable case for which all criteria are completely wrong at predicting the hard tensile strength is for the material system MR60H/NB4708. In this case, the nominal CPT is the highest of the NIAR dataset (0.32004 mm, see Table D.3) and the failure mode is a multi-mode failure, see Fig. D.3. As mentioned earlier in Sect. 1.6 and a couple more times, the thicker the ply, the more prone it is to delamination and matrix-dominated failure, which is not a failure mode in line with the present framework's assumptions. Moreover, the reported multi-mode failure is a clear indicator that this case does not fulfill the method's hypotheses.
  It should be pointed out that even if the LPF MFH method seems to be the most accurate, all the methods generally predict strengths in a very narrow range. This is correlated by Table 4.7, from which it is readily seen that all criteria lead to approximately the same mean error and standard deviation regarding open-hole strength prediction. On the contrary, the methods behave very differently as far as the unnotched strength is concerned. This might be due to the already identified poor sensitivity of predicted hard tensile strength to the unnotched strength, see Chap. 2. It should be noted that while $\mathscr{R}_{ss}^{0}$ was kept constant in Chap. 2 in order to stress the sensitivity of OH predictions w.r.t. UN strength, in this case $\mathscr{R}_{ss}^{0,\text{calib.}}$ varies from one UN criterion to another so that previous explanation is only a guess.
  As a conclusion, the LPF MFH criterion should be used if possible, but the use of another criteria such as the max-strain criterion might also work well.
- **Hard OHC**:
  The open-hole hard compressive strength is systematically over-estimated, whatever the unnotched criterion used, see Table 4.7. The FPF 0 criterion gives the less unsafe predictions.
- **Soft OH**:
  The open-hole soft strength was already mentioned as a no-go zone for the present framework, since it was generally under-predicted by more than 20%, especially in compression. Therefore, even if the max-strain criterion is appealing for reducing the committed error, it is still very disappointing.

Layup	Loading	MS		UC		UCD		LPF mRoM		LPF MFH		FPF 0	
		μ[%]	σ[%]	μ[%]	σ[%]	μ[%]	σ[%]	μ[%]	σ[%]	μ[%]	σ[%]	μ[%]	σ[%]
QUASI	OHT	-0.0	0.0	-0.0	0.0	-0.0	0.0	-0.0	0.0	-0.0	0.0	-0.0	0.0
	OHC	0.0	0.0	0.0	0.0	0.0	0.0	0.0	0.0	0.0	0.0	0.0	0.0
HARD	OHT	-8.9	8.5	-10.1	8.9	-9.2	9.2	-9.3	9.7	-8.6	9.8	-9.0	8.6
	OHC	13.3	6.5	12.9	6.5	16.8	6.6	16.2	6.9	15.6	6.8	9.2	6.4
SOFT	OHT	-10.8	10.3	-17.3	9.2	-29.0	9.0	-23.5	8.2	-22.7	8.1	-9.5	10.2
	OHC	-24.6	4.2	-25.7	4.3	-34.5	5.0	-32.2	4.9	-32.1	5.0	-31.2	4.9

Table 4.7: Mean error of open-hole strength prediction, for Max-Strain (MS), Unit Circle with intact (UC) and degraded (UCD) elastic properties, Last Ply Failure criterion with mRoM (LPF mRoM) and MFH (LPF MFH) degradation methods and the First Ply Failure on the 0° ply only (FPF 0). Error closest to zero is colored in blue. For detailed case by case open-hole strength prediction, refer to Table E.6. Mean (μ) and standard deviation (σ) are provided, in percent. Calibration is performed on QI lay-ups.

As a reminder, provided that the thickness of the plies is homogeneous through-the-thickness, the framework will predict the same open-hole strength regardless of the thickness. The method is therefore not capable of predicting varying strength resulting from varying ply thickness. However, as previously noticed, the method is expected to work well in case of thin-ply laminates that do not fail by delamination, expected to fail for thicker plies that are generally more prone to delamination, which is in contradiction with the framework's hypothesis. The framework is not capable of predicting the *inverse* hole size effect neither.

4.3.3 Best practice

In Sect. 4.3.1 and Sect. 4.3.2, the influence of using a given unnotched strength criterion has been discussed. In the following, an attempt will be made to use the best practice rules derived above regarding the unnotched strength prediction. For that sake, instead of using the same criterion irrespective of the layup and loading, the unnotched criterion will be adapted to each of the 6 following cases: quasi-isotropic, hard and soft lay-ups, each in tension or compression. A summary of the chosen criteria is shown in Table 4.8. For shortening notations, the ensemble of choices in Table 4.8 will be named BEST criterion hereinbelow, standing for Best Estimate of the unnotched STrength. In cases where material strength data is incomplete, i.e. not enough strengths are provided to apply Tsai-Wu-based criteria (e.g. FPF 0 or LPF mRoM), a fall-back method must be chosen. For QI lay-ups in compression, it is chosen to be the max-strain criterion, showing good agreement with the experimental data whereas for hard coupons in compression, the degraded unit circle with MFH degradation method is preferred.

	QI	Soft	Hard
UNT	UCD	UC	UC
UNC	FPF 0 ↳MS	MS	LPF mRoM ↳UCD

Table 4.8: BEST configuration, with fall-back methods in case of insufficient strength data for applying Tsai-Wu-based criterion.

A comparison of the BEST criterion with all the other criteria is shown in Table E.7, for unnotched strength prediction. Detailed notched prediction is also shown in Table E.8. Mean errors and standard deviations for UN strength are given in Table 4.9 and in Table 4.10 for the notched strength. Bar charts are provided in Fig. E.1 to E.3, showing both UN and OH prediction. As awaited, the criterion outperforms all the others, since it is a mixing of the unnotched criteria on a per layup and per loading basis.

Layup	Loading	BEST		MS		UC		UCD		LPF mRoM		LPF MFH		FPF 0	
		μ[%]	σ[%]	μ[%]	σ[%]	μ[%]	σ[%]	μ[%]	σ[%]	μ[%]	σ[%]	μ[%]	σ[%]	μ[%]	σ[%]
QUASI	UNT	-8.3	10.7	15.9	13.4	3.6	12.7	-8.3	10.7	6.1	10.8	4.1	11.2	13.3	12.1
	UNC	-0.3	8.8	-2.4	8.1	-4.5	7.8	-16.2	6.7	-14.1	9.0	-11.2	8.5	-0.8	8.8
HARD	UNT	-10.8	9.3	8.1	7.8	-10.8	9.3	-19.2	8.0	-2.9	13.8	-3.4	11.6	4.9	9.6
	UNC	0.1	9.2	13.1	10.3	8.8	10.2	1.0	10.3	1.8	8.9	5.5	9.7	2.3	8.0
SOFT	UNT	-9.2	14.6	20.9	18.3	-9.2	14.6	-35.5	12.2	-21.6	13.7	-20.4	14.0	14.5	21.0
	UNC	-14.1	7.6	-14.1	7.6	-19.3	7.6	-42.2	7.0	-36.5	10.3	-35.1	10.1	-29.9	9.2

Table 4.9: Mean error of the unnotched strength prediction for best practice (BEST), Max-Strain (MS), Unit Circle with intact (UC) and degraded (UCD) elastic properties, Last Ply Failure criterion with mRoM (LPF mRoM) and MFH (LPF MFH) degradation methods and the First Ply Failure on the 0° ply only (FPF 0). Error closest to zero is colored in blue. For detailed case by case unnotched strength prediction, refer to Table E.7. Mean (μ) and standard deviation (σ) are provided, in percent.

Layup	Loading	BEST		MS		UC		UCD		LPF mRoM		LPF MFH		FPF 0	
		μ[%]	σ[%]	μ[%]	σ[%]	μ[%]	σ[%]	μ[%]	σ[%]	μ[%]	σ[%]	μ[%]	σ[%]	μ[%]	σ[%]
QUASI	OHT	-0.0	0.0	-0.0	0.0	-0.0	0.0	-0.0	0.0	-0.0	0.0	-0.0	0.0	-0.0	0.0
	OHC	0.0	0.0	0.0	0.0	0.0	0.0	0.0	0.0	0.0	0.0	0.0	0.0	0.0	0.0
HARD	OHT	-5.9	8.8	-8.9	8.5	-10.1	8.9	-9.2	9.2	-9.3	9.7	-8.6	9.8	-9.0	8.6
	OHC	8.4	6.4	13.3	6.5	12.9	6.5	16.8	6.6	16.2	6.9	15.6	6.8	9.2	6.4
SOFT	OHT	-14.1	10.0	-10.8	10.3	-17.3	9.2	-29.0	9.0	-23.5	8.2	-22.7	8.1	-9.5	10.2
	OHC	-25.1	4.0	-24.6	4.2	-25.7	4.3	-34.5	5.0	-32.2	4.9	-32.1	5.0	-31.2	4.9

Table 4.10: Mean error of the open-hole strength prediction, for best practice (BEST), Max-Strain (MS), Unit Circle with intact (UC) and degraded (UCD) elastic properties, Last Ply Failure criterion with mRoM (LPF mRoM) and MFH (LPF MFH) degradation methods and the First Ply Failure on the 0° ply only (FPF 0). Error closest to zero is colored in blue. For detailed case by case open-hole strength prediction, refer to Table E.8. Mean (μ) and standard deviation (σ) are provided, in percent. Calibration was performed on QI lay-ups.

It is easily seen from Table 4.10 that the hard open-hole tensile strength prediction works satisfactorily, with largest errors for MR60H/NB4708 (-22%, index 10), CytecT40-800/Cycom5215 (-19%, index 6) and IM7G/MTM45-1 (-12%, index 5), see Fig. E.2. The use of the experimental unnotched strength does not seem to provide any better results for these three cases. It is noted that in addition to having the thickest nominal ply thickness, MR60H-NB4708 is reported to fail in multi-mode so that the framework is not expected to work well. The two remaining cases were reported to fail by mixed lateral/multi-mode failure and angled mode, respectively. It is very important to note that while being erroneous, these predictions are safe. As a side note, it was reported that the IM7G/MTM45-1

hard tensile tests sometimes ended up with delamination (DGM) and longitudinal splitting (SGM), see [51, p. 205]. The fact that the predicted hard tensile open-hole strength of IM7G/MTM45-1 using BEST is close to the one predicted using experimental UN strength is a stroke of luck. Indeed, the hard UNT strength is definitely under-estimated but looking at the calibrated $\mathscr{R}^0_{ss}$, it is higher when using BEST than when the experimental UN strength is used, since the QI UNT strength was also under-estimated. The higher steady-state value luckily compensate for the under-prediction of the hard unnotched tensile strength.

As regards the hard open-hole compressive strength, the notched strength predictions are unsafe, the largest errors occuring for IM7G/EpoxyEP2202 (18%, index 8) and IM7G/MTM45-1 (20%, index 5), see Fig. E.2. Unfortunately, the predominant failure mode is reported to be lateral for both cases, in line with the framework's assumptions. The predictions made with the experimental unnotched strength are not satisfactory either. For IM7G/EpoxyEP2202, it is unclear if the large error in OH strength comes from the calibration of $\mathscr{R}^0_{ss}$ since no experimental UNC strength was provided. Regarding IM7G/MTM45-1, some further comments can be made. Firstly, a large scatter among the 7 normalized experimental hard OH strength has been noticed, see [51, p. 231], ranging from 304 MPa to 390 MPa, approximately. The reported normalized experimental strength of 344 MPa was taken as the average of those 7 tested coupons and might be questionable since the reported coefficient of variation of the measured OH compressive strengths was as large as 8%. Eventually, the hard laminate Young modulus is reported to be 84.46 GPa but LPT predicts 90.96 GPa, a difference of 7.7% in one of the very basic components of the framework. As a conclusion, while analyzing the error in open-hole predictions, a lot of factors come into play. Moreover, it is of paramount importance to keep in mind that composite materials are characterized by variability of material properties and fiber orientation, requiring a statistical analysis rather than a deterministic one [3].

As the soft open-hole strength is concerned, no improvement is noticed when using the BEST criterion, as expected. The soft strength predictions are still mainly under-estimated. As a reminder, this is due to multiple reasons. Firstly, the soft coupons are generally failing by angled or multi-mode failure modes. A large majority of soft tensile coupons failed by angled mode, probably because of the very high proportion of 45° plies. Moreover, the onset of macroscopic failure might also be preceded by local-level delamination, especially for compressive coupons. Eventually, as mentioned in Chap. 3, plastic deformation might occur in the vicinity of crack tip. Since these facts are not modeled by the semi-analytical framework, it is concluded that it should not be used for predicting the notched strength of soft coupons.

Unfortunately, the NIAR dataset does not provide other hole diameters than 6.35 mm. Therefore, the ability of the present framework to predict hard strength with varying hole size can not be estimated.

4.4 Conclusions

In this chapter, unnotched strength criteria have been analyzed in details, namely the Last Ply Failure with two different degradation methods (modified Rules of Mixtures and Mean-Field Homogenization), the Unit Circle with intact and degraded elastic properties, and the First Ply Failure on the 0° ply only, with intact elastic properties. Best practice rules have been derived for predicting the unnotched

strength in RTD conditions, see Table 4.8. These rules specify which unnotched criterion should be used for given loading and lay-up for best UN strength prediction. The unnotched strength prediction is therefore generally better. Using these best practice rules for predicting hard notched strength has been shown beneficial, as it is generally in very good agreement with experimental data, except if the reported experimental failure modes are not supported by the present framework (delamination, angled failure or splitting). However, the notched strength prediction of soft coupons still suffers from huge under-estimations.

A summary of the accuracy obtained with the above framework, i.e. full elastic characterization, BEST unnotched strength criterion and calibration of an average $\mathscr{R}$-curve, is shown in Table 4.11. Compared to the framework in which a simple max-strain criterion is used, see Table 3.4, hard compressive strength has been improved, since both the mean error and the number of predictions in a ±10% error range get better, see Table 4.10 (BEST and MS labeled columns). The hard tensile strength has also been improved a little. Regarding soft strength, no improvement is noticed.

Layup		Hard		Soft	
Loading		OHT	OHC	OHT	OHC
Number of predictions in	±10%	7/10	8/10	0/10	0/10
	±15%	8/10	8/10	5/10	0/10

Table 4.11: Summary of the acuracy of the framework, with full elastic characterization, BEST criterion for the unnotched strength and calibration of an average $\mathscr{R}$-curve on the strength of a QI lay-up. Case by case prediction can be found in Fig. E.1 to E.3.

5 Residual Curing Stresses

In this chapter, residual thermal stresses due to curing are included in the framework stated above. Indeed, as explained in Sect. G.1, the fabrication process of laminated unidirectional composites induces residual stresses due to the temperature difference between fabrication and testing environments. The method will be assessed on the NIAR dataset [10] since for each material report, the temperature of each environment is provided. The curing temperature is generally given in process specification document, referenced in the material report.

5.1 Method

In this section, the method applied to take into account the residual stresses is exposed. It is based on thermo-elasticity.

Assuming that the temperature field is uniform across the thickness of the laminate[1], and assuming linear elasticity, let the stresses be expressed as:

$$\boldsymbol{\sigma} = \mathbb{E} : \boldsymbol{\varepsilon} + \boldsymbol{\sigma}_R, \tag{5.1}$$

where $\boldsymbol{\sigma}_R$ is the residual Cauchy stress tensor due to thermal stresses. The thermal expansion in the ply (i) in the *global* axes due to a temperature difference ΔT can be written as follows:

$$\boldsymbol{\varepsilon}_R^{(i)} = \boldsymbol{\alpha}^{(i)} \left(T_{\text{test}} - T_{\text{cure}}\right) \tag{5.2}$$

$$= \boldsymbol{\alpha}^{(i)} \Delta T \tag{5.3}$$

where the thermal expansion tensor of the ply (i), $\boldsymbol{\alpha}^{(i)}$, can be expressed from a suitable rotation of the thermal expansion tensor of the 0° ply $\boldsymbol{\alpha}^0$:

$$\boldsymbol{\alpha}^0 = \begin{pmatrix} \alpha_L & 0 & 0 \\ 0 & \alpha_T & 0 \\ 0 & 0 & \alpha_T \end{pmatrix}, \tag{5.4}$$

[1] Some authors mentioned that a finite-width composite laminate is in fact under a thre-dimensional non-uniform state of stress, with boundary layers at the free edges that can cause premature delamination [52].

with α_L and α_T the longitudinal and transverse expansion coefficients of the material. It is thus assumed that the ply expands as a transversely isotropic material. The lack of information about thermal expansion coefficients has been compensated for by using default values: $-3\cdot10^{-8\circ}\,\mathrm{C}^{-1}$ for α_L and $3\cdot10^{-5\circ}\,\mathrm{C}^{-1}$ for α_T. If the total strain of the laminate is denoted by $\boldsymbol{\varepsilon}^*$, the stress in the ply (i) may be written as:

$$\boldsymbol{\sigma}^{(i)} = \mathbb{E}^{(i)} : \left(\boldsymbol{\varepsilon}^* - \boldsymbol{\varepsilon}_R^{(i)}\right) \tag{5.5}$$

$$= \mathbb{E}^{(i)} : \left(\boldsymbol{\alpha}^* - \boldsymbol{\alpha}^{(i)}\right)\Delta T, \tag{5.6}$$

where $\boldsymbol{\alpha}^*$ is the thermal expansion tensor of the laminate. At rest, forces are balanced, implying:

$$\sum_i^N t^{(i)}\boldsymbol{\sigma}^{(i)} = \mathbf{0} \tag{5.7}$$

$$\Leftrightarrow \sum_i^N t^{(i)}\mathbb{E}^{(i)} : \left(\boldsymbol{\varepsilon}^* - \boldsymbol{\alpha}^{(i)}\Delta T\right) = \mathbf{0} \tag{5.8}$$

$$\Leftrightarrow \left(\sum_i^N t^{(i)}\mathbb{E}^{(i)}\right) : \boldsymbol{\varepsilon}^* = \Delta T \sum_i^N \mathbb{E}^{(i)} : \boldsymbol{\alpha}^{(i)} \tag{5.9}$$

$$\Leftrightarrow \boldsymbol{\varepsilon}^* = \Delta T \left(\sum_i^N t^{(i)}\mathbb{E}^{(i)}\right)^{-1} : \left(\sum_i t^{(i)}\mathbb{E}^{(i)} : \boldsymbol{\alpha}^{(i)}\right) = \boldsymbol{\alpha}^*\Delta T, \tag{5.10}$$

from which $\boldsymbol{\alpha}^*$ is easily extracted:

$$\boldsymbol{\alpha}^* = \left(\sum_i^N t^{(i)}\mathbb{E}^{(i)}\right)^{-1} : \left(\sum_i t^{(i)}\mathbb{E}^{(i)} : \boldsymbol{\alpha}^{(i)}\right) \tag{5.11}$$

Eventually, the residual stresses in the ply (i), in the direction of the fibers of the 0° ply (i.e. in the *global* axes), is expressed as:

$$\boldsymbol{\sigma}_R^{(i)} = \Delta T\mathbb{E}^{(i)} : \left(\boldsymbol{\alpha}^* - \boldsymbol{\alpha}^{(i)}\right) \tag{5.12}$$

The above method looks very similar to the developments of Miller [53]. In fact, the above method was not derived with usual laminate plate theory notation, but can be matched with results found in Miller [53]. In this work, the linear coefficients of thermal expansion α and the bending coefficients of the thermal straining χ for a laminate are defined as:

$$\left\{\begin{array}{c}\alpha\\ \chi\end{array}\right\}_L = \frac{1}{\Delta T}\left[\begin{array}{cc}A & B\\ B & D\end{array}\right]^{-1}\left\{\begin{array}{c}N\\ M\end{array}\right\}_T, \tag{5.13}$$

where A, B, D are the extensional, extensional-bending, and bending laminate constitutive matrices, respectively, and N and M are the stress resultants and stress couples of the laminate. The subscripts L and T stands for laminate and thermal, respectively. In the context of the present report, only symmetrical balanced laminates are considered, such that the B matrix vanishes. Therefore, the thermal expansion matrix α_L is given by $\alpha_L = \Delta T^{-1}A^{-1}N_T$.

This procedure is completely analogous to Eq. (5.11) since:

$$N_{T,i} = \int_{-h/2}^{h/2} Q_{ij}\alpha_j\Delta T\,dz = \sum_{I=1}^{N} Q_{ij}^{(I)}\alpha_j^{(I)}\Delta T\,t^{(I)}, \tag{5.14}$$

$$A_{ij} = \int_{-h/2}^{h/2} Q_{ij}\, dz = \sum_{I=1}^{N} Q_{ij}^{(I)}\, t^{(I)}. \tag{5.15}$$

The C++ function computing the laminate expansion tensor $\boldsymbol{\alpha}^*$ has been validated against [54]. A detailed explanation of the procedure can be found in Sect. F.1.

There remains to incorporate the residual stresses in the framework stated in the previous chapter, see Chap. 4.

5.2 Residual stresses for Max-Strain and Unit Circle

If one uses Unit Circle criterion, see Sect. 4.2, the residual stresses are included in the criterion as follows:

$$\begin{aligned} X_r^T &= X^T - \boldsymbol{\sigma}_{R,11}^0, \\ X_r^C &= X^C + \boldsymbol{\sigma}_{R,11}^0. \end{aligned} \tag{5.16}$$

Eq. (5.16) are easy to interpret. If curing induces tensile residual stresses, the effective tensile strength is reduced, whereas the effective compressive strength increases. On the contrary, if curing induces compressive residual stresses, the effective compressive strength decreases whereas the effective tensile strength increases. A similar procedure is applied for the unit circle with degraded properties (UCD) and the max-strain criterion (MS).

The method Eq. (5.16) does not lead to any noticeable change in the unnotched strength prediction. This is expected as the residual stresses in the *global* axes of 0° plies is very low, see Table 5.1a.

5.3 Residual stresses for Tsai-Wu criterion and alike

5.3.1 First approach

The procedure that was adopted as a first approach for incorporating residual stresses in the Tsai-Wu criterion is very similar to that of the Unit Circle, see Sect. 5.2. The initial material strengths are simply replaced by:

$$\begin{aligned} X_r^T &= X^T - \boldsymbol{\sigma}_R^{(i),\theta}{}_{,11} \\ X_r^C &= X^C + \boldsymbol{\sigma}_R^{(i),\theta}{}_{,11} \\ Y_r^T &= Y^T - \boldsymbol{\sigma}_R^{(i),\theta}{}_{,22} \\ Y_r^C &= Y^C + \boldsymbol{\sigma}_R^{(i),\theta}{}_{,22} \\ S_r &= S - \boldsymbol{\sigma}_R^{(i),\theta}{}_{,12} \end{aligned}$$

where the residual stresses $\boldsymbol{\sigma}_R^{(i),\theta}$ used is the residual stress in the direction of the fibers of the ply (i) (i.e. *local* axes), oriented with an angle θ, which is not the same as the residual stress derived in Sect. 5.1 but a rotated one, see Sect. F.1.

The method exposed hereinabove is not adapted at all if one wants to take into account the residual stresses due to curing. In the following, the reason why such a method fails is exposed, with an example on the AS4/MTM45-1 from NIAR in CTD conditions, for a First Ply Failure on the 0° ply only criterion. Fig. 5.1 shows the 0° envelope in both stress and strain space, for three distinct cases: with the experimental strengths, i.e. without incorporating residual thermal stresses, with residual stresses taken into account and interaction factor of -0.5, and with a null interaction factor. Table 5.1a gives the initial strengths and those after subtracting the residual stresses. It is noted that the transverse tensile strength Y^T has been decreased by nearly 100%, and there exists some material systems for which it even became negative, thus preventing the use of Tsai-Wu-based failure criterion. It is also noted that the longitudinal strengths are left nearly unchanged since the residual stresses in the fiber direction is very small and that the shear strength remains unchanged for the very reason that no residual shear stress exists in a 0° ply. Since the Tsai-Wu envelope in the stress space must go through the 4 ply strengths X^T, X^C, Y^T ,Y^C, the supplementary requirement that the envelope is closed leads to an oblate envelope, see Fig. 5.1. In the ε_x-ε_y strain space, there are also 4 anchor points through which the envelope is required to pass, see Eq. (5.17), that explain why the envelope gets stretched as the transverse tensile strength decreases, see Fig. 5.1. Indeed, the two longitudinal strengths are nearly aligned with the transverse tensile strength, artificially increasing the strength of the ply in tension. Therefore, one needs to deal with residual stresses in another manner. It must be noted that the above approach was used in the beginning because it was very easy to integrate into computational code: only the strengths are changed.

$$\begin{aligned}&\left(\frac{X^T}{E_1};\frac{-\nu_{12}X^T}{E_1}\right),\left(\frac{X^C}{E_1};\frac{\nu_{12}X^C}{E_1}\right),\\&\left(\frac{-\nu_{21}Y^T}{E_2};\frac{Y^T}{E_2}\right),\left(\frac{\nu_{21}Y^C}{E_2};\frac{Y^C}{E_2}\right).\end{aligned} \tag{5.17}$$

Strength	Exp. [MPa]	Final [MPa]
X^T	1814.011	1817.621
X^C	1598.274	1594.664
Y^T	48.953	1.044
Y^C	264.414	312.323
S	94.577	94.577

(a) Experimental ply strengths (*Exp.*) and ply strengths after subtracting the residual thermal stresses in the local ply orthotropic axes (*Final*) are given.

E_x^L [MPa]	76061.835
ν_{xy}^L [-]	0.422

(b) Laminate elastic properties.

Table 5.1: Some material properties for the material system AS4/MTM45-1 from NIAR [10], in CTD environmental condition, for the 0° ply in a stacking sequence $[0/45/0/90/0/-45/0/45/0/-45]$.

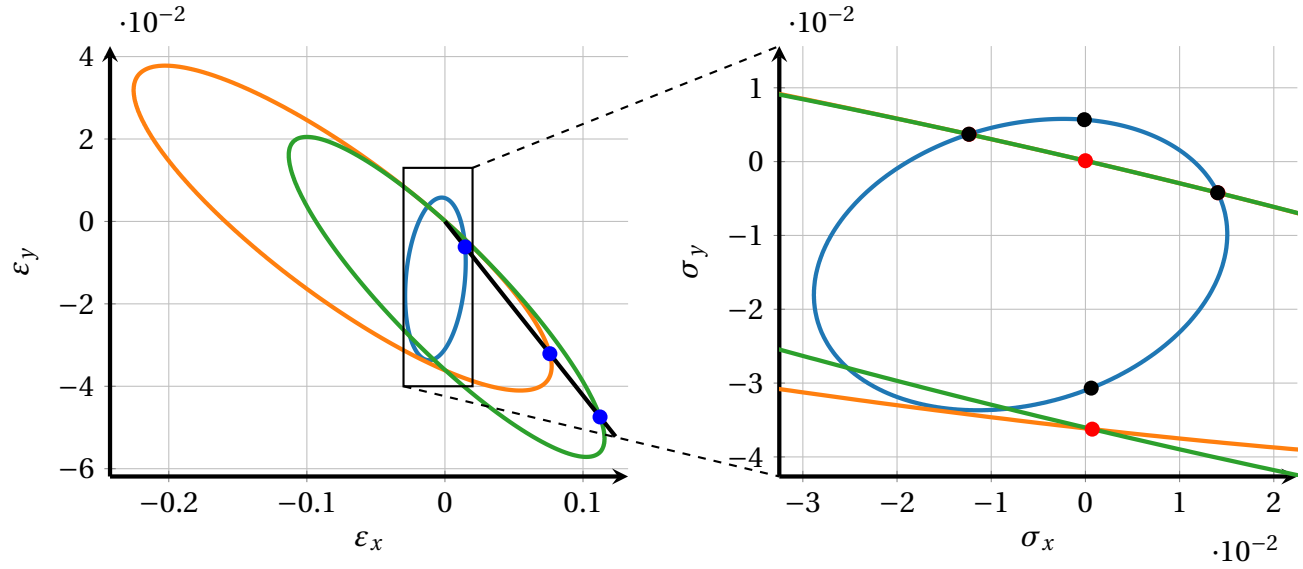

(a) Strain space envelopes (left) and zoom on the zone of interest (right). Anchor points are shown: initial strength (●) and modified strength according to Sect. 5.3.1 (●). The intersections between the envelopes and the black solid line of slope $-\nu_{xy}^{L}$ (●) give the following strength: 1113.98 MPa, 5780.20 MPa, 8544.55 MPa.

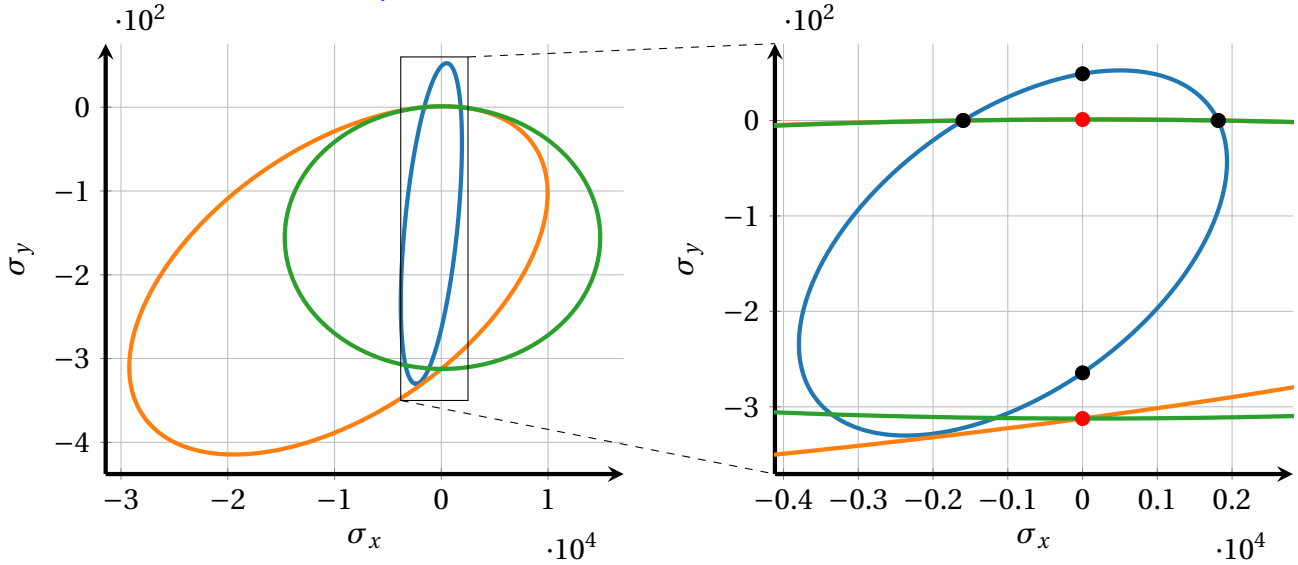

(b) Stress space envelopes (left) and zoom on the zone of interest (right). Anchor points are shown: initial strength (●) and modified strength according to Sect. 5.3.1 (●).

Figure 5.1: Tsai-Wu failure envelope of the 0° ply of AS4/MTM45-1 from NIAR in CTD condition, without residual thermal stresses (—), with residual thermal stresses incorpated as in Sect. 5.3.1 (—) and with residual thermal stresses and a null interaction term (—). The strengths are given in Table 5.1. It must be noted that some anchor points overlap due to nearly unchanged strength after subtracting residual stresses. The stacking sequence is $[0/45/0/90/0/-45/0/45/0/-45]$.

5.3.2 Second approach

In the previous sections, the residual stresses were taken into account by changing the material strengths, thereby changing the failure envelope. Incorporated to the unit circle or the max-strain criterion, residual stresses does not significantly affect the ultimate predicted strength. Regarding Tsai-Wu-like

criteria, the previous method was concluded not efficient and misbehaving because of the closed-envelope restriction.

Therefore, a new approach is proposed, see Fig. 5.2. Instead of changing the strengths of each ply before drawing its envelope and start from a zero state of strain, the initial state of strain is taken as the residual thermal strain state in the 0° direction of the laminate, named *global axes* hereinafter. Whereas 0° and 90° plies will not undergo residual shear stresses, the −45° (or any other angle) ply will exhibit some non-negligible mechanical shear strains, see Sect. F.2. Therefore, the Tsai-Wu criterion described in Sect. 4.1.1 must be solved in the ε_x-ε_y-γ_{xy} strain space instead of the ε_x-ε_y strain space as it was done previously. That is to say, the terms related to shear in Eq. (4.5) are not discarded anymore. It is to be noted that Fig. 5.2 is representing a case in which γ_{xy} is zero. Assuming linear elasticity, the following can be inserted in Eq. (4.5):

$$\begin{aligned}\varepsilon_x &= \boldsymbol{\varepsilon}_{R}^{(i)}{}_{,11} + \Delta\varepsilon_x,\\ \varepsilon_y &= \boldsymbol{\varepsilon}_{R}^{(i)}{}_{,22} - \nu_{xy}^{L}\Delta\varepsilon_x,\\ \gamma_{xy} &= \boldsymbol{\varepsilon}_{R}^{(i)}{}_{,12},\end{aligned}$$

and it remains to solve for $\Delta\varepsilon_x$[2], see Fig. 5.2. The ultimate strength is given by $E_x^L \cdot \Delta\varepsilon_x$.

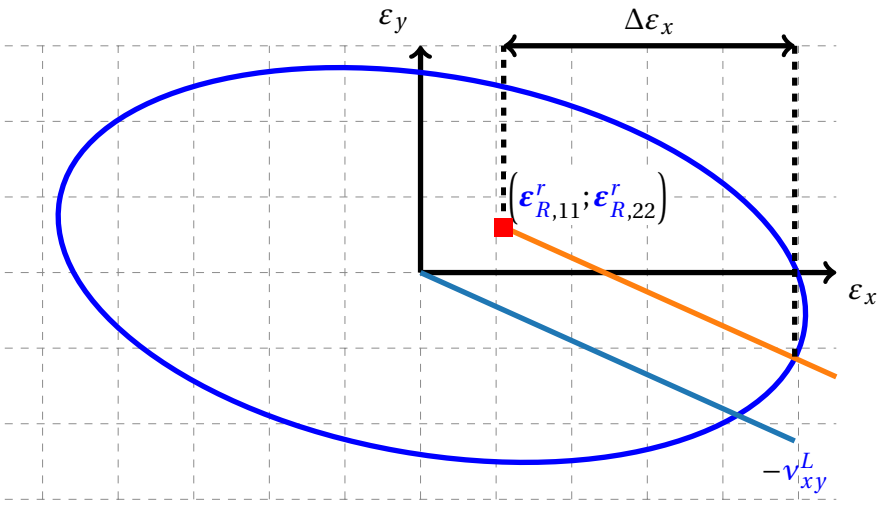

Figure 5.2: Schematic view of the method to integrate the residual thermal stresses, see Sect. 5.3.2. The initial state of strain of the ply is not the origin but the state of residual thermal strains. The line of slope $-\nu_{xy}^L$ is simply shifted.

Tables F.1, F.3 and F.5 show a comparison of the predicted unnotched strength for the Tsai-Wu-based failure criteria with and without the residual thermal stresses, alongside with the BEST criterion. Tables F.2, F.4 and F.6 show the predicted open-hole strength when those criteria are used. These comparisons are made for RTD, CTD and ETW environmental conditions. Mean errors and standard deviations are presented in Tables 5.3a to 5.3c for the open-strength prediction and in Tables 5.2a to 5.2c for unnotched strength prediction.

In order to be complete, it is very important to keep in mind that the errors shown in the aforementioned tables can be misleading. Indeed, when material data is not sufficient to apply a criterion,

[2]Note that Eq. (4.5) becomes simply a quadratic function of $\Delta\varepsilon_x$, from which two roots are extracted: the tensile and compressive longitudinal strain-to-failure of the laminate.

the fall-back method in the C++ implementation of the framework in the Unit Circle. Therefore, if the initial criterion was a First Ply Failure, the Unit Circle with intact properties is used, whereas the degraded Unit Circle is used if the criterion to apply was a Last Ply Failure. In the tables showing case by case results, the duplicated results are removed. For instance, if all criteria fall-back to the unit circle, only one value will be shown. That being said, the results can be discussed.

CTD conditions As a preliminary remark, it is noted that compressive strength is never given in the NIAR dataset, neither for unnotched nor for notched strength.

Regarding unnotched strength prediction in CTD conditions, the BEST criterion, which does not take into account residual stresses, is still very good. Nevertheless, it is observed that the unnotched strength prediction using Tsai-Wu-based criteria is enhanced in some cases when incorporating the residual stresses. A striking example is the MR60H/NB4708 material system for which the Last Ply Failure with modified Rules of Mixtures and residual thermal stresses (*mRoM TRS* in Table F.1) is nearly equal to the experimentally measured unnotched strength whereas the error in the predicted UN strength was as high as 26% when the residual strains were ignored.

As the hard tensile open-hole strength is concerned, the errors are remarkably small when the BEST criterion is used, see Tables 5.2a and F.1. The soft tensile strength is still overly under-predicted.

As a conclusion, for CTD conditions, it seems that the unnotched strength can be improved by taking into account residual thermal stresses. However, the open-hole strength prediction should still be performed with the best practice rules, leading to hard tensile strengths that are in very good agreement with experimental data.

RTD conditions The UN strength is still better described by the BEST criterion. The notched predictions are therefore not expected to be enhanced when thermal residual stresses are taken into account, which is indeed the case, see Tables 5.2b and F.3.

ETW conditions The unnotched quasi-isotropic strength might be predicted with the First Ply Failure on the 0° ply, with thermal residual stresses incorporated. However, it is noted that for the cases in which it is not the best criterion, it is in fact far from the experimental value, see MR60H/NB4708 for instance (Table F.5). For quasi-isotropic lay-ups in compression, the BEST criterion should be applied, i.e. First Ply Failure on the 0° ply without thermal residual stresses. Looking at the mean errors only, the BEST criterion should also be used for hard and soft unnotched strengths, since it has the benefit to provide generally conservative predictions.

Regarding the notched prediction of hard compressive and soft tensile coupons, the FPF 0 criterion seems to be a good choice. For hard tensile coupons and soft compressive coupons, the framework seems not adapted. It should be noted that for concluding relevant rules of best practice for ETW conditions, more data is needed.

Layup	Loading	BEST		mRoM		mRoM TRS		MFH		MFH TRS		FPF0		FPF0 TRS	
		μ[%]	σ[%]	μ[%]	σ[%]	μ[%]	σ[%]	μ[%]	σ[%]	μ[%]	σ[%]	μ[%]	σ[%]	μ[%]	σ[%]
QUASI	UNT	-3.2	13.0	12.7	15.1	9.2	17.9	11.4	16.8	9.2	18.3	17.2	14.8	7.7	21.3
	UNC	nan	nan	nan	nan	nan	nan	nan	nan	nan	nan	nan	nan	nan	nan
HARD	UNT	-5.3	9.9	-1.8	8.0	-11.6	17.1	-1.6	7.2	-9.3	15.3	4.0	5.3	-3.4	10.3
	UNC	nan	nan	nan	nan	nan	nan	nan	nan	nan	nan	nan	nan	nan	nan
SOFT	UNT	-4.2	16.6	-13.2	16.4	-19.6	20.4	-12.2	16.6	-18.1	19.7	10.6	23.9	5.5	18.1
	UNC	nan	nan	nan	nan	nan	nan	nan	nan	nan	nan	nan	nan	nan	nan

(a) Mean errors of the unnotched strength prediction in CTD.

Layup	Loading	BEST		mRoM		mRoM TRS		MFH		MFH TRS		FPF0		FPF0 TRS	
		μ[%]	σ[%]	μ[%]	σ[%]	μ[%]	σ[%]	μ[%]	σ[%]	μ[%]	σ[%]	μ[%]	σ[%]	μ[%]	σ[%]
QUASI	UNT	-8.3	10.7	6.1	10.8	3.2	13.3	4.1	11.2	1.7	12.2	13.3	12.1	7.6	11.8
	UNC	-0.3	8.8	-14.1	9.0	-21.3	10.8	-11.2	8.5	-18.0	9.8	-0.8	8.8	-45.1	22.8
HARD	UNT	-10.8	9.3	-2.9	13.8	-14.2	15.0	-3.4	11.6	-12.3	13.8	4.9	9.6	2.6	7.8
	UNC	0.1	9.2	1.8	8.9	-3.8	9.1	5.5	9.7	0.2	9.2	2.3	8.0	-36.8	22.3
SOFT	UNT	-9.2	14.6	-21.6	13.7	-28.4	15.3	-20.4	14.0	-26.8	15.2	14.5	21.0	16.1	20.9
	UNC	-14.1	7.6	-36.5	10.3	-41.9	11.7	-35.1	10.1	-40.2	11.3	-29.9	9.2	-62.2	22.0

(b) Mean errors of the unnotched strength prediction in RTD.

Layup	Loading	BEST		mRoM		mRoM TRS		MFH		MFH TRS		FPF0		FPF0 TRS	
		μ[%]	σ[%]	μ[%]	σ[%]	μ[%]	σ[%]	μ[%]	σ[%]	μ[%]	σ[%]	μ[%]	σ[%]	μ[%]	σ[%]
QUASI	UNT	-17.6	4.5	-25.4	10.2	-31.7	11.0	-25.9	9.9	-32.6	11.5	6.7	10.2	3.7	11.3
	UNC	-1.8	14.4	-18.8	10.5	-24.8	10.6	-11.7	12.2	-18.1	11.9	-1.8	14.4	-36.3	18.4
HARD	UNT	-22.8	2.6	-37.3	6.5	-44.5	5.3	-36.3	7.4	-43.9	7.4	10.7	11.6	10.0	12.6
	UNC	-2.9	10.2	-2.9	10.2	-9.4	9.5	6.2	10.8	-1.2	9.1	-4.3	9.5	-38.0	13.2
SOFT	UNT	-20.0	10.7	-43.4	5.3	-48.4	6.6	-41.7	6.0	-47.2	7.8	29.0	20.4	31.0	19.8
	UNC	-15.4	8.0	-39.2	7.4	-44.6	7.8	-34.3	7.6	-40.3	7.9	-40.9	9.3	-64.7	15.3

(c) Mean errors of the unnotched strength prediction in ETW.

Table 5.2: Prediction of unnotched strength, comparison of the following criteria: Best Practise (BEST), Last Ply Failure with mRoM (*mRoM*) and MFH (*MFH*) degradation method without Thermal Residual Stresses and with Thermal Residual Stresses (*mRoM TRS* and *MFH TRS*, respectively), First Ply Failure with (*FPF0 TRS*) and without (*FPF0*) Thermal Residual Stresses and BEST criterion. The experimental OH strength is given in the column labeled *exp*. Case by case unnotched strength predictions are given in Tables F.1, F.3 and F.5.

Layup	Loading	BEST		mRoM		mRoM TRS		MFH		MFH TRS		FPF0		FPF0 TRS	
		μ[%]	σ[%]	μ[%]	σ[%]	μ[%]	σ[%]	μ[%]	σ[%]	μ[%]	σ[%]	μ[%]	σ[%]	μ[%]	σ[%]
QUASI	OHT	0.0	0.0	0.0	0.0	0.0	0.0	0.0	0.0	0.0	0.0	0.0	0.0	0.0	0.0
	OHC	nan	nan	nan	nan	nan	nan	nan	nan	nan	nan	nan	nan	nan	nan
HARD	OHT	-1.1	7.3	-4.7	8.2	-7.4	10.0	-4.2	7.9	-6.1	9.7	-4.7	7.5	0.1	5.9
	OHC	nan	nan	nan	nan	nan	nan	nan	nan	nan	nan	nan	nan	nan	nan
SOFT	OHT	-15.1	10.9	-22.7	7.8	-26.4	8.6	-21.9	8.1	-25.3	8.4	-15.8	11.1	-16.4	10.6
	OHC	nan	nan	nan	nan	nan	nan	nan	nan	nan	nan	nan	nan	nan	nan

(a) Mean errors of the open-hole strength prediction in CTD.

Layup	Loading	BEST		mRoM		mRoM TRS		MFH		MFH TRS		FPF0		FPF0 TRS	
		μ[%]	σ[%]	μ[%]	σ[%]	μ[%]	σ[%]	μ[%]	σ[%]	μ[%]	σ[%]	μ[%]	σ[%]	μ[%]	σ[%]
QUASI	OHT	-0.0	0.0	-0.0	0.0	-0.0	0.0	-0.0	0.0	-0.0	0.0	-0.0	0.0	-0.0	0.0
	OHC	0.0	0.0	0.0	0.0	0.0	0.0	0.0	0.0	0.0	0.0	0.0	0.0	-0.0	0.0
HARD	OHT	-5.9	8.8	-9.3	9.7	-11.9	10.2	-8.6	9.8	-10.7	10.4	-9.0	8.6	-8.0	8.6
	OHC	8.4	6.4	16.2	6.9	20.8	9.3	15.6	6.8	19.1	8.0	9.2	6.4	12.4	0.8
SOFT	OHT	-14.1	10.0	-23.5	8.2	-27.1	9.2	-22.7	8.1	-26.1	9.0	-9.5	10.2	-10.6	10.9
	OHC	-25.1	4.0	-32.2	4.9	-34.0	5.9	-32.1	5.0	-34.0	5.6	-31.2	4.9	-28.4	1.1

(b) Mean errors of the open-hole strength prediction in RTD.

Layup	Loading	BEST		mRoM		mRoM TRS		MFH		MFH TRS		FPF0		FPF0 TRS	
		μ[%]	σ[%]	μ[%]	σ[%]	μ[%]	σ[%]	μ[%]	σ[%]	μ[%]	σ[%]	μ[%]	σ[%]	μ[%]	σ[%]
QUASI	OHT	0.0	0.0	0.0	0.0	0.0	0.0	0.0	0.0	-0.0	0.0	0.0	0.0	0.0	0.0
	OHC	-0.0	0.0	0.0	0.0	-0.0	0.0	-0.0	0.0	0.0	0.0	-0.0	0.0	-0.0	0.0
HARD	OHT	-12.3	8.5	-13.1	4.0	-15.9	0.0	-12.0	4.5	-15.2	0.0	-12.3	8.2	-11.2	8.7
	OHC	2.6	6.3	13.2	5.6	14.7	5.9	11.5	5.3	13.1	5.7	2.1	5.9	-3.7	0.0
SOFT	OHT	-17.5	3.1	-33.1	1.9	-36.4	0.0	-30.2	0.7	-35.1	0.0	1.6	11.0	3.3	10.4
	OHC	-25.4	7.6	-32.7	8.1	-34.7	9.5	-31.6	8.3	-34.0	8.9	-38.0	8.7	-21.0	0.0

(c) Mean errors of the open-hole strength prediction in ETW.

Table 5.3: Prediction of open-hole strength, comparison of the following criteria: Best Practise (BEST), Last Ply Failure with mRoM (*mRoM*) and MFH (*MFH*) degradation method without Thermal Residual Stresses and with thermal stresses (*mRoM TRS* and *MFH TRS*, respectively), First Ply Failure with (*FPF0 TRS*) and without (*FPF0*) Thermal Residual Stresses and BEST criterion. The experimental OH strength is given in the column labeled *exp*. A *nan*-valued cell means that no experimental strength was found in the NIAR dataset. Calibration is performed on QI lay-ups. Case by case open-hole strength predictions are given in Tables F.2, F.4 and F.6.

5.4 Conclusion

In this chapter, residual thermal stresses due to the difference in temperature between the curing environment and the testing environment have been taken into account. For criteria such a the Unit Circle or the max-strain criterion, the way residual stresses were incorporated, i.e. changing the longitudinal strength, was proven not usefull, as the predictions are not enhanced. For Tsai-Wu-based criteria, an approach considering the initial state of strain of each ply in the *global* axes was used. The Tsai-Wu-based criteria with and without residual stresses were tested in CTD, RTD and ETW

conditions. For the CTD environment, taking into account residual stresses helped to enhance the unnotched prediction. However, the open-hole prediction should still be performed with the BEST criterion, and leads to very good results, considering that an average calibrated $\mathscr{R}$-curve is used. Regarding the RTD environment, the BEST criterion still applies, such that residual thermal stresses can be disregarded. Eventually, in ETW environment, the unnotched strength is reasonnably well predicted if the First Ply Failure on the 0° ply with thermal residual stresses criterion is used for QI tensile strength and the BEST is applied otherwise. However, the soft UN strengths are poorly predicted. Regarding the notched strength, the hard compressive and soft tensile strength are captured, but the framework fails at predicting the hard tensile and soft compressive strength.

6 Conclusion

This report was concerned with the evaluation and validation of a recently proposed semi-analytical approach to predict open-hole strength of unidirectional coupons, based solely on the longitudinal Young modulus, strength and $\mathscr{R}$-curve of the 0° ply [4]. Efforts were put on evaluating the framework's elementary building blocks, namely the Trace theory, the laminate plate theory, the unnotched strength criterion and the coupled stress-energy failure criterion, on several datasets. A calibration method was also proposed to cope with the lack of data regarding the $\mathscr{R}$-curve. Residual stresses due to curing were also incorporated in the framework.

First, the building blocks of the semi-analytical method proposed in [4] were presented. The first one is the Trace theory, see Sect. 1.1.2, that was initially proposed in [43]. This theory is based on the empirical observation that if one normalizes the elastic properties of a lamina w.r.t. the trace of its in-plane stiffness matrix, one recovers coefficients that are common to a large range of CFRP. For instance, in RTD environmental conditions, the longitudinal Young modulus of the lamina is equal to 88% of the trace of the in-plane stiffness matrix. Therefore, if only the longitudinal Young modulus of the lamina is known, based on the trace, the other lamina elastic constants can be found. It was noticed that the trace of the in-plane stiffness has a very simple expression, that was not seen in previous work. In this report, the Trace theory coefficients reported in [43] were used to compute the elastic properties of quasi-isotropic laminates for the 10 unidirectional material systems that were identified in the NIAR dataset, thanks to the Laminate Plate Theory. These laminate constants were compared with the ones computed based on the experimental lamina elastic constants. It was concluded that the loss of accuracy in RTD was nearly always less or equal to 3%. However, for CTD, ETW and ETW2 conditions, the loss of accuracy is not negligible if the Trace theory coefficients reported in [43] are used. Indeed, especially in ETW and ETW2 conditions, the errors were as high as ten percent. Therefore, new coefficients were proposed for the aforementioned environmental conditions. With these new coefficients, the error in quasi-isotropic laminate elastic properties was reduced to 4% or less.

The second building block of the method is the laminate unnotched strength criterion. Furtado et al. [4] used the max-strain criterion. This criterion is very simple and requires the longitudinal lamina Young modulus and strength, only. Using this criterion, the unnotched strength of any laminate can be predicted.

The third building block presents a method, initially proposed in Camanho et al. [8], that is con-

cerned with the calculation of the $\mathscr{R}$-curve of the laminate (or, alternatively, its critical energy release rate). Using the experimentally measured lamina $\mathscr{R}$-curve, which is an input of the framework, the classical laminate plate theory, and assuming that the crack propagates identically in all the plies of the laminate, considered balanced and symmetric, it is possible to compute the $\mathscr{R}$-curve of the laminate, see Sect. 1.3. It is important to note that during this work, an error was found in the method. Indeed, the authors that first published the approximation of the orthotropy correction factor χ (Eq. (1.4)) released a corrigenda that Furtado et al. [4] were not aware of. This correction changes the open-hole prediction by a few percent, towards higher predictions.

Once the laminate elastic properties, $\mathscr{R}$-curve and unnotched strength are known, it remains to compute the open-hole strength of the laminate. Assuming that a crack develops perpendicularly to the applied load due to fiber-dominated failure, see Fig. 1.3, Cornetti et al. [17] proposed to combine an average stress criterion and an energy-based criterion, see Sect. 1.4.1 and Sect. 1.4.2, respectively. Therefore, a system of two equations with two unknowns must be solved. The first unknown is the crack extension at failure, and the second one is the remote applied load leading to ultimate failure. In fact, this system of equations is quite general and can be particularized to centered crack, ellipsoidal and circular holes. Indeed, the stress field along the ligament section and the energy release rate appearing in Eq. (1.10) are kept general by Cornetti et al. [17]. In order to solve the system, the stress field is approximated with an analytical expression, first developed in [22], see Sect. 1.4.4.1. The energy release rate of the laminate is approximated by the energy release rate of an isotropic plate with a central hole, corrected with the equivalent modulus of the laminate, see Sect. 1.4.4.2.

The framework as proposed in [4] is summarized in Fig. 1.4.

The above framework was first implemented in `C++`, and validated against the results found in [4]. The method was found capable of very accurately predicting the open-hole strength of several CFRP and the hole size effect, i.e. the decreasing open-hole strength as the hole diameter increases.

In order to further validate the performances of the method, it was necessary to introduce a calibration method to cope with the fact that, in general, the $\mathscr{R}$-curve is never measured in usual test campaigns. Two methods were proposed: the calibration of a constant critical energy release rate and the calibration of an average $\mathscr{R}$-curve that is based on the 4 $\mathscr{R}$-curves reported in [4]. The idea is to use the framework with the knowlegdge of the open-hole strength, and to use it to back-calculate the steady-state $\mathscr{R}$-curve or the critical energy release rate of the lamina, see Sect. 2.1. The open-hole predictions that were made using calibration were found to be as good as or better than the predictions made with the experimentally measured data. It was noticed that the calibrated steady-state value of the average $\mathscr{R}$-curve is generally very close to the steady-state value of experimentally measured $\mathscr{R}$-curve found in [4]. Moreover, the $\mathscr{R}$-curve is representative of the physical process of unidirectional composite fracture under uniaxial loading, whereas the constant energy release rate is more an artificial mean, whose calibrated value is not representative of the steady-state value of the $\mathscr{R}$-curve.

Thanks to the calibration method, the framework was evaluated successfully on several other material systems whose $\mathscr{R}$-curve was not given in the data sheets. The hole size effect was also captured with the calibrated average $\mathscr{R}$-curve, see Sect. 2.2. However, it was noted that even if the framework works well for thin-ply laminate, exhibiting a brittle-like failure and a decreasing notched strength for increasing hole size, it can not be used for computing the notched strength of thick-laminates, that are generally more prone to delamination and exhibit a *inversed* hole size effect.

Until this point, the calibration was mainly performed on quasi-isotropic lay-ups. However, in the NIAR dataset, the open-hole experimental strengths are always given for quasi-isotropic, hard and soft lay-ups. Therefore, a choice must be made regarding the lay-up on which calibration is performed. The framework can then be assessed on the two remaining strengths. In order to motivate the choice, a sensitivity analysis was conducted on 10 material systems in RTD conditions, see Sect. 2.3. The lay-up that should be prefered should be the less sensitive to the unnotched strength to cope with the inaccuracy of the unnotched criterion, and the more sensitive to the given open-hole strength on which calibration is performed. It was concluded that calibration on hard lay-ups should be prefered if available. However, the quasi-isotropic lay-ups are generally the first lay-up that is tested. Therefore, for the rest of the present work, calibration was performed on quasi-isotropic lay-ups.

Using the experimental unnotched strength that is given in the NIAR dataset instead of using the max-strain criterion was shown to be a better choice, see Chap. 3. Therefore, the rest of this report was concerned with improving the unnotched strength prediction. For that sake, two options were followed: changing the unnotched criterion and taking into account residual stresses due to curing of the laminate, see Chap. 4 and Chap. 5, respectively.

Alongside with the max-strain criterion, 5 criteria were evaluated on the NIAR dataset in RTD conditions, for tensile and compressive loadings, and for quasi-isotropic, hard and soft laminates. This is a total of 60 experimental unnotched strengths that can be used to assess the capabilities of each unnotched criteria. Tsai-Wu-based failure criteria were considered first, see Sect. 4.1. The First Ply Failure was concluded way too conservative as the failure envelopes of the 45° and 90° plies were limiting. Tsai et al. [43] proposed to degrade the matrix of the lamina in order to change its elastic properties, thereby changing the shape of the failure envelopes and increasing the predicted strength. This method is named Last Ply Failure. Two methods were proposed for degradation of the lamina elastic properties, namely a modified rules of mixtures and a mean-field homogenization technique, see Sect. 4.1.2.1 and Sect. 4.1.2.2, respectively. The first conclusion was that the modified rules of mixtures provided a way too low lamina Poisson ratio. However, when computing the laminate properties from the degraded lamina properties and applying the Last Ply Failure, both methods were found more or less equivalent, with the method based on mean-field homogenization being a little more acurate on the unnotched prediction.

When the Last Ply Failure criterion was first used, it was noticed that for a lot of cases, the 0° ply failure envelope was driving failure. Therefore, a criterion based solely on the intact failure envelope of the 0° ply was proposed, see Sect. 4.1.3. It was shown to be a good unnotched strength criterion, compared to Last Ply approach, especially on hard coupons. The last unnotched criterion that was analyzed is the Unit Circle, initially proposed by Tsai et al. [43], see Sect. 4.2. This failure criterion was proposed as a conservative approximation to the Last Ply Failure envelope of laminates. Instead of using the 5 lamina strengths as Tsai-Wu-based criterion do, the Unit Circle relies on the longitudinal Young modulus and strength only. Tsai et al. [43] proposed to use the degraded lamina properties to go from the Unit Circle in the strain space to the Unit Circle in the stress space and compute the unnotched strength. However, it was noticed that using the intact properties is beneficial in most cases.

Once all the criteria have been presented, they were compared with each other. A best practice rule was derived, telling which unnotched criterion should be used under given loading and lay-up, see Table 4.8. Using this rule enhances the unnotched strength prediction as well as the notched

strength prediction, when calibration is applied on RTD coupons of the NIAR dataset.

The second method that was proposed to enhance the unnotched strength prediction is related to residual thermal stresses due to the difference in temperature between the autoclave and the testing environment. Taking into account such residual stresses is expected to improve unnotched strength prediction. An approach was proposed to deal with residual thermal stresses using the Unit Circle and the max-strain criterion, but no noticeable improvement was shown, see Sect. 5.2. Then, the residual thermal stresses were introduced in the Tsai-Wu-based criteria, by changing the 5 lamina strengths according to the residual thermal stresses in the *local* axes. This method was proved to be completely wrong, and it was attributed to both transverse tensile strength approaching zero and the close-envelope requirement. Another approach was then developed, that makes use of the initial state of strain due to the residual thermal stresses. The method was integrated in the 3 Tsai-Wu-based unnotched criteria and compared in CTD, RTD and ETW environments, for both unnotched and notched strength. It was concluded that the unnotched strength is not enhanced in RTD, whereas it helps in some cases for CTD and ETW environments, see Sect. 5.4. Regarding open-hole predictions, they should be done with the best practice rules in CTD and leads to strengths that are in very good agreement with experimental data. The best practice rules still apply for notched strength in RTD environment. As the predictions in ETW environment are concerned, it was concluded that hard compressive and soft tensile strengths can be relatively accurately predicted, but the framework fails at predicting the hard tensile and soft compressive notched strength.

To conclude, the present work implemented a recently proposed semi-analytical framework to compute notched strength of unidirectional composites. An extensive validation campaign under various environmental conditions and lay-ups, a calibration method to relieve the need for characterizing a $\mathscr{R}$-curve as well as a comprehensive study of some unnotched failure criteria were presented. The framework accurately predicts the open-hole strength of a wide range of CFRPs, keeping in mind that only the elastic, strength and $\mathscr{R}$-curve of the lamina are used.

A

Trace Theory

In this chapter, the study of the Trace theory validity has been performed on the NIAR dataset, for the 10 unidirectional material systems that were found in [10], in 4 environmental conditions, namely CTD, RTD, ETW and ETW2. Only tensile properties were considered. Table A.1 contains the tensile properties of the ply, the Trace of the in-plane stiffness matrix Eq. (1.2) and the trace-normalized elastic properties. Trace theory factors can be extracted, see Table 1.2. Tables A.2 and A.3 contain the elastic properties of QI laminates computed with the Trace factors found in [7] and with Trace factors from Table 1.2, respectively. More information about the NIAR dataset can be found in Chap. D.

Material system	Env. cond.	E_1 [GPa]	E_2 [GPa]	ν_{12} [-]	G_{12} [GPa]	Trace [GPa]	$\frac{E_1}{\text{Trace}}$	$\frac{E_2}{\text{Trace}}$	$\frac{G_{12}}{\text{Trace}}$
AS4/8552	RTD	111.49	9.86	0.335	4.83	132.22	0.843	0.075	0.037
AS4/8552	CTD	106.39	10.76	0.335	5.58	129.66	0.821	0.083	0.043
AS4/8552	ETW	114.87	7.86	0.386	2.34	128.68	0.893	0.061	0.018
MTM45-1/HTS40F13	RTD	117.35	8.69	0.350	3.93	135.05	0.869	0.064	0.029
MTM45-1/HTS40F13	CTD	118.87	9.17	0.365	4.83	139.02	0.855	0.066	0.035
MTM45-1/HTS40F13	ETW	120.66	7.93	0.326	2.76	135.01	0.894	0.059	0.020
MTM45-1/HTS40F13	ETW2	120.66	7.38	0.396	2.07	133.41	0.904	0.055	0.016
MR60H/NB4708	RTD	127.21	8.48	0.355	3.79	144.42	0.881	0.059	0.026
MR60H/NB4708	CTD	124.59	9.58	0.359	4.41	144.34	0.863	0.066	0.031
MR60H/NB4708	ETW	126.17	6.96	0.367	2.48	139.10	0.907	0.050	0.018
IM7/8552	RTD	138.17	9.72	0.356	4.69	158.60	0.871	0.061	0.030
IM7/8552	CTD	142.58	10.55	0.362	5.93	166.49	0.856	0.063	0.036
IM7/8552	ETW	140.45	8.14	0.383	2.14	154.13	0.911	0.053	0.014
Cytec5250/T650	RTD	125.90	9.72	0.304	4.96	146.52	0.859	0.066	0.034
Cytec5250/T650	CTD	123.90	10.62	0.308	5.72	147.06	0.842	0.072	0.039
Cytec5250/T650	ETW	127.48	5.86	0.388	1.38	137.03	0.930	0.043	0.010
AS4/MTM45	RTD	117.35	8.62	0.310	3.65	134.17	0.875	0.064	0.027
AS4/MTM45	CTD	116.04	9.79	0.300	4.48	135.76	0.855	0.072	0.033
AS4/MTM45	ETW	118.87	8.14	0.320	2.41	132.72	0.896	0.061	0.018
AS4/MTM45	ETW2	135.34	8.76	0.350	2.28	149.80	0.903	0.058	0.015
IM7G/EpoxyEP2202	RTD	141.06	9.62	0.317	4.57	160.86	0.877	0.060	0.028
IM7G/EpoxyEP2202	CTD	142.20	10.57	0.300	5.76	165.32	0.860	0.064	0.035
IM7G/EpoxyEP2202	ETW	147.71	8.58	0.304	3.37	163.87	0.901	0.052	0.021
IM7G/MTM45-1	RTD	139.55	8.41	0.361	3.62	156.37	0.892	0.054	0.023
IM7G/MTM45-1	CTD	140.72	8.96	0.346	4.36	159.55	0.882	0.056	0.027
IM7G/MTM45-1	ETW	139.62	7.52	0.373	2.47	153.18	0.911	0.049	0.016
IM7G/MTM45-1	ETW2	140.79	6.96	0.389	2.24	153.35	0.918	0.045	0.015
CYTECT40-800/CYCOM5215	RTD	128.73	8.62	0.366	3.74	146.06	0.881	0.059	0.026
CYTECT40-800/CYCOM5215	CTD	129.97	9.38	0.306	4.64	149.57	0.869	0.063	0.031
CYTECT40-800/CYCOM5215	ETW	129.07	7.31	0.362	2.78	142.96	0.903	0.051	0.019
Cytec5320/T650	RTD	126.18	9.84	0.326	4.95	147.06	0.858	0.067	0.034
Cytec5320/T650	CTD	118.98	10.56	0.325	5.78	142.31	0.836	0.074	0.041
Cytec5320/T650	ETW	127.79	8.91	0.334	3.77	145.31	0.879	0.061	0.026
Cytec5320/T650	ETW2	125.84	7.54	0.337	2.24	138.78	0.907	0.054	0.016
Mean				**0.344**			**0.880**	**0.061**	**0.026**
Std dev.				0.028			0.026	0.009	0.009
Coef. var [%]				8.240			2.910	14.113	33.127
MeanRTD				**0.338**			**0.871**	**0.063**	**0.029**
Coef. var [%]				6.348			1.537	8.646	13.548
MeanCTD				**0.331**			**0.854**	**0.068**	**0.035**
Coef. var [%]				7.563			1.928	10.494	13.130
MeanETW				**0.354**			**0.903**	**0.054**	**0.018**
Coef. var [%]				8.207			1.448	11.064	22.245
MeanETW2				**0.368**			**0.908**	**0.053**	**0.015**
Coef. var [%]				6.807			0.644	9.075	3.606

Table A.1: Trace Theory factors on the NIAR dataset, based on tensile properties.

Elastic properties	AS4/8552								MTM45-1/HTS40F13							
	RTD		CTD		ETW				RTD		CTD		ETW		ETW2	
$E_1{}^L$	44.383	4.2	43.615	7.3	42.728	-2.6			45.201	0.8	46.642	2.7	45.037	-2.3	44.268	-4.0
$E_2{}^L$	44.383	4.2	43.615	7.3	42.728	-2.6			45.201	0.8	46.642	2.7	45.037	-2.3	44.268	-4.0
$\nu_{12}{}^L$	0.313	1.8	0.306	-0.4	0.343	11.5			0.322	4.6	0.315	2.3	0.331	7.7	0.345	12.1
$G_{12}{}^L$	16.900	3.8	16.692	7.4	15.905	-5.2			17.097	-0.2	17.738	2.2	16.915	-4.0	16.456	-6.6
Elastic properties	MR60H/NB4708								IM7/8552							
	RTD		CTD		ETW				RTD		CTD		ETW			
$E_1{}^L$	48.304	-0.6	48.315	1.5	46.346	-3.8			53.122	0.6	55.927	2.7	51.146	-4.7		
$E_2{}^L$	48.304	-0.6	48.315	1.5	46.346	-3.8			53.122	0.6	55.927	2.7	51.146	-4.7		
$\nu_{12}{}^L$	0.324	5.3	0.322	4.5	0.335	8.7			0.320	3.9	0.311	1.1	0.345	12.1		
$G_{12}{}^L$	18.242	-1.8	18.277	0.4	17.364	-5.8			20.124	-0.3	21.330	2.4	19.015	-7.3		
Elastic properties	Cytec5250/T650								AS4/MTM45							
	RTD		CTD		ETW				RTD		CTD		ETW		ETW2	
$E_1{}^L$	49.250	2.4	49.513	4.6	45.468	-6.6			44.930	0.2	45.570	2.8	44.195	-2.7	49.748	-3.8
$E_2{}^L$	49.250	2.4	49.513	4.6	45.468	-6.6			44.930	0.2	45.570	2.8	44.195	-2.7	49.748	-3.8
$\nu_{12}{}^L$	0.309	0.4	0.304	-1.3	0.345	12.1			0.321	4.2	0.313	1.8	0.336	9.2	0.343	11.4
$G_{12}{}^L$	18.812	2.3	18.989	4.9	16.901	-9.2			17.012	-0.7	17.350	2.4	16.538	-4.7	18.522	-6.3
Elastic properties	IM7G/EpoxyEP2202								IM7G/MTM45-1							
	RTD		CTD		ETW				RTD		CTD		ETW		ETW2	
$E_1{}^L$	53.937	0.1	55.632	2.4	54.786	-2.9			52.246	-2.0	53.446	-0.6	50.980	-4.4	51.006	-5.2
$E_2{}^L$	53.937	0.1	55.632	2.4	54.786	-2.9			52.246	-2.0	53.446	-0.6	50.980	-4.4	51.006	-5.2
$\nu_{12}{}^L$	0.317	2.9	0.305	-0.8	0.325	5.7			0.327	6.2	0.320	3.8	0.337	9.7	0.339	10.2
$G_{12}{}^L$	20.483	-0.6	21.308	2.6	20.671	-4.2			19.686	-3.4	20.252	-1.5	19.059	-6.5	19.047	-7.4
Elastic properties	CYTECT40-800/CYCOM5215								Cytec5320/T650							
	RTD		CTD		ETW				RTD		CTD		ETW		ETW2	
$E_1{}^L$	48.807	-0.7	50.222	1.2	47.677	-3.3			49.377	2.4	47.907	5.4	48.603	-0.4	46.189	-3.9
$E_2{}^L$	48.807	-0.7	50.222	1.2	47.677	-3.3			49.377	2.4	47.907	5.4	48.603	-0.4	46.189	-3.9
$\nu_{12}{}^L$	0.327	6.1	0.312	1.5	0.332	7.9			0.312	1.5	0.304	-1.2	0.324	5.2	0.337	9.6
$G_{12}{}^L$	18.396	-2.2	19.134	0.8	17.898	-5.1			18.811	2.1	18.368	5.7	18.357	-1.6	17.268	-6.0

Table A.2: Quasi-isotropic laminate elastic properties computed from tensile data found in the NIAR dataset using LPT, see Table A.1. The unit system is GPa. Alongside with the values computed with full ply elastic characterization, errors when trace theory is used are presented, in percent. Errors larger than 3% are in red. Trace theory coefficients used are presented in Table 1.1. Supplementary information on the NIAR dataset: see Chap. D.

Elastic properties	AS4/8552								MTM45-1/HTS40F13							
	RTD		CTD		ETW				RTD		CTD		ETW		ETW2	
$E_1{}^L$	44.383	4.2	43.615	6.4	42.728	2.5			45.201	0.8	46.642	1.8	45.037	2.8	44.268	2.3
$E_2{}^L$	44.383	4.2	43.615	6.4	42.728	2.5			45.201	0.8	46.642	1.8	45.037	2.8	44.268	2.3
$\nu_{12}{}^L$	0.313	1.8	0.306	-0.8	0.343	4.5			0.322	4.6	0.315	1.9	0.331	0.8	0.345	3.7
$G_{12}{}^L$	16.900	3.8	16.692	6.5	15.905	1.3			17.097	-0.2	17.738	1.3	16.915	2.6	16.456	1.4
Elastic properties	MR60H/NB4708								IM7/8552							
	RTD		CTD		ETW				RTD		CTD		ETW			
$E_1{}^L$	48.304	-0.6	48.315	0.6	46.346	1.2			53.122	0.6	55.927	1.8	51.146	0.3		
$E_2{}^L$	48.304	-0.6	48.315	0.6	46.346	1.2			53.122	0.6	55.927	1.8	51.146	0.3		
$\nu_{12}{}^L$	0.324	5.3	0.322	4.2	0.335	1.8			0.320	3.9	0.311	0.7	0.345	5.0		
$G_{12}{}^L$	18.242	-1.8	18.277	-0.4	17.364	0.7			20.124	-0.3	21.330	1.6	19.015	-0.9		
Elastic properties	Cytec5250/T650								AS4/MTM45							
	RTD		CTD		ETW				RTD		CTD		ETW		ETW2	
$E_1{}^L$	49.250	2.4	49.513	3.7	45.468	-1.8			44.930	0.2	45.570	1.9	44.195	2.4	49.748	2.5
$E_2{}^L$	49.250	2.4	49.513	3.7	45.468	-1.8			44.930	0.2	45.570	1.9	44.195	2.4	49.748	2.5
$\nu_{12}{}^L$	0.309	0.4	0.304	-1.7	0.345	5.0			0.321	4.2	0.313	1.4	0.336	2.3	0.343	3.1
$G_{12}{}^L$	18.812	2.3	18.989	4.1	16.901	-3.0			17.012	-0.7	17.350	1.5	16.538	1.8	18.522	1.7
Elastic properties	IM7G/EpoxyEP2202								IM7G/MTM45-1							
	RTD		CTD		ETW				RTD		CTD		ETW		ETW2	
$E_1{}^L$	53.937	0.1	55.632	1.5	54.786	2.2			52.246	-2.0	53.446	-1.5	50.980	0.6	51.006	1.0
$E_2{}^L$	53.937	0.1	55.632	1.5	54.786	2.2			52.246	-2.0	53.446	-1.5	50.980	0.6	51.006	1.0
$\nu_{12}{}^L$	0.317	2.9	0.305	-1.1	0.325	-1.0			0.327	6.2	0.320	3.5	0.337	2.7	0.339	1.9
$G_{12}{}^L$	20.483	-0.6	21.308	1.8	20.671	2.4			19.686	-3.4	20.252	-2.3	19.059	-0.1	19.047	0.6
Elastic properties	CYTECT40-800/CYCOM5215								Cytec5320/T650							
	RTD		CTD		ETW				RTD		CTD		ETW		ETW2	
$E_1{}^L$	48.807	-0.7	50.222	0.2	47.677	1.8			49.377	2.4	47.907	4.5	48.603	4.8	46.189	2.4
$E_2{}^L$	48.807	-0.7	50.222	0.2	47.677	1.8			49.377	2.4	47.907	4.5	48.603	4.8	46.189	2.4
$\nu_{12}{}^L$	0.327	6.1	0.312	1.1	0.332	1.0			0.312	1.5	0.304	-1.5	0.324	-1.4	0.337	1.4
$G_{12}{}^L$	18.396	-2.2	19.134	-0.0	17.898	1.5			18.811	2.1	18.368	4.8	18.357	5.1	17.268	2.0

Table A.3: Quasi-isotropic laminate elastic properties computed from tensile data found in the NIAR dataset using LPT, see Table A.1. The unit system is GPa. Alongside with the values computed with full ply elastic characterization, errors when corrected trace theory is used are presented, in percent. Errors larger than 3% are in red. Corrected trace theory coefficients used are presented in Table 1.2. Supplementary information on the NIAR dataset: see Chap. D.

B

Data from Furtado's paper

The material data used to reproduce the results found in [4] are presented. It should be noted that in order to reproduce the tensile notched predictions of M40JB/ThinPreg 80EP found in [4], the reported critical energy release rate $\mathcal{G}_{Ic}^{0}$ has been changed from 61 to 47.7 N/mm, see Table B.3. Moreover, as discussed in Chap. 2, the compressive ply longitudinal strength of IM7/8552 reported in [4] might be replaced by the one found in [29], see Table B.2.

Materialsystem	E_1 [Mpa]	E_2 [Mpa]	G_{12} [Mpa]	ν_{12} [-]
IM7/8552	171420	9080	5290	0.32
T800/M21	172000	8900	5000	0.32
T700/AR2527	110000	7400	4200	0.3
M40JB/ThinPreg80EP/CF	222000	7010	4661	0.314
T700/M21	130000	8300	4500	0.32

Table B.1: Ply elastic properties, from [4].

Material system	0° ply strength [MPa]	
	Tension	Compression
IM7/8552	2326	1200 or 1690[a]
T800/M21	3039	1669
T700/AR2527	2300	1500
M40JB/ThinPreg 80EP/CF	2250	1052
T700/M21	2000	1300

[a] The compressive strength was reported to be 1690 MPa in [29].

Table B.2: Longitudinal ply strengths, from [4].

Material system	$\mathscr{R}$-curve of the 0° ply Eq. (1.11)				$\mathscr{G}^0_{Ic}$	Ref.
	$\mathscr{R}_{ss}$	l_{fpz}	ζ	η		
Tension						
IM7/8552	205	2.63	0.319	3.65	-	[15]
T800/M21	283	1.14	0.758	3.53	-	[15]
T700/AR2527	254	1.92	0.423	4	-	[15]
M40JB/ThinPreg 80EP	-	-	-	-	61 or 47.7[a]	[b]
T700/M21	-	-	-	-	391	[b]
Compression						
IM7/8552	61	1.43	0.513	4.29	-	[39]
T800/M21	-	-	-	-	37	[b]
T700/AR2527	-	-	-	-	43	[b]

[a] In order to reproduce results shown in [4], $\mathscr{G}^0_{Ic}$ was modified from the reported value 61 [N/mm] to 47.7 [N/mm].
[b] These values are back-computed from either QI laminate open-hole strength or fracture toughness, see [4, Table 5].

Table B.3: $\mathscr{R}$-curve parameters of the 0° ply of the carbon/epoxy systems used in [4].

C Calibration method: supplementary data

This chapter contains supplementary material that supports the developments made in Chap. 2.

ϕ [mm]	R [N/mm]
0.5	188.45
1.0	134.33
2.0	148.52
3.2	146.69
4.0	160.86
6.0	168.63
6.4	179.69
8.0	137.70
10.0	154.31
12.7	191.26
25.4	193.59
50.8	287.80

Table C.1: Calibration of the average tensile $\mathscr{R}$-curve Sect. 2.1.2 on the IM7/8552 material system from [4]. The calibration has been performed on all the hole sizes that were available. Mean value is 174.32 [N/mm], standard deviation [N/mm] is 39.53, coefficient of variation is 22.67%.

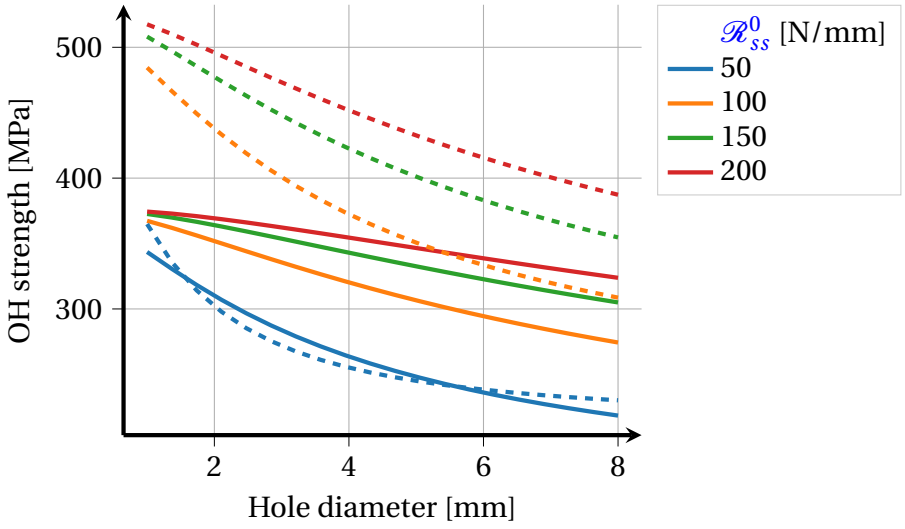

Figure C.1: Prediction of open-hole compressive strength for IM7/8552, as of function of the hole diameter. Dashed lines correspond to IM7/8552-CCS (X^C = 1690 MPa). Solid lines corresponds to IM7/8552 (X^C = 1200 MPa). Hole-to-width ratio fixed to 1/6.

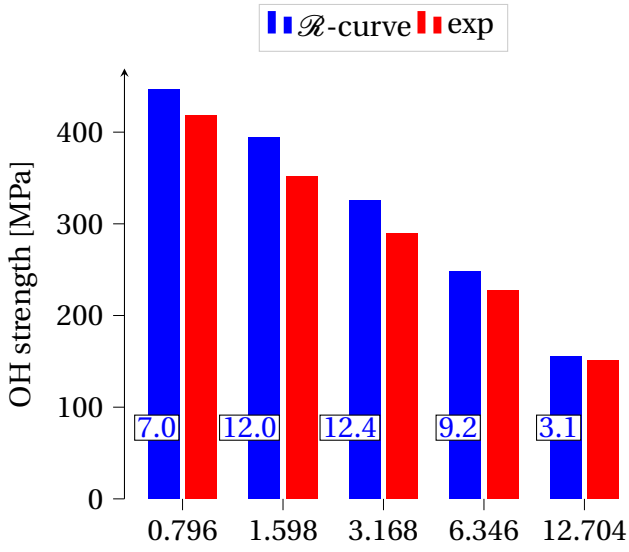

Figure C.2: Prediction of the compressive open-hole strength of IM7/8552, using the elastic properties and experimental $\mathscr{R}$-curve of [4] and the experimental unnotched strength of [40]. The x-axis is the hole diameter [mm]. The width of all coupons is 25.4 mm.

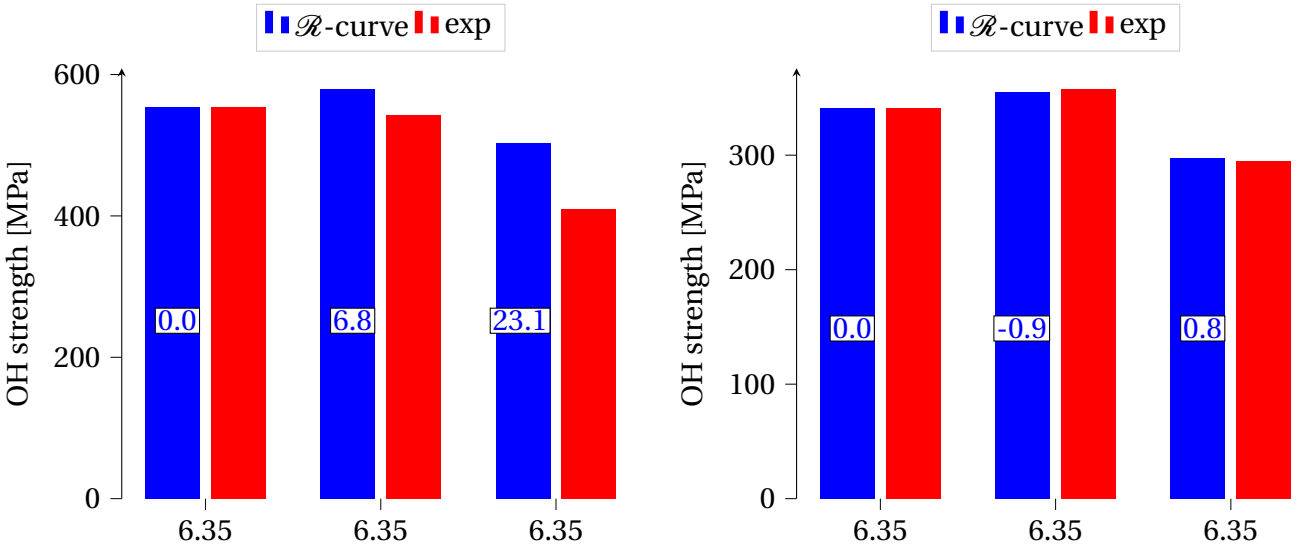

(a) Tension.

(b) Compression.

Figure C.3: Prediction of the tensile and compressive open-hole strength for results presented in [41]. Lay-up is, from left to right: $[45/0/-45/90]_{2s}$, $[60/0/-60]_{3s}$, $[30/60/90/-60/-30]_{2s}$. Results are obtained by applying the max-strain criterion for the unnotched strength, and the calibration of $\mathscr{R}^0_{ss}$ on the $[45/0/-45/90]_{2s}$ laminate. Full elastic characterization was used. Hole diameter is always 6.35 mm. Width is always 38.1 mm.

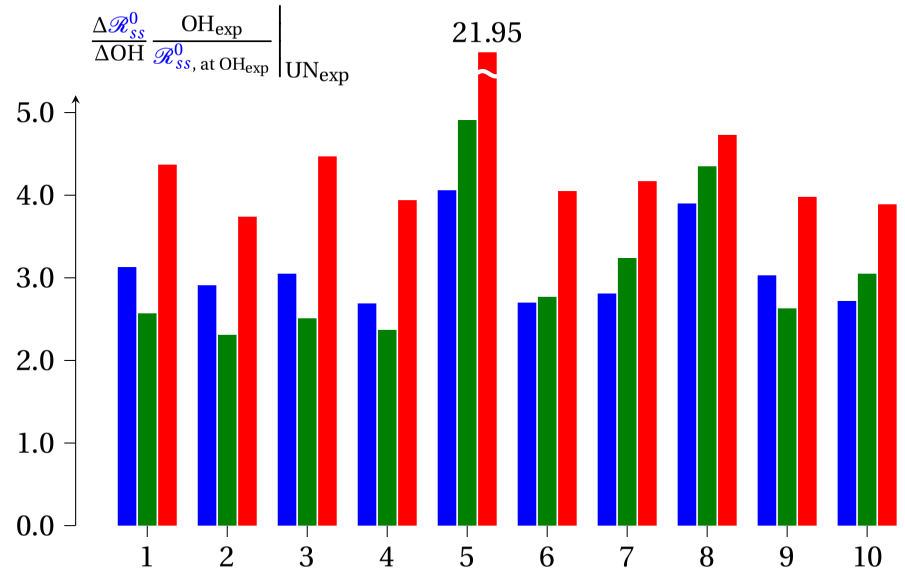

(a) QI (▮▮), hard (▮▮), soft (▮▮). Sensitivity of calibrated $\mathscr{R}^0_{ss}$ w.r.t. open-hole tensile strength, for a fixed unnotched strength equal to the experimental tensile unnotched strength.

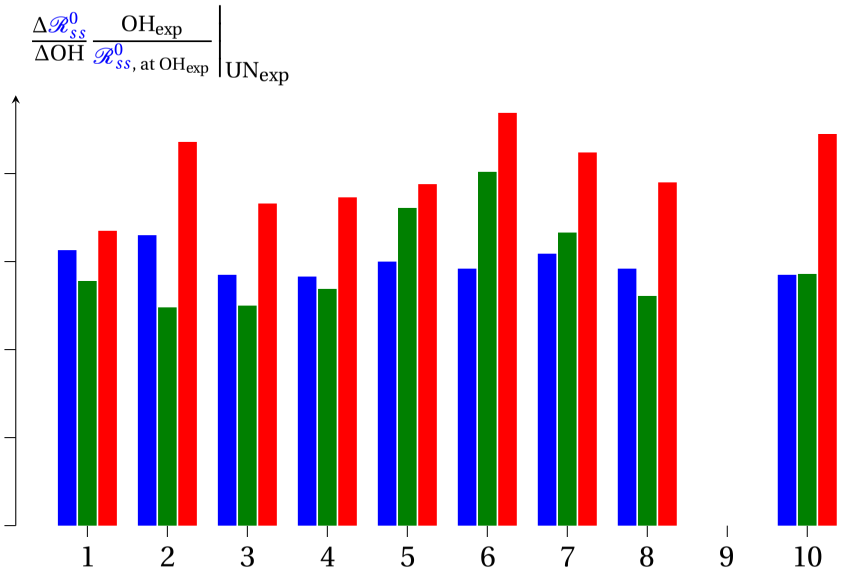

(b) QI (▮▮), hard (▮▮), soft (▮▮). Sensitivity of calibrated $\mathscr{R}^0_{ss}$ w.r.t. open-hole compressive strength, for a fixed unnotched strength equal to the experimental compressive unnotched strength.

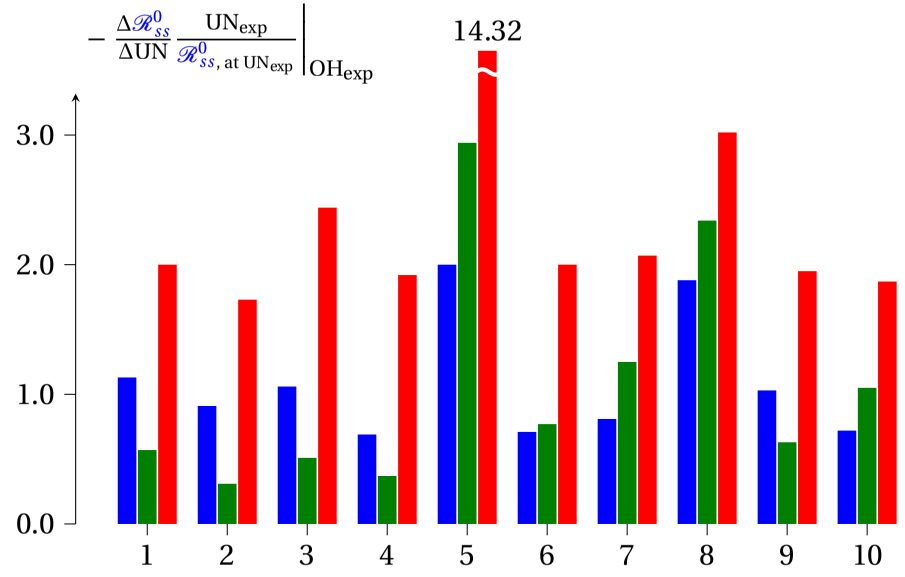

(c) QI (▮▮), hard (▮▮), soft (▮▮). Sensitivity of calibrated $\mathscr{R}^0_{ss}$ w.r.t. unnotched tensile strength, for a fixed open-hole strength equal to the experimental tensile open-hole strength.

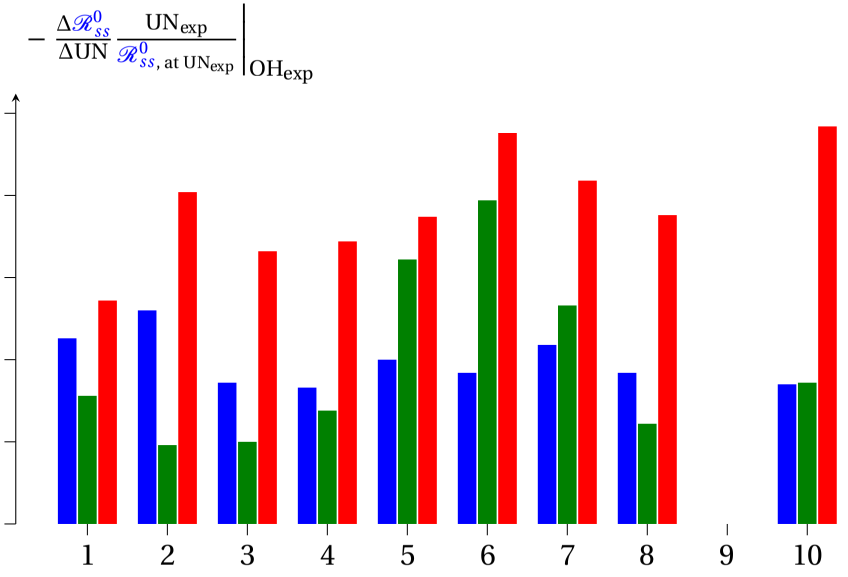

(d) QI (▮▮), hard (▮▮), soft (▮▮). Sensitivity of calibrated $\mathscr{R}^0_{ss}$ w.r.t. unnotched compressive strength, for a fixed open-hole strength equal to the experimental compressive open-hole strength.

Figure C.4: Sensitivity of the calibrated steady-state value of the $\mathscr{R}$-curve, in RTD conditions. The values are calculated as in Eq. (2.4) (p. 37). Material systems are IM7/8552 (1), AS4/8552 (2), Cytec5250/T650 (3), Cytec5320/T650 (4), MR60H/NB4708 (5), MTM45-1/HTS40F13 (6), AS4/MTM45 (7), CYTECT40-800/CYCOM5215 (8), IM7G/EpoxyEP2202 (9), IM7G/MTM45-1 (10).

D NIAR dataset

This appendix gathers some supplementary information about the NIAR dataset [10].

D.1 Unidirectional material systems from NIAR

The NIAR dataset contains a handfull of characterized material systems, among which only the unidirectional composites were chosen [10]. Table D.1 recaps all the material systems extracted from this dataset, as well as the reference to the material data report. It is to be noted that the material properties were always taken as the normalized ones, by default. However, in case of missing normalized values, measured values were considered.

Material system	Fiber	Reference
AS4/8552	AS4	[55]
MTM45-1/HTS40F13	HTS40F13	[56]
MR60H/NB44708	MR60H	[9]
IM7/8552	IM7	[31]
Cytec5250/T650	T650	[57]
AS4/MTM45	AS4	[58]
IM7G/EpoxyEP2202	IM7	[59]
IM7G/MTM45-1	IM7	[51]
CYTECT40/800/CYCOM5215	T800S	[60]
Cytec5320/T650	T650	[61]

Table D.1: List of available unidirectional composites available in the NIAR dataset [10], with the corresponding fiber. The longitudinal Young modulus of the fibers are given in Table E.1.

D.2 Shear strength

In general, the final shear strength is not provided in NIAR's data sheets. However, the strengths at 0.2% offset $F_{12}^{0.2\%}$ and 5% strain $F_{12}^{5\%}$ are generally given. In this way, the final in-plane shear strength F_{12} can be approximated by:

$$F_{12} = F_{12}^{5\%} + 0.005 \frac{F_{12}^{5\%} - F_{12}^{0.2\%}}{0.05 - \left(0.002 + \dfrac{F_{12}^{0.2\%}}{G_{12}}\right)}.$$

This approximation is also shown in Fig. D.1.

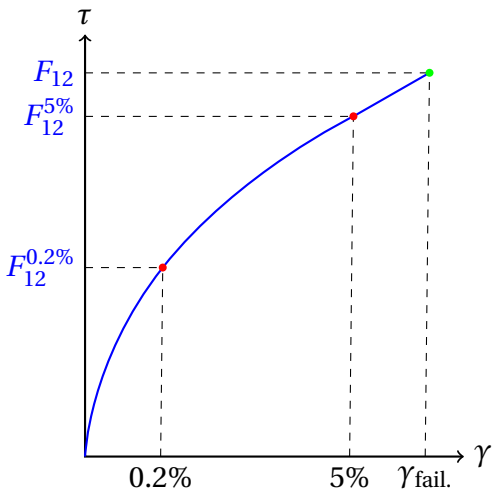

Figure D.1: Shear strength from strengths at 0.2% offset and 5% strain. Not to scale.

D.3 Failure modes: identification codes

Alongside with elastic properties and strengths, the NIAR dataset provides the predominant failure mode of each and every tested coupon under a coded string format. This code is based on three characters whose meaning is described in Tables D.2a to D.2c.

D.4 Results of the framework, in RTD conditions

In the following, the results that can be obtained with the framework evaluated in Chap. 3 are shown in Fig. D.2 to D.4. The environmental conditions are those of Room Temperature Dry kind of environment, shortened RTD. The failure mode of each test is written inside the bar charts. Note that in order to lighten the figures, the material systems are replaced by numbers, from 1 to 10. They are sorted by increasing cured ply thickness, i.e. material system numbered 1 has the thinnest plies. Table D.3

Failure area	Code
Inside grip/tab	I
At grip/tab	A
Gage	G
Multiple areas	M
Tab adhesive	T
Various	V
Unknown	U

(a) Second character.

Failure location	Code
Bottom	B
Top	T
Left	L
Right	R
Middle	M
Various	V
Unknown	U

(b) Third character.

Failure mode	Code
Angled	A
Brooming	B
End-crushing	C
Delamination	D
Euler buckling	E
Through-thickness	H
Kink bands	K
Lateral	L
Multi-mode	M(x,y,z)
Long-splitting	S
Transverse shear	T
Explosive	X
Other	O

(c) First character.

Table D.2: Failure modes identification codes, after [62].

shows which material system corresponds to which number, as well as the nominal cured ply thickness. The results obtained when using the Trace theory and max-strain criterion are shown in Fig. D.5 to D.7. The calibrated values of the steady-state $\mathscr{R}$-curve $\mathscr{R}_{ss}^{0,\text{calib.}}$ are shown in Table D.4.

ID	Material system	Nominal cured ply tickness [mm]
1	Cytec5250/T650	0.1397
2	Cytec5320/T650	0.1397
3	MTM45-1/HTS40F13	0.1397
4	AS4/MTM45	0.1397
5	IM7G/MTM45-1	0.1397
6	CYTECT40-800/CYCOM5215	0.14478
7	IM7/8552	0.18288
8	IM7G/EpoxyEP2202	0.18288
9	AS4/8552	0.18796
10	MR60H/NB4708	0.32004

Table D.3: Integer identifier for material systems of the NIAR dataset, sorted by increasing order of nominal cured ply thickness.

Material system	Loading	$\mathscr{R}_{ss}^{0,\text{calib.}}$ NTT [N/mm]	$\mathscr{R}_{ss}^{0,\text{calib.}}$ TT [N/mm]
Cytec5250-T650	OHT	158.7	160.6
Cytec5250-T650	OHC	146.1	153.9
Cytec5320-T650	OHT	124.8	126.2
Cytec5320-T650	OHC	159.0	168.5
MTM45-1-HTS40F13	OHT	214.3	211.1
MTM45-1-HTS40F13	OHC	184.4	189.7
AS4-MTM45	OHT	215.0	209.2
AS4-MTM45	OHC	133.7	134.7
IM7G-MTM45-1	OHT	234.2	218.4
IM7G-MTM45-1	OHC	129.2	122.0
CYTECT40-800-CYCOM5215	OHT	216.9	207.2
CYTECT40-800-CYCOM5215	OHC	112.9	111.3
IM7-8552	OHT	158.9	155.7
IM7-8552	OHC	131.1	133.0
IM7G-EpoxyEP2202	OHT	289.6	282.1
IM7G-EpoxyEP2202	OHC	131.9	132.4
AS4-8552	OHT	123.4	126.5
AS4-8552	OHC	162.5	182.3
MR60H-NB4708	OHT	260.7	249.7
MR60H-NB4708	OHC	88.4	87.5

Table D.4: Calibrated values of the steady-state average $\mathscr{R}$-curve on the QI lay-ups of the NIAR dataset, in RTD conditions. $\mathscr{R}_{ss}^{0,\text{calib.}}$ NTT: using the max-strain unnotched criterion and the full elastic characterization (No Trace Theory). $\mathscr{R}_{ss}^{0,\text{calib.}}$ TT: using max-strain unnotched criterion and Trace Theory.

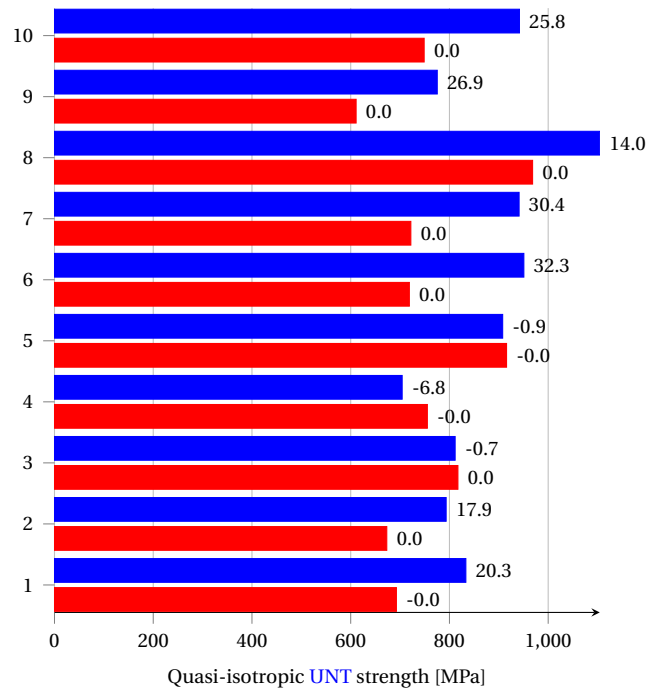

(a) Quasi-isotropic UNT strength : using experimental unnotched strength (), using Max-Strain ().

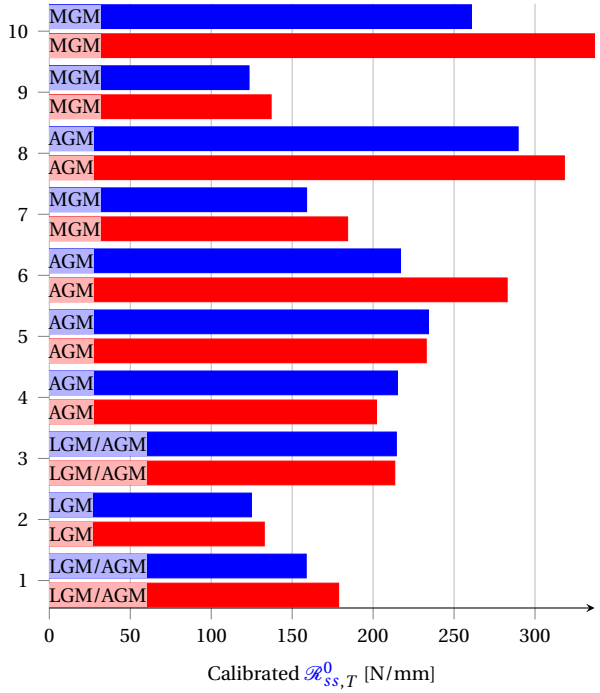

(b) Calibrated $\mathscr{R}^0_{ss,T}$: using experimental unnotched strength (), using Max-Strain ().

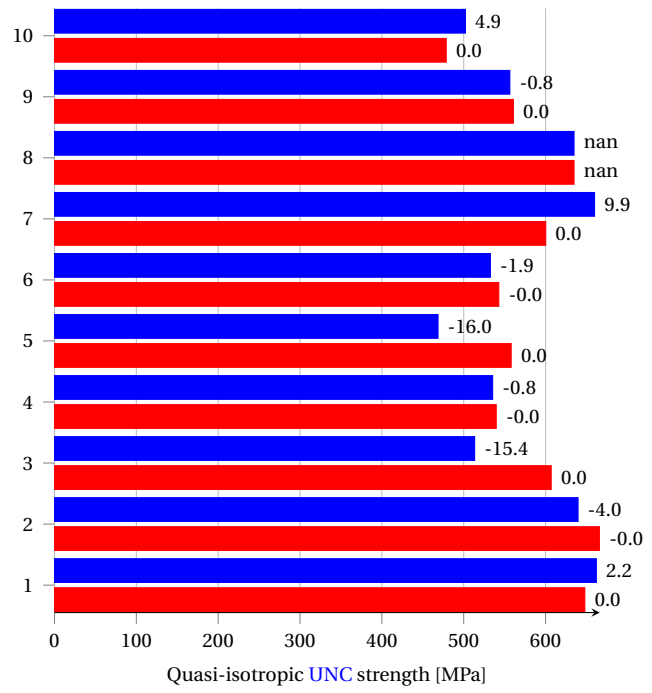

(c) Quasi-isotropic UNC strength : using experimental unnotched strength (), using Max-Strain ().

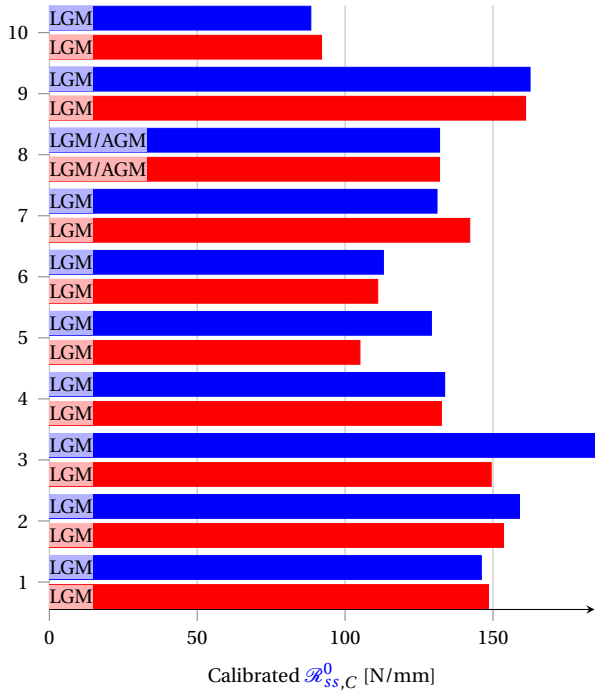

(d) Calibrated $\mathscr{R}^0_{ss,C}$: using experimental unnotched strength (), using Max-Strain ().

Figure D.2: Prediction of unnotched strength and open-hole strength on the NIAR dataset, for QI coupons. The failure mode is given for each case, see Sect. D.3. The error of the prediction w.r.t. the expected strength is given on the right of each bar. A *nan* valued error means that no experimental strength was given. A missing bar means that no solution was found to the coupled energy-stress criterion. The material system corresponding to the integers on the y-axis can be found in Table D.3. They are classified by increasing nominal cured ply thickness. Calibration of an average $\mathscr{R}$-curve on the QI OH strength, in RTD environment.

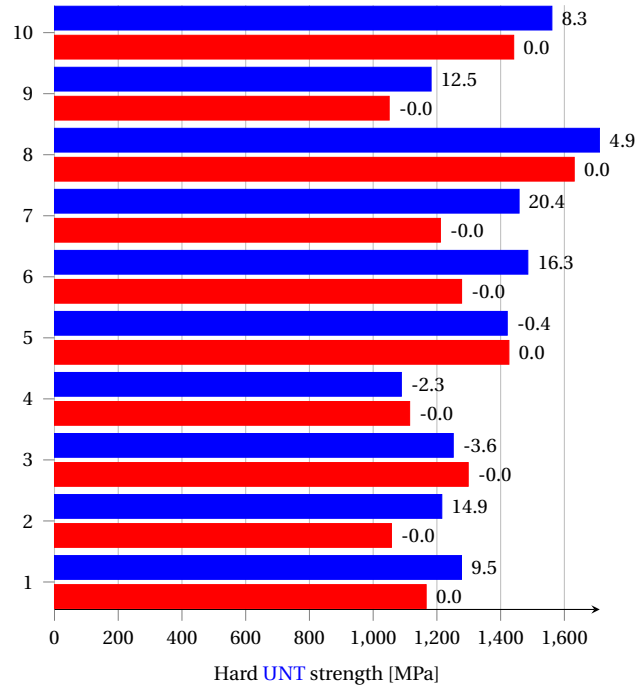

(a) Hard UNT strength : using experimental unnotched strength (), using Max-Strain ().

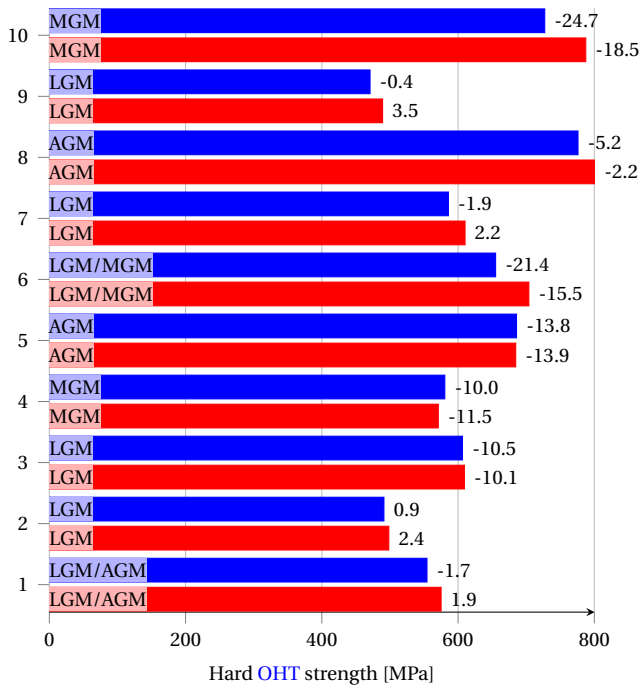

(b) Hard OHT strength : using experimental unnotched strength (), using Max-Strain ().

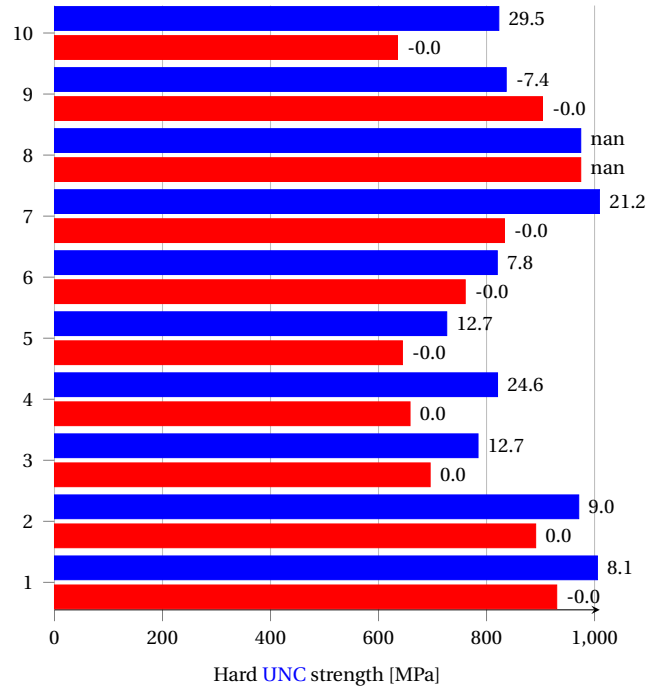

(c) Hard UNC strength : using experimental unnotched strength (), using Max-Strain ().

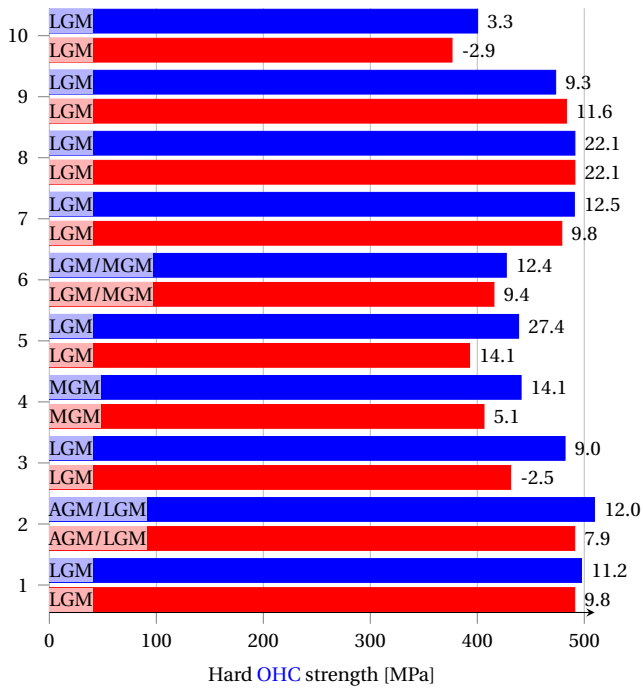

(d) Hard OHC strength : using experimental unnotched strength (), using Max-Strain ().

Figure D.3: Prediction of unnotched strength and open-hole strength on the NIAR dataset, for hard coupons. The failure mode is given for each case, see Sect. D.3. The error of the prediction w.r.t. the expected strength is given on the right of each bar. A *nan* valued error means that no experimental strength was given. A missing bar means that no solution was found to the coupled energy-stress criterion. The material system corresponding to the integers on the y-axis can be found in Table D.3. They are classified by increasing nominal cured ply thickness. Calibration of an average $\mathscr{R}$-curve on the QI OH strength, in RTD environment.

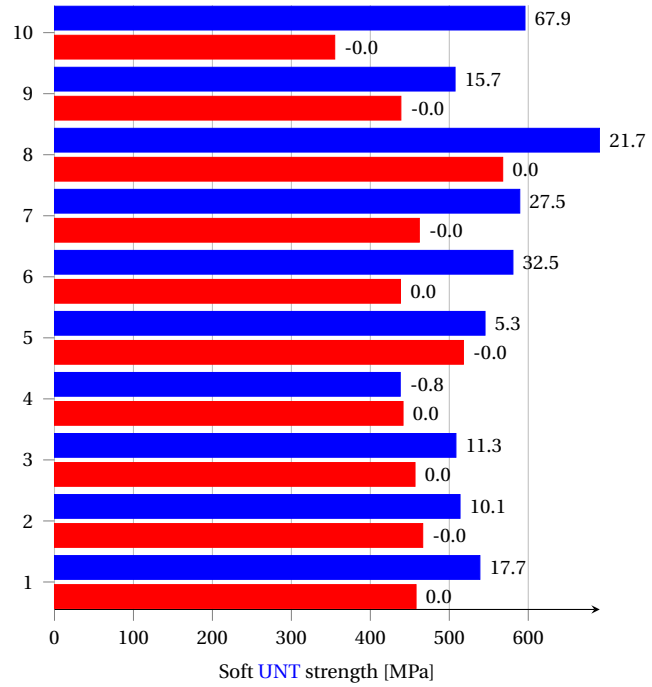

(a) Soft UNT strength : using experimental unnotched strength (), using Max-Strain ().

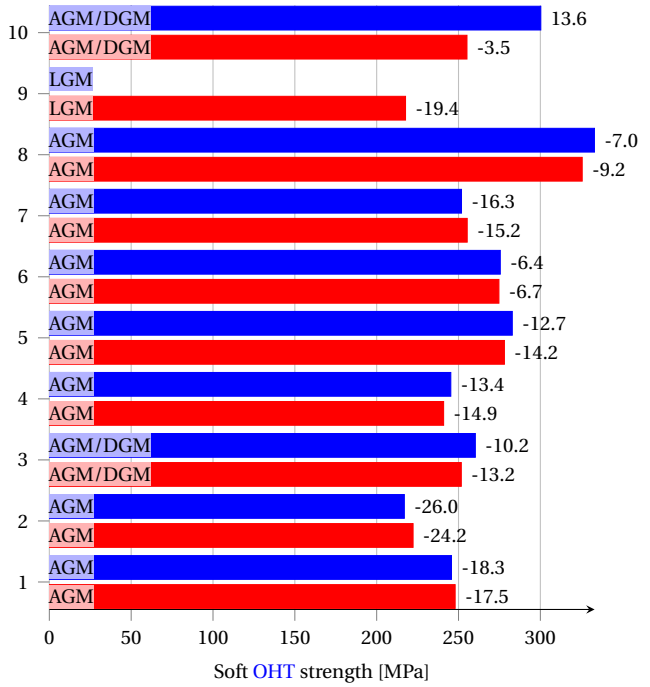

(b) Soft OHT strength : using experimental unnotched strength (), using Max-Strain ().

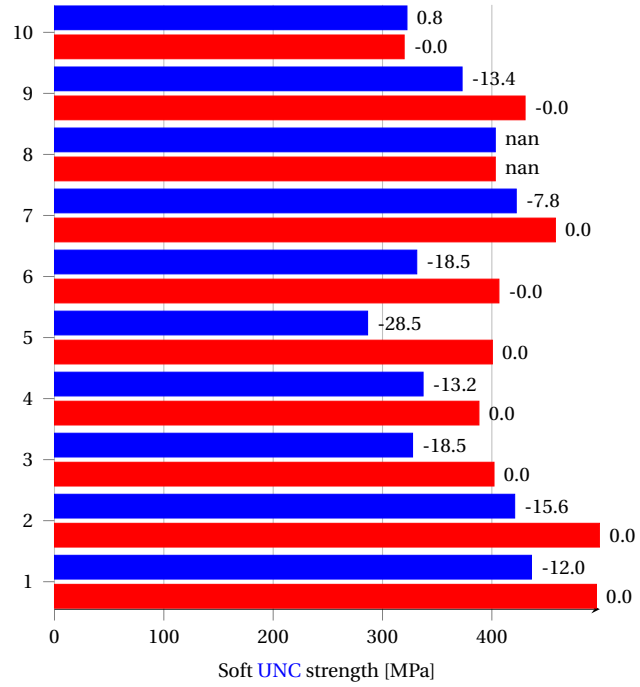

(c) Soft UNC strength : using experimental unnotched strength (), using Max-Strain ().

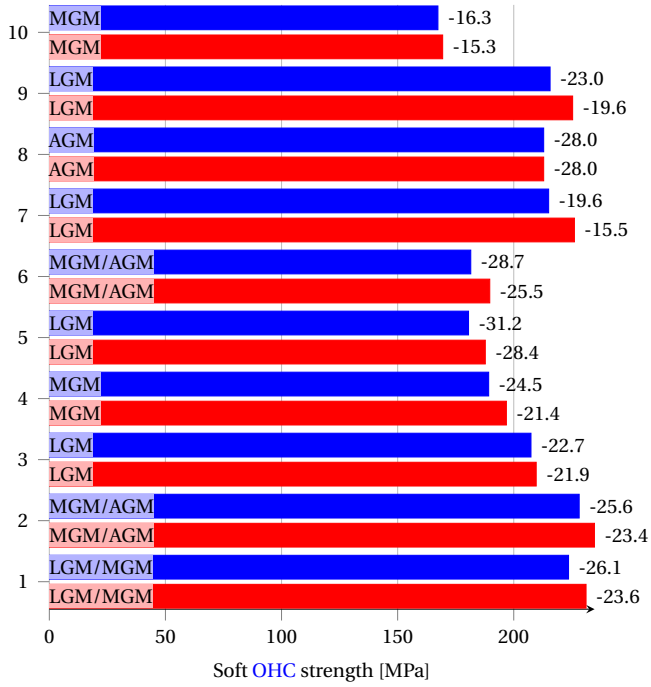

(d) Soft OHC strength : using experimental unnotched strength (), using Max-Strain ().

Figure D.4: Prediction of unnotched strength and open-hole strength on the NIAR dataset, for soft coupons. The failure mode is given for each case, see Sect. D.3. The error of the prediction w.r.t. the expected strength is given on the right of each bar. A *nan* valued error means that no experimental strength was given. A missing bar means that no solution was found to the coupled energy-stress criterion. The material system corresponding to the integers on the y-axis can be found in Table D.3. They are classified by increasing nominal cured ply thickness. Calibration of an average $\mathscr{R}$-curve on the QI OH strength, in RTD environment.

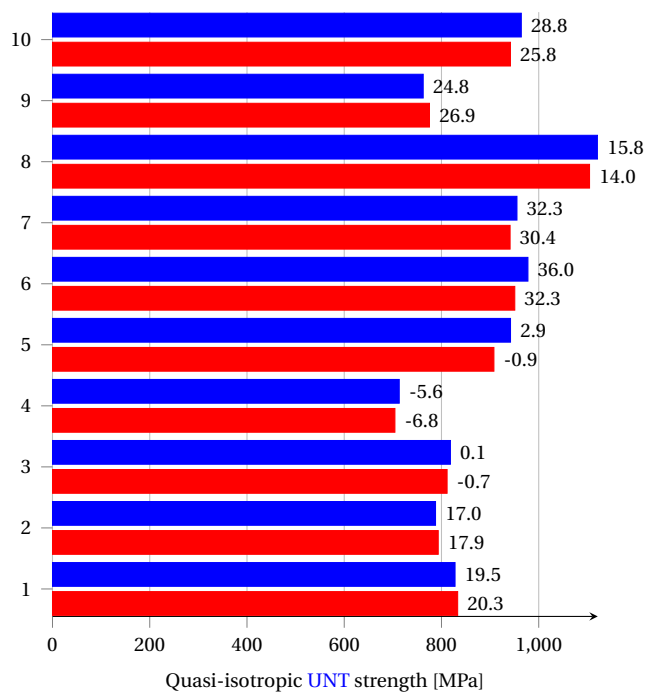

(a) Quasi-isotropic UNT strength : using Max-Strain (MS) without Trace theory (), using Trace theory ().

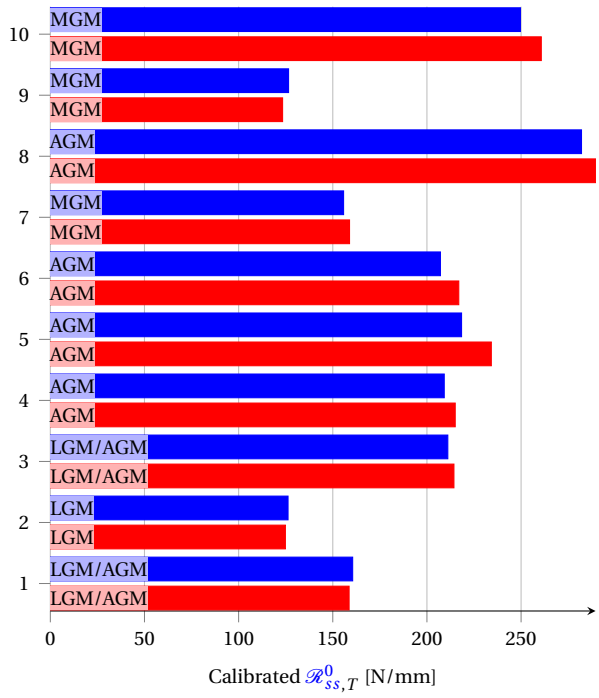

(b) Calibrated $\mathscr{R}^0_{ss,T}$: using Max-Strain (MS) without Trace theory (), using Trace theory ().

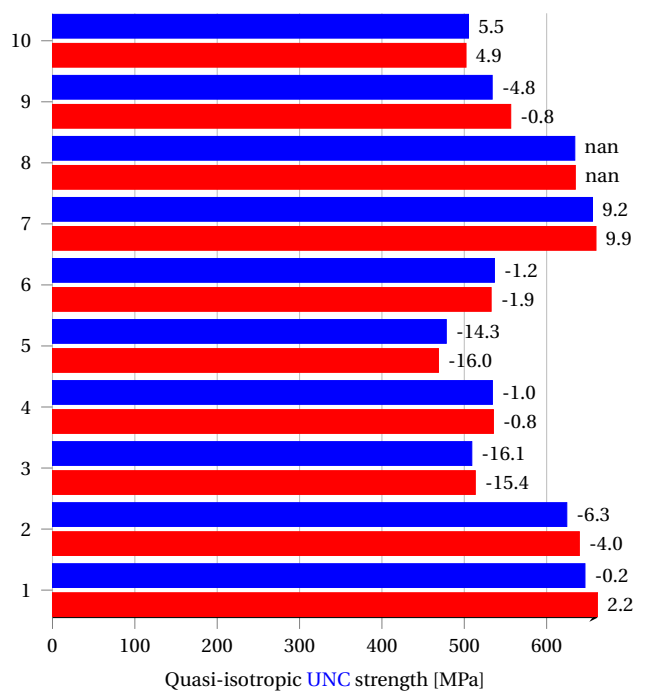

(c) Quasi-isotropic UNC strength : using Max-Strain (MS) without Trace theory (), using Trace theory ().

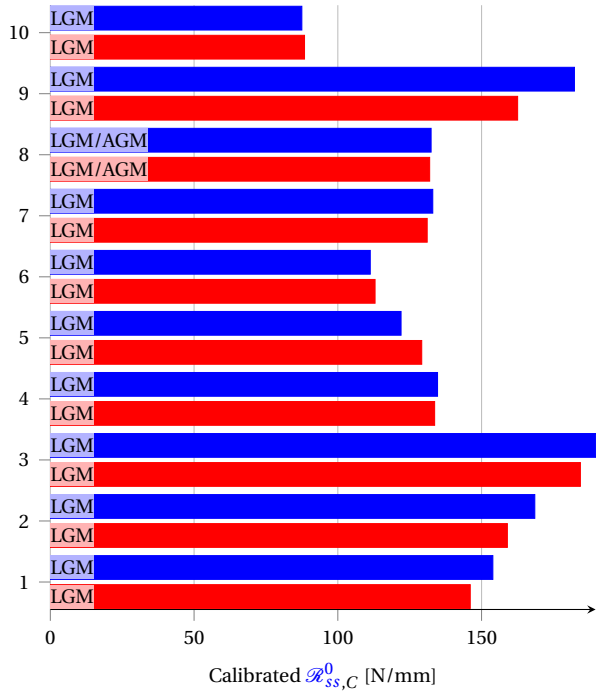

(d) Calibrated $\mathscr{R}^0_{ss,C}$: using Max-Strain (MS) without Trace theory (), using Trace theory ().

Figure D.5: Prediction of unnotched strength and open-hole strength on the NIAR dataset, for QI coupons. The failure mode is given for each case, see Sect. D.3. The error of the prediction w.r.t. the expected strength is given on the right of each bar. A *nan* valued error means that no experimental strength was given. A missing bar means that no solution was found to the coupled energy-stress criterion. The material system corresponding to the integers on the y-axis can be found in Table D.3. They are classified by increasing nominal cured ply thickness. Calibration of an average $\mathscr{R}$-curve on the QI OH strength, in RTD environment.

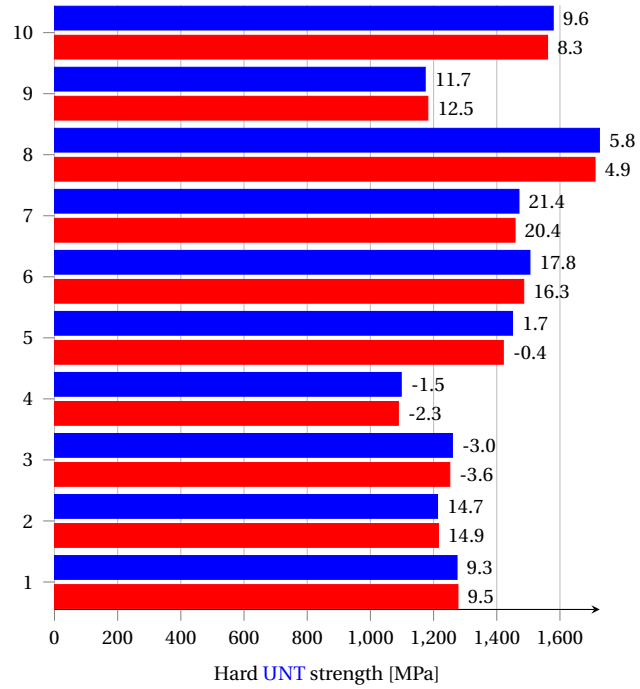

(a) Hard UNT strength : using Max-Strain (MS) without Trace theory (), using Trace theory ().

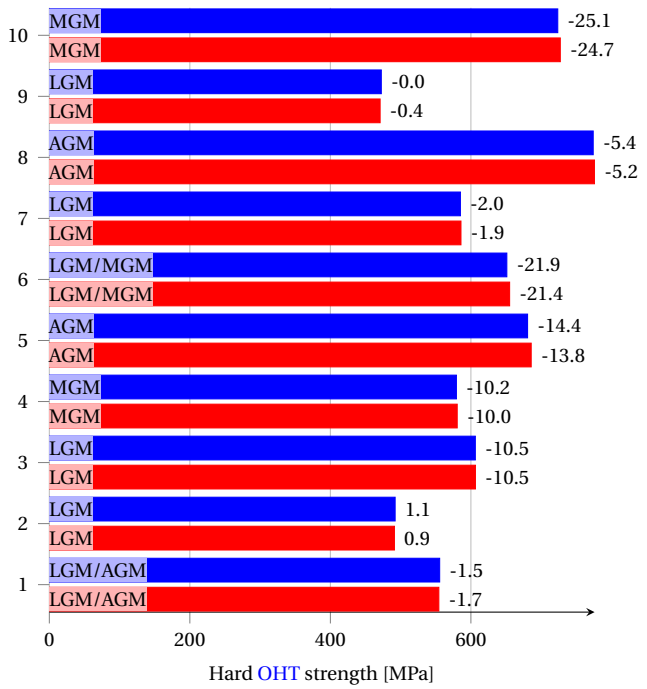

(b) Hard OHT strength : using Max-Strain (MS) without Trace theory (), using Trace theory ().

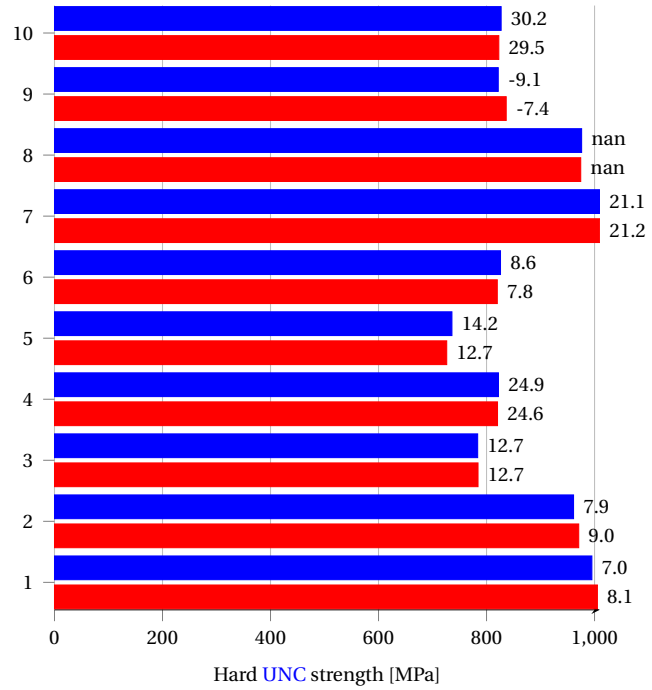

(c) Hard UNC strength : using Max-Strain (MS) without Trace theory (), using Trace theory ().

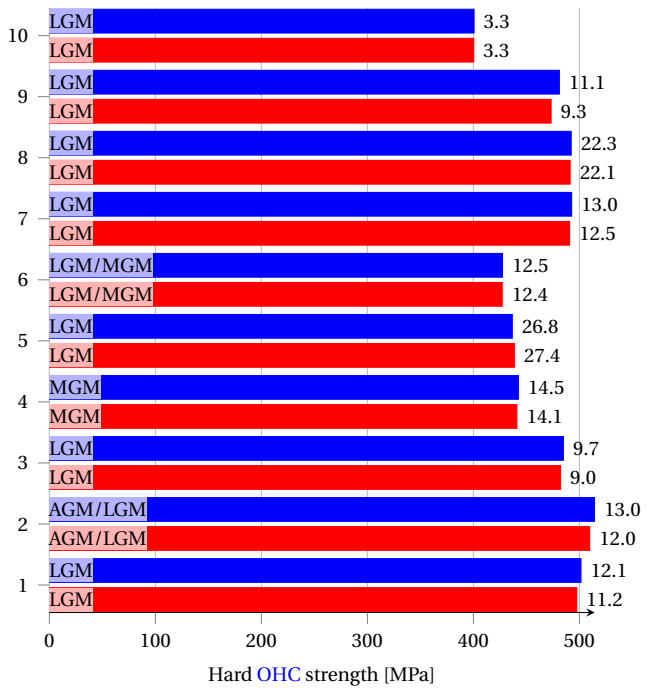

(d) Hard OHC strength : using Max-Strain (MS) without Trace theory (), using Trace theory ().

Figure D.6: Prediction of unnotched strength and open-hole strength on the NIAR dataset, for hard coupons. The failure mode is given for each case, see Sect. D.3. The error of the prediction w.r.t. the expected strength is given on the right of each bar. A *nan* valued error means that no experimental strength was given. A missing bar means that no solution was found to the coupled energy-stress criterion. The material system corresponding to the integers on the y-axis can be found in Table D.3. They are classified by increasing nominal cured ply thickness. Calibration of an average $\mathscr{R}$-curve on the QI OH strength, in RTD environment.

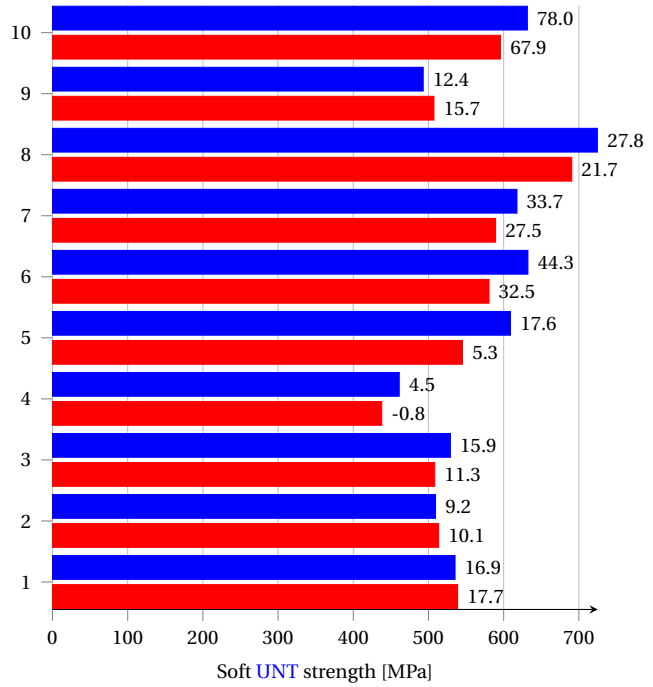

(a) Soft UNT strength : using Max-Strain (MS) without Trace theory (), using Trace theory ().

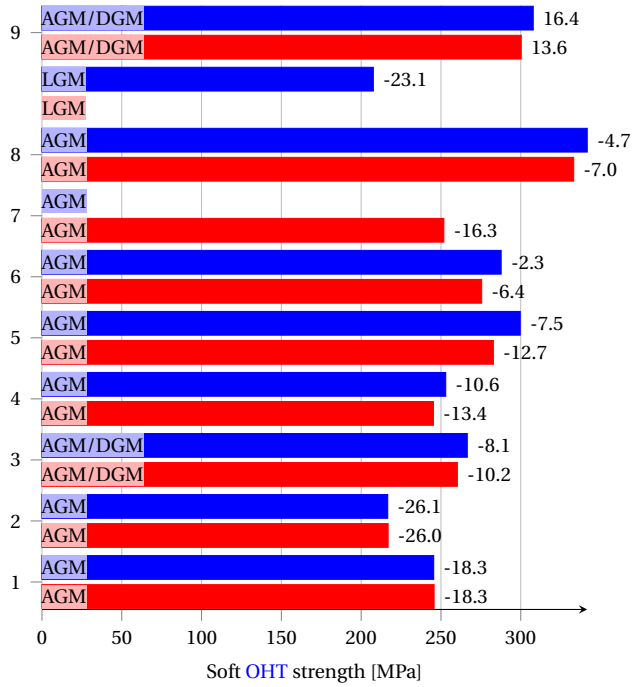

(b) Soft OHT strength : using Max-Strain (MS) without Trace theory (), using Trace theory ().

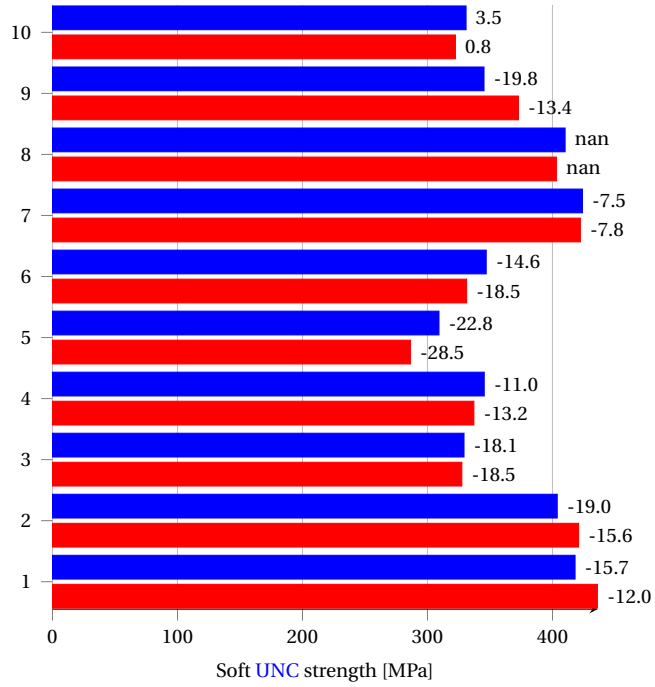

(c) Soft UNC strength : using Max-Strain (MS) without Trace theory (), using Trace theory ().

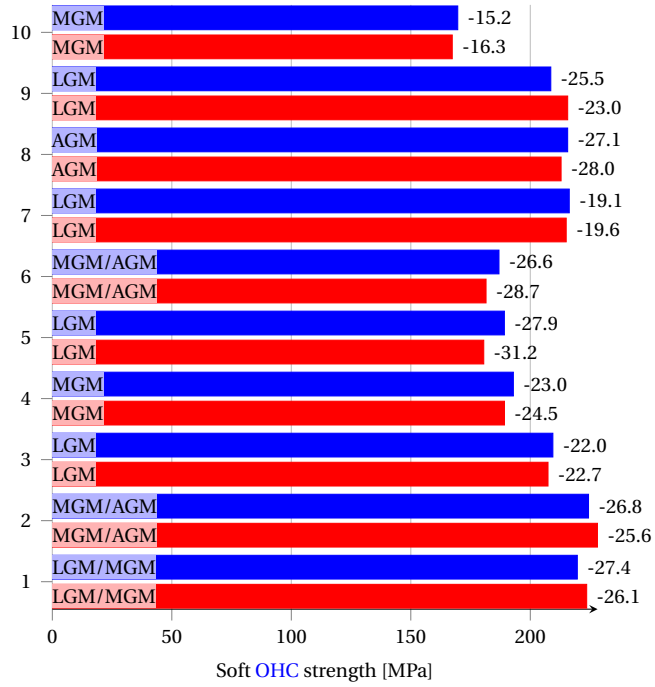

(d) Soft OHC strength : using Max-Strain (MS) without Trace theory (), using Trace theory ().

Figure D.7: Prediction of unnotched strength and open-hole strength on the NIAR dataset, for soft coupons. The failure mode is given for each case, see Sect. D.3. The error of the prediction w.r.t. the expected strength is given on the right of each bar. A *nan* valued error means that no experimental strength was given. A missing bar means that no solution was found to the coupled energy-stress criterion. The material system corresponding to the integers on the y-axis can be found in Table D.3. They are classified by increasing nominal cured ply thickness. Calibration of an average $\mathscr{R}$-curve on the QI OH strength, in RTD environment.

E

Unnotched strength: supplementary data

E.1 Fiber properties

Fiber name	Longitudinal Young modulus [GPa]	Reference
AS4	231	[63]
T800S	294	[64]
IM7	276	[65]
MR60H	290	[66]
T650	255	[67]
HTS40F13	239	[68]

Table E.1: Properties of the fibers used in the NIAR dataset, see Table D.1.

E.2 Results

Material	Lay-up	Loading	exp	LPF mRoM	LPF MFH
IM7-8552 CPT : 0.18288 mm	QUASI	UNT	721.81	885.21	853.88
		UNC	600.19	562.48	589.26
	HARD	UNT	1210.93	1457.23	1419.17
		UNC	833.16	890.31	933.72
	SOFT	UNT	462.02	383.41	390.11
		UNC	458.09	284.33	293.43
AS4-8552 CPT : 0.18796 mm	QUASI	UNT	610.94	711.22	686.57
		UNC	560.68	461.54	481.22
	HARD	UNT	1050.21	1173.39	1137.18
		UNC	903.56	728.43	760.37
	SOFT	UNT	438.64	320.16	323.15
		UNC	430.37	237.16	242.71
Cytec5250-T650 CPT : 0.1397 mm	QUASI	UNT	692.58	-	-
		UNC	647.97	-	-
	HARD	UNT	1166.25	-	-
		UNC	929.90	-	-
	SOFT	UNT	457.88	-	-
		UNC	495.66	-	-
Cytec5320-T650 CPT : 0.1397 mm	QUASI	UNT	673.08	730.54	705.28
		UNC	666.23	540.12	559.65
	HARD	UNT	1057.28	1205.65	1168.06
		UNC	890.92	856.43	889.19
	SOFT	UNT	466.31	376.52	381.59
		UNC	498.70	276.62	281.89
MR60H-NB4708 CPT : 0.32004 mm	QUASI	UNT	748.77	787.68	820.78
		UNC	478.63	427.30	453.11
	HARD	UNT	1440.94	1121.19	1162.83
		UNC	635.08	722.49	766.41
	SOFT	UNT	354.87	357.08	370.70
		UNC	319.78	234.33	246.64
MTM45-1-HTS40F13 CPT : 0.1397 mm	QUASI	UNT	817.17	753.47	729.91
		UNC	606.88	440.90	457.34
	HARD	UNT	1298.21	1181.10	1206.62
		UNC	695.54	700.82	727.75
	SOFT	UNT	456.57	308.94	313.32
		UNC	401.96	225.29	230.32
AS4-MTM45 CPT : 0.1397 mm	QUASI	UNT	755.25	664.38	639.61
		UNC	539.72	456.20	476.72
	HARD	UNT	1114.40	1100.09	1063.66
		UNC	658.31	719.97	753.18
	SOFT	UNT	441.40	302.44	309.51
		UNC	388.17	229.45	236.45
CYTECT40-800-CYCOM5215 CPT : 0.14478 mm	QUASI	UNT	718.78	-	-
		UNC	542.89	-	-
	HARD	UNT	1277.39	-	-
		UNC	760.49	-	-
	SOFT	UNT	438.16	-	-
		UNC	406.45	-	-
IM7G-EpoxyEP2202 CPT : 0.18288 mm	QUASI	UNT	968.43	1030.69	1002.11
		UNC	0.00	549.00	566.17
	HARD	UNT	1630.88	1493.81	1521.06
		UNC	0.00	874.44	902.97
	SOFT	UNT	567.61	387.69	391.12
		UNC	0.00	280.47	285.00
IM7G-MTM45-1 CPT : 0.1397 mm	QUASI	UNT	915.69	865.17	836.35
		UNC	557.99	411.63	428.87
	HARD	UNT	1425.91	1102.53	1131.20
		UNC	644.18	654.62	682.66
	SOFT	UNT	517.87	285.34	290.94
		UNC	400.45	208.20	214.11

Total	ALL	45		11	34
Total	QI UNT	8		4	4
Total	QI UNC	7		0	7
Total	HARD UNT	8		1	7
Total	HARD UNC	7		5	2
Total	SOFT UNT	8		1	7
Total	SOFT UNC	7		0	7

Table E.2: Comparison of unnotched strength prediction on the NIAR dataset, for RTD conditions. Compared criterions are: Last-Ply-Failure with mRoM degradation (LPF mRoM) and Last-Ply-Failure with MFH degradation (LPF MFH). The experimental unnotched strength is given in the column labeled *exp*. Unit system is MPa. The colored cell is always representative of the criterion with the smallest error. Red cells are for unsafe prediction. Green cells are for safe predictions. If the mterial properties were not sufficient for applying the criterions, a dash is written in the cell. A yellow cell means that the experimental unnotched strength was missing. Below, a summary of which criterion was the most predictive, for each loading and layup case. The light blue cell indicates which criterion was best, and orange-colored cells denote equally ranked criteria.

Material	Lay-up	Loading	exp	LPF mRoM	LPF MFH	FPF 0
IM7-8552 CPT : 0.18288 mm	QUASI	UNT	721.81	885.21	853.88	940.86
		UNC	600.19	562.48	589.26	691.64
	HARD	UNT	1210.93	1457.23	1419.17	1482.34
		UNC	833.16	890.31	933.72	912.17
	SOFT	UNT	462.02	383.41	390.11	601.04
		UNC	458.09	284.33	293.43	326.68
AS4-8552 CPT : 0.18796 mm	QUASI	UNT	610.94	711.22	686.57	776.25
		UNC	560.68	461.54	481.22	572.64
	HARD	UNT	1050.21	1173.39	1137.18	1198.61
		UNC	903.56	728.43	760.37	751.36
	SOFT	UNT	438.64	320.16	323.15	514.45
		UNC	430.37	237.16	242.71	288.34
Cytec5250-T650 CPT : 0.1397 mm	QUASI	UNT	692.58	-	-	-
		UNC	647.97	-	-	-
	HARD	UNT	1166.25	-	-	-
		UNC	929.90	-	-	-
	SOFT	UNT	457.88	-	-	-
		UNC	495.66	-	-	-
Cytec5320-T650 CPT : 0.1397 mm	QUASI	UNT	673.08	730.54	705.28	791.14
		UNC	666.23	540.12	559.65	650.26
	HARD	UNT	1057.28	1205.65	1168.06	1231.01
		UNC	890.92	856.43	889.19	867.17
	SOFT	UNT	466.31	376.52	381.59	522.07
		UNC	498.70	276.62	281.89	325.69
MR60H-NB4708 CPT : 0.32004 mm	QUASI	UNT	748.77	787.68	820.78	939.63
		UNC	478.63	427.30	453.11	528.12
	HARD	UNT	1440.94	1121.19	1162.83	1563.14
		UNC	635.08	722.49	766.41	718.35
	SOFT	UNT	354.87	357.08	370.70	595.97
		UNC	319.78	234.33	246.64	275.56
MTM45-1-HTS40F13 CPT : 0.1397 mm	QUASI	UNT	817.17	753.47	729.91	810.84
		UNC	606.88	440.90	457.34	529.90
	HARD	UNT	1298.21	1181.10	1206.62	1246.69
		UNC	695.54	700.82	727.75	711.85
	SOFT	UNT	456.57	308.94	313.32	496.47
		UNC	401.96	225.29	230.32	258.62
AS4-MTM45 CPT : 0.1397 mm	QUASI	UNT	755.25	664.38	639.61	705.28
		UNC	539.72	456.20	476.72	527.32
	HARD	UNT	1114.40	1100.09	1063.66	1101.06
		UNC	658.31	719.97	753.18	689.53
	SOFT	UNT	441.40	302.44	309.51	438.68
		UNC	388.17	229.45	236.45	236.76
CYTECT40-800-CYCOM5215 CPT : 0.14478 mm	QUASI	UNT	718.78	-	-	-
		UNC	542.89	-	-	-
	HARD	UNT	1277.39	-	-	-
		UNC	760.49	-	-	-
	SOFT	UNT	438.16	-	-	-
		UNC	406.45	-	-	-
IM7G-EpoxyEP2202 CPT : 0.18288 mm	QUASI	UNT	968.43	1030.69	1002.11	1104.48
		UNC	0.00	549.00	566.17	635.04
	HARD	UNT	1630.88	1493.81	1521.06	1701.21
		UNC	0.00	874.44	902.97	868.12
	SOFT	UNT	567.61	387.69	391.12	672.64
		UNC	0.00	280.47	285.00	315.39
IM7G-MTM45-1 CPT : 0.1397 mm	QUASI	UNT	915.69	865.17	836.35	906.72
		UNC	557.99	411.63	428.87	485.55
	HARD	UNT	1425.91	1102.53	1131.20	1417.10
		UNC	644.18	654.62	682.66	662.38
	SOFT	UNT	517.87	285.34	290.94	534.80
		UNC	400.45	208.20	214.11	228.46

Total	ALL	45		5	12	28
Total	QI UNT	8		1	4	3
Total	QI UNC	7		0	2	5
Total	HARD UNT	8		0	3	5
Total	HARD UNC	7		3	2	2
Total	SOFT UNT	8		1	1	6
Total	SOFT UNC	7		0	0	7

Table E.3: Comparison of unnotched strength prediction on the NIAR dataset, for RTD conditions. Compared criteria are: Last-Ply-Failure with mRoM degradation (LPF mRoM), Last-Ply-Failure with MFH degradation (LPF MFH) and First-Ply-Failure on the 0° ply only (FPF 0). The experimental unnotched strength is given in the column labeled *exp*. Unit system is MPa. The colored cell is always representative of the criterion with the smallest error. Red cells are for unsafe prediction. Green cells are for safe predictions. If the material properties were not sufficient for applying the criteria, a dash is written in the cell. A yellow cell means that the experimental unnotched strength was missing. Below, a summary of which criterion was the most predictive, for each loading and layup case. The light blue cell indicates which criterion was best.

Material	Lay-up	Loading	exp	UC	UCD
IM7-8552 CPT : 0.18288 mm	QUASI	UNT	721.81	855.41	761.61
		UNC	600.19	644.54	567.30
	HARD	UNT	1210.93	1232.18	1123.97
		UNC	833.16	967.31	897.74
	SOFT	UNT	462.02	452.97	320.89
		UNC	458.09	393.74	279.49
AS4-8552 CPT : 0.18796 mm	QUASI	UNT	610.94	709.40	612.78
		UNC	560.68	543.46	463.54
	HARD	UNT	1050.21	1015.21	906.04
		UNC	903.56	802.73	730.83
	SOFT	UNT	438.64	399.59	263.20
		UNC	430.37	348.68	230.86
Cytec5250-T650 CPT : 0.1397 mm	QUASI	UNT	692.58	774.59	675.37
		UNC	647.97	643.60	555.49
	HARD	UNT	1166.25	1123.93	1013.96
		UNC	929.90	956.16	872.26
	SOFT	UNT	457.88	439.48	296.69
		UNC	495.66	401.42	270.64
Cytec5320-T650 CPT : 0.1397 mm	QUASI	UNT	673.08	738.36	643.86
		UNC	666.23	620.94	535.83
	HARD	UNT	1057.28	1071.20	968.06
		UNC	890.92	920.76	840.44
	SOFT	UNT	466.31	420.91	283.96
		UNC	498.70	386.04	260.33
MR60H-NB4708 CPT : 0.32004 mm	QUASI	UNT	748.77	803.66	718.09
		UNC	478.63	495.02	439.45
	HARD	UNT	1440.94	1193.80	1088.25
		UNC	635.08	801.55	755.29
	SOFT	UNT	354.87	449.76	347.38
		UNC	319.78	313.54	243.15
MTM45-1-HTS40F13 CPT : 0.1397 mm	QUASI	UNT	817.17	721.11	638.60
		UNC	606.88	503.37	441.80
	HARD	UNT	1298.21	1020.84	927.31
		UNC	695.54	756.76	702.05
	SOFT	UNT	456.57	373.40	262.27
		UNC	401.96	308.77	220.36
AS4-MTM45 CPT : 0.1397 mm	QUASI	UNT	755.25	648.01	577.16
		UNC	539.72	520.56	459.44
	HARD	UNT	1114.40	940.33	861.80
		UNC	658.31	780.17	723.50
	SOFT	UNT	441.40	347.01	250.24
		UNC	388.17	309.84	224.35
CYTECT40-800-CYCOM5215 CPT : 0.14478 mm	QUASI	UNT	718.78	830.28	741.20
		UNC	542.89	524.24	467.49
	HARD	UNT	1277.39	1180.35	1058.86
		UNC	760.49	796.23	747.05
	SOFT	UNT	438.16	400.35	291.21
		UNC	406.45	315.63	234.89
IM7G-EpoxyEP2202 CPT : 0.18288 mm	QUASI	UNT	968.43	964.63	856.68
		UNC	0.00	624.86	552.85
	HARD	UNT	1630.88	1356.53	1225.78
		UNC	0.00	946.67	882.89
	SOFT	UNT	567.61	485.53	340.73
		UNC	0.00	383.93	277.36
IM7G-MTM45-1 CPT : 0.1397 mm	QUASI	UNT	915.69	764.72	696.27
		UNC	557.99	462.29	417.38
	HARD	UNT	1425.91	1058.89	976.66
		UNC	644.18	707.93	669.18
	SOFT	UNT	517.87	354.05	266.20
		UNC	400.45	274.34	210.39

Total	ALL	57		43	14
Total	QI UNT	10		4	6
Total	QI UNC	9		8	1
Total	HARD UNT	10		10	0
Total	HARD UNC	9		3	6
Total	SOFT UNT	10		9	1
Total	SOFT UNC	9		9	0

Table E.4: Comparison of unnotched strength prediction on the NIAR dataset, for RTD conditions. Compared criteria are: Unit Circle (UC) and Unit Circle with degraded properties using the MFH method (UCD). The experimental unnotched strength is given in the column labeled *exp*. Unit system is MPa. The colored cell is always representative of the criterion with the smallest error. Red cells are for unsafe prediction. Green cells are for safe predictions. If the material properties were not sufficient for applying the criteria, a dash is written in the cell. A yellow cell means that the experimental unnotched strength was missing. Below, a summary of which criterion was the most predictive, for each loading and layup case. The light blue cell indicates which criterion was best.

Material	Lay-up	Loading	exp	MS	UC	UCD	LPF mRoM	LPF MFH	FPF 0
IM7-8552 CPT : 0.18288 mm	QUASI	UNT	721.81	941.09	855.41	761.61	885.21	853.88	940.86
		UNC	600.19	659.89	644.54	567.30	562.48	589.26	691.64
	HARD	UNT	1210.93	1457.85	1232.18	1123.97	1457.23	1419.17	1482.34
		UNC	833.16	1009.67	967.31	897.74	890.31	933.72	912.17
	SOFT	UNT	462.02	589.22	452.97	320.89	383.41	390.11	601.04
		UNC	458.09	422.29	393.74	279.49	284.33	293.43	326.68
AS4-8552 CPT : 0.18796 mm	QUASI	UNT	610.94	775.29	709.40	612.78	711.22	686.57	776.25
		UNC	560.68	556.37	543.46	463.54	461.54	481.22	572.64
	HARD	UNT	1050.21	1181.75	1015.21	906.04	1173.39	1137.18	1198.61
		UNC	903.56	836.40	802.73	730.83	728.43	760.37	751.36
	SOFT	UNT	438.64	507.29	399.59	263.20	320.16	323.15	514.45
		UNC	430.37	372.76	348.68	230.86	237.16	242.71	288.34
Cytec5250-T650 CPT : 0.1397 mm	QUASI	UNT	692.58	833.25	774.59	675.37	-	-	-
		UNC	647.97	662.08	643.60	555.49	-	-	-
	HARD	UNT	1166.25	1277.09	1123.93	1013.96	-	-	-
		UNC	929.90	1005.26	956.16	872.26	-	-	-
	SOFT	UNT	457.88	538.72	439.48	296.69	-	-	-
		UNC	495.66	436.22	401.42	270.64	-	-	-
Cytec5320-T650 CPT : 0.1397 mm	QUASI	UNT	673.08	793.29	738.36	643.86	730.54	705.28	791.14
		UNC	666.23	639.70	620.94	535.83	540.12	559.65	650.26
	HARD	UNT	1057.28	1215.29	1071.20	968.06	1205.65	1168.06	1231.01
		UNC	890.92	970.67	920.76	840.44	856.43	889.19	867.17
	SOFT	UNT	466.31	513.58	420.91	283.96	376.52	381.59	522.07
		UNC	498.70	420.85	386.04	260.33	276.62	281.89	325.69
MR60H-NB4708 CPT : 0.32004 mm	QUASI	UNT	748.77	941.80	803.66	718.09	787.68	820.78	939.63
		UNC	478.63	502.10	495.02	439.45	427.30	453.11	528.12
	HARD	UNT	1440.94	1560.74	1193.80	1088.25	1121.19	1162.83	1563.14
		UNC	635.08	822.69	801.55	755.29	722.49	766.41	718.35
	SOFT	UNT	354.87	595.82	449.76	347.38	357.08	370.70	595.97
		UNC	319.78	322.34	313.54	243.15	234.33	246.64	275.56
MTM45-1-HTS40F13 CPT : 0.1397 mm	QUASI	UNT	817.17	811.52	721.11	638.60	753.47	729.91	810.84
		UNC	606.88	513.36	503.37	441.80	440.90	457.34	529.90
	HARD	UNT	1298.21	1251.24	1020.84	927.31	1181.10	1206.62	1246.69
		UNC	695.54	784.21	756.76	702.05	700.82	727.75	711.85
	SOFT	UNT	456.57	508.37	373.40	262.27	308.94	313.32	496.47
		UNC	401.96	327.45	308.77	220.36	225.29	230.32	258.62
AS4-MTM45 CPT : 0.1397 mm	QUASI	UNT	755.25	704.21	648.01	577.16	664.38	639.61	705.28
		UNC	539.72	535.35	520.56	459.44	456.20	476.72	527.32
	HARD	UNT	1114.40	1088.40	940.33	861.80	1100.09	1063.66	1101.06
		UNC	658.31	820.30	780.17	723.50	719.97	753.18	689.53
	SOFT	UNT	441.40	437.85	347.01	250.24	302.44	309.51	438.68
		UNC	388.17	337.09	309.84	224.35	229.45	236.45	236.76
CYTECT40-800-CYCOM5215 CPT : 0.14478 mm	QUASI	UNT	718.78	950.73	830.28	741.20	-	-	-
		UNC	542.89	532.59	524.24	467.49	-	-	-
	HARD	UNT	1277.39	1485.28	1180.35	1058.86	-	-	-
		UNC	760.49	819.87	796.23	747.05	-	-	-
	SOFT	UNT	438.16	580.56	400.35	291.21	-	-	-
		UNC	406.45	331.29	315.63	234.89	-	-	-
IM7G-EpoxyEP2202 CPT : 0.18288 mm	QUASI	UNT	968.43	1104.49	964.63	856.68	1030.69	1002.11	1104.48
		UNC	0.00	634.80	624.86	552.85	549.00	566.17	635.04
	HARD	UNT	1630.88	1711.06	1356.53	1225.78	1493.81	1521.06	1701.21
		UNC	0.00	974.38	946.67	882.89	874.44	902.97	868.12
	SOFT	UNT	567.61	690.56	485.53	340.73	387.69	391.12	672.64
		UNC	0.00	403.12	383.93	277.36	280.47	285.00	315.39
IM7G-MTM45-1 CPT : 0.1397 mm	QUASI	UNT	915.69	907.82	764.72	696.27	865.17	836.35	906.72
		UNC	557.99	468.61	462.29	417.38	411.63	428.87	485.55
	HARD	UNT	1425.91	1420.67	1058.89	976.66	1102.53	1131.20	1417.10
		UNC	644.18	726.25	707.93	669.18	654.62	682.66	662.38
	SOFT	UNT	517.87	545.23	354.05	266.20	285.34	290.94	534.80
		UNC	400.45	286.33	274.34	210.39	208.20	214.11	228.46

Total	ALL	57		18	15	7	4	2	11
Total	QI UNT	10		2	1	6	0	0	1
Total	QI UNC	9		3	2	0	0	1	3
Total	HARD UNT	10		3	5	0	0	0	2
Total	HARD UNC	9		1	1	1	3	1	2
Total	SOFT UNT	10		0	6	0	1	0	3
Total	SOFT UNC	9		9	0	0	0	0	0

Table E.5: Comparison of unnotched strength prediction on the NIAR dataset, for RTD conditions. Compared criteria are: Max-Strain (MS), Unit Circle (UC), Unit Circle with Degraded properties using MFH (UCD), Last-Ply-Failure with mRoM degradation (LPF mRoM), Last-Ply-Failure with MFH degradation (LPF MFH) and First-Ply-Failure on the 0° ply only (FPF 0). The experimental unnotched strength is given in the column labeled *exp*. Unit system is MPa. The colored cell is always representative of the criterion with the smallest error. Red cells are for unsafe prediction. Green cells are for safe predictions. If the material properties were not sufficient for applying the criteria, a dash is written in the cell. A yellow cell means that the experimental unnotched strength was missing. Below, a summary of which criterion was the most predictive, for each loading and layup case. The light blue cell indicates which criterion was best.

Material	Lay-up	Loading	exp	MS	UC	UCD	LPF mRoM	LPF MFH	FPF 0
IM7-8552 CPT : 0.18288 mm	QUASI	OHT	406.79	158.90	163.03	175.27	160.98	163.15	158.91
		OHC	338.39	131.08	133.33	151.88	153.63	145.00	127.43
	HARD	OHT	597.02	585.84	583.19	587.90	589.57	592.81	585.93
		OHC	436.02	490.71	489.44	502.17	502.70	500.20	474.24
	SOFT	OHT	300.96	251.81	243.35	214.91	228.45	230.96	0.00
		OHC	267.52	215.02	212.09	189.80	192.11	192.75	195.53
AS4-8552 CPT : 0.18796 mm	QUASI	OHT	328.40	123.35	125.46	136.65	125.35	127.07	123.34
		OHC	325.98	162.54	167.52	232.95	236.26	209.49	157.23
	HARD	OHT	472.64	470.78	468.85	473.60	474.48	477.06	470.76
		OHC	432.85	473.23	470.88	492.85	493.52	490.30	450.14
	SOFT	OHT	270.07	0.00	205.73	177.87	190.91	192.41	0.00
		OHC	280.13	215.64	211.92	176.21	180.21	180.58	190.56
Cytec5250-T650 CPT : 0.1397 mm	QUASI	OHT	384.66	158.66	163.95	183.37	163.95	163.95	163.95
		OHC	343.63	146.06	149.29	176.80	149.29	149.29	149.29
	HARD	OHT	564.20	554.35	551.55	559.50	-	-	-
		OHC	447.40	497.39	495.68	510.19	-	-	-
	SOFT	OHT	300.54	245.69	237.64	205.50	-	-	-
		OHC	302.40	223.59	219.89	191.09	-	-	-
Cytec5320-T650 CPT : 0.1397 mm	QUASI	OHT	341.99	124.83	126.82	137.10	127.30	129.26	124.87
		OHC	350.90	158.97	163.72	203.58	200.33	187.86	156.65
	HARD	OHT	486.75	491.15	489.76	495.58	495.75	498.48	491.31
		OHC	455.16	509.66	507.13	524.25	526.17	524.04	489.97
	SOFT	OHT	293.27	216.89	213.50	187.70	206.98	208.95	0.00
		OHC	306.71	228.17	223.63	190.84	198.26	198.30	205.63
MR60H-NB4708 CPT : 0.32004 mm	QUASI	OHT	476.77	260.73	302.52	366.08	310.82	294.76	261.12
		OHC	262.62	88.41	89.39	101.25	105.35	97.45	85.50
	HARD	OHT	965.75	727.21	712.16	719.30	699.28	699.27	727.84
		OHC	387.69	400.30	399.87	412.19	411.79	408.39	382.59
	SOFT	OHT	264.41	300.27	284.71	254.93	252.52	255.63	300.45
		OHC	199.95	167.34	166.68	156.70	155.31	156.21	157.38
MTM45-1-HTS40F13 CPT : 0.1397 mm	QUASI	OHT	416.93	214.34	238.65	287.57	227.83	235.41	214.47
		OHC	327.09	184.37	191.32	286.37	289.33	247.25	174.92
	HARD	OHT	677.69	606.44	594.84	601.86	612.85	623.76	606.15
		OHC	442.02	482.01	479.35	502.87	503.20	499.62	454.85
	SOFT	OHT	289.99	260.27	239.82	198.81	214.23	217.47	258.67
		OHC	268.41	207.41	203.39	171.91	175.25	175.62	180.55
AS4-MTM45 CPT : 0.1397 mm	QUASI	OHT	395.69	215.02	238.18	299.67	230.09	242.92	214.69
		OHC	301.71	133.67	137.87	167.66	170.21	156.28	135.86
	HARD	OHT	645.14	580.50	570.48	580.90	596.46	601.11	582.06
		OHC	386.45	440.93	438.72	452.26	453.15	450.72	417.16
	SOFT	OHT	283.10	245.28	228.58	191.66	210.11	215.37	245.32
		OHC	250.42	189.19	185.08	162.79	165.67	166.33	161.80
CYTECT40-800-CYCOM5215 CPT : 0.14478 mm	QUASI	OHT	451.06	216.91	236.86	269.64	236.86	236.86	236.86
		OHC	292.34	112.95	114.68	132.81	114.68	114.68	114.68
	HARD	OHT	833.23	655.10	646.13	647.29	-	-	-
		OHC	379.83	427.11	426.05	438.15	-	-	-
	SOFT	OHT	294.34	275.51	251.20	214.54	-	-	-
		OHC	254.55	181.48	179.41	162.35	-	-	-
IM7G-EpoxyEP2202 CPT : 0.18288 mm	QUASI	OHT	534.98	289.57	319.32	370.99	301.94	308.58	289.57
		OHC	337.31	131.94	133.69	153.63	155.23	148.65	131.90
	HARD	OHT	818.39	776.04	762.48	767.28	768.87	778.67	775.44
		OHC	402.37	491.20	490.19	503.80	503.78	502.08	476.01
	SOFT	OHT	358.36	333.15	305.60	254.71	268.01	270.61	331.34
		OHC	295.77	212.88	210.66	189.48	191.11	190.96	194.63
IM7G-MTM45-1 CPT : 0.1397 mm	QUASI	OHT	468.91	234.19	280.66	335.30	243.30	251.25	234.39
		OHC	295.58	129.18	132.31	170.30	178.95	156.67	122.18
	HARD	OHT	795.59	685.80	663.34	665.39	646.69	659.51	685.70
		OHC	344.26	438.58	436.94	453.14	452.29	449.15	414.99
	SOFT	OHT	323.92	282.84	246.64	206.29	209.13	213.02	281.39
		OHC	262.35	180.52	177.95	158.10	157.82	158.33	158.19

Total	ALL	40		19	4	2	0	5	10
Total	QI OHT	0		0	0	0	0	0	0
Total	QI OHC	0		0	0	0	0	0	0
Total	HARD OHT	10		2	1	2	0	4	1
Total	HARD OHC	10		0	2	0	0	0	8
Total	SOFT OHT	10		7	1	0	0	1	1
Total	SOFT OHC	10		10	0	0	0	0	0

Table E.6: Comparison of OH strength prediction on the NIAR dataset based on average $\mathscr{R}$-curve calibration, for RTD conditions. Compared criteria are: Max-Strain (MS), Unit Circle (UC), Unit Circle with Degraded properties using MFH (UCD), Last-Ply-Failure with mRoM degradation (LPF mRoM)and with MFH degradation (LPF MFH) and First-Ply-Failure on the 0° ply only (FPF 0). The experimental OH strength is given in the column labeled *exp*. Unit system is MPa. The colored cell is always representative of the criterion with the smallest error. Red and green cells are for unsafe and safe predictions, respectively. If the material properties were not sufficient for applying the criteria, a dash is written in the cell. A yellow cell means that no solution was found to the coupled energy-stress criterion Eq. (1.10). Below, a summary of which criterion was the most predictive, for each loading and layup case. The light blue cell indicates which criterion was best. Calibration was performed on strengths in light orange. Calibrated $\mathscr{R}_{ss}^{0,\text{calib.}}$ values are shown in light brown, in [N/mm].

Material	Lay-up	Loading	exp	BEST	MS	UC	UCD	LPF mRoM	LPF MFH	FPF 0
IM7-8552 CPT : 0.18288 mm	QUASI	UNT	721.81	761.61	941.09	855.41	761.61	885.21	853.88	940.86
		UNC	600.19	691.64	659.89	644.54	567.30	562.48	589.26	691.64
	HARD	UNT	1210.93	1232.18	1457.85	1232.18	1123.97	1457.23	1419.17	1482.34
		UNC	833.16	890.31	1009.67	967.31	897.74	890.31	933.72	912.17
	SOFT	UNT	462.02	452.97	589.22	452.97	320.89	383.41	390.11	601.04
		UNC	458.09	422.29	422.29	393.74	279.49	284.33	293.43	326.68
AS4-8552 CPT : 0.18796 mm	QUASI	UNT	610.94	612.78	775.29	709.40	612.78	711.22	686.57	776.25
		UNC	560.68	572.64	556.37	543.46	463.54	461.54	481.22	572.64
	HARD	UNT	1050.21	1015.21	1181.75	1015.21	906.04	1173.39	1137.18	1198.61
		UNC	903.56	728.43	836.40	802.73	730.83	728.43	760.37	751.36
	SOFT	UNT	438.64	399.59	507.29	399.59	263.20	320.16	323.15	514.45
		UNC	430.37	372.76	372.76	348.68	230.86	237.16	242.71	288.34
Cytec5250-T650 CPT : 0.1397 mm	QUASI	UNT	692.58	675.37	833.25	774.59	675.37	-	-	-
		UNC	647.97	662.08	662.08	643.60	555.49	-	-	-
	HARD	UNT	1166.25	1123.93	1277.09	1123.93	1013.96	-	-	-
		UNC	929.90	872.26	1005.26	956.16	872.26	-	-	-
	SOFT	UNT	457.88	439.48	538.72	439.48	296.69	-	-	-
		UNC	495.66	436.22	436.22	401.42	270.64	-	-	-
Cytec5320-T650 CPT : 0.1397 mm	QUASI	UNT	673.08	643.86	793.29	738.36	643.86	730.54	705.28	791.14
		UNC	666.23	650.26	639.70	620.94	535.83	540.12	559.65	650.26
	HARD	UNT	1057.28	1071.20	1215.29	1071.20	968.06	1205.65	1168.06	1231.01
		UNC	890.92	856.43	970.67	920.76	840.44	856.43	889.19	867.17
	SOFT	UNT	466.31	420.91	513.58	420.91	283.96	376.52	381.59	522.07
		UNC	498.70	420.85	420.85	386.04	260.33	276.62	281.89	325.69
MR60H-NB4708 CPT : 0.32004 mm	QUASI	UNT	748.77	718.09	941.80	803.66	718.09	787.68	820.78	939.63
		UNC	478.63	528.12	502.10	495.02	439.45	427.30	453.11	528.12
	HARD	UNT	1440.94	1193.80	1560.74	1193.80	1088.25	1121.19	1162.83	1563.14
		UNC	635.08	722.49	822.69	801.55	755.29	722.49	766.41	718.35
	SOFT	UNT	354.87	449.76	595.82	449.76	347.38	357.08	370.70	595.97
		UNC	319.78	322.34	322.34	313.54	243.15	234.33	246.64	275.56
MTM45-1-HTS40F13 CPT : 0.1397 mm	QUASI	UNT	817.17	638.60	811.52	721.11	638.60	753.47	729.91	810.84
		UNC	606.88	529.90	513.36	503.37	441.80	440.90	457.34	529.90
	HARD	UNT	1298.21	1020.84	1251.24	1020.84	927.31	1181.10	1206.62	1246.69
		UNC	695.54	700.82	784.21	756.76	702.05	700.82	727.75	711.85
	SOFT	UNT	456.57	373.40	508.37	373.40	262.27	308.94	313.32	496.47
		UNC	401.96	327.45	327.45	308.77	220.36	225.29	230.32	258.62
AS4-MTM45 CPT : 0.1397 mm	QUASI	UNT	755.25	577.16	704.21	648.01	577.16	664.38	639.61	705.28
		UNC	539.72	527.32	535.35	520.56	459.44	456.20	476.72	527.32
	HARD	UNT	1114.40	940.33	1088.40	940.33	861.80	1100.09	1063.66	1101.06
		UNC	658.31	719.97	820.30	780.17	723.50	719.97	753.18	689.53
	SOFT	UNT	441.40	347.01	437.85	347.01	250.24	302.44	309.51	438.68
		UNC	388.17	337.09	337.09	309.84	224.35	229.45	236.45	236.76
CYTECT40-800-CYCOM5215 CPT : 0.14478 mm	QUASI	UNT	718.78	741.20	950.73	830.28	741.20	-	-	-
		UNC	542.89	532.59	532.59	524.24	467.49	-	-	-
	HARD	UNT	1277.39	1180.35	1485.28	1180.35	1058.86	-	-	-
		UNC	760.49	747.05	819.87	796.23	747.05	-	-	-
	SOFT	UNT	438.16	400.35	580.56	400.35	291.21	-	-	-
		UNC	406.45	331.29	331.29	315.63	234.89	-	-	-
IM7G-EpoxyEP2202 CPT : 0.18288 mm	QUASI	UNT	968.43	856.68	1104.49	964.63	856.68	1030.69	1002.11	1104.48
		UNC	0.00	635.04	634.80	624.86	552.85	549.00	566.17	635.04
	HARD	UNT	1630.88	1356.53	1711.06	1356.53	1225.78	1493.81	1521.06	1701.21
		UNC	0.00	874.44	974.38	946.67	882.89	874.44	902.97	868.12
	SOFT	UNT	567.61	485.53	690.56	485.53	340.73	387.69	391.12	672.64
		UNC	0.00	403.12	403.12	383.93	277.36	280.47	285.00	315.39
IM7G-MTM45-1 CPT : 0.1397 mm	QUASI	UNT	915.69	696.27	907.82	764.72	696.27	865.17	836.35	906.72
		UNC	557.99	485.55	468.61	462.29	417.38	411.63	428.87	485.55
	HARD	UNT	1425.91	1058.89	1420.67	1058.89	976.66	1102.53	1131.20	1417.10
		UNC	644.18	654.62	726.25	707.93	669.18	654.62	682.66	662.38
	SOFT	UNT	517.87	354.05	545.23	354.05	266.20	285.34	290.94	534.80
		UNC	400.45	286.33	286.33	274.34	210.39	208.20	214.11	228.46

Total	ALL	57		34	8	4	0	1	2	8
Total	QI UNT	10		6	2	1	0	0	0	1
Total	QI UNC	9		4	2	2	0	0	1	0
Total	HARD UNT	10		5	3	0	0	0	0	2
Total	HARD UNC	9		4	1	1	0	0	1	2
Total	SOFT UNT	10		6	0	0	0	1	0	3
Total	SOFT UNC	9		9	0	0	0	0	0	0

Table E.7: Comparison of unnotched strength prediction on the NIAR dataset, for RTD conditions. Compared criteria are: Best Practise (glsBEST), Max-Strain (MS), Unit Circle (UC), Unit Circle with Degraded properties using MFH (UCD), Last-Ply-Failure with mRoM degradation (LPF mRoM), Last-Ply-Failure with MFH degradation (LPF MFH) and First-Ply-Failure on the 0° ply only (FPF 0). The experimental unnotched strength is given in the column labeled *exp*. Unit system is MPa. The colored cell is always representative of the criterion with the smallest error. Red cells are for unsafe prediction. Green cells are for safe predictions. If the material properties were not sufficient for applying the criteria, a dash is written in the cell. A yellow cell means that the experimental unnotched strength was missing. Below, a summary of which criterion was the most predictive, for each loading and layup case. The light blue cell indicates which criterion was best.

Material	Lay-up	Loading	exp	BEST	MS	UC	UCD	LPF mRoM	LPF MFH	FPF 0
IM7-8552 CPT : 0.18288 mm	QUASI	OHT	406.79	175.27	158.90	163.03	175.27	160.98	163.15	158.91
		OHC	338.39	127.43	131.08	133.33	151.88	153.63	145.00	127.43
	HARD	OHT	597.02	600.63	585.84	583.19	587.90	589.57	592.81	585.93
		OHC	436.02	471.16	490.71	489.44	502.17	502.70	500.20	474.24
	SOFT	OHT	300.96	249.43	251.81	243.35	214.91	228.45	230.96	0.00
		OHC	267.52	212.76	215.02	212.09	189.80	192.11	192.75	195.53
AS4-8552 CPT : 0.18796 mm	QUASI	OHT	328.40	136.65	123.35	125.46	136.65	125.35	127.07	123.34
		OHC	325.98	157.23	162.54	167.52	232.95	236.26	209.49	157.23
	HARD	OHT	472.64	485.87	470.78	468.85	473.60	474.48	477.06	470.76
		OHC	432.85	444.49	473.23	470.88	492.85	493.52	490.30	450.14
	SOFT	OHT	270.07	212.15	0.00	205.73	177.87	190.91	192.41	0.00
		OHC	280.13	213.38	215.64	211.92	176.21	180.21	180.58	190.56
Cytec5250-T650 CPT : 0.1397 mm	QUASI	OHT	384.66	183.37	158.66	163.95	183.37	163.95	163.95	163.95
		OHC	343.63	146.06	146.06	149.29	176.80	149.29	149.29	149.29
	HARD	OHT	564.20	575.95	554.35	551.55	559.50	-	-	-
		OHC	447.40	479.12	497.39	495.68	510.19	-	-	-
	SOFT	OHT	300.54	246.74	245.69	237.64	205.50	-	-	-
		OHC	302.40	223.59	223.59	219.89	191.09	-	-	-
Cytec5320-T650 CPT : 0.1397 mm	QUASI	OHT	341.99	137.10	124.83	126.82	137.10	127.30	129.26	124.87
		OHC	350.90	156.65	158.97	163.72	203.58	200.33	187.86	156.65
	HARD	OHT	486.75	506.16	491.15	489.76	495.58	495.75	498.48	491.31
		OHC	455.16	487.89	509.66	507.13	524.25	526.17	524.04	489.97
	SOFT	OHT	293.27	219.70	216.89	213.50	187.70	206.98	208.95	0.00
		OHC	306.71	227.02	228.17	223.63	190.84	198.26	198.30	205.63
MR60H-NB4708 CPT : 0.32004 mm	QUASI	OHT	476.77	366.08	260.73	302.52	366.08	310.82	294.76	261.12
		OHC	262.62	85.50	88.41	89.39	101.25	105.35	97.45	85.50
	HARD	OHT	965.75	752.43	727.21	712.16	719.30	699.28	699.27	727.84
		OHC	387.69	383.20	400.30	399.87	412.19	411.79	408.39	382.59
	SOFT	OHT	264.41	298.68	300.27	284.71	254.93	252.52	255.63	300.45
		OHC	199.95	165.30	167.34	166.68	156.70	155.31	156.21	157.38
MTM45-1-HTS40F13 CPT : 0.1397 mm	QUASI	OHT	416.93	287.57	214.34	238.65	287.57	227.83	235.41	214.47
		OHC	327.09	174.92	184.37	191.32	286.37	289.33	247.25	174.92
	HARD	OHT	677.69	629.14	606.44	594.84	601.86	612.85	623.76	606.15
		OHC	442.02	451.47	482.01	479.35	502.87	503.20	499.62	454.85
	SOFT	OHT	289.99	250.91	260.27	239.82	198.81	214.23	217.47	258.67
		OHC	268.41	204.48	207.41	203.39	171.91	175.25	175.62	180.55
AS4-MTM45 CPT : 0.1397 mm	QUASI	OHT	395.69	299.67	215.02	238.18	299.67	230.09	242.92	214.69
		OHC	301.71	135.86	133.67	137.87	167.66	170.21	156.28	135.86
	HARD	OHT	645.14	607.72	580.50	570.48	580.90	596.46	601.11	582.06
		OHC	386.45	424.32	440.93	438.72	452.26	453.15	450.72	417.16
	SOFT	OHT	283.10	240.55	245.28	228.58	191.66	210.11	215.37	245.32
		OHC	250.42	190.19	189.19	185.08	162.79	165.67	166.33	161.80
CYTECT40-800-CYCOM5215 CPT : 0.14478 mm	QUASI	OHT	451.06	269.64	216.91	236.86	269.64	236.86	236.86	236.86
		OHC	292.34	112.95	112.95	114.68	132.81	114.68	114.68	114.68
	HARD	OHT	833.23	674.88	655.10	646.13	647.29	-	-	-
		OHC	379.83	415.64	427.11	426.05	438.15	-	-	-
	SOFT	OHT	294.34	259.85	275.51	251.20	214.54	-	-	-
		OHC	254.55	181.48	181.48	179.41	162.35	-	-	-
IM7G-EpoxyEP2202 CPT : 0.18288 mm	QUASI	OHT	534.98	370.99	289.57	319.32	370.99	301.94	308.58	289.57
		OHC	337.31	131.90	131.94	133.69	153.63	155.23	148.65	131.90
	HARD	OHT	818.39	800.15	776.04	762.48	767.28	768.87	778.67	775.44
		OHC	402.37	477.07	491.20	490.19	503.80	503.78	502.08	476.01
	SOFT	OHT	358.36	317.65	333.15	305.60	254.71	268.01	270.61	331.34
		OHC	295.77	212.86	212.88	210.66	189.48	191.11	190.96	194.63
IM7G-MTM45-1 CPT : 0.1397 mm	QUASI	OHT	468.91	335.30	234.19	280.66	335.30	243.30	251.25	234.39
		OHC	295.58	122.18	129.18	132.31	170.30	178.95	156.67	122.18
	HARD	OHT	795.59	694.85	685.80	663.34	665.39	646.69	659.51	685.70
		OHC	344.26	412.79	438.58	436.94	453.14	452.29	449.15	414.99
	SOFT	OHT	323.92	254.88	282.84	246.64	206.29	209.13	213.02	281.39
		OHC	262.35	177.79	180.52	177.95	158.10	157.82	158.33	158.19

Total	ALL	40		21	12	1	2	0	1	3
Total	QI OHT	0		0	0	0	0	0	0	0
Total	QI OHC	0		0	0	0	0	0	0	0
Total	HARD OHT	10		7	0	1	2	0	0	0
Total	HARD OHC	10		8	0	0	0	0	0	2
Total	SOFT OHT	10		3	5	0	0	0	1	1
Total	SOFT OHC	10		3	7	0	0	0	0	0

Table E.8: Comparison of OH strength prediction on the NIAR dataset based on average $\mathscr{R}$-curve calibration, for RTD conditions. Compared criteria are: Best Practise (BEST), Max-Strain (MS), Unit Circle (UC), Unit Circle with Degraded properties using MFH (UCD), Last-Ply-Failure with mRoM degradation (LPF mRoM)and with MFH degradation (LPF MFH) and First-Ply-Failure on the 0° ply only (FPF 0). The experimental OH strength is given in the column labeled *exp*. Unit system is MPa. The colored cell is always representative of the criterion with the smallest error. Red and green cells are for unsafe and safe predictions, respectively. If the material properties were not sufficient for applying the criteria, a dash is written in the cell. A yellow cell means that no solution was found to the coupled energy-stress criterion Eq. (1.10). Below, a summary of which criterion was the most predictive, for each loading and layup case. The light blue cell indicates which criterion was best. Calibration was performed on strengths in light orange. Calibrated $\mathscr{R}_{ss}^{0,\text{calib.}}$ values are shown in light brown, in [N/mm].

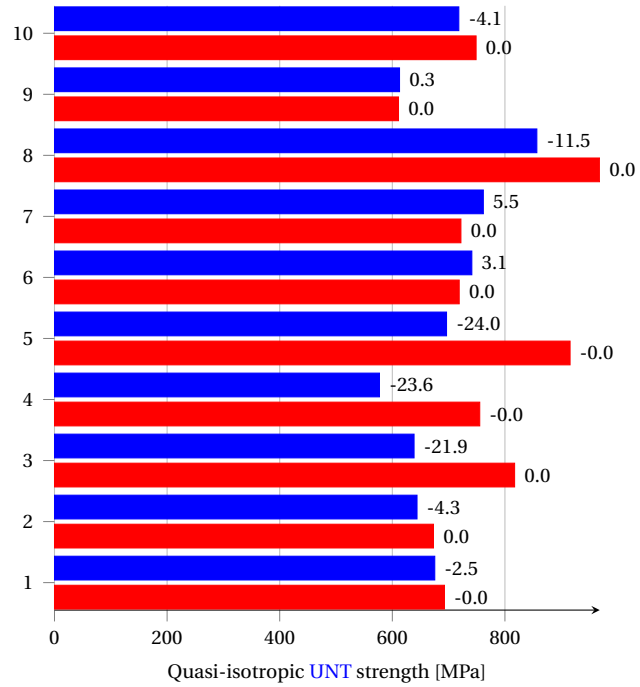

(a) Quasi-isotropic UNT strength : using experimental unnotched strength ( ), using BEST ( ).

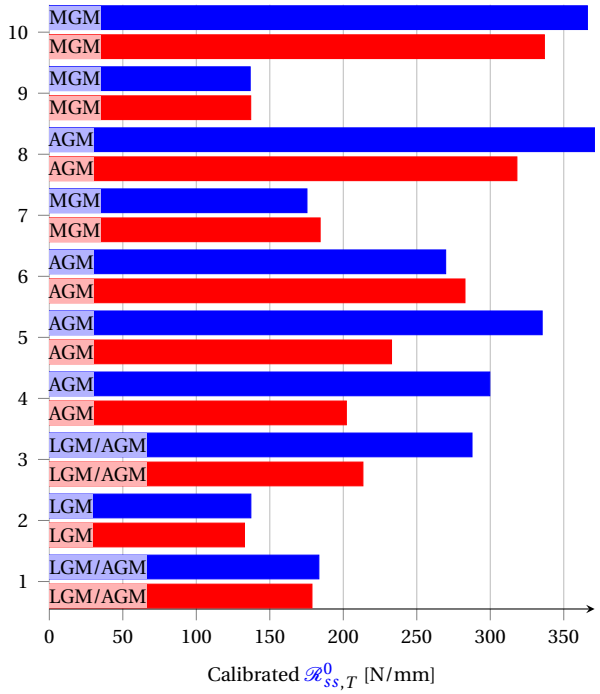

(b) Calibrated $\mathscr{R}^0_{ss,T}$: using experimental unnotched strength ( ), using BEST ( ).

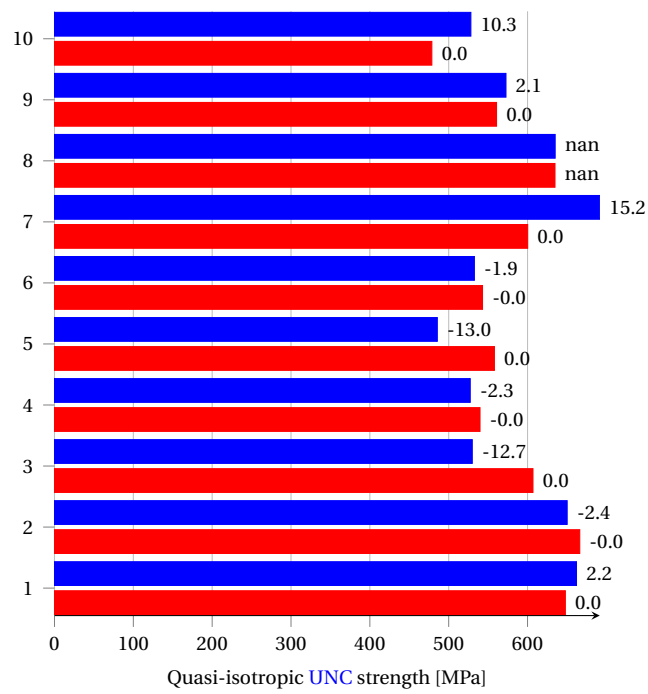

(c) Quasi-isotropic UNC strength : using experimental unnotched strength ( ), using BEST ( ).

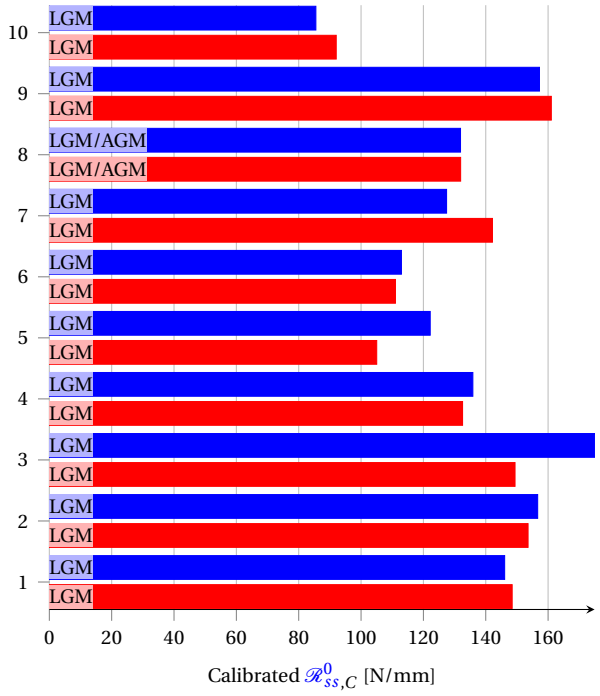

(d) Calibrated $\mathscr{R}^0_{ss,C}$: using experimental unnotched strength ( ), using BEST ( ).

Figure E.1: Prediction of unnotched strength and open-hole strength on the NIAR dataset, for QI coupons. The failure mode is given for each case, see Sect. D.3. The error of the prediction w.r.t. the expected strength is given on the right of each bar. A *nan* valued error means that no experimental strength was given. A missing bar means that no solution was found to the coupled energy-stress criterion. The material system corresponding to the integers on the y-axis can be found in Table D.3. They are classified by increasing nominal cured ply thickness. Calibration of an average $\mathscr{R}$-curve on the QI OH strength, in RTD environment.

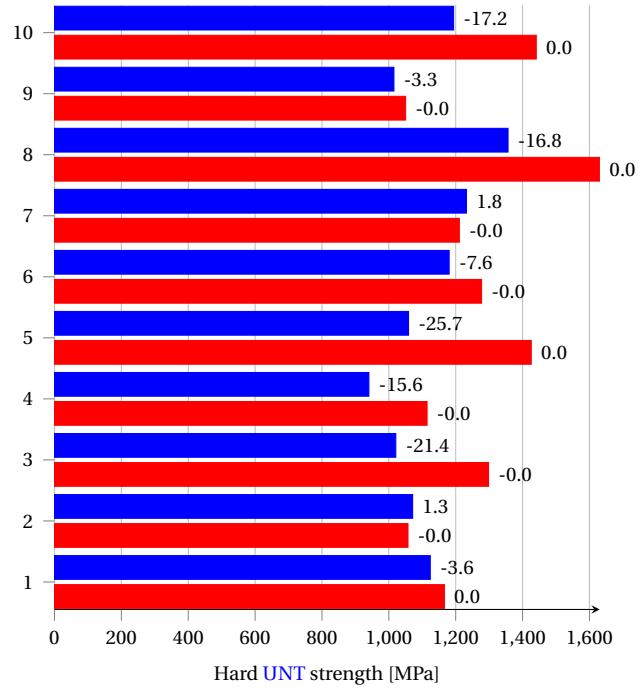

(a) Hard UNT strength : using experimental unnotched strength (=), using BEST (=).

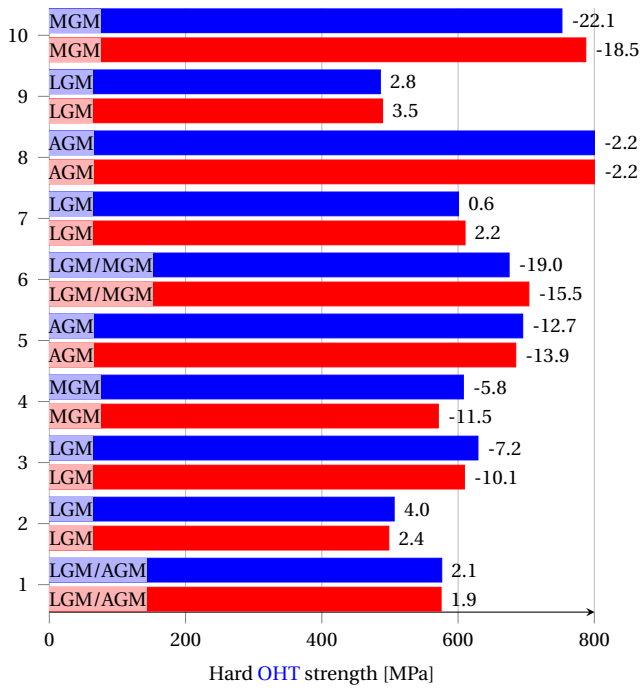

(b) Hard OHT strength : using experimental unnotched strength (=), using BEST (=).

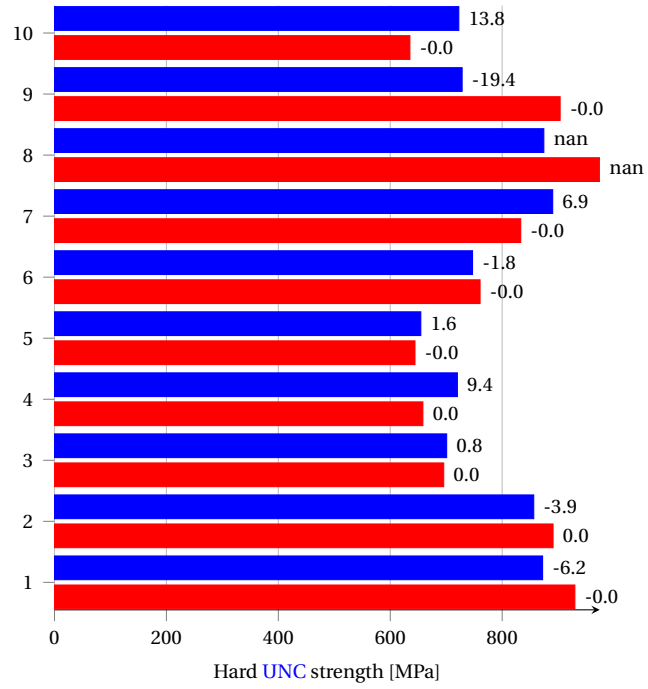

(c) Hard UNC strength : using experimental unnotched strength (=), using BEST (=).

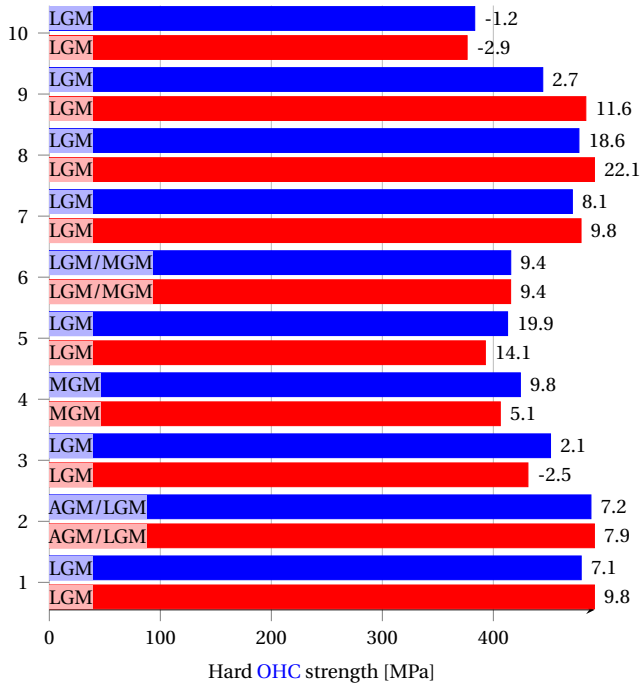

(d) Hard OHC strength : using experimental unnotched strength (=), using BEST (=).

Figure E.2: Prediction of unnotched strength and open-hole strength on the NIAR dataset, for hard coupons. The failure mode is given for each case, see Sect. D.3. The error of the prediction w.r.t. the expected strength is given on the right of each bar. A *nan* valued error means that no experimental strength was given. A missing bar means that no solution was found to the coupled energy-stress criterion. The material system corresponding to the integers on the y-axis can be found in Table D.3. They are classified by increasing nominal cured ply thickness. Calibration of an average $\mathscr{R}$-curve on the QI OH strength, in RTD environment.

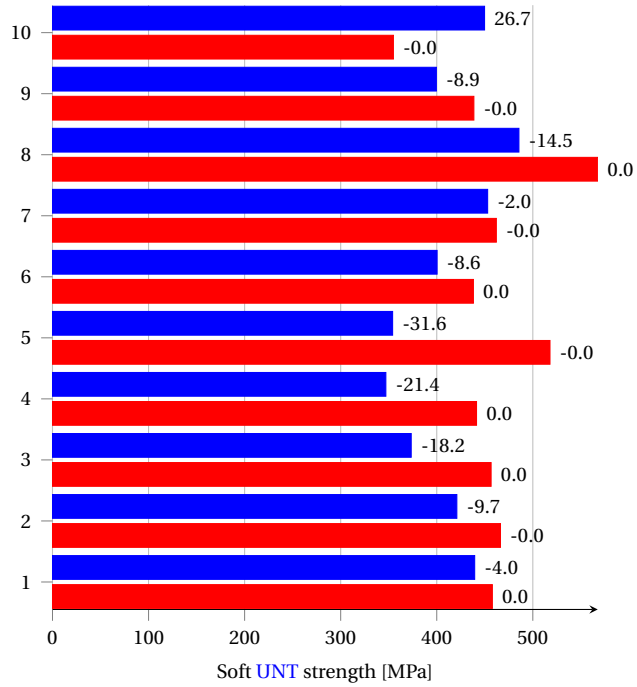

(a) Soft UNT strength : using experimental unnotched strength (), using BEST ().

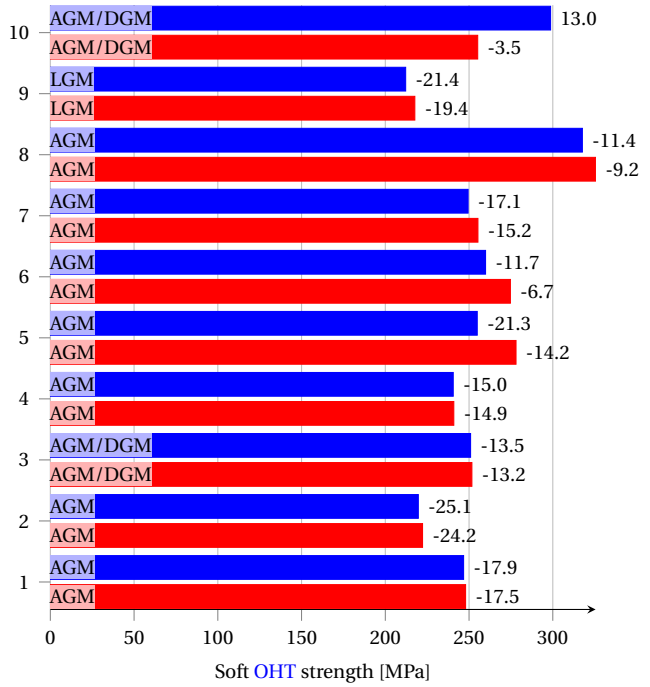

(b) Soft OHT strength : using experimental unnotched strength (), using BEST ().

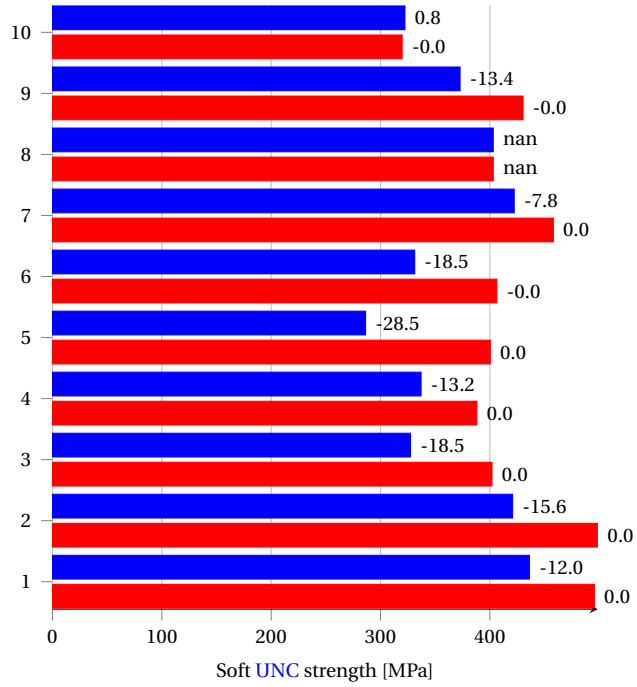

(c) Soft UNC strength : using experimental unnotched strength (), using BEST ().

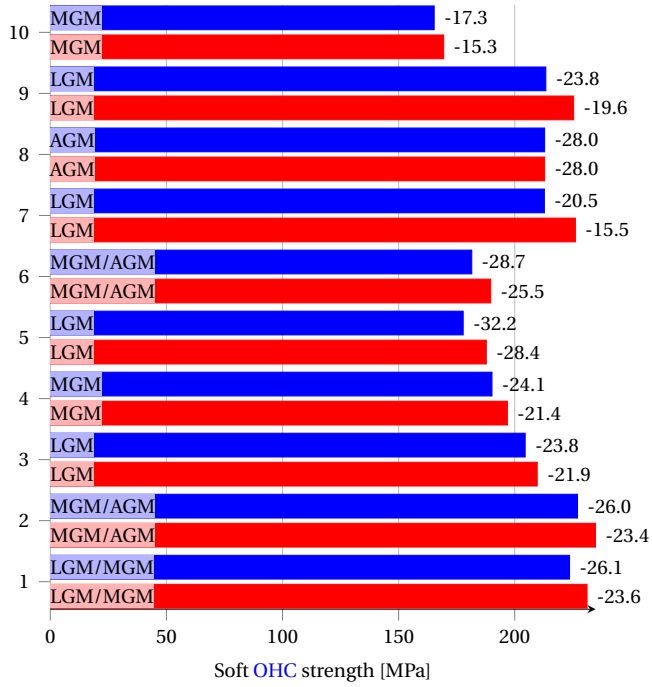

(d) Soft OHC strength : using experimental unnotched strength (), using BEST ().

Figure E.3: Prediction of unnotched strength and open-hole strength on the NIAR dataset, for soft coupons. The failure mode is given for each case, see Sect. D.3. The error of the prediction w.r.t. the expected strength is given on the right of each bar. A *nan* valued error means that no experimental strength was given. A missing bar means that no solution was found to the coupled energy-stress criterion. The material system corresponding to the integers on the y-axis can be found in Table D.3. They are classified by increasing nominal cured ply thickness. Calibration of an average $\mathscr{R}$-curve on the QI OH strength, in RTD environment.

F Residual stresses

F.1 Residual thermal stresses: details

This section is dedicated to a more detailed view of how residual stresses were implemented. It follows these steps:

1. Compute the elastic stiffness tensor of the 0° ply, $\mathbb{E}^0$, using the 4 lamina elastic constants;
2. Assuming that the plies thermally expand as transversely isotropic materials, compute the thermal expansion tensor of the 0° ply, $\boldsymbol{\alpha}^0$, using the longitudinal and transverse thermal expansion coefficients α_L and α_T;
3. Loop over the plies to compute the laminate thermal expansion tensor $\boldsymbol{\alpha}^*$ by accumulating the two terms in the right-hand side of Eq. (5.11):
   (a) Rotate $\mathbb{E}^0$ and $\boldsymbol{\alpha}^0$ by θ to obtain the ply elastic stiffness tensor $\mathbb{E}^{(i)}$ and thermal expansion tensor $\boldsymbol{\alpha}^{(i)}$ in the *global* axes;
   (b) Accumulate;
4. Inverse the first term of the right-hand side of Eq. (5.11) and compute $\boldsymbol{\alpha}^*$;
5. Loop over the plies to compute the residual stresses in each ply, in the local fiber direction $\theta^{(i)}$, i.e. in the *local* axes:
   (a) Compute the residual stresses in the ply (i) in the *global* axes:

$$\boldsymbol{\sigma}_R^{(i)} = \Delta T \mathbb{E}^{(i)} : \left(\boldsymbol{\alpha}^* - \boldsymbol{\alpha}^{(i)}\right);$$

   (b) Rotate $\boldsymbol{\sigma}_R^{(i)}$ by $-\theta$ to obtain $\boldsymbol{\sigma}_R^{(i),\theta}$, i.e. the residual stresses in the ply (i) in the *local* axes.

F.2 Total, mechanical and thermal strains

Assuming LPT holds, each ply of a symmetric and balanced laminate will undergo the same strains as the others. Be the appearent strain due to temperature difference or uniaxial loading, there is no shear strain in the *global* axes. The strains can be decomposed into two contributing parts, namely

the mechanical strains $\boldsymbol{\varepsilon}_{\text{mech}}$ and the thermal strains $\boldsymbol{\varepsilon}_R$:

$$\boldsymbol{\varepsilon}_{\text{tot}} = \boldsymbol{\varepsilon}_{\text{mech}} + \boldsymbol{\varepsilon}_R.$$

In the following, the stresses and strains in each ply is described, considering either *global* or *local* axes.

F.2.1 Without thermal stresses

In this case, it is considered that there is no influence of the temperature on the initial state of the laminate. Therefore, under uniaxial loading, one has:

- In the *global* axes:
  - There is no shear strain since the laminate is balanced.
  - There is shear stress in the angled plies[1]. However, this shear stress does not induce shear strain. For instance, the shear stress in ±45° plies is equal but of opposite sign such that the resulting shear strain in the global axis is zero.
- In the *local* axes:
  - There is both shear stress and shear strain in the angled plies.

F.2.2 With thermal stresses only

The case of thermally expanded laminate is now considered. For such a case, the following observations are made:

- In the *global* axes:
  - The is no total shear strain.
  - There are thermal shear strains in the angled plies, but since the total shear strain is zero, there are also mechanical shear strains and consequently, there are shear stresses.
- In the *local* axes:
  - There is total shear strain in angled plies, but not thermal shear strain. Therefore, there is mechanical shear strain and shear stresses.

F.2.3 With thermal stresses

This case is a superposition of the above cases.

F.3 Supplementary plots and tables

[1] Angled plies are plies whose angle is not 0° or 90°.

Material	Lay-up	Loading	exp	BEST	mRoM	mRoM TRS	MFH	MFH TRS	FPF0	FPF0 TRS
IM7-8552 CPT : 0.18288 mm	QUASI	UNT	684.99	771.77	894.34	911.17				
		UNC								
	HARD	UNT	1200.93	1307.03		1308.51				
		UNC								
	SOFT	UNT	484.15	523.01		527.10				
		UNC								
AS4-8552 CPT : 0.18796 mm	QUASI	UNT	580.61	640.75	760.87	778.35				
		UNC								
	HARD	UNT	1029.94	1100.23		1102.31				
		UNC								
	SOFT	UNT	459.26	462.28		467.14				
		UNC								
Cytec5250-T650 CPT : 0.1397 mm	QUASI	UNT	671.27	657.72	771.13	785.01				
		UNC								
	HARD	UNT	1120.88	1104.47		1105.59				
		UNC								
	SOFT	UNT	480.08	444.73		445.57				
		UNC								
Cytec5320-T650 CPT : 0.1397 mm	QUASI	UNT	637.85	637.44	746.73	763.75				
		UNC								
	HARD	UNT	995.35	1083.88		1085.60				
		UNC								
	SOFT	UNT	491.61	447.32		452.06				
		UNC								
MR60H-NB4708 CPT : 0.32004 mm	QUASI	UNT	638.59	708.34	807.89	638.40	816.04	687.08	907.42	525.11
		UNC								
	HARD	UNT	1378.61	1224.40	1174.34	855.11	1233.61	925.25	1543.30	1319.45
		UNC								
	SOFT	UNT	346.94	475.47	374.98	306.11	393.30	326.80	608.89	514.17
		UNC								
MTM45-1-HTS40F13 CPT : 0.1397 mm	QUASI	UNT	799.52	653.13	750.16	741.63	719.37	707.59	807.51	575.70
		UNC								
	HARD	UNT	1269.53	1085.98	1240.77	1037.70	1194.48	1105.32	1263.91	1084.27
		UNC								
	SOFT	UNT	505.66	428.87	360.01	302.28	368.94	315.82	541.62	508.52
		UNC								
AS4-MTM45 CPT : 0.1397 mm	QUASI	UNT	780.00	573.27	651.15	628.58	622.85	597.95	699.44	0.00
		UNC								
	HARD	UNT	1091.37	962.95	1082.96	913.59	1039.81	977.93	1113.98	811.28
		UNC								
	SOFT	UNT	480.01	379.03	337.28	272.74	343.55	285.98	478.62	401.11
		UNC								
CYTECT40-800-CYCOM5215 CPT : 0.14478 mm	QUASI	UNT	716.16	746.18	849.12	855.39				
		UNC								
	HARD	UNT	1273.88	1195.13		1195.17				
		UNC								
	SOFT	UNT	464.16	437.65		433.96				
		UNC								
IM7G-EpoxyEP2202 CPT : 0.18288 mm	QUASI	UNT	962.38	908.00	1073.28	1061.43	1037.02	1023.20	1168.21	1016.74
		UNC								
	HARD	UNT	1727.85	1500.27	1674.87	1316.99	1721.10	1386.64	1816.21	1695.34
		UNC								
	SOFT	UNT	608.23	579.91	440.63	377.03	446.82	388.63	774.08	768.39
		UNC								
IM7G-MTM45-1 CPT : 0.1397 mm	QUASI	UNT	901.08	739.42	899.96	768.41	867.82	806.39	949.10	778.88
		UNC								
	HARD	UNT	1431.01	1156.26	1231.30	892.02	1262.68	936.53	1497.05	1360.45
		UNC								
	SOFT	UNT	540.76	405.40	319.72	259.14	325.51	268.16	593.59	580.33
		UNC								

Total	ALL	30		12	2	5	1	1	5	4
Total	QI UNT	10		5	1	1	0	0	2	1
Total	QI UNC	0		0	0	0	0	0	0	0
Total	HARD UNT	10		3	1	2	1	0	2	1
Total	HARD UNC	0		0	0	0	0	0	0	0
Total	SOFT UNT	10		4	0	2	0	1	1	2
Total	SOFT UNC	0		0	0	0	0	0	0	0

Table F.1: Comparison of UN strength prediction on the NIAR dataset, for CTD conditions. Compared criteria are: Best Practise (BEST), Last Ply Failure with mRoM (*mRoM*) and MFH (*MFH*) degradation method without residual thermal stresses and with thermal stresses (*mRoM TRS* and *MFH TRS*, respectively), First Ply Failure with (*FPF0 TRS*) and without (*FPF0*) and BEST criterion. The experimental OH strength is given in the column labeled *exp*. Unit system is MPa. The colored cell is always representative of the criterion with the smallest error. Red and green cells are for unsafe and safe predictions, respectively. If the material properties were not sufficient for applying the criteria, the cell is empty. A yellow cell means that no solution was found to the coupled energy-stress criterion Eq. (1.10). Below, a summary of which criterion was the most predictive, for each loading and layup case. The light blue cell indicates which criterion was best.

Material	Lay-up	Loading	exp	BEST	mRoM	mRoM TRS	MFH	MFH TRS	FPF0	FPF0 TRS
IM7-8552 CPT : 0.18288 mm	QUASI	OHT	398.17	161.05						
		OHC								
	HARD	OHT	542.96	588.22	570.96	570.17				
		OHC								
	SOFT	OHT	316.81	259.65	252.91	252.95				
		OHC								
AS4-8552 CPT : 0.18796 mm	QUASI	OHT	310.61	112.58						
		OHC								
	HARD	OHT	431.34	451.77	444.03	444.60				
		OHC								
	SOFT	OHT	276.20	207.84	204.39	204.68				
		OHC								
Cytec5250-T650 CPT : 0.1397 mm	QUASI	OHT	368.59	162.05						
		OHC								
	HARD	OHT	533.59	550.89	526.26	524.76				
		OHC								
	SOFT	OHT	311.09	242.77	233.27	232.78				
		OHC								
Cytec5320-T650 CPT : 0.1397 mm	QUASI	OHT	324.78	116.15						
		OHC								
	HARD	OHT	449.55	477.64	464.28	463.87				
		OHC								
	SOFT	OHT	303.76	215.44	209.97	210.10				
		OHC								
MR60H-NB4708 CPT : 0.32004 mm	QUASI	OHT	455.81	309.69						0.00
		OHC								
	HARD	OHT	876.67	726.65	674.99	633.17	683.90	643.45	696.28	0.00
		OHC								
	SOFT	OHT	263.38	297.17	252.03	235.96	257.83	241.88	293.83	0.00
		OHC								
MTM45-1-HTS40F13 CPT : 0.1397 mm	QUASI	OHT	421.75	279.50						
		OHC								
	HARD	OHT	654.59	644.81	628.68	598.57	633.55	623.13	615.35	712.69
		OHC								
	SOFT	OHT	317.09	273.00	238.23	215.68	244.03	224.05	273.46	325.83
		OHC								
AS4-MTM45 CPT : 0.1397 mm	QUASI	OHT	396.38	297.32						0.00
		OHC								
	HARD	OHT	624.39	618.68	600.03	571.87	605.69	605.44	586.41	0.00
		OHC								
	SOFT	OHT	297.99	257.31	227.74	201.23	233.74	211.05	257.90	0.00
		OHC								
CYTECT40-800-CYCOM5215 CPT : 0.14478 mm	QUASI	OHT	441.47	244.79						
		OHC								
	HARD	OHT	704.64	658.18	629.28	628.08				
		OHC								
	SOFT	OHT	305.78	268.98	259.16	257.88				
		OHC								
IM7G-EpoxyEP2202 CPT : 0.18288 mm	QUASI	OHT	537.58	337.88						
		OHC								
	HARD	OHT	805.08	808.66	781.84	738.47	792.67	757.30	775.81	795.81
		OHC								
	SOFT	OHT	380.16	343.83	290.93	266.45	294.65	272.84	345.97	357.80
		OHC								
IM7G-MTM45-1 CPT : 0.1397 mm	QUASI	OHT	459.12	264.50						
		OHC								
	HARD	OHT	745.12	683.17	650.24	597.35	661.02	603.77	667.67	701.70
		OHC								
	SOFT	OHT	336.26	266.89	223.15	197.47	226.77	201.25	283.62	300.74
		OHC								

Total	ALL	20		10	2	2	1	0	1	4
Total	QI OHT	0		0	0	0	0	0	0	0
Total	QI OHC	0		0	0	0	0	0	0	0
Total	HARD OHT	10		5	2	2	0	0	0	1
Total	HARD OHC	0		0	0	0	0	0	0	0
Total	SOFT OHT	10		5	0	0	1	0	1	3
Total	SOFT OHC	0		0	0	0	0	0	0	0

Table F.2: Comparison of OH strength prediction on the NIAR dataset with calibration of an average $\mathscr{R}$-curve on QI lay-ups, for CTD conditions. Compared criteria are: Best Practise (BEST), Last Ply Failure with mRoM (*mRoM*) and MFH (*MFH*) degradation method without residual thermal stresses and with thermal stresses (*mRoM TRS* and *MFH TRS*, respectively), First Ply Failure with (*FPF0 TRS*) and without (*FPF0*) and BEST criterion. The experimental OH strength is given in the column labeled *exp*. Unit system is MPa. The colored cell is always representative of the criterion with the smallest error. Red and green cells are for unsafe and safe predictions, respectively. If the material properties were not sufficient for applying the criteria, the cell is empty. A yellow cell means that no solution was found to the coupled energy-stress criterion Eq. (1.10). Below, a summary of which criterion was the most predictive, for each loading and layup case. The light blue cell indicates which criterion was best.

Material	Lay-up	Loading	exp	BEST	mRoM	mRoM TRS	MFH	MFH TRS	FPF0	FPF0 TRS
IM7-8552 CPT : 0.18288 mm	QUASI	UNT	721.81	761.61	885.21	874.21	853.88	840.22	940.86	855.07
		UNC	600.19	691.64	562.48	504.98	589.26	535.21		310.11
	HARD	UNT	1210.93	1232.18	1457.23	1214.83	1419.17	1264.68	1482.34	1409.53
		UNC	833.16	890.31		826.52	933.72	874.13	912.17	467.98
	SOFT	UNT	462.02	452.97	383.41	339.39	390.11	348.66	601.04	599.46
		UNC	458.09	422.29	284.33	253.80	293.43	264.96	326.68	128.94
AS4-8552 CPT : 0.18796 mm	QUASI	UNT	610.94	612.78	711.22	706.50	686.57	679.53	776.25	713.24
		UNC	560.68	572.64	461.54	412.25	481.22	435.00		255.13
	HARD	UNT	1050.21	1015.21	1173.39	980.20	1137.18	1016.00	1198.61	1148.78
		UNC	903.56	728.43		677.05	760.37	712.58	751.36	398.06
	SOFT	UNT	438.64	399.59	320.16	281.60	323.15	287.15	514.45	518.41
		UNC	430.37	372.76	237.16	210.62	242.71	218.12	288.34	114.14
Cytec5250-T650 CPT : 0.1397 mm	QUASI	UNT	692.58	675.37	774.59	784.86				
		UNC	647.97	662.08	643.60	628.41				
	HARD	UNT	1166.25	1123.93		1124.67				
		UNC	929.90	872.26	956.16	954.42				
	SOFT	UNT	457.88	439.48		441.23				
		UNC	495.66	436.22	401.42	393.66				
Cytec5320-T650 CPT : 0.1397 mm	QUASI	UNT	673.08	643.86	730.54	726.09	705.28	698.94	791.14	723.93
		UNC	666.23	650.26	540.12	491.19	559.65	514.38		333.58
	HARD	UNT	1057.28	1071.20	1205.65	1183.61	1168.06	1143.33	1231.01	1172.35
		UNC	890.92	856.43		804.72	889.19	842.00	867.17	500.32
	SOFT	UNT	466.31	420.91	376.52	337.74	381.59	345.92	522.07	521.14
		UNC	498.70	420.85	276.62	250.31	281.89	257.84	325.69	150.54
MR60H-NB4708 CPT : 0.32004 mm	QUASI	UNT	748.77	718.09	787.68	694.70	820.78	728.88	939.63	890.02
		UNC	478.63	528.12	427.30	386.75	453.11	414.59		238.28
	HARD	UNT	1440.94	1193.80	1121.19	946.79	1162.83	993.61	1563.14	1553.01
		UNC	635.08	722.49		674.19	766.41	720.48	718.35	374.75
	SOFT	UNT	354.87	449.76	357.08	320.59	370.70	335.09	595.97	598.38
		UNC	319.78	322.34	234.33	208.56	246.64	222.12	275.56	115.32
MTM45-1-HTS40F13 CPT : 0.1397 mm	QUASI	UNT	817.17	638.60	753.47	752.06	729.91	725.23	810.84	777.12
		UNC	606.88	529.90	440.90	397.72	457.34	416.92		253.96
	HARD	UNT	1298.21	1020.84	1181.10	981.77	1206.62	1016.37	1246.69	1240.63
		UNC	695.54	700.82		655.30	727.75	685.56	711.85	390.55
	SOFT	UNT	456.57	373.40	308.94	274.52	313.32	281.07	496.47	519.18
		UNC	401.96	327.45	225.29	202.15	230.32	208.81	258.62	112.05
AS4-MTM45 CPT : 0.1397 mm	QUASI	UNT	755.25	577.16	664.38	654.83	639.61	626.89	705.28	625.74
		UNC	539.72	527.32	456.20	404.57	476.72	428.22		168.26
	HARD	UNT	1114.40	940.33	1100.09	916.60	1063.66	961.58	1101.06	1050.34
		UNC	658.31	719.97		662.49	753.18	699.41	689.53	284.07
	SOFT	UNT	441.40	347.01	302.44	262.51	309.51	271.73	438.68	446.77
		UNC	388.17	337.09	229.45	201.85	236.45	210.64	236.76	63.84
CYTECT40-800-CYCOM5215 CPT : 0.14478 mm	QUASI	UNT	718.78	741.20	830.28	833.60				
		UNC	542.89	532.59	524.24	511.39				
	HARD	UNT	1277.39	1180.35		1180.33				
		UNC	760.49	747.05	796.23	795.33				
	SOFT	UNT	438.16	400.35		397.58				
		UNC	406.45	331.29	315.63	308.62				
IM7G-EpoxyEP2202 CPT : 0.18288 mm	QUASI	UNT	968.43	856.68	1030.69	1027.55	1002.11	995.91	1104.48	1087.76
		UNC	0.00	635.04	549.00	499.78	566.17	519.84		338.06
	HARD	UNT	1630.88	1356.53	1493.81	1268.76	1521.06	1305.92	1701.21	1710.49
		UNC	0.00	874.44		822.23	902.97	854.35	868.12	515.18
	SOFT	UNT	567.61	485.53	387.69	349.22	391.12	355.12	672.64	702.30
		UNC	0.00	403.12	280.47	254.22	285.00	260.53	315.39	156.35
IM7G-MTM45-1 CPT : 0.1397 mm	QUASI	UNT	915.69	696.27	865.17	740.02	836.35	774.10	906.72	866.99
		UNC	557.99	485.55	411.63	361.35	428.87	381.50		183.59
	HARD	UNT	1425.91	1058.89	1102.53	886.99	1131.20	924.64	1417.10	1404.64
		UNC	644.18	654.62		598.32	682.66	630.00	662.38	301.63
	SOFT	UNT	517.87	354.05	285.34	246.99	290.94	254.79	534.80	554.48
		UNC	400.45	286.33	208.20	181.64	214.11	189.24	228.46	77.80

Total	ALL	57		29	2	7	4	4	10	1
Total	QI UNT	10		4	0	0	0	3	3	0
Total	QI UNC	9		6	1	0	2	0	0	0
Total	HARD UNT	10		2	0	2	0	1	4	1
Total	HARD UNC	9		3	0	4	2	0	0	0
Total	SOFT UNT	10		5	1	1	0	0	3	0
Total	SOFT UNC	9		9	0	0	0	0	0	0

Table F.3: Comparison of UN strength prediction on the NIAR dataset, for RTD conditions. Compared criteria are: Best Practise (BEST), Last Ply Failure with mRoM (*mRoM*) and MFH (*MFH*) degradation method without residual thermal stresses and with thermal stresses (*mRoM TRS* and *MFH TRS*, respectively), First Ply Failure with (*FPF0 TRS*) and without (*FPF0*) and BEST criterion. The experimental OH strength is given in the column labeled *exp*. Unit system is MPa. The colored cell is always representative of the criterion with the smallest error. Red and green cells are for unsafe and safe predictions, respectively. If the material properties were not sufficient for applying the criteria, the cell is empty. A yellow cell means that no solution was found to the coupled energy-stress criterion Eq. (1.10). Below, a summary of which criterion was the most predictive, for each loading and layup case. The light blue cell indicates which criterion was best.

Material	Lay-up	Loading	exp	BEST	mRoM	mRoM TRS	MFH	MFH TRS	FPF0	FPF0 TRS
IM7-8552 CPT : 0.18288 mm	QUASI	OHT	406.79	175.27						
		OHC	338.39	127.43						0.00
	HARD	OHT	597.02	600.63	589.57	579.71	592.81	587.68	585.93	592.42
		OHC	436.02	471.16	502.70	517.76	500.20	511.89	474.24	0.00
	SOFT	OHT	300.96	249.43	228.45	216.78	230.96	220.53	0.00	254.88
		OHC	267.52	212.76	192.11	185.65	192.75	187.20	195.53	0.00
AS4-8552 CPT : 0.18796 mm	QUASI	OHT	328.40	136.65						
		OHC	325.98	157.23						0.00
	HARD	OHT	472.64	485.87	474.48	466.45	477.06	472.41	470.76	473.98
		OHC	432.85	444.49	493.52	523.48	490.30	512.11	450.14	0.00
	SOFT	OHT	270.07	212.15	190.91	180.51	192.41	182.97	0.00	
		OHC	280.13	213.38	180.21	170.45	180.58	172.18	190.56	0.00
Cytec5250-T650 CPT : 0.1397 mm	QUASI	OHT	384.66	183.37						
		OHC	343.63	146.06						
	HARD	OHT	564.20	575.95	551.55	550.04				
		OHC	447.40	479.12	495.68	499.26				
	SOFT	OHT	300.54	246.74	237.64	237.34				
		OHC	302.40	223.59	219.89	219.99				
Cytec5320-T650 CPT : 0.1397 mm	QUASI	OHT	341.99	137.10						
		OHC	350.90	156.65						0.00
	HARD	OHT	486.75	506.16	495.75	495.89	498.48	498.65	491.31	495.89
		OHC	455.16	487.89	526.17	544.44	524.04	538.35	489.97	0.00
	SOFT	OHT	293.27	219.70	206.98	199.20	208.95	202.13	0.00	219.27
		OHC	306.71	227.02	198.26	191.20	198.30	192.16	205.63	0.00
MR60H-NB4708 CPT : 0.32004 mm	QUASI	OHT	476.77	366.08						
		OHC	262.62	85.50						0.00
	HARD	OHT	965.75	752.43	699.28	675.02	699.27	679.62	727.84	739.30
		OHC	387.69	383.20	411.79	424.71	408.39	417.94	382.59	0.00
	SOFT	OHT	264.41	298.68	252.52	243.06	255.63	247.38	300.45	305.31
		OHC	199.95	165.30	155.31	150.70	156.21	152.45	157.38	0.00
MTM45-1-HTS40F13 CPT : 0.1397 mm	QUASI	OHT	416.93	287.57						
		OHC	327.09	174.92		0.00				
	HARD	OHT	677.69	629.14	612.85	578.09	623.76	592.66	606.15	613.43
		OHC	442.02	451.47	503.20	0.00	499.62	524.48	454.85	
	SOFT	OHT	289.99	250.91	214.23	198.87	217.47	203.31	258.67	264.93
		OHC	268.41	204.48	175.25	0.00	175.62	168.11	180.55	
AS4-MTM45 CPT : 0.1397 mm	QUASI	OHT	395.69	299.67						
		OHC	301.71	135.86						0.00
	HARD	OHT	645.14	607.72	596.46	561.97	601.11	584.70	582.06	605.53
		OHC	386.45	424.32	453.15	474.01	450.72	466.21	417.16	0.00
	SOFT	OHT	283.10	240.55	210.11	192.42	215.37	199.13	245.32	259.85
		OHC	250.42	190.19	165.67	157.88	166.33	159.62	161.80	0.00
CYTECT40-800-CYCOM5215 CPT : 0.14478 mm	QUASI	OHT	451.06	269.64						
		OHC	292.34	112.95						
	HARD	OHT	833.23	674.88	646.13	645.33				
		OHC	379.83	415.64	426.05	429.85				
	SOFT	OHT	294.34	259.85	251.20	250.16				
		OHC	254.55	181.48	179.41	179.40				
IM7G-EpoxyEP2202 CPT : 0.18288 mm	QUASI	OHT	534.98	370.99						
		OHC	337.31	131.90						0.00
	HARD	OHT	818.39	800.15	768.87	732.07	778.67	745.51	775.44	778.65
		OHC	402.37	477.07	503.78	518.33	502.08	514.11	476.01	0.00
	SOFT	OHT	358.36	317.65	268.01	251.21	270.61	255.07	331.34	335.26
		OHC	295.77	212.86	191.11	185.81	190.96	186.17	194.63	0.00
IM7G-MTM45-1 CPT : 0.1397 mm	QUASI	OHT	468.91	335.30						
		OHC	295.58	122.18		976.49				0.00
	HARD	OHT	795.59	694.85	646.69	613.05	659.51	617.83	685.70	694.22
		OHC	344.26	412.79	452.29	487.90	449.15	473.51	414.99	0.00
	SOFT	OHT	323.92	254.88	209.13	191.83	213.02	195.36	281.39	287.92
		OHC	262.35	177.79	157.82	148.80	158.33	151.00	158.19	0.00

Total	ALL	40		30	0	0	1	1	3	5
Total	QI OHT	0		0	0	0	0	0	0	0
Total	QI OHC	0		0	0	0	0	0	0	0
Total	HARD OHT	10		8	0	0	0	1	1	0
Total	HARD OHC	10		8	0	0	0	0	2	0
Total	SOFT OHT	10		4	0	0	1	0	0	5
Total	SOFT OHC	10		10	0	0	0	0	0	0

Table F.4: Comparison of OH strength prediction on the NIAR dataset with calibration of an average $\mathscr{R}$-curve on QI lay-ups, for RTD conditions. Compared criteria are: Best Practise (BEST), Last Ply Failure with mRoM (*mRoM*) and MFH (*MFH*) degradation method without residual thermal stresses and with thermal stresses (*mRoM TRS* and *MFH TRS*, respectively), First Ply Failure with (*FPF0 TRS*) and without (*FPF0*) and BEST criterion. The experimental OH strength is given in the column labeled *exp*. Unit system is MPa. The colored cell is always representative of the criterion with the smallest error. Red and green cells are for unsafe and safe predictions, respectively. If the material properties were not sufficient for applying the criteria, the cell is empty. A yellow cell means that no solution was found to the coupled energy-stress criterion Eq. (1.10). Below, a summary of which criterion was the most predictive, for each loading and layup case. The light blue cell indicates which criterion was best.

Material	Lay-up	Loading	exp	BEST	mRoM	mRoM TRS	MFH	MFH TRS	FPF0	FPF0 TRS
IM7-8552 CPT : 0.18288 mm	QUASI	UNT	775.38	657.10	586.22	521.71	574.59	503.68	801.34	758.09
		UNC	397.69	471.59	370.93	336.23	416.48	377.70		259.74
	HARD	UNT	1292.28	956.94	808.56	709.07	814.05	706.40	1321.64	1292.23
		UNC	547.58	572.50		528.77	634.75	584.31	560.16	320.09
	SOFT	UNT	373.49	290.68	219.66	197.55	226.80	201.73	465.94	468.01
		UNC	280.00	245.95	174.72	157.05	191.60	171.42	155.48	75.51
AS4-8552 CPT : 0.18796 mm	QUASI	UNT	656.24	506.19	487.12	433.59	482.84	425.40	602.91	565.58
		UNC	433.89	421.99	324.14	294.80	361.58	334.00		249.43
	HARD	UNT	996.91	768.62	681.50	596.65	690.44	601.14	989.61	959.84
		UNC	606.81	498.98		463.16	556.35	522.29	502.49	307.67
	SOFT	UNT	332.12	251.89	190.08	171.03	196.49	175.62	369.83	369.05
		UNC	314.40	226.17	154.67	139.48	170.37	155.89	147.23	76.51
Cytec5250-T650 CPT : 0.1397 mm	QUASI	UNT	668.24	610.34	479.89	411.08	421.70	340.40	747.99	706.75
		UNC	386.80	406.63	323.68	283.02	372.92	316.36		211.35
	HARD	UNT	1170.04	864.01	671.05	566.34	621.26	496.96	1242.32	1210.26
		UNC	464.43	496.80		443.10	554.05	476.33	501.88	270.59
	SOFT	UNT	336.19	250.70	184.02	159.65	180.48	148.56	425.89	425.59
		UNC	233.25	205.83	149.98	129.61	164.53	135.53	136.94	63.19
Cytec5320-T650 CPT : 0.1397 mm	QUASI	UNT	725.25	579.71	662.90	661.76	642.91	639.76	706.86	699.09
		UNC	563.14	524.93	451.68	423.84	467.46	441.73		362.80
	HARD	UNT								
		UNC								
	SOFT	UNT								
		UNC								
MR60H-NB4708 CPT : 0.32004 mm	QUASI	UNT	750.36	627.13	449.54	441.82	474.07	466.32	930.44	930.47
		UNC	280.82	350.97	280.24	276.25	308.38	304.54		328.37
	HARD	UNT	1165.42	949.59	660.56	646.98	697.29	683.88	1545.21	1550.42
		UNC	476.84	466.65		461.42	512.75	507.65	458.34	430.22
	SOFT	UNT	321.36	333.55	210.00	206.76	221.70	218.46	550.72	553.24
		UNC	222.77	201.73	150.53	148.09	164.49	162.14	164.60	152.80
MTM45-1-HTS40F13 CPT : 0.1397 mm	QUASI	UNT	0.00	637.32	639.58	589.48	673.95	624.08	809.97	799.11
		UNC	514.90	449.31	387.50	364.48	414.54	392.97		308.44
	HARD	UNT								
		UNC								
	SOFT	UNT								
		UNC								
AS4-MTM45 CPT : 0.1397 mm	QUASI	UNT	0.00	509.69	513.83	467.60	511.49	463.16	647.64	641.56
		UNC	440.85	338.69	300.27	278.91	318.83	298.76		210.17
	HARD	UNT								
		UNC								
	SOFT	UNT								
		UNC								
CYTECT40-800-CYCOM5215 CPT : 0.14478 mm	QUASI	UNT	772.08	634.74	495.72	443.12	524.81	472.15	889.39	867.22
		UNC	421.06	380.59	307.64	280.85	336.02	310.27		227.68
	HARD	UNT	1180.45	919.65	677.39	592.35	717.54	633.81	1406.13	1410.73
		UNC	567.44	478.18		444.75	521.92	489.51	475.36	297.35
	SOFT	UNT	389.90	286.81	184.44	166.23	194.54	176.71	506.36	521.47
		UNC	283.44	214.00	148.12	134.39	159.63	146.36	145.81	80.89
IM7G-EpoxyEP2202 CPT : 0.18288 mm	QUASI	UNT	949.79	740.26	806.70	720.80	837.80	753.88	977.47	980.52
		UNC	444.33	463.85	418.22	382.88	434.92	401.66		262.45
	HARD	UNT	1425.26	1120.81	1055.20	910.70	1088.63	949.30	1496.40	1534.35
		UNC	621.82	663.14		622.35	690.49	652.30	629.62	384.99
	SOFT	UNT	494.62	367.28	278.68	251.63	285.06	259.43	544.88	578.06
		UNC	304.67	284.92	209.62	190.90	215.40	197.85	207.89	110.33
IM7G-MTM45-1 CPT : 0.1397 mm	QUASI	UNT	0.00	675.46	598.13	545.94	599.54	544.38	918.40	912.60
		UNC	485.53	408.84	341.18	317.47	366.95	342.50		276.99
	HARD	UNT								
		UNC								
	SOFT	UNT								
		UNC								

Total	ALL	41		19	1	1	5	1	8	6
Total	QI UNT	7		1	0	0	0	0	3	3
Total	QI UNC	10		6	1	0	3	0	0	0
Total	HARD UNT	6		1	0	0	0	0	3	2
Total	HARD UNC	6		1	0	1	2	1	1	0
Total	SOFT UNT	6		4	0	0	0	0	1	1
Total	SOFT UNC	6		6	0	0	0	0	0	0

Table F.5: Comparison of UN strength prediction on the NIAR dataset, for ETW conditions. Compared criteria are: Best Practise (BEST), Last Ply Failure with mRoM (*mRoM*) and MFH (*MFH*) degradation method without residual thermal stresses and with thermal stresses (*mRoM TRS* and *MFH TRS*, respectively), First Ply Failure with (*FPF0 TRS*) and without (*FPF0*) residual thermal stresses and BEST criterion. The experimental OH strength is given in the column labeled *exp*. Unit system is MPa. The colored cell is always representative of the criterion with the smallest error. Red and green cells are for unsafe and safe predictions, respectively. If the material properties were not sufficient for applying the criterion or if the criterion leads the same prediction as BEST, the cell is empty. A yellow cell means that no solution was found to the coupled energy-stress criterion Eq. (1.10). Below, a summary of which criterion was the most predictive, for each loading and layup case. The light blue cell indicates which criterion was best.

Material	Lay-up	Loading	exp	BEST	mRoM	mRoM TRS	MFH	MFH TRS	FPF0	FPF0 TRS
IM7-8552 CPT : 0.18288 mm	QUASI	OHT	461.74	368.34		0.00				
		OHC	244.90	74.97						0.00
	HARD	OHT	791.93	670.84	641.05	0.00	655.37		695.18	708.41
		OHC	320.05	334.94	366.25	374.56	361.21	366.03	332.18	0.00
	SOFT	OHT	264.69	220.77	178.96	0.00	185.39		265.71	272.19
		OHC	177.61	136.99	125.27	120.70	127.24	122.92	109.95	0.00
AS4-8552 CPT : 0.18796 mm	QUASI	OHT	356.32	273.01		0.00				
		OHC	228.15	78.52						0.00
	HARD	OHT	545.17	529.94	503.09	0.00	510.78		536.25	548.12
		OHC	333.43	305.33	341.69	351.93	337.76	343.27	306.22	0.00
	SOFT	OHT	221.18	187.26	151.13	0.00	155.99		213.06	219.12
		OHC	182.09	130.89	116.51	111.44	119.55	115.84	105.27	0.00
Cytec5250-T650 CPT : 0.1397 mm	QUASI	OHT	388.17	247.49		0.00				
		OHC	248.49	107.57	223.37	0.00				
	HARD	OHT	627.49	558.33	544.22	0.00			580.63	589.13
		OHC	318.26	334.26	378.02	0.00	367.59	372.91	336.11	
	SOFT	OHT	236.49	181.83	150.62	0.00			218.62	222.33
		OHC	176.30	132.69	118.73	0.00	120.14	109.45	103.00	
Cytec5320-T650 CPT : 0.1397 mm	QUASI	OHT	364.33	196.29						
		OHC	307.71	134.69						0.00
	HARD	OHT								
		OHC								
	SOFT	OHT								
		OHC								
MR60H-NB4708 CPT : 0.32004 mm	QUASI	OHT	515.93	0.00					339.40	
		OHC	203.19	61.49						
	HARD	OHT	990.29	0.00					796.91	797.57
		OHC	296.89	290.38	326.07	327.70	320.45	321.44	288.07	285.78
	SOFT	OHT	248.00	0.00					311.44	311.93
		OHC	136.38	121.60	113.38	112.81	115.19	114.77	110.36	107.69
MTM45-1-HTS40F13 CPT : 0.1397 mm	QUASI	OHT	437.61	359.17						
		OHC	287.99	146.76						0.00
	HARD	OHT								
		OHC								
	SOFT	OHT								
		OHC								
AS4-MTM45 CPT : 0.1397 mm	QUASI	OHT	379.28	387.02		1069.45		0.00		
		OHC	261.93	253.81	0.00					
	HARD	OHT								
		OHC								
	SOFT	OHT								
		OHC								
CYTECT40-800-CYCOM5215 CPT : 0.14478 mm	QUASI	OHT	464.36	476.85	0.00				256.45	
		OHC	228.91	79.34						0.00
	HARD	OHT	919.83	671.75	0.00				681.70	687.62
		OHC	295.92	309.76	347.67	361.11	343.12	350.57	308.86	0.00
	SOFT	OHT	273.65	223.53	0.00				272.16	276.51
		OHC	194.02	133.32	115.53	110.01	118.09	113.98	107.02	0.00
IM7G-EpoxyEP2202 CPT : 0.18288 mm	QUASI	OHT	512.91	444.83						
		OHC	250.58	73.39						0.00
	HARD	OHT	803.29	760.13	703.74	675.96	704.38	680.84	747.75	751.06
		OHC	321.64	359.05	373.20	381.38	371.69	378.33	353.25	0.00
	SOFT	OHT	316.10	271.66	215.14	201.12	217.66	205.00	301.23	306.64
		OHC	232.92	151.99	138.56	135.41	138.80	136.02	134.19	0.00
IM7G-MTM45-1 CPT : 0.1397 mm	QUASI	OHT	504.97	604.31	0.00					
		OHC	239.66	79.38						0.00
	HARD	OHT								
		OHC								
	SOFT	OHT								
		OHC								

Total	ALL	24		9	0	0	1	0	6	8
Total	QI OHT	0		0	0	0	0	0	0	0
Total	QI OHC	0		0	0	0	0	0	0	0
Total	HARD OHT	6		1	0	0	0	0	0	5
Total	HARD OHC	6		2	0	0	1	0	3	0
Total	SOFT OHT	6		0	0	0	0	0	3	3
Total	SOFT OHC	6		6	0	0	0	0	0	0

Table F.6: Comparison of OH strength prediction on the NIAR dataset with calibration of an average $\mathscr{R}$-curve on QI lay-ups, for ETW conditions. Compared criteria are: Best Practise (BEST), Last Ply Failure with mRoM (*mRoM*) and MFH (*MFH*) degradation method without residual thermal stresses and with thermal stresses (*mRoM TRS* and *MFH TRS*, respectively), First Ply Failure with (*FPF0 TRS*) and without (*FPF0*) and BEST criterion. The experimental OH strength is given in the column labeled *exp*. Unit system is MPa. The colored cell is always representative of the criterion with the smallest error. Red and green cells are for unsafe and safe predictions, respectively. If the material properties were not sufficient for applying the criteria, the cell is empty. A yellow cell means that no solution was found to the coupled energy-stress criterion Eq. (1.10). Below, a summary of which criterion was the most predictive, for each loading and layup case. The light blue cell indicates which criterion was best.

G Definitions

G.1 Symmetric and balanced laminates

G.1.1 Symmetry

A composite laminate is generally composed of several plies, each ply being oriented with a specific angle with respect to the longitudinal direction of the composite (the 0° direction). A symmetric laminate is such that there is an even number of plies[1]; taking the mid-plane of the laminate, the plies above it are mirroring the plies below the mid-plane. For instance, [0/90/45/45/90/0] is symmetric whereas [0/90/45/0] is not. The main interest in doing symmetric laminates is the dramatic reduction in thermal twisting as the laminate is cooled down after curing. Indeed, the fabrication process of composite laminates generally consists in stacking the impregnated plies at room temperature before placing them in an autoclave for curing. At elevated temperatures, the extension of the plies do not create warping. However, when the laminate is cooled down, the plies contract in different manners depending on their orientation. If the lay-up is symmetric, there is a symmetry in the thermal residual stresses preventing warping.

Mathematically, the flexural and tensile behaviors of the laminate are independent, leading to independent A and D matrices [69, p. 255].

G.1.2 Balancing

A laminate is said to be balanced if it has equal numbers of "+θ" and "-θ" angled plies. If a laminate is both symmetric and balanced, the in-plane normal shear coupling terms disappear [69, p. 237].

[1] It must be noted that the laminate is still considered symmetric if it has an odd number of plies, with the central ply being a 0° or 90° ply.

List of Figures

List of Tables

References

[1] Federal Aviation Administration. “Advisory Circular”. In: (Aug. 2010). URL: https://www.faa.gov/documentLibrary/media/Advisory_Circular/AC_20-107B_with_change_1.pdf.

[2] B. Yancey. *Material Certification of Laminated Composites*. Oct. 2016. URL: https://insider.altairhyperworks.com/material-certification-laminated-composites/ (visited on 04/15/2019).

[3] O. Vallmajó et al. “Virtual calculation of the B-value allowables of notched composite laminates”. In: *Composite Structures* 212 (Mar. 2019), pp. 11–21. DOI: https://doi.org/10.1016/j.compstruct.2018.12.049.

[4] C. Furtado et al. “Prediction of size effects in open-hole laminates using only the Young’s modulus, the strength, and the $\mathscr{R}$-curve of the 0° ply”. In: *Composites Part A: Applied Science and Manufacturing* 101 (Oct. 2017), pp. 306–317. URL: https://doi.org/10.1016/j.compositesa.2017.04.014.

[5] National Programme on Technology Enhanced Learning. *Introduction to Classical Plate Theory*. June 2012. URL: https://nptel.ac.in/courses/101104010/16 (visited on 04/15/2019).

[6] S. W. Tsai and J. D. D. Melo. *Composite Materials design and testing - Unlocking mystery with invariants*. Ed. by Department of Aeronautics Composites Design Group and Stanford University Astronautics. 2015.

[7] S. W. Tsai and J. D. D. Melo. “An invariant-based theory of composites”. In: *Composites Science and Technology* 100 (Aug. 2014), pp. 237–243. URL: https://doi.org/10.1016/j.compscitech.2014.06.017.

[8] P. P. Camanho and G. Catalanotti. “On the relation between the mode I fracture toughness of a composite laminate and that of a 0° ply: Analytical model and experimental validation”. In: *Engineering Fracture Mechanics* 78.13 (Aug. 2011), pp. 2535–2546. URL: https://doi.org/10.1016/j.engfracmech.2011.06.013.

[9] K.-L. Poon. *Newport Adhesives and Composites NCT4708 MR60H 300gsm 38% RC Unidirectional Qualification Material Property Data Report*. National Institute For Aviation Research, Aug. 2011. URL: https://www.wichita.edu/research/NIAR/Research/newport-nct4708/4708-Unitape-2.pdf (visited on 02/15/2019).

[10] *National Center for Advanced Materials Performance*. Wichita State University. URL: https://www.wichita.edu/research/NIAR/Research/ncamp.php# (visited on 02/06/2019).

[11] A. Arteiro et al. "A micro-mechanics perspective to the invariant-based approach to stiffness". In: *Composites Science and Technology* 176 (2019), pp. 72–80. ISSN: 0266-3538. DOI: https://doi.org/10.1016/j.compscitech.2019.04.002. URL: http://www.sciencedirect.com/science/article/pii/S0266353818328938.

[12] G. Bao et al. "The role of material orthotropy in fracture specimens for composites". In: *International Journal of Solids and Structures* 29.9 (), pp. 1105–1116. URL: https://doi.org/10.1016/0020-7683(92)90138-J.

[13] G. Bao, S. H. Z. Suo, and Fan B. "Corrigenda". In: *Int. J. Solids Structures* 29.16 (1992), p. 2115. URL: https://www.sciencedirect.com/science/article/pii/0020768392901983.

[14] S.T. Pinho, P. Robinson, and L. Iannucci. "Fracture toughness of the tensile and compressive fibre failure modes in laminated composites". In: *Composites Science and Technology* 66.13 (Oct. 2016), pp. 2069–2079. URL: https://doi.org/10.1016/j.compscitech.2005.12.023.

[15] G. Catalanotti et al. "Determination of the mode I crack resistance curve of polymer composites using the size-effect law". In: *Engineering Fracture Mechanics* 118 (Mar. 2014), pp. 49–65. URL: https://doi.org/10.1016/j.engfracmech.2013.10.021.

[16] A. Arteiro et al. "Large damage capability of non-crimp fabric thin-ply laminates". In: *Composites Part A: Applied Science and Manufacturing* 63 (2014), pp. 110–122. ISSN: 1359-835X. DOI: https://doi.org/10.1016/j.compositesa.2014.04.002. URL: http://www.sciencedirect.com/science/article/pii/S1359835X14001043.

[17] P. Cornetti et al. "Finite fracture mechanics: A coupled stress and energy failure criterion". In: *Engineering Fracture Mechanics* 73 (2006), pp. 2021, 2033. URL: https://doi.org/10.1016/j.engfracmech.2006.03.010.

[18] P. P. Camanho et al. "A finite fracture mechanics model for the prediction of the open-hole strength of composite laminates". In: *Composites Part A: Applied Science and Manufacturing* 45.8 (Aug. 2012), pp. 1219–1225.

[19] J. M. Whitney and R. J. Nuismer. ""Stress fracture criteria for laminated composites containing stress concentrations". In: *Journal of Composite Materials* 8.3 (July 1974), pp. 253–265. DOI: https://doi.org/10.1177/002199837400800303.

[20] S. C. Tan. "Laminated Composites Containing an Elliptical Opening. I. Approximate Stress Analyses and Fracture Models". In: *Journal of Composite Materials* 10 (1987), pp. 925–948. DOI: https://doi.org/10.1177%2F002199838702101004.

[21] N. M. Pugno and R. S. Ruoff. "Quantized fracture mechanics". In: *Philosophical Magazine* 84.27 (2004), pp. 2829–2845. DOI: 10.1080/14786430412331280382.

[22] S. C. Tan. *Stress Concentrations in Laminated Composites*. Ed. by CRC Press. 1994. ISBN: 9781566760775.

[23] A. J. Konish and J. M. Whitney. "Approximate Stresses in an Orthotropic Plate Containing a Circular Hole". In: *Journal of Composite Materials* 9.2 (1975), pp. 157–166. DOI: 10.1177/002199837500900206

[24] J. C. Newman. "A Nonlinear Fracture Mechanics Approach to the Growth of Small Cracks". In: *AGARD(NATO)* 328.6 (Apr. 1983), p. 28.

[25] URL: https://en.wikipedia.org/wiki/Brent%27s_method#Implementations (visited on 02/21/2019).

[26] URL: http://mathworld.wolfram.com/LobattoQuadrature.html (visited on 02/19/2019).

[27] P. P. Camanha, P. Maimi, and CG. Davila. "Prediction of size effects in notched laminates using continuum damage mechanics". In: *Composites Science and Technology* 67 (2007), pp. 2715–2727.

[28] X. Xu et al. "Unification of strength scaling between unidirectional, quasi-isotropic, and notched carbon/epoxy laminates". In: *Composites Part A: Applied Science and Manufacturing* 90 (Nov. 2016), pp. 296–305.

[29] J. Lee and C. Soutis. "Measuring the notched compressive strength of composite laminates: speciment size effects." In: *Composites Science and Technology* 68.12 (Sept. 2008). DOI: https://doi.org/10.1016/j.compscitech.2007.09.003.

[30] M. Bessa. "Meso-mechanical model of the structural integrity of advanced composite laminates". Master's Thesis. Mechanical Engineering Department, University of Porto, 2010.

[31] K. Marlett. *Hexcel 8552 IM7 Unidirectional Prepreg 190 gsm and 35%RC Qualification Material Property Data Report*. Apr. 2011. URL: https://www.wichita.edu/research/NIAR/Documents/Qual-CAM-RP-2009-015-Rev-B-Hexcel-8552-IM7-MPDR-04.16.19.pdf (visited on 02/15/2019).

[32] G. H. Ercin et al. "Size effects on the tensile and compressive failure of notched composite laminates". In: *ECCM15 - 15th European conference on composite materials* (June 2012).

[33] C. Furtado et al. "Selective ply-level hybridisation for improved notched response of composite laminates". In: *Composite Structures* 145 (2016), pp. 1–14.

[34] A. Arteiro et al. "Notched response of non-crimp fabric thin-ply laminates". In: *Composites Science and Technology* 79 (2013), pp. 97–114.

[35] M. R. Wisnom and S. R. Hallett. "The role of delamination in strength, failure mechanism and hole size effect in open hole tensile tests on quasi-isotropic laminates". In: *Composites Part A: Applied Science and Manufacturing* 40.4 (2009), pp. 335–342. ISSN: 1359-835X. DOI: https://doi.org/10.1016/j.compositesa.2008.12.013. URL: http://www.sciencedirect.com/science/article/pii/S1359835X08003266.

[36] P. P. Camanho and P. Maimi. *Size effects on the strength of notched composites. 16th International Conference On Composite Materials*. English. 2007. URL: http://iccm-central.org/Proceedings/ICCM16proceedings/contents/pdf/TueB/TuBA2-03sp_camanhop222032p.pdf (visited on 04/05/2019).

[37] A. Arteiro. "Structura Mechanics of Thin-Ply Laminated Composites". English. PhD Thesis. Porto: Faculty of Engineering, University of Porto, 2016.

[38] P. P. Camanho et al. "Prediction of in situ strengths and matrix cracking in composites under transverse tension and in-plane shear". In: *Composites: Part A* 37 (2006), pp. 165–176.

[39] G. Catalanotti, J. Xavier, and P.P. Camanho. "Measurement of the compressive crack resistance curve of composites using the size effect law". In: *Composites Part A: Applied Science and Manufacturing* 56 (2014), pp. 300–307. ISSN: 1359-835X. DOI: https://doi.org/10.1016/j.compositesa.2013.10.017. URL: http://www.sciencedirect.com/science/article/pii/S1359835X13002923.

[40] A. J. Hodge, A. T. Nettles, and J. R. Jackson. “Comparison of Open-Hole Compression Strength and Compression After Impact Strength on Carbon Fiber/Epoxy Laminates for the Ares I Composite Interstage”. In: (Mar. 2011). URL: https://ntrs.nasa.gov/search.jsp?R=20110008641 (visited on 05/23/2019).

[41] S. B. Clay and P. M. Knoth. “Experimental results of quasi-static testing for calibration and validation of composite progressive damage analysis methods”. In: *Journal of Composite Materials* 51.10 (2017), pp. 1333–1353. DOI: 10.1177/0021998316658539. eprint: https://doi.org/10.1177/0021998316658539. URL: https://doi.org/10.1177/0021998316658539.

[42] P. J. Callus. *The Effects of Hole-size and Environment on the Mechanical Behaviour of a Quasi-isotropic AS4/3501-6 Laminate in Tension, Compression and Bending*. Victoria, Australia: Air Vehicles Division, Defence Science and Technology Organisation, Nov. 2007.

[43] S. W. Tsai and J. D. D. Melo. “A unit circle failure criterion for carbon fiber reinforced polymer composites”. In: *Composites Science and Technology* 123 (Feb. 2016), pp. 71–78. URL: https://doi.org/10.1016/j.compscitech.2015.12.011.

[44] P.A. Carraro and M. Quaresimin. “A stiffness degradation model for cracked multidirectional laminates with cracks in multiple layers”. In: *International Journal of Solids and Structures* 58 (2015), pp. 34–51.

[45] S. W. Tsai and H. T. Hahn. *Introduction to composite materials*. Ed. by Inc. Technomic Publishing Co. 1980. ISBN: 9780877622888.

[46] *Mechanical Behaviors of a Lamina*. English. URL: https://www.efunda.com/formulae/solid_mechanics/composites/comp_lamina_egnu.cfm (visited on 03/22/2019).

[47] *Mean-field homogenization*. URL: https://abaqus-docs.mit.edu/2017/English/SIMACAEMATRefMap/simamat-c-meanfieldhomogenization.htm (visited on 04/25/2019).

[48] e-Xstream Engineering. *User’s Manual. Release 2018.1*. English. 2018.

[49] L. Wu et al. “An incremental-secant mean-field homogenization method with second statistical moments for elasto-visco-plastic composite materials”. In: *Mechanics of Materials* 114 (2017), pp. 180–200. ISSN: 0167-6636. DOI: https://doi.org/10.1016/j.mechmat.2017.08.006.

[50] T. Mura. *Micromechanics of Defects in Solids*. Ed. by Martinus Nijhoff Publishers. Second, revised edition. 1987. ISBN: 902473343X.

[51] E Lian. *SOLVAY (Formerly known as Advanced Composites Group) MTM45-1/ IM7-145 32%RW 12k IM7 Unidirectional 145 gsm Qualification Material Property Data Report*. URL: https://www.wichita.edu/research/NIAR/Research/cytec-mtm45-1/CAM-RP-2008-007-Rev-B-ACG-IM7-Uni-3.28.2018-FINAL-MPDR.pdf (visited on 02/15/2019).

[52] C. T. Herakovich and D. M. Wong. “Influence of residual stresses on the tensile strength of composite-metal sandwich laminates”. In: *Experimental Mechanics* 17.11 (Nov. 1977), pp. 409–414. DOI: https://doi.org/10.1007/BF02324237.

[53] A. K. Miller. “Thermal Expansion coefficients for laminates obtained from invariant lamina properties”. In: *Fibre Science and Technology* 13.5 (Aug. 1980), pp. 397–409. DOI: https://doi.org/10.1016/0015-0568(80)90012-3.

[54] H.T. Hahn and N.J. Pagano. “Curing Stresses in Composite Laminates”. In: *Journal of Composite Materials* 9.1 (1975), pp. 91–106. DOI: doi:10.1177/002199837500900110.

[55] K. Marlett. *Hexcel 8552 AS4 Unidirectional Prepreg at 190 gsm and 35% RC Qualification Material Property Data Report*. May 2011. URL: https://www.wichita.edu/research/NIAR/Research/hexcel-8552/AS4-Unitape-2.pdf (visited on 02/15/2019).

[56] M. Michelle and T. Vinsensius. *CYTEC (Formerly Advanced Composites Group) 12K HTS5631 Unidirectional MTM45-1/HTS(12k)-145-32%RW Qualification Material Property Data Report*. Mar. 2016. URL: https://www.wichita.edu/research/NIAR/Research/cytec-mtm45-1/12K-HTS5631-Unidirectional-HTS40-2.pdf.

[57] M. Man. *Cytec Cycom 5250-5 T650 Unitape Gr 145 32% RC Qualification Material Property Data Report*. Oct. 2017. URL: https://www.wichita.edu/research/NIAR/Research/cytec-5250-5/T650-Unitape-2.pdf (visited on 02/15/2019).

[58] E. Clarkson. *CYTEC (Formerly Advanced Composites Group) MTM45-1/ 12K AS4 145gsm 32%RW Unidirectional Qualification Statistical Analysis Report*. Mar. 2016. URL: https://www.wichita.edu/research/NIAR/Research/cytec-mtm45-1/12K-AS4-Unidirectional-3.pdf (visited on 02/15/2019).

[59] M. Man and T. Vinsensius. *Solvay Cytec Cycom EP 2202 IM7G Unitape Gr 190 RC 33% Qualification Material Property Data Report*. Aug. 2017. URL: https://www.wichita.edu/research/NIAR/Research/cytec-ep2202/IM7G-Unitape-2.pdf (visited on 02/15/2019).

[60] M. Man. *Cytec Cycom 5215 T40-800 Unitape Gr 145 33% RC Qualification Material Property Data Report*. July 2012. URL: https://www.wichita.edu/research/NIAR/Research/cytec-5215/T40-800-Unitape-2.pdf (visited on 02/15/2019).

[61] M. Man. *Solvay Cytec Cycom 5320-1 T650 Unitape Qualification Material Property Data Report*. Jan. 2017. URL: https://www.wichita.edu/research/NIAR/Research/cytec-5320-1/T650-Unitape-2.pdf (visited on 02/15/2019).

[62] ASTM International. *ASTM D3410 / D3410M-16, Standard Test Method for Compressive Properties of Polymer Matrix Composite Materials with Unsupported Gage Section by Shear Loading*. West Conshohocken, 2016. DOI: 10.1520/D3410_D3410M-16. URL: http://www.astm.org/cgi-bin/resolver.cgi?D3410D3410M (visited on 03/24/2019).

[63] Hexcel Corporation. *HexTow AS4A - Carbon Fiber*. 2016. URL: https://www.hexcel.com/user_area/content_media/raw/AS4A_HexTow_DataSheet.pdf (visited on 03/14/2019).

[64] Toray Carbon Fibers America Inc. *Torayca T800S Data Sheet*. URL: https://www.toraycma.com/file_viewer.php?id=4464 (visited on 03/14/2019).

[65] Hexcel Corporation. *HexTow Carbon Fiber*. 2018. URL: https://flipflashpages.uniflip.com/3/105023/1095189/pub/document.pdf (visited on 03/14/2019).

[66] Grafil Inc. *Pyrofil MR60H 24K*. 2008. URL: https://www.rockwestcomposites.com/downloads/MR60H-24K_(02-2008).pdf (visited on 03/14/2019).

[67] Cytec Engineerd Materials. *Thornel T-650/35 PAN-Based Fiber*. 2012. URL: https://www.fibermaxcomposi
com/shop/datasheets/T650.pdf (visited on 03/14/2019).

[68] Swiss Composite. *Tenax-E HTS40 F13 12K 800tex*. 2010. URL: https://www.swiss-composite.ch/pdf/t-Tenax-Datenblatt.pdf (visited on 03/14/2019).

[69] D. Gay and S. V. Hoa. *Composite Materials Design and applications*. Ed. by CRC Press. 2007. ISBN: 1-4200-4519-9.